# Mitochondrial bioenergetics and transporter-mediated metabolism in *Schizosaccharomyces pombe*

Dissertation

zur Erlangung des Grades

des Doktors der Naturwissenschaften

der Naturwissenschaftlich-Technischen Fakultät

der Universität des Saarlandes

von

## Vasileios Delis

Saarbrücken

2016

*To Eva*

Tag des Kolloguiums:   04.10.2016

Dekan:   Prof. Dr. Dirk Bähre

Berichterstatter:   Prof. Dr. Elmar Heinzle

Prof. Dr. Manfred Schmitt

Vorsitz:   Prof. Dr. Volkhard Helms

Akad. Mitarbeiter:   Dr.-Ing. M. Kohlstedt

# Acknowledgements

Science, my boy, is made up of mistakes, but they are mistakes which it is useful to make, because they lead little by little to the truth.

Jules Verne, Journey to the Center of the Earth

# Table of Contents

# List of abbreviations

Following is a list of all relevant abbreviations and acronyms that were used throughout this thesis.

## Cellular localization

CYT: cytosolic compartment

EX: extracellular space

IMM: inner mitochondrial membrane

IMS: mitochondrial intermembrane space

MIT: mitochondrial compartment

OMM: outer mitochondrial membrane

## Mitochondrial transporters

ANT: adenine nucleotide translocator

CTP: citrate transporter

DIC: dicarboxylate carrier

DIC: dicarboxylate carrier protein

DTC: di-/tricarboxylate carrier

MPC: mitochondrial pyruvate carrier

OAC: oxaloacetate carrier

OGC: oxoglutarate carrier

POR: porin

POR: porin

SFC: succinate/fumarate carrier

SFC: succinate/fumarate carrier or antiporter

VDAC: voltage-dependent annion carrier, porin

YEA6: NAD transporter

YMUC: yeast mitochondrial unspecific channel

## Enzymes and pathways

ADH: alcohol dehydrogenase

ALD: aldehyde dehydrogenase

ALD: aldehyde dehydrogenase

ATPase: mitochondrial matrix ATP synthase

CS: citrate synthase

GA3P-DH: glyceraldehyde 3-phospate dehydrogenase

GUT2: glycerol 3-phosphate dehydrogenase

MAE2: malic enzyme

MDH: malate dehydrogenase

NDE1/2: external mitochondrial NADH dehydrogenases

NDI: internal mitochondrial NADH dehydrogenases

PCX: pyruvate carboxylase

PDC: pyruvate decarboxylase

PDH: pyruvate dehydrogenase complex

PPP: pentose phosphate pathway

TCA: tricarboxylic acid cycle

## Metabolites and redox precursors

$\alpha$KG: $\alpha$-ketoglutarate

3PG: 3-phosphoglycerate

A(X)P (AMP, ADP, ATP): mono-, di- or triphosphate adenosine nucleotide

AAD: acetaldehyde

AcCoA: acetyl-CoA

ACE: acetate

ASP: aspartate

cis-ACO: cis-aconitate

CIT: citrate

cytc: cytochrome $c$

E4P: erythrose 4-phosphate

EtOH: ethanol

F6P: fructose 6-phosphate

FAD/FADH$_2$: oxidized and reduced flavin adenine dinucleotide

FUM: fumarate

G6P: glucose 6-phosphate

GA3P: glyceraldehyde 3-phosphate

GLC: glucose

GLU: glutamate

GLYC: glycerine

ICI: isocitrate

isoPM: isopropylmalate

MAL: malate

NAD/NADH: oxidized and reduced nicotinamide adenine dinucleotide

NADP/NADPH: oxidized and reduced nicotinamide adenine dinucleotide phosphate

OAA: oxaloacetate

OG or oxoG: oxoglutarate

oxoAd: oxoadipate

PEP: phosphoenolpyruvate

PYR: pyruvate

Q: ubiquinone

$QH_2$: ubiquinol

SUC: succinate

## Others

amp: ampicillin

Ap5A: P1,P5-di(adenosine-5')pentaphosphate

BCAA: branched-chain amino acids

CDW: cell dry weight

$D_{crit}$: critical dilution rate

DHAP: dihydroxyacetone phosphate

DMSO: dimethyl sulfoxide

DTT: dithiothreitol

ER: endoplasmic reticulum

G418: geneticin

HPLC: high pressure liquid chromatography

IS: ion source

kan: kanamycin

kanMX: kanamycin resistance selection marker

LB: lysogeny broth medium

MCF: mitochondrial carrier family

MDV: mass distribution vector

MFA: metabolic flux analysis

MIMS: membrane inlet mass spectrometer

MM: minimal medium

MTF: 5-methyltetrahydrofolate

natMX: nourseothricin resistance selection marker

$O.D_{595nm}$: optical density at a wavelength of 595 nm

$O.D_{600nm}$: optical density at a wavelength of 600 nm

ORF: open reading frame

ORF: open reading frame

OUR: oxygen uptake rate

P/O: phosphate/oxygen ratio

P: product

PCR: polymerase chain reaction

PEEK: polyether ether ketone

QF: quadropole filter

ROS: reactive oxygen species

ROT: rotenone

RPM: rounds per minute

S: substrate

SD: synthetic defined medium

SEM: secondary electron multiplier

SGD: *Saccharomyces* genome database

UPR: unfolded protein response

UPR: unfolded protein response

WGD: whole genome duplication

WT: wild type

X: biomass

YES: yeast extract sucrose medium

# Abstract

Currently we possess a limited understanding on mitochondrial transporters in the model organism *Schizosaccharomyces pombe* and of the nature and the extent of regulation that is exerted from these mitochondrial carrier proteins on mitochondrial and cytosolic pathways.

A systems biology approach was applied towards dynamically quantifying the metabolism of NADH, $FADH_2$ and NAD-linked substrates which spanned over three compartments (cytosol, mitochondrial intermembrane space and mitochondrial matrix) and was mediated by specific membrane-bound transporters. In particular, by utilizing a selective permeabilization method in cytosol-mimicking conditions, exogenous substrates were delivered in a targeted manner directly on the cytosolic side of the outer mitochondrial membrane.

In this manner we could propose the existence of a dicarboxylate carrier protein docked on the inner mitochondrial membrane that could be specifically inhibited and also identify an outer mitochondrial membrane porin linking via metabolite channeling the cytosolic formation of NADH to its oxidation in the intermembrane mitochondrial space. Furthermore, the deletion of the genes encoding for the functional subunits of the mitochondrial pyruvate carrier (MPC) revealed in whole cells a metabolic bottleneck at the pyruvate node with extended metabolic implications for the ethanol and acetate biosynthetic pathways. Based on the *in situ* characterization of selectively permeabilized MPC-deficient strains we hypothesize that the MPC machinery is part of a larger transmembrane metabolon connecting pyruvate transport to mitochondrial respiration, ATP synthesis and exchange for cytosolic ADP. As such, the MPC could affect metabolic pathways in the cytosol and the mitochondrial matrix, influence the P/O ratio and reveal itself as part of an extended metabolon possibly regulating the Crabtree effect.

# Zusammenfassung

Derzeit ist unser Verständnis über mitochondriale Transporter bei dem Modelorganismus *Schizosaccharomyces pombe* noch sehr begrenzt, ebenso wie die Natur und der regulatorische Umfang von solchen mitochondrialen Carrier-Proteinen innerhalb mitochondrial- und zytosolisch-lokalisierten Stoffwechselwegen.

Zur dynamischen Quantifizierung des Metabolismus von NADH, $FADH_2$, und NAD-gekoppelten Substraten, der sich über drei Kompartimente erstreckt (Zytosol, mitochondrialer Intermembranraum und Matrix) und über Membran-gebundene Transporter vermittelt wird, wurde eine systembiologische Methode angewandt. Insbesondere wurden durch die selektive Permeabilisierung der Plasmamembran unter zytosol-nachahmenden Bedingungen exogene Substrate gezielt auf die zytosolische Seite der mitochondrialen Außenmembran abgegeben.

Dies führte zu der Annahme, dass ein Dikarbonsäure Membrantransporter existiert, der an der inneren mitochondrialen Membran lokalisiert ist und spezifisch inhibiert werden kann. Gleichzeitig wurde ein Porin identifiziert, das sich an der mitochondrialen Außenmembran befindet und mittels Metabolit-Channeling die zytosolische Synthese von NADH in seine oxidierte Form im mitochondrialen Intermembranraum verknüpft. Darüber hinaus führte die Deletion der Gene für die funktionellen Untereinheiten des mitochondrialen Pyruvattransporters (MPC) am Pyruvatknotenpunkt zu einem metabolischen Bottleneck mit erweiterten metabolischen Auswirkungen auf die Ethanol- und Acetatstoffwechselwege. Basierend auf der *in situ* Charakterisierung, der selektiv-permeabilisierten Deletionsmutanten des mitochondrialen Pyruvattransporters, wurde die Hypothese erstellt, dass die MPC-Maschinerie Teil eines größeren Metabolons ist, das den Pyruvattransport zur mitochondrialen Atmungskette, die ATP Synthese, sowie deren Austausch zu zytosolischem ADP miteinander verknüpft. Dadurch kann die MPC Maschinerie enzymatische Aktivitäten, sowohl im Zytosol, als auch in der mitochondrialen Matrix beeinflussen, den P/O-Wert beeinflussen und als Teil eines Metabolons möglicherweise den Crabtree-Effekt regulieren.

# Chapter 1

# Objectives

This work focused on elucidating the metabolic crosstalk between the cytosol and the mitochondrial matrix of the yeast *Schizosaccharomyces pombe*. In this context the aim was to set as the starting point the quantification of *in vivo* carbon fluxes at a steady state throughout the central metabolism of *S. pombe* and subsequently identify points of carbon exchange between the two subcellular compartments. The subsequent target was to proceed with the dynamic characterization of the transporter-mediated metabolism of respiratory substrates by mitochondria through these points.

The core of this work lied in establishing a suitable experimental system that would preserve an intact intracellular architecture and membrane structures while maintaining the functionality of membrane transporters and enzymes residing in the vicinity of these proteins in either side of the outer and the inner mitochondrial membrane. The first target was to identify the proper conditions and permeabilizing compound that would be employed for the selective permeabilization of the plasma membrane in a proper cytosol-mimicking buffer. Then it would be investigated whether these conditions would allow for intact mitochondria to possess a functional respiratory chain in the presence of exogenously supplied substrates and at the same time whether mitochondrial oxygen uptake would be coupled to the intramitochondrial synthesis of metabolic energy in the form of ATP (*in situ* studies). Therefore, in order to characterize dynamically the metabolism of these substrates in the *in situ* system we focused mostly on developing a sealed mini-reactor, where selectively permeabilized cells would be added and incubated in the presence of appropriate substrates. The mini-reactor could then be coupled to a mass-spectrometer for the dynamic quantification of produced gases ($O_2$, $CO_2$, acetaldehyde) along with a suitable sampling system allowing for the subsequent chromatographic quantification of carboxylates, redox precursors and adenosine nucleotides.

Particular emphasis was given on identifying the mitochondrial transporter system facilitating the entry of pyruvate into the mitochondrial matrix. Pyruvate is

not only the end-product of glycolysis but also lies at the node where carbon fluxes partition between the fermentative pathway and the mitochondrial metabolism of this carboxylate in the TCA cycle. The distribution of the fluxes at this node is of central interest as it is the basis for the Crabtree effect and the onset of ethanol biosynthesis in yeasts. The molecular mechanism of pyruvate transport and the genes encoding it have been a matter of debate for many years until only recently where the mitochondrial pyruvate carrier (MPC) was identified in only a handful of model organisms except *S. pombe*. Therefore we focused on creating a set of deletion mutants for the gene sequences that were inferred from homology to express the MPC in *S. pombe*. The metabolic implications of a genetically perturbed MPC could then be examined with physiological studies aiming on the growth of these strains on glucose in batch cultures compared to the wild type along with steady state kinetics for substrate uptake and product formation. The final goal would be then to apply the *in situ* methodology for dynamically quantifying mitochondrial metabolism for the wild type and mutant strains in the presence of pyruvate and examine its metabolism at the pyruvate node and whether the MPC exerts any control on mitochondrial function and/or adjacent metabolic pathways.

# Chapter 2

# Theoretical Fundaments

## 2.1 *Schizosaccharomyces pombe* as a model organism

*Schizosaccharomyces pombe* (Figure 2.1) is a unicellular eukaryote belonging to the class of Ascomycetes and was first isolated from East African millet beer in 1893 by P. Lindner. However *S. pombe* was established as a laboratory strain during the 1950s by Urs Leupold who isolated among others the wild type 972 (h-). This strain and its derivatives are used today throughout the world for *S. pombe* studies.
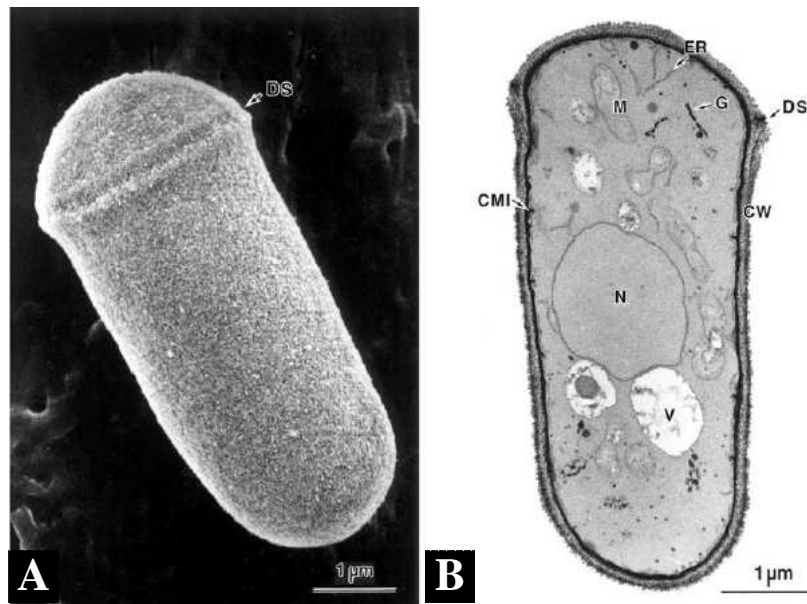


Figure 2.1: Imaging of the surface and ultrastructure of a fixated single *S. pombe* cell. Images obtained by scanning electron microscopy (SEM) [A] and transmission electron microscopy (TEM) [B]. CM, cell membrane; CMI, invagination of cell membrane; CW, cell wall; DS, division scar; ER, endplasmic reticulum; G, Golgi apparatus; M, mitochondrion; N, nucleus; V, vacuole. Images from (Osumi, 2012).

Cells possess a cylindrical shape with a typical length of 7 - 15 $\mu$m and a diameter around 2 - 4 $\mu$m. Due to how *S. pombe* cells undergo cell division like higher eukaryotes by means of fission instead by budding (like *S. cerevisiae*) (Balasubramanian et al., 2004), *S. pombe* is alternatively called fission yeast. The fision yeast genome is usually haploid and after meiosis and sporulation daughter cells form a linear tetrad ascus (Forsburg, 2003). The haploid genome of *S. pombe* was the sixth organism and second unicellular one to be fully sequenced (Wood et al., 2002) and its ~13.8 Mb genome is organized in three chromosomes (5.7 Mb, 4.6 Mb and 3.5 Mb), possessing 300 - 1000 times larger centromeres than *S. cerevisiae* (35 kb, 65 kb and 110 kb) (Giga-Hama et al., 2007). Fission yeast entered the post-genomic era with the construction of a genome-wide set of gene deletions covering 98.4 % of the organism's genome (Kim et al., 2010) and it is predicted to have 5054 protein coding genes (Hoffman et al., 2015), with 90 % of the gene products attributed to one cellular compartment (Matsuyama et al., 2006).

The two yeasts have diverged from each other 330 - 420 million years ago (Giga-Hama et al., 2007). There are over 300 genes that were lost in *S. cerevisiae* and further 300 genes that diverged compared to *S. pombe* (Aravind et al., 2000), placing the fission yeast closer to the common ancestor of both yeast organisms. Therefore highly conserved or divergent biological mechanisms shared or not between the two yeast systems (and studied in a complementary manner in both yeast organisms) can provide information to elucidate their function in higher organisms as well. Moreover, divergent or conserved biological systems in *S. pombe* and *S. cerevisiae* can reveal the plasticity of mechanisms that evolved into more complex ones in higher eukaryotes.

An example for a conserved mechanism between *S. pombe* and vertebrates but not between the latter and *S. cerevisiae* is the inhibitory phosphorylation of tyrosine in Cdc2 (cell cycle kinase subunit) which leads to cell cycle arrest as a response to DNA damage (Rhind et al., 1997). Another mechanism that is partially divergent and partially conserved between *S. pombe* and *S. cerevisiae* is the signal transduction pathway as a response to the secretion of mating pheromones, with the conserved part being structurally homologous to a kinase module (MAP/ERK kinases) from higher eukaryotes (Neiman et al., 1993). Furthermore there are proteins that interact with *S. pombe* centromeres that are homologous to mammalian ones whereas no such proteins are found in *S. cerevisiae* (Hoffman et al., 2015).

By studying the divergence of biological mechanisms in both organisms, two distinct mechanisms were found characteristic of the unfolded protein response (UPR) in the endoplasmic reticulum (ER), both of which are used interchangeably by mammalian cells. More specifically the UPR in mammalian cells entails the activation of Ire1 (inositol-requiring enzyme-1) which leads to the splicing of specific mRNAs

and to a transcriptional response which boosts the expression of ER components, thus increasing the capacity of this compartment (higher capacity for high load of unfolded proteins). Another mechanism that relies on Ire1 activation (activation of X-box-binding protein 1) leads to the degradation of mRNAs that encode proteins that enter the ER (decreasing the load of unfolded proteins) also known as regulated Ire1-dependent decay (RIDD) (Hollien and Weissman, 2006; Hollien et al., 2009). *S. cerevisiae* relies only on the former mRNA splicing mechanism, whereas *S. pombe* possesses the latter RIDD mechanism to cope with the unfolded protein stress upon the ER (Kimmig et al., 2012).

Another important characteristic is that 43 % of the *S. pombe* genes entail introns in their ORFs (Yanagida, 2002; Braun et al., 2005), whereas this feature has been lost in *S. cerevisiae* (Russell and Nurse, 1986) and instead a high reverse transcriptase activity is found but no RNAi mechanism as in *S. pombe* (Hoffman et al., 2015). Further similarities to higher eukaryotes consist of genes involved in post-translational modifications and DNA replication (Aravind et al., 2000; Giga-Hama et al., 2007) that are absent in *S. cerevisiae*.

The fact that the fission yeast shares many common traits with higher organisms (or traits complementary to those of *S. cerevisiae* origin), the complete sequencing of its genome and the existence of well-established experimental protocols applied on it, make *S. pombe* an important model organism. Studies have been more focused on cell cycle regulation and differentiation but attempts have also been made based on *S. pombe* for the heterologous expression of proteins derived from plants and animals.

These proteins can consist of complicated molecules, such as glycosylated ones which can be successfully expressed and secreted in *S. pombe* due to the aforementioned similarities (mRNA splicing machinery) (Kukuruzinska et al., 1987) to higher eukaryotes. Another trait of *S. pombe* that supports its role as a host for the heterologous protein production is the presence of a well developed Golgi apparatus and glycosyltransferase activity, which is not found in other yeasts (Idiris et al., 2006, 2010). In this context there are various examples reported concerning the expression of heterologous proteins such as the human lipocortin I (Tohda et al., 1994) or the secretion of heterologous proteins, as human lysosomal acid lipase (Ikeda et al., 2004) that carries as a secretory signal peptide the precursor of a mating pheromone (P-factor) derived from the *map2* gene of mutated *S. pombe* cells (Imai and Yamamoto, 1994).

## 2.2 Physiology of *S. pombe*

*S. pombe* can grow aerobically during glucose-limitation and non glucose-limiting conditions. Fully aerobic metabolism is achieved during the former conditions and respirofermentative metabolism is activated during the latter (Queiroz et al., 1993), with a P/O of 1.28 for both conditions. During the respirofermentative metabolism of glucose, ethanol is the main metabolic by-product whereas during respiratory metabolism low concentrations of glycerol, pyruvate and acetate are produced (de Jong-Gubbels et al., 1996).

### 2.2.1 The Crabtree effect

During the metabolism of glucose at high growth rates (during steady state) and in respiratory conditions *S. pombe*, just like *S. cerevisiae*, triggers its fermentative pathway producing in the process ethanol and $CO_2$ at a loss of biomass (von Meyenburg, 1969; Postma et al., 1989). This so called long-term Crabtree effect is typical of Crabtree-positive yeasts, whereas Crabtree-negative yeasts do not synthesize ethanol under such conditions. Other than the long-term Crabtree effect, yeasts are also characterized by the short-term Crabtree effect, when under glucose-limiting conditions (glucose uptake under a threshold value during steady state) and in the presence of oxygen a glucose pulse is applied and ethanol biosynthesis is triggered (Urk et al., 1989, 1990). Even under glucose-limiting and aerobic conditions however the fermentative pathway of Crabtree-positive yeasts has been found to be upregulated (Hagman and Piškur, 2015).

Various explanations have been given for the onset of the Crabtree effect. From an evolutionary scope, the ability of yeast cells to ferment glucose might have appeared simultaneously with the appearance of fruits (Hagman et al., 2013). According to this hypothesis, ancient yeasts had to develop a way to out-compete bacteria that were able to consume fruit sugars and possessed faster growth rates than them. Therefore, yeasts developed means to synthesize acetate and ethanol that could eliminate bacterial cells that would otherwise consume fruit sugars. This biochemical adaptation was possibly triggered in ancient yeasts like *S. pombe* by the loss of complex I from the respiratory chain. Evolutionary it was further refined with the *URA1* horizontal transfer and the whole genome duplication, leading to the fine-tuned Crabtree effect of the more recent *Saccharomyces* lineage, where cells can grow on ethanol as a sole carbon source (Hagman et al., 2014; Dashko et al., 2014; Kurtzman and Robnett, 2003).

The biochemical and regulatory differences for the onset of the long- and the short-term Crabtree effect have been hard to draw from each other. For example,

*K. lactis*, a yeast long classified as a long-term Crabtree-negative yeast, has been recently found to be a Crabtree-positive yeast in regards of the short-term effect (Hagman et al., 2014).

The short-term Crabtree effect and the presence of ethanol, triggered by the transition from glucose limitation to glucose excess (Urk et al., 1989) in the presence of oxygen, was not caused by the inability of mitochondria to oxidize pyruvate or by a repressed TCA cycle. The comparison of Crabtree positive (*S. cerevisiae*, *S. pombe*) and Crabtree negative yeasts (*C. utilis*) in terms of the short-term Crabtree effect, revealed that the pyruvate decarboxylase activity was higher in the former yeasts accompanied by acetate and ethanol excretion (Urk et al., 1990). A computational analysis of the short-term Crabtree effect (after the application of a glucose pulse to the system) simulating fluxes through a central metabolism kinetic model, predicted an increase of the flux through the pyruvate decarboxylase and the alcohol dehydrogenase and simultaneously a decrease of the flux through the acetaldehyde dehydrogenase and the acetyl-coA synthetase (Kesten et al., 2015). In both *S. pombe* and *S. cerevisiae* the pyruvate decarboxylase enzyme is found in high levels during respiratory growth with the activity of the enzyme increasing when the glucose uptake rate increased in a glucose-limited culture (de Jong-Gubbels et al., 1996).

It has been postulated that the underlying basis for the long-term Crabtree effect is a reduced respiratory capacity (Pronk et al., 1996) and a low TCA cycle activity due to glucose repression which further induces overflow metabolism at the pyruvate node. The long-term Crabtree effect was partially encountered in *S. cerevisiae* by the expression of an alternative NADH oxidase which targeted the mitochondria and caused an up-regulation of genes expressing TCA cycle enzymes (Vemuri et al., 2007). The deletion or overexpresion of the mitochondrial NAD transporter in *S. cerevisiae* had no effect on the glucose uptake rate where the long-term Crabtree-effect became evident (Agrimi et al., 2011) in continuous glucose cultivations, thus the decisive trigger was the overflow metabolism at the pyruvate node.

The analysis of the *in vivo* fluxes ($^{13}$C metabolic flux analysis) of the central metabolism of Crabtree-negative and Crabtree-positive yeasts during batch cultivations confirmed that ethanol secretion and the glycolytic flux correlated with glucose uptake as well as the TCA cycle flux with the glycolytic flux whereas for the Crabtree-negative yeasts there was no such correlation (Christen and Sauer, 2011). The TCA cycle activity was higher than that for Crabtree-positive yeasts that possessed the same glycolytic flux. The differences between the central metabolism of Crabtree-positive and Crabtree-negative yeasts are illustrated in Figure 2.2, A & B based on the results by Christen and Sauer (Christen and Sauer, 2011).
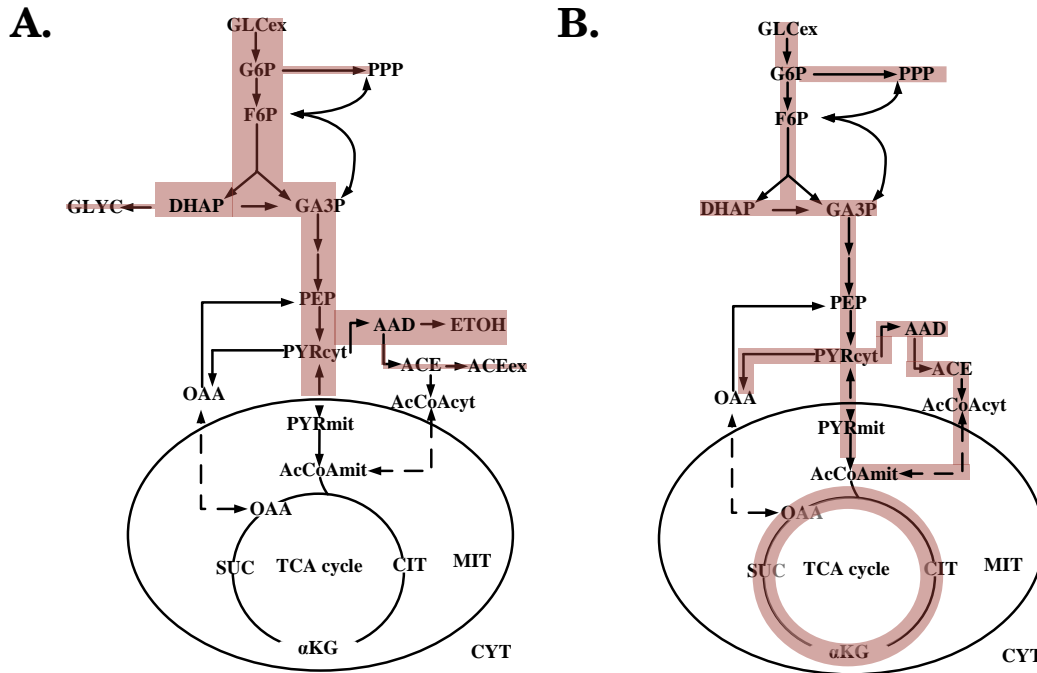
Figure 2.2: Graphical representation of the most pronounce changes (marked with color) of *in vivo* fluxes through the central metabolism of Crabtree-positive [A] and Crabtree negative yeasts [B]. All reactions represented are active in all cases. Figure adapted from (Christen and Sauer, 2011). GLCex: external glucose; G6P: glucose 6-phospate; F6P; fructose 6-phospate; PPP: pentose phosphate pathway; DHAP: dihydroxyacetone phosphate; GLYC: glycerol; GA3P: glyceraldehyde 3-phosphate; PEP: phosphoenolpyruvate; PYR: pyruvate; OAA: oxaloacetate; AAD: acetaldehyde; ETOH: ethanol; ACE: acetate; AcCoA: acetyl-CoA; SUC: succinate; CIT: citrate; $\alpha$-KG: $\alpha$-ketoglutarate; TCA cycle: tricarboxylic acid cycle; MIT: mitochondrial compartment; CYT: cytosolic compartment.

Recently it has been proposed, that there is a common underlying cause for both the short-term and the long-term Crabtree effect, which is the overflow of metabolism. In this case an increased anaerobic glycolysis corresponding to high glucose uptake even in the presence of oxygen, preceded evolutionary the glucose repression of respiration (Hagman and Piškur, 2015). According to the authors, this latter trait of more refined sensing of glucose (activation of signal transduction pathways by glucose and glycolytic fluxes) was gained by yeasts relatively late after the whole genome duplication event, fine-tuning the long-term Crabtree effect.

### 2.2.2   Carbon uptake and central metabolism of *S. pombe*

A common trait of Crabtree-positive yeasts is the energy-independent sugar up-take, whereas Crabtree-negative yeasts facilitate sugar transfer to the cytosol in an energy-dependent manner (Hagman and Piškur, 2015). *S. cerevisiae* relies on facilitated diffusion driven by a concentration gradient, whereas in *S. pombe* a $H^+$-ATPase pumps protons out of a cell, creating an electrochemical gradient, thus enabling $H^+$/hexose symport (Hoefer and Nassar, 1987; Heiland et al., 2000).

*S. pombe* with only 6 hexose transporters (compared to 17 *HXT* transporters and *GAL2* in *S. cerevisiae* expressing carriers for hexose transport) (Reinders and Ward, 2001; Jansen et al., 2006) is able to grow on glucose, fructose, glycerol and maltose but not on galactose, sucrose, pyruvate, acetate, DL-lactate, glutamate and malate (Heslot et al., 1970; Osothsilp and Subden, 1986; Heiland et al., 2000; Reinders and Ward, 2001; Matsuzawa et al., 2010). Acetate can be metabolized in the presence of glucose (Tsai et al., 1987) or glycerol (Klement et al., 2011).

Another difference between the two yeasts propably also stemming from the fact that the *S. cerevisiae* genome has accumulated more changes than the *S. pombe* one (WGD, horizontal gene transfer etc.), is that *S. pombe* can not utilize ethanol as the sole carbon source, whereas ethanol can be metabolized in the presence of glucose (de Jong-Gubbels et al., 1996) in *S. cerevisiae*. This is propably caused by the absence of isocitrate lyase and malate synthase in *S. pombe* cells, which explains why no functional glyoxylate cycle is found in fission yeast. (Tsai et al., 1987; Fiechter and Seghezzi, 1992; de Jong-Gubbels et al., 1996).

During glucose uptake and metabolism under aerobic conditions *S. pombe*, as a Crabtree-positive yeast, produces ethanol as the main metabolic by-product, either during batch cultivations or after surpassing the $D_{crit}$ ($D_{crit}$ = 0.16 $h^{-1}$) (de Jong-Gubbels et al., 1996) in glucose-limited cultures. Metabolic energy in the form of ATP is generated at a great extent glycolytically (and at a smaller extent mitochondrially) by the activities of 6-phosphofructokinase (encoded by *pfk1*), phosphoglycerate kinase (encoded by *pgk1*) and pyruvate kinase (encoded by *pyk1*). With carbon flux being mostly diverted towards the fermentative pathway (Crabtree effect), NADH that is produced in the cytosol glycolytically (glyceraldehyde 3-phosphate dehydrogenase activity) can be mainly oxidized by the alcohol dehydrogenase yielding ethanol. Two alcohol dehydrogenases have been functionally characterized in *S. pombe*, namely Adh1p which is cytosolic (Russell and Hall, 1983) and Adh4p (Crichton et al., 2007), which is mitochondrial. Other predicted *S. pombe* sequences encoding alcohol dehydrogenases based on information from the PomBase database (Wood et al., 2012; McDowall et al., 2015) are *adh8* and SPBC337.11.

Following the fate of NADH in the cytosol, NADH can be formed by the cy-

tosolic malic enzyme, Mae2p, functioning in the carboxylating direction while re-plenishing cytosolic pyruvate pools. This enzyme has been found to be unaffected by the presence of L-malate, however an increase of glucose concentration from 2 % to 8 % induced the *mae2* expression (Viljoen et al., 1999) in *S. pombe*. This NAD-dependent malic enzyme is part of the anaplerosis linking malate to pyruvate, which can be carboxylated in an ATP-dependent manner to yield oxaloacetate. However in *S. pombe*, oxaloacetate can not be converted into PEP as there is no PEP-carboxykinase activity (the first enzyme of gluconeogenesis). A further gluconeogenic gene, *fbp1*, encoding the fructose-1,6-biphosphatase enzyme is repressed in the presence of glucose (Hoffman and Winston, 1991; de Jong-Gubbels et al., 1996).

Another point for NAD reduction would be at the acetaldehyde dehydrogenase point of the metabolism, although this enzyme can be found as an NADP-dependent isoform as well. Downstream from this dehydrogenase lies the ATP-dependent acetyl-CoA synthetase, forming acetyl-CoA from acetate. The cytosolic acetyl-CoA synthetase in *S. cerevisiae* links the entry of carbon into the fermentative pathway (pyruvate decarboxylase) with the supply of the mitochondria with acetyl-CoA via the carnitine-acetyl-CoA shuttle (CAT2, YAT1 and YAT2). It has been postulated that such a shuttle system has to exist in *S. pombe* even if there are still no known candidates (Sohn et al., 2012). Both genes expressing the acetaldehyde dehydrogenase and the acetyl-CoA synthetase enzymes are expressed constituvely in *S. pombe* (de Jong-Gubbels et al., 1996).

The compartmentalized TCA cycle functions in the mitochondria of *S. pombe* cells and participates in energy generation and formation of metabolic precursors for anabolic reactions, like the biosynthesis of branched-chain amino acids (BCAA). Various metabolites synthesized or consumed in the TCA cycle take part in shuttle reactions bridging the cytosol with the mitochondrial matrix, as will be examined in subsequent parts.

## 2.3 The mitochondrial respiratory chain

The respiratory chain of yeasts (see Figure 2.3) in general comprises of multienzymic complexes that are docked in the inner mitochondrial membrane (IMM) and their function is to mediate the transport of electrons to the smaller mobile components, namely ubiquinone and cytochrome *c*. The transport of electrons occurs while some complexes (complexes III and IV) pump protons throughout the IMM, generating an electrochemical proton gradient. The final acceptor of electrons is molecular oxygen which is thus consumed during mitochondrial respiration and the transmembrane proton gradient or proton-motive force provides the needed energy for the final complex (complex V or ATP synthase) of the respiratory chain to synthesize metabolic energy in the form of ATP. The generation of energy as ATP from ADP and phosphate during mitochondrial respiration is called oxidative phosphorylation.
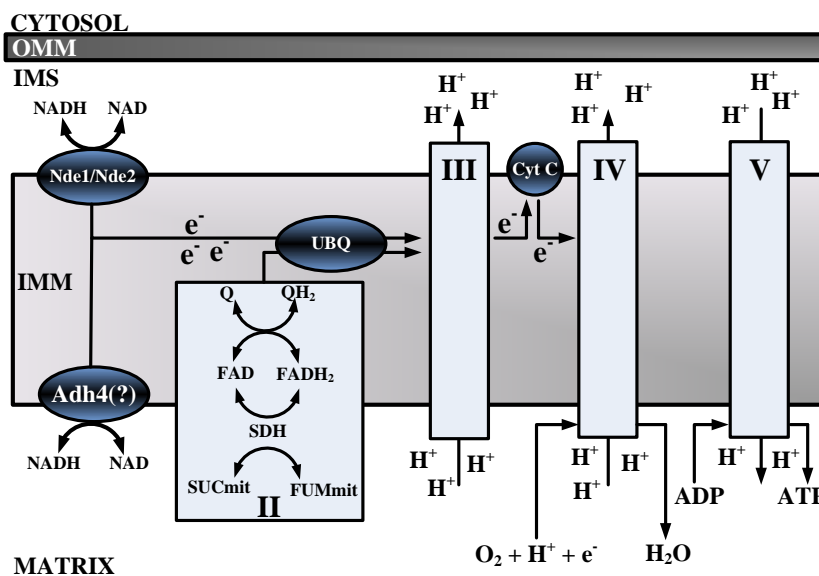


Figure 2.3: Mitchell's chemiosmotic hypothesis, number of protons ($H^+$) not indicative of actual proton translocation stoichiometry for each proton-pumping complex.

Electrons are removed from the reducing equivalents NADH and $FADH_2$, that may originate from glycolytic reactions, the TCA cycle or the oxidation of fatty acids. The oxidation of cytosolic NADH takes place at the IMM-docked, external NADH dehydrogenases (Nde1p and Nde2p) which are encoded by sequences SPBC947.15c and SPAC3A11.07 and face the intermembrane space (IMS). These sequences are homologous to the *NDE1* and *NDE2* genes of *S. cerevisiae* encoding for separate, external NADH-dehydrogenases (Luttik et al., 1998). It is unknown whether *S. pombe* possesses an internal, mitochondrial matrix-facing NADH dehydrogenase

as the one present (Ndip) in *S. cerevisiae* (De Vries et al., 1992), which is capable of oxidizing mitochondrial NADH. However, an alcohol dehydrogenase isoform has been identified in *S. pombe* (Adh4p), residing in the mitochondrial matrix that is capable of oxidizing internal NADH. This enzyme is controlled by ubiquinol ($QH_2$) oxidation when NADH is the enzymatic substrate and by ubiquinone (Q) reduction when ethanol is the substrate (Crichton et al., 2007).

Neither of these NADH dehydrogenases, either internal or external, are present in mammalian mitochondria, that instead possess a multimeric complex I (composed of 43 subunits in mammals (Kerscher et al., 2002)) capable of pumping protons during the transfer of electrons to the ubiquinone pool and being sensitive to inhibition by rotenone.

However fungi other than *S. cerevisiae* and *S. pombe*, like *Neurospora crassa* and *Yarrowia lipolytica*, possess a complex I, similar to the mamalian one (with 35 or more subunits), and additionally express NADH dehydrogenases facing towards the mitochondrial matrix and the IMS (*N. crassa*) (Duarte et al., 2003; Videira, 1998) or towards the IMS alone (*Y. lipolytica*) (Kerscher et al., 2002), similar to mitochondrial NADH dehydrogenases in plants (potato and *A. thaliana*) (Fernie et al., 2004). Furthermore, the respiratory chain of *S. pombe* is non-branched as there are no alternative oxidases (AOX) (Moore et al., 1992) (identified as a cyanide-resistant branch of the respiratory chain) as part of the respiratory chain (present in *Y. lipolytica*, *Aspergillus niger*, some members of the Animalia and plants). Alternative oxidases bypass complexes III and IV and transfer electrons from the ubiquinol pool to molecular oxygen, depriving energy from the ATP synthase (McDonald and Vanlerberghe, 2004).

The *S. pombe* complex I has been shown to be insensitive to rotenone inhibition (Heslot et al., 1970; Moore et al., 1992) just like its counterpart from *S. cerevisiae*. Furthermore, mammalian mitochondria due to the lack of external NADH dehydrogenases (as in yeast mitochondria) rely on shuttle mechanisms that couple the oxidation of cytosolic NADH to NADH dehydrogenases residing in the mitochondrial matrix. The absence of proton pumping from the *S. pombe* NADH dehydrogenases would result to complex I not generating proton-motive force, similar to complex II, which will be covered further on. Therefore assuming the *in vivo* P/O ratio equal to unity as it has been calculated for *S. cerevisiae* (Verduyn et al., 1991; Bakker et al., 2001) the subsequent respiratory yield of ATP on glucose for growing cells would be 16 mol ATP per mol glucose.

Another source of electrons that can be transferred to the ubiquinone pool stems from the oxidation of succinate by the mitochondrial succinate dehydrogenase which comprises complex II of the mitochondrial respiratory chain and is simultaneously part of the TCA cycle. The reducing precursor in this case is $FADH_2$. Complex

II is a non proton-pumping multimeric component of the respiratory chain that spans the internal mitochondrial membrane and consists of proteins Sdh1p, Sdh2p, Sdh3p and Sdh4p. Sdh1p is the FAD-binding flavoprotein facing the mitochondrial matrix, Sdh2p is a hydrophilic iron-sulfur protein (FeS component), Sdh3p is the cytochrome *b* and Sdh4p an inner membrane docking protein. Sdh3p and Sdh4p comprise a hydrophobic heme-containing dimer. In *S. cerevisiae* the role of heme *b* was investigated and it was ruled out that its presence is needed for either stabilizing the multimeric complex or increasing its catalytic efficiency (Oyedotun et al., 2007). During $FADH_2$ oxidation in the presence of succinate, electrons are transferred through the FeS cluster and towards the hydrophobic components where ubiquinone is bound and subsequently reduced to ubiquinol. The total stoichiometry is two electrons per ubiquinone being reduced.

Ubiquinol is then oxidized at complex III, which is also known as the $bc_1$ complex (ubiquinol: cytochrome *c* oxidoreductase), consisting of 10 subunits in *S. cerevisiae* and is one of the most conserved structures throughout mitochondria of various organisms (Joseph-Horne et al., 2001). The overall reaction catalyzed by complex III is described by equation 2.1.

$$QH_2 + 2\,cytc^{3+} + 2\,H_{mm}^+ \longleftrightarrow Q + 2\,cytc^{2+} + 4\,H_{ims}^+ \tag{2.1}$$
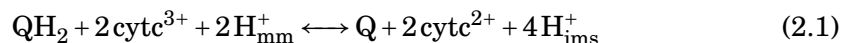
The apparent function of this complex is to catalyze the oxidation of ubiquinol and the transfer of electrons to the cytochrome *c* pool, while pumping protons ($H_{mm}^+$) from the mitochondrial matrix to the IMS ($H_{ims}^+$). Transfer of electrons takes place at cytochromes *b* and $c_1$ and at the Rieske iron-sulfur proteins. This electron transfer is part of the Q cycle and entails the binding of ubiquinone at two sites, namely the $Q_N$ and $Q_P$ reaction centres. At the $Q_N$ quinone reduction site facing the mitochondrial matrix (also called N side), half of the electrons are recycled towards the ubiquinone pool and protons are taken up from the mitochondrial matrix. At the second reaction centre, $Q_P$, electrons from reduced ubiquinone are accepted and half of them are split back to the ubiquinone pool and the rest towards cytochrome *c* through the Rieske FeS cluster and the heme-containing cytochrome $c_1$. Cytochrome $c_1$ along with the Rieske FeS domain face the IMS (P side of the membrane) while the heme-containing $b_L$ and $b_H$ of cytochrome *b* are located within the inner mitochondrial membrane (Scheffler, 1999). Yeast complex III shows no proteolytic activity as its mammalian counterpart does and also no cytochrome *c* reductase activity (Joseph-Horne et al., 2001).

After electrons are transferred to the mobile carrier cytochrome *c*, the latter is released from complex III and is subsequently bound on the terminal acceptor of electrons of the mitochondrial respiratory chain, complex IV (cytochrome *c* oxidase)

where the following reaction takes place (2.2):

$$O_2 + 4\,cytc^{2+} + 8\,H^+_{mm} \longrightarrow 2\,H_2O + 4\,cytc^{3+} + 4\,H^+_{ims} \tag{2.2}$$
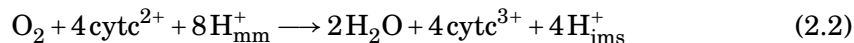
The yeast complex is composed of 9 subunits and contains two heme centres and two copper centres (Scheffler, 1999) and at this complex one molecule of oxygen is reduced and two molecules of water are produced. Two cytochrome $c$ molecules are needed to be bound on the subunit II of the cytochrome $c$ oxidase (IMS facing, P side) in order for one molecule of oxygen to be consumed. Cytochrome $c$ molecules transfer their electrons to a binuclear copper centre ($Cu_A$) that contains two atoms and from there electrons are transferred to the iron-containing heme $a$ of subunit I, then to the adjacent heme $a_3$ and subsequently to another copper centre ($Cu_B$). For each pair of electrons transferred from cytochrome $c$, four protons are taken up from the mitochondrial matrix (N side) and two are released in the IMS (P side), which is thermodynamically equivalent to the translocation of four protons (Wikstrom and Hummer, 2012). On the other hand, at complex III, the other proton-pumping complex of the respiratory chain, for every pair of electrons transferred, two protons are taken up from the N side and four are released on the P side, making the process thermodynamically equivalent to the translocation of two protons (Hinkle, 2005). Complex III does not have a lower proton-motive force than complex IV. These two complexes act in parallel in the mitochondrial proton circuit (thus have the same proton-motive force) but due to the lower redox potential span at complex III, less energy is required for proton translocation across the membranes and subsequently less charge (or proton) translocation stoichiometry (n = H$^+$/O) is needed (Nicholls and Ferguson, 2002). The relationship betweeen these parameters is better exhibited with equation 2.3:

$$n\Delta p = 2\Delta E_h \tag{2.3}$$

where n is the H$^+$/O stoichiometry of a respiratory chain complex, $\Delta E_h$ the redox potential difference and $\Delta$p the proton-motive force. Equation 2.3 can be extended to account for the mitochondrial membrane potential $\Delta\psi$ as follows:

$$n\Delta p = 2(\Delta E_h + \Delta\psi) \tag{2.4}$$

The final complex connecting the consumption of oxygen and the build-up of proton-motive force to the generation of energy in the form of ATP in the mitochondrial matrix, is the ATP synthase ($F_1F_0$-ATPase). The ATP synthase or complex V relies on proton translocation and consists in total of 13 core subunits in yeast. These multimeric complexes form dimers organized in rows along mitochondrial cristae (Davies et al., 2012). A highly conserved lollipop-like structure protruding

with its round head into the mitochondrial matrix, is composed of three $\alpha$ subunits separated from each other by an equal number of catalytic $\beta$ chains while the $\alpha_3\beta_3$ complex surrounds a central $\gamma$ stalk that is able to rotate (Ferguson, 2010). The $F_1$ matrix sector of the polypeptide complex is where ADP and inorganic phosphate react to form ATP. Rotational momentum is gained by the passage of protons from the IMS to the mitochondrial matrix through the $F_0$ part of the complex comprised of polypeptides 8, 6 and 9 (analogous to mammalian, chloroplast and bacterial a, b and c polypeptides respectively) that are stabilized onto the inner mitochondrial membrane. The $\gamma$ stalk in yeast is structurally connected with the $F_0$ subsector of the complex via subunit $\delta$ (Duvezin-Caubet et al., 2003), whereas subunit $\varepsilon$ couples proton translocation from $F_0$ to ATP synthesis at $F_1$. In yeast the $F_0$ rotor has 10 c-subunits forming a ring which rotates when protons are translocated from the IMS, thus forcing the central stalk ($\gamma$) of the $F_1$ subunit to perform a 360° rotation (Noji et al., 1997; Dautant et al., 2010). After a full clockwise rotation three molecules of ATP are synthesized by the $F_1$ rotor subunit (Watt et al., 2010). The rotation changes conformationally the catalytic centres of the $F_1$ sector of the complex, thus releasing newly formed ATP and preparing the active centre for the entry of ADP and inorganic phosphate.

The spatial organization of the respiratory complexes in the respiratory chain governs not only the efficiency of the transfer of electrons and subsequently the efficiency of oxidative phosphorylation, but is also important for regulating the generation of reactive oxygen species (ROS), the redox balance and the exchange of TCA cycle intermediates between the cytosol and the mitochondrial matrix. There have been various models proposed that describe the spatial configuration of respiratory complexes in the inner mitochondrial membrane. The oldest one, also called the random diffusion model (fluid model) (Hackenbrock et al., 1986), regarded respiratory complexes being independent from each other with the mobile elements (ubiquinone and cytochrome $c$) freely diffusing in the IMM. The next model proposed was radically different from the fluid model, proposing the organization of respiratory complexes into supercomplexes (SCs) allowing for more efficient electron transfer and stability of the chain (Schägger and Pfeiffer, 2000). More recently, a third model has been proposed based on fibroblast mouse cells (Acín-Pérez et al., 2008), called the plasticity model, which integrated parts of both previous models and proposed the dynamic existence of both supercomplexes and of independent respiratory complexes (reviewed in (Dudkina et al., 2010; Acin-Perez and Enriquez, 2014; Genova and Lenaz, 2014)). The plasticity model holds the mammalian complex I in a central position which is able to associate with complex III, complexes III and V, complexes II and III and IV, complexes III and IV (Acín-Pérez et al., 2008).

However in yeast cells, where no complex I exists as in mammalian cells, the

respiratory chain is organized in a supercomplex that operates as a single unit. Complex II and complex III are functionally associated in *S. cerevisiae* with neither ubiquinone nor cytochrome *c* exhibiting pool behaviour (Boumans et al., 1998). Both elements of the respiratory chain that were previously described as mobile (freely diffusing in the lateral membrane plane), are rather channeled between the respiratory complexes. Furthermore, depending on the cultivation conditions (glucose or lactate as the carbon source), complex III can exist as a free dimer ($III_2$) or form a supercomplex with complex IV either in the form of a complex III dimer with a monomer of complex IV ($III_2IV_1$) or as two dimers of complexes III and IV ($III_2IV_2$) (Schägger and Pfeiffer, 2000). The switch from glucose to lactate increases the presence of the $III_2IV_2$ supercomplex and decreases the presence of the free dimer of complex III. Single particle electron microscopy studies in yeast have elucidated the 3D structure of the $III_2IV_2$ dimer (Heinemeyer et al., 2007), where the short distance between the binding sites of complexes III and IV for cytochrome *c* serves to allow for metabolite channeling in the respiratory chain and subsequently increase the efficiency of electron transport.

The structural association of complexes III and IV is attributed to the phospholipid cardiolipin (Zhang et al., 2002; Wenz et al., 2009), which assists to stabilize the supercomplex and increases the efficiency of cytochrome *c* oxidase (complex IV). Cardiolipin has been found to physically bind the yeast ADP/ATP translocator protein (Aac2p) in the vicinity of complex IV (thus to the III/IV supercomplex), thus increasing the efficiency of ATP synthesis (Claypool et al., 2008). Another phospholipid crucial for the assembly of the aforementioned supercomplex is the phospholipid phosphatidylethanolamine (Böttinger et al., 2012).

## 2.4  Mitochondrial transporters of *S. pombe* and shuttle systems

The inner mitochondrial membrane except of harbouring the machinery with which cells produce energy, serves also as the boundary where the active transport of various metabolites links the compartmentalized enzymatic activities of the cytosol to the mitochondrial matrix. Single carrier proteins (30-34 kDa proteins encoded by the nuclear genome) control the transfer of organic acids, inorganic phosphate, redox precursors, adenosine phosphates, metals and protons towards the cytosol and the mitochondria even when oxygen is not driving oxidative phosphorylation (Palmieri et al., 2000). Despite the fact that such molecules pass mostly unhampered through the outer mitochondrial membrane, the inner mitochondrial membrane is normally a non-permeable barrier for such molecules allowing only the diffusion of small molecules like $CO_2$ and $O_2$ (LaNoue and Schoolwerth, 1979).

There are mainly three modes of transport of metabolites through the inner mitochondrial membrane: an active exchange of molecules that reside in either sides of the membranes (antiport), unidirectional transport and symport of a metabolite along with a proton from one side to the other (Palmieri, 2013). The mode of transport may either yield a net movement of charge to the other side of the IMM (electrogenic transport) or may lead to zero net charge being transported (electroneutral transport). Such mitochondrial proteins belong to the mitochondrial carrier family with structural elements being common between them. They possess regions with 100 amino acids-long sequences tandemly repeated three times and each repeat consists of two hydrophobic $\alpha$ helices (Palmieri et al., 2011, 2006; Palmieri, 2004). Each homologous repeat carries a characteristic motif PX[D/E]XX[K/R]X[K/R]-(20-30 residues)-[D/E]GXXXX-[W/Y/F][K/R]G, with the sequence sometimes being modified in one or more repeats of each carrier protein.

For the past 35 years mitochondrial carriers were considered to be organized in dimers, however only recently it has been proposed that based on comparing existing methodologies, their caveats and sequence/structure data (Arco and Satrustegui, 2005) a monomer is most likely to describe mitochondrial transporters (reviewed in (Kunji and Crichton, 2010)). A dimeric model would kinetically rely on a simultaneous transport mechanism where two substrates bind simultaneously to the transporter system. On the other hand, a monomer could kinetically function as a ping-pong mechanism, relying on the binding of the substrate to the binding site and the rotational interchange between a closed and an open state before the release of a substrate on the other side (Palmieri and Pierri, 2010; Ruprecht et al., 2014). In such a model called the single binding centre gated pore mechanism (Klingen-

berg, 1989), salt-bridges created by charged residues could regulate the access of the substrate to the internal cavity of the transporter by opening or closing the gate in either side of the inner mitochondrial membrane.
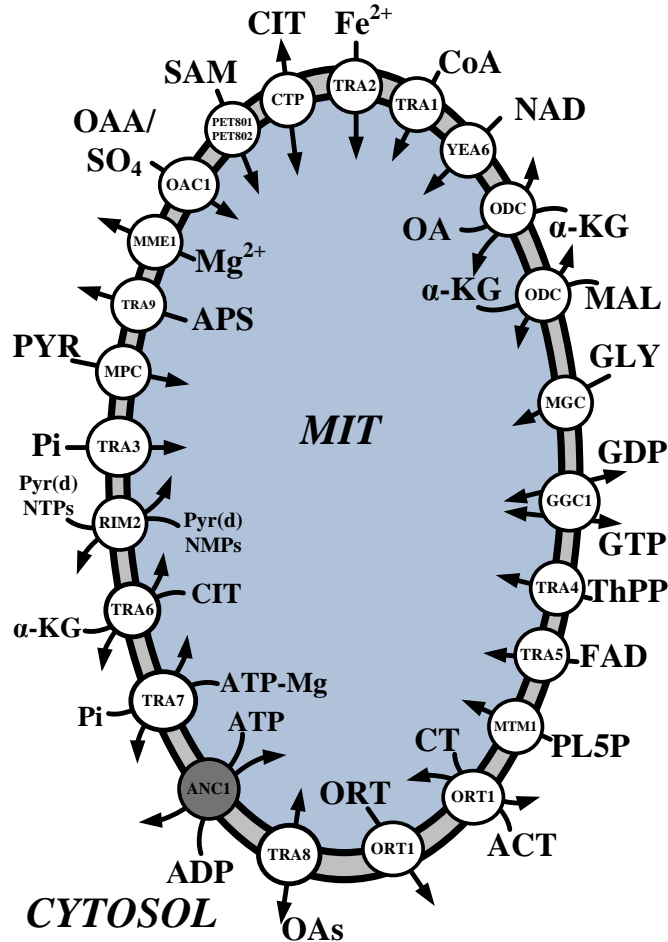


Figure 2.4: All *S. pombe* members of the mitochondrial carrier family, anchored on the inner mitochondrial membrane. Identity and function of transporters assessed experimentally is illustrated with grey color and the rest of the transporters are inferred based on their homology to known *S. cerevisiae* sequences. Transporters coded by genes with an unassigned name, are depicted with the prefix TRA. ANC1: SPBC530.10c; OAC1: SPAC139.02c; PET801: SPAC12B10.09; PET802: SPBC1271.11; CTP: SPAC19G12.05; TRA1: SPAC17H9.08; TRA2: SPAC4G8.08 and SPAC8C9.12c; TRA3: SPBC1703.13c; TRA4: SPBC1604.04; TRA5: SPBC27B12.09c; TRA6: SPBC83.13; TRA7: SPBC12D12.05c; TRA8: SPAC4G9.20c; TRA9: SPAPB17E12.12c; ODC: SPAC328.09; MGC: SPAC823.10c; ORT1:SPBC29A3.11c; RIM2: SPAC688.09; MME1: SPCC1442.03; GGC1: SPCC1682.09c; MTM1: SPBP23A10.06; YEA6: SPAC227.03c; MPC (Mpc1p and Mpc2p): SPCC1235.11 and SPAC24B11.09. ORT: ornithine; ACT: acylcarnitine; CT: carnitine; PYR: pyruvate; OAA: oxaloacetate; CIT: citrate; OA: oxoadipate; $\alpha$-KG: $\alpha$-ketoglutarate; GLY: glycine; ThPP: thiamine pyrophosphate; ORT: ornithine; MAL: malate; pyr(d)NTPs: (deoxy)pyrimidine nucleoside triphosphates; pyr(d)NMPS: (deoxy)pyrimidine nucleoside monophosphates; Oas: organic acids; NTs: nucleotides; PL5P: pyridoxal 5'-phosphate; APS: adenosine 5'-phosphosulfate; SAM: S-adenosylmethionine.

Concerning the members of mitochondrial carriers in *S. cerevisiae* their number had been assumed to be 35 gene-encoded proteins in the past (Palmieri et al., 2000; Palmieri, 2004; Hildyard and Halestrap, 2003a) with 27 distinct functions (Arco and Satrustegui, 2005). However, Ugo1p, was found to be structurally bound on the outer mitochondrial membrane so the number of mitochondrial carriers in yeast has been revised to be 34 (Palmieri et al., 2006). Nonetheless, after the elucidation of the mitochondrial pyruvate carrier in *S. cerevisiae*, which consists of two subunits encoded by *MPC1*, *MPC2* and *MPC3* (Herzig et al., 2012; Bricker et al., 2012), the number of gene-members of the mitochondrial carrier family will rise. *A. thaliana* has been predicted to consist of 58 members (Picault et al., 2004; Palmieri, 2013) and the number of the mitochondrial solute carrier family (SLC25) of *H. sapiens* has been reported to be around 50 (Palmieri et al., 2011) with closer estimates setting this number to 57 (Pär et al., 2011) and 53 carriers (Palmieri, 2013).

The higher number of mitochondrial carriers in *S. cerevisiae* and *A. thaliana* can be attributed to evolutionary events like WGDs (whole genome duplications) or gene duplications that expanded the number of members of this family. Many of these paralogues or duplicates where maintained and conserved even after gene loss/divergence since they provided advantages to the host organisms (Arco and Satrustegui, 2005; Palmieri et al., 2011).

The search for *S. pombe* proteins from the PomBase database accounting for mitochondrial localization, transport activity and homology to known *S. cerevisiae* mitochondrial carriers (Mitochondrial Carrier Family, MCF) from the SGD database (Cherry et al., 2012), yielded 25 gene sequences with 24 distinct functions. A previous comparison of the *S. pombe* genome to human SLC25 genes revealed 23 sequences encoding mitochondrial carriers (Pär et al., 2011). Major representatives of the *S. pombe* proteins with mitochondrial carrier function are summarized in Figure 2.4, where it is evident that only minimal experimental information is available on the identity and function of most mitochondrial carriers of *S. pombe* as compared to those from *S. cerevisiae*.

From the 24 proteins depicted in Figure 2.4, the sole protein sequence that has been experimentally assayed is that for the ADP/ATP translocator of *S. pombe*, Anc1p (gene sequence: SPBC530.10c) (Couzin et al., 1996; Trézéguet et al., 1999). The exchange of ADP for ATP is an electrogenic process due to the passage of a molecule of $ADP^{3-}$ for each $ATP^{4-}$. The homologous ADP/ATP translocator in *S. cerevisiae* is expressed by three distinct genes, namely *AAC1*, *AAC2* and *AAC3*. In general, mitochondrial carriers are identified as follows in the post-genomic era. Proteins of unknown function are compared to known mitochondrial carriers in order to identify the signature domains (tripartite structure etc.) in the unknown sequences. Subsequently, the gene sequences encoding these products are overex-

pressed in *E. coli* and/or in *S. cerevisiae* cells, are then isolated and functionally reconstituted in artificial liposomes. Their functional characteristics (type of transport, metabolites being transported, inhibition studies, kinetic characteristics) are then assayed.

The striking difference between *S. pombe* and *S. cerevisiae* is that the former lacks a significant number of mitochondrial carriers, that are usually also found in other higher organisms. More specifically, *S. pombe* mitochondria lack proteins of the MCF like the succinate/fumarate antiporter (SFC), the dicarboxylate carrier protein (DIC) and a carnitine carrier (CRC). However, based on homology alone, the Ort1p product (encoded by SPBC29A3.11c, Figure 2.4) exhibits similarities to both the yeast ornithine carrier (ORT1) as well as to the carnitine-dependent carrier of acetyl-CoA (CRC1).

The succinate/fumarate carrier in *S. cerevisiae* (Palmieri et al., 1997) exchanges mitochondrial fumarate for cytosolic succinate, thus enabling the continuous operation of the mitochondrial succinate dehydrogenase and the electron flow at the mitochondrial electron transport chain. The physiological function of the dicarboxylate carrier protein in yeast is the exchange of cytosolic succinate for inorganic phosphate and other organic acids that can be transported are malate and malonate, while phenylsuccinate acts as a potent inhibitor of the transporter (Palmieri et al., 1996). Therefore concerning the fate of succinate uptake in *S. pombe* a possible (but not strong) candidate would be the protein homologous to the yeast oxoglutarate/citrate carrier (OGC; encoded by *YHM2* in *S. cerevisiae*) that normally exchanges mitochondrial citrate for cytosolic oxoglutarate but can also transport to a lesser extent succinate (Castegna et al., 2010a). The OGC transporter in *S. cerevisiae* is not sensitive to phenylsuccinate inhibition.

Another mitochondrial carrier absent from the *S. pombe* MCF is the one facilitating the exchange of aspartate for glutamate. This carrier in *S. cerevisiae* encoded by genes *AGC1* and *AGC2*, is homologous to the human calcium-dependent aralar1 and citrin carriers of the SLC25 family, that are parts of the aspartate-glutamate NADH shuttle system (Cavero et al., 2003). The aspartate-glutamate exchanger along with the oxodicarboxylate carrier in *S. cerevisiae* (ODC1 and ODC2) have been shown to comprise the malate-aspartate shuttle, which functions as a redox shuttle able to transfer reducing equivalents across the mitochondrial membrane (Palmieri et al., 2001; Cavero et al., 2003). Furthermore, the Agc1p in *S. cerevisiae* also functions as a uniport for glutamate uptake from the mitochondria since there is no yeast mitochondrial glutamate carrier as in mammalian cells (Arco and Satrustegui, 2005) where two such isoforms exist (Gutiérrez-Aguilar and Baines, 2013).

The oxodicarboxylate carrier (ODC) which is able to exchange cytosolic $\alpha$-ketoglu-

tarate (or malate) for mitochondrially synthesized 2-oxoadipate exists in *S. pombe* and is the gene product of sequence SPAC328.09 (ODC protein in Figure 2.4). Therefore, the absence of a glutamate carrier and subsequently of a NADH redox shuttle in *S. pombe* could be an indication that *S. pombe* mitochondria possess a mitochondrially-localized glutamate dehydrogenase, whereas *S. cerevisiae* mitochondria are known to lack this enzymatic activity (Cavero et al., 2003).

Table 2.1: The genetic sequences coding for the carboxylate/ketoacid subfamily of the mitochondrial carriers for various organisms. Data were mined from existing literature and from the PomBase database (Picault et al., 2004; Arco and Satrustegui, 2005; Palmieri et al., 2011; Haferkamp and Schmitz-Esser, 2012; Palmieri, 2013; Li et al., 2014). DIC: dicarboxylate carrier; OGC: oxoglutarate carrier; DTC: di-/tricarboxylate carrier; SFC: succinate/fumarate carrier; CTP (yeast): citrate transporter; CiC (mammalian): citrate carrier; ODC: oxodicarboxylate carrier; OAC: oxaloacetate carrier; MPC: mitochondrial pyruvate carrier; MAL: malate; SUC: succinate; Pi: inorganic phosphate; OG: oxoglutarate; CIT: citrate; SUC: succinate; FUM: fumarate: ; ICI: isocitrate; PEP: phosphoenolpyruvate; cis-ACO: cis-aconitate; oxoAd: oxoadipate; oxoG: oxoglutarate; isoPM: isopropylmalate; PYR: pyruvate. n.h. denotes that there is no homologous sequence existing or until now identified.

| Protein | Substrates | *S. cerevisiae* | *S. pombe* | *A. thaliana* | *H. sapiens* |
| --- | --- | --- | --- | --- | --- |
| DIC | MAL, SUC, Pi, sulfate, thiosulfate | YLR348c | n.h. | At2g22500, At4g24570, At5g09470 | SLC25A10 |
| OGC | OG, MAL | YHM2 | SPBC83.13 | n.h. | SLC25A11 |
| DTC | OG, CIT | n.h. | n.h. | At5g19760 | n.h. |
| SFC | SUC, FUM | YJR095w | n.h. | At5g01340 | n.h. |
| CTP , CiC | CIT, ICI, MAL, PEP, cis-ACO | YBR291c | SPAC19G12.05 | n.h. | SLC25A1 |
| ODC | oxoAd, oxoG | YPL134C, YOR222w | SPAC328.09 | n.h. | SLC25A21 |
| OAC | OAA, isoPM, MAL, sulfate | YKL120W | SPAC139.02c | n.h. | SLC25A34, SLC25A35 |
| MPC | PYR | YGL080W, YHR162W, YGR243W | SPCC1235.11, SPAC24B11.09 | At5g20090, At4g05590, At4g22310, At4g14695 | MPC1, MPC2 |

Continuing to focus on carboxylates, the citrate transporter, that was one of the early mitochondrial carriers characterized in *S. cerevisiae* (Kaplan et al., 1995; Xu, 2000; Aluvila et al., 2010), has a homologous structure in *S. pombe* which is encoded by gene SPAC19G12.05. The physiological role of this carrier in yeast is the exchange of cytosolic citrate or isocitrate plus a proton for another tricarboxylate, while in mammalian cells the citrate carrier protein (CiC) is able to exchange citrate for malate or PEP and is linked with tumor cell proliferation (Catalina-Rodriguez et al., 2012). Citrate can serve as a substrate for the citrate lyase in the cytosol and yield OAA and acetyl-CoA that can be used in lipid biosynthetic pathways.

Table 2.1 summarizes the transport of tri-and dicarboxylates into and out of the mitochondrial matrix for four diverse organisms, while details on the transport of succinate, fumarate, malate and pyruvate will be covered experimentally in subsequent parts of this work. The mitochondrial pyruvate carrier is not yet categorized as part of the SLC family in humans, but is nevertheless illustrated here along with the other mitochondrial carriers of carboxylic acids. In mammalian cells the MPC has been implicated, even before being identified, as a member of the pyruvate-citrate and the pyruvate-malate shuttle along with SLC members DIC and CiC (Palmieri, 2004).

To summarize, as it can be seen from the cumulative comparison of various mitochondrial carriers between yeasts and higher organisms (Table 2.1), some functionalities are widely conserved (MPC), others are organism-specific (DTC, CiC, CTP), while others are missing. *S. pombe* is the organism of the aforementioned four species that possesses the smallest number of mitochondrial carriers in total (experimentally identified or inferred from homology), which can be seen as analogous to its genome being subjected to less evolutionary changes than that of *S. cerevisiae*. Added to this, plant orthologues have been described as hybrid transporters compared to their yeast and mammalian counterparts, since they are able to catalyze the transport of a broader range of metabolites.

An example are the DTC and DIC transporters from *A. thaliana*, where the former (DTC) shares traits with the oxoglutarate and citrate carriers of mammalian cells while the latter (DIC) combines the functionality of transporters OAC and DIC from yeast (Haferkamp and Schmitz-Esser, 2012). The versatility of mitochondrial carriers is therefore proportional to the different needs, environments and evolutionary history that are characteristic of their host organisms, along with the differences in the topology and specificity of enzymatic activities on either side of the mitochondrial boundary.

Therefore, mitochondrial carriers have to be seen as part of a wider network which comprises a membrane metabolon and not as isolated carriers that only me-

diate the transfer of a metabolite. There are various examples where metabolite channeling between compartmentalized enzymes takes place near mitochondrial carriers (Moraes and Reithmeier, 2012):

- Parts of the urea cycle are associated with the IMM and employ the ornithine-citrulline antiporter in rat liver mitochondria thus regenerating ornithine in the cytosol which can be uptaken from the mitochondria to form citrulline again.

- Elements of the arginine biosynthetic pathway along with the mitochondrial transfer of glutamate and arginine (mitochondrial glutamate uptake and ornithine efflux) are associated with each other in yeast mitochondria.

- The malate/citrate shuttle is connected with enzymes of the TCA cycle which in turn are associated with the inner mitochondrial membrane thus functiong as a complex and forming a metabolon. Here metabolite channeling is believed to take place between these enzymes along an electrostatic channel (Vélot et al., 1997).

## 2.5  Selective permeabilization of membranes for *in situ* studies

Selective permeabilization as a technique has been firstly developed by Reeves and Sols (Reeves and Sols, 1973), for the study of the *E. coli* phosphofructokinase, by making the cell membrane permeable to externally supplied substrates. This was achieved by a toluene-freezing technique and studies employing the permeabilization of the cell membrane have been coined as *in situ* studies. It was then that it was firstly realized that an enzyme's regulatory role in a metabolic network is better revealed with *in situ* studies than *in vitro*. Toluene-based permeabilization was then further applied on *S. cerevisiae* cells for the analysis of cytosolic enzymes (Serrano et al., 1973).

It has been argued that classical mitochondrial isolation techniques employing homogenization and centrifugation could lead to the mitochondrial fraction being underestimated, structurally and functionally compromised with loss of its spatial interactions to other cellular components (cytoskeleton, endoplasmic reticulum) (Picard et al., 2011). The interactions that are lost during traditional mitochondrial isolation techniques are connected to microcomparmentation and metabolite channeling and are fundamentally depending on the intactness of the intracellular architecture (Kuznetsov et al., 2008; Salabei et al., 2014).

Such caveats are surpassed with the selective permeabilization of cells. By applying low concentrations of permeabilizing agents, such as detergents (Triton-X, saponin, digitonin) or antibiotics (nystatin, filipin) the plasma membrane is made permeable allowing for the soluble, small-sized elements of the cytosol to leak out through ∿8 nm-large pores (Perry et al., 2013). At the same time, the membranes of intracellular structures such as the endoplasmic reticulum and mitochondria, remain intact. In this work we have focused on digitonin as the permeabilizing agent of choice.

Digitonin has the ability to bind stoichiometrically with its hydrophobic steroid core on cholesterol (in higher organisms) or ergosterol (in yeast cells and fungi) disrupting the lipid bilayer in a concentration-dependent manner. However membranes of other intracellular compartments, in specific of mitochondria, contain little (outer mitochondrial membrane) to virtually no ergosterol (inner mitochondrial membrane), thus they cannot be attacked by digitonin and retain their intactness and association with other subcellular structures. Subsequently, exogenous substrates can be applied to activate in a targeted manner metabolic pathways of the cytosol and of the mitochondrial matrix, transporters docked on the outer and inner mitochondrial membranes and the respiratory chain.

We have seen in previous parts that mitochondrial membrane tranporters can be functionally associated with neighbouring enzymes in either side of the membrane and that metabolite channeling takes place during electron transfer in the respiratory chain. Therefore the application of an *in situ* approach is vital in order to quantitatively characterize in a targeted manner the activity of all these interconnected elements of the mitochondrial membrane without disrupting the physiological spatial relationship between organelles and the cytoskeleton.

Selective permeabilization of yeast cells (*S. cerevisiae* and *K. fragilis*) has been routinely applied for the characterization of the activities of cytosolic enzymes, where incubation with 0.01 % (w/v) digitonin for under 60 min permeabilized the plasma membrane but did not cause leaking of proteins to the extracellular space (Cordeiro and Freire, 1995; Freire et al., 1998). Digitonin has also been used as one of the permeabilizing agent of choice for the *in situ* quantification of mitochondrial respiration of mammalian cells and tissues in two-chamber titration-injection respirometers (Saks et al., 1998; Kuznetsov et al., 2008) and in well-plates (Wahrheit et al., 2015). Also it was verified that *S. cerevisiae* peroxisomal enzymes start leaking out at concentrations of digitonin over 0.03 - 0.06 % (w/v) (Zhang and Lazarow, 1995). Therefore, at a carefully chosen digitonin concentration yeast cells can be successfully permeabilized while retaining their cytosolic enzymes and intact intracellular organelles.

Complete permeabilization of recombinant *S. pombe* cells has been demonstrated for studying the cytosolic UDP-glucose 6-dehydrogenase by applying 0.3 % (v/v) Triton X-100 as the permeabilizing agent (Weyler et al., 2015). Selective permeabilization of the plasma membrane has been demonstrated in *S. pombe* but not for measuring compartmented enzymatic activities *in situ* or mitochondrial function. One study focused on the permeabilization of the plasma membrane with $CuCl_2$ and the examination of $Ca^{2+}$ transport across the vacuolar membrane (Chardwiriyapreecha et al., 2009) while another study was based on nystatin-permeabilization and monitored again vacuolar $Ca^{2+}$ uptake (Halachmi et al., 1992). The apparent lack of *in situ* studies on *S. pombe* are in strong contrast with the growing number of publications focusing on *S. cerevisiae* (Avéret et al., 1998; Manon and Guérin, 1998; Boubekeur et al., 1999, 2001; Avéret et al., 2002; Påhlman et al., 2002; Díaz-Ruiz et al., 2008).

## 2.6 $^{13}$C metabolic flux analysis for *in vivo* studies

In order to quantify *in vivo* the metabolic network of an organism and gain insight into the cellular physiology and regulatory mechanisms, the method of metabolic flux analysis (MFA) is applied (Stephanopoulos et al., 1998). The calculation of intracellular fluxes is based on:

1. a model describing major intracellular reactions

2. mass balances around intracellular metabolites

3. measured extracellular fluxes that consist of uptake rates of substrates and production rates of metabolites at a metabolic steady-state

The outcome is a flux map depicting all biochemical reactions of the network and an estimate of the steady-state rate at which each reaction occurs (Stephanopoulos et al., 1998).

Furthermore MFA is used for the examination of the rigidity or flexibility of branching points according to changes (e.g. genetic modifications, different carbon sources) and/or for comparative studies between strains with a modified genetic background in order to identify alternative pathways. When MFA was firstly established it relied on the stoichiometry of the metabolic network (stoichiometric MFA). The disadvantage of this approach is that it fails when taking into account parallel metabolic networks, metabolic cycles that are not coupled to measurable fluxes and bidirectional reactions occurring at the same time (Wiechert, 2001). This obstacle can be avoided by applying MFA along with $^{13}$C labeled substrates.

### 2.6.1 MFA with $^{13}$C labeled substrates

Metabolic flux analysis with $^{13}$C-labeled substrates, such as [1-$^{13}$C]-glucose, and the analysis of labeling distribution amongst the metabolites of the considered metabolic network provides the following advantages. It generates a more detailed analysis of alternative pathways, of metabolite channelling, of the compartmentation of fluxes partitioning at boundary interfaces (between cytosol and mitochondrial) and of bidirectional fluxes (Wittmann et al., 2002).

As it was mentioned before, the isotope of choice is mostly carbon with an isotope mass of 13. This is the most straightforward choice which takes advantage of the transfer of carbons from substrates to products during the rearrangement of the carbon skeleton of metabolites throughout the metabolic network. This kind of carbon rearrangement is based on enzymatic specificity and the cleavage or formation of carbon-carbon bonds (Wittmann et al., 2002). Labeled carbon atoms are

distributed through the metabolic network and the subsequent isotopic enrichment of the intracellular pools can be quantified either by nuclear magnetic resonance (NMR) or mass spectrometry (MS) (Wiechert, 2001).

The combination of measured extracellular fluxes along with the measured intracellular labeling pattern of metabolites, leads to the computation of intracellular fluxes as illustrated in Figure 2.5. The existence of stable isotopes other than $^{13}C$, that are naturally occurring in metabolites, demands correcting for their presence (Wittmann and Heinzle, 2008).
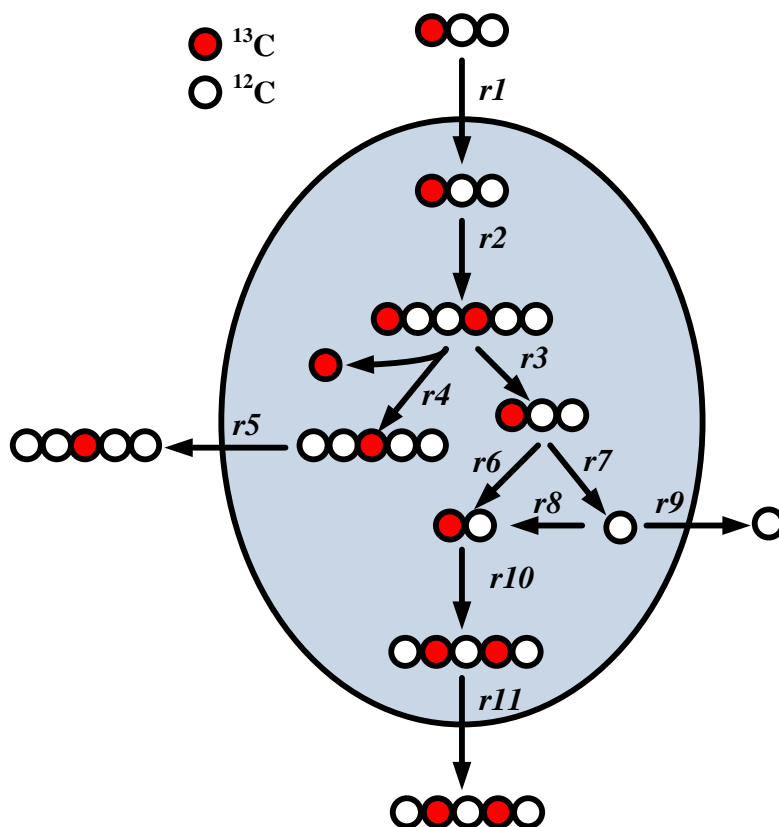


Figure 2.5: Flow of carbon from a substrate into a metabolic network and to various products. The measured extracellular fluxes and the measured intracellular labeling pattern lead to the determination of the intracellular fluxes. Labeled carbon $^{13}C$ illustrated with red filling and non-labeled carbon with no filling. Extracellular fluxes: $r_1$, $r_5$, $r_9$ and $r_{11}$. Intracellular fluxes: $r_2$, $r_3$, $r_4$, $r_6$, $r_7$, $r_8$, $r_{10}$.

Another prerequisite for performing stationary metabolic flux analysis is that $^{13}C$ labeling experiments are performed during the isotopic steady-state of the metabolism, where the labeling pattern of the metabolites does not change over time. The analysis of the isotopic enrichment of intracellular pools of aminoacids by means of MS differentiates between mass isotopomers, whereas employing NMR

can differentiate between positional isotopomers (Wittmann and De Graaf, 2005). The term isotopomer derives from the terms isotope and isomer and describes the different labeling patterns which a metabolite can possess (Wiechert, 2001).

Isotopomers are categorized into positional isotopomers, mass isotopomers and cumulated isotopomers (cumomers) as summarized in Figure 2.6. Positional isotopomers have an exact labeling pattern, defined by a specific number of $^{13}C$ atoms in specific positions of the metabolite. A metabolite with n carbon atoms can have $2^n$ different positional isotopomers. A mass isotopomer on the other hand is not defined by the position of the $^{13}C$ atoms in the molecule but by the number of them (Wittmann and Heinzle, 2005). A metabolite with n carbon atoms has n+1 mass isotopomers. Accordingly, mass isotopomers that differ by the number of labeled carbon atoms can be resolved with mass spectrometry and positional isotopomers can be assessed by NMR, thus measuring the specific labeling degree of single atoms (fractional enrichment) (Wittmann and De Graaf, 2005).
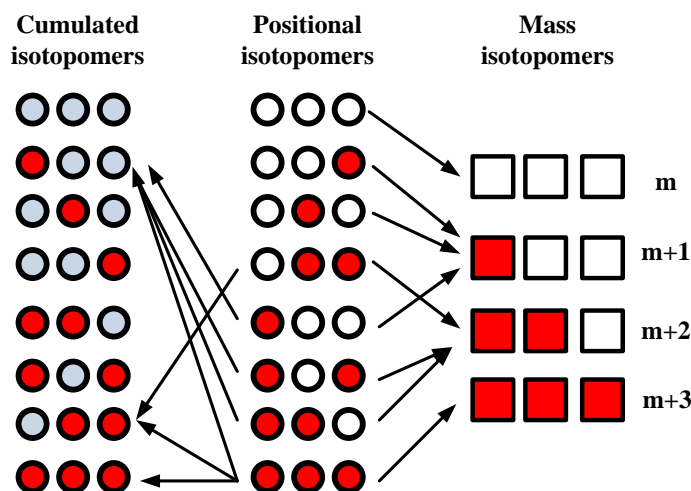


Figure 2.6: Cumulated isotopomers, positional isotopomers and mass isotopomers for a molecule with three carbon atoms, which are either $^{12}C$ (white), $^{13}C$ (red) or not specified (blue). The arrows denote the grouping of positional isotopomers in cumomers and mass isotopomers (Wittmann et al., 2002).

The isotopomer distribution of a metabolite is comprised of the percentage of each isotopomer within a metabolite pool (isotopomer fractions), whereas the sum of all fractions is one (Wiechert, 2001). In the case of cumomers or cumulated isotopomer fractions (Wiechert et al., 1999) the isotopomers that have in common the labeling at the same carbon atom also belong to the same cumomer fraction (Wittmann et al., 2002). For example for a molecule with 3 carbon atoms, three 1-cumomer fractions occur that are single labeled and are identical to the frac-

tional enrichment. A 1-cumomer fraction ($c_{1xx}$), a 2-cumomer fraction ($c_{x11}$) and a 3-cumomer fraction ($c_{111}$) are illustrated in Figure 2.6.

### 2.6.2   Flux estimation

The quantification of the *in vivo* activities of the pathways that comprise the central metabolic network of *S. pombe* is based on the labeling pattern of proteinogenic amino acids and on the stoichiometric data obtained for the substrate uptake and product formation rates (ethanol, glycerol, pyruvate) from steady-state batch cultivations.

The calculated flux maps were based on simulated and measured mass distribution vectors, which were the input data for a metabolic modelling program, namely XFluxGate, developed by Yang and based on published methods (Yang et al., 2008) using a decomposition algorithm utilizing the elementary metabolite unit (EMU) framework (Antoniewicz et al., 2007). The mathematical modelling program was based on MATLAB R2012b (and R2008b) as a computational platform.

# Chapter 3

# Materials and Methods

## 3.1 Organisms

### 3.1.1 *Schizosaccharomyces pombe*

Fission yeast strains were based on the haploid wild-type strain *Schizosaccha-romyces pombe* CBS 356 (CBS, Centraalbureau voor Schimmelcultures, Utrecht, The Netherlands) with a h$^-$ mating type. The mutant strain ED668(BG_0000H8) with a deletion of the gene expressing the voltage-dependent anion-selective channel (gene sequence: SPAC1635.01) with genotype orf$\Delta$:kanMX4 *ade6*-M216 *ura4*-D18 *leu1*-32 was purchased from Bioneer Corporation (Daejeon, Korea).

Strains constructed in this work are summarized as following:

- *mpc1*$\Delta$: Strain containing the *mpc1* (SPCC1235.11) gene deletion, encoding the Mpc1p subunit of the mitochondrial pyruvate carrier protein.

- *mpc2*$\Delta$: Strain containing the *mpc2* ( SPAC24B11.09) gene deletion, encoding the Mpc2p subunit of the mitochondrial pyruvate carrier protein.

- *mpc1*$\Delta$*mpc2*$\Delta$: Strain containing the *mpc1* and *mpc2* gene deletions, encoding both subunits of the mitochondrial pyruvate carrier protein.

### 3.1.2 *Escherichia coli*

The *E. coli* strain BL21-Gold(DE3) was used for the amplification of plasmids. They possess a $BF^-$ *ompT hsdS* ($r_B^- m_B^-$ ) $dcm^+$ $Tet^r$ gal $\lambda(DE3)$ *endA* Hte genotype and were purchased from Stratagene (La Jolla, USA).

## 3.2 Plasmids

The plasmids used for the needs of strain construction are summarized in Table 3.1 (see plasmid vector maps in Appendix).

Table 3.1: General characteristics of plasmids used.

| plasmid name | Length | Characteristics | Supplier |
|---|---|---|---|
| **pUG6** | 4009 bp | Vector providing resistance to G418 (geneticin), *kan*MX; *Kan$^r$*, *Amp$^r$* | Euroscarf |
| **pAG25** | 3704 bp | Vector providing resistance to nourseothricin, *nat*MX; *Amp$^r$* | Euroscarf |

## 3.3   Primers

All oligonucleotides used in this work were supplied by Sigma-Aldrich and are described in detail in Tables 3.2 and 3.3 .

Table 3.2: Oligonucleotides used for the disruption of the *mpc1* gene.

| Primer | Sequence ($5' \rightarrow 3'$) |
| --- | --- |
| Primers used for the construction of the gene disruption cassette | |
| **$5'$-upstream1** | ATAATTGGTCCTGTTCGAATTTACC |
| **$3'$-upstream1** | GGTGACCCGGCGGGGACAAGGCAAGCTGTT TATACCTCAATCAGTTGATGAATATTGG |
| **$5'$-*nat*MX** | CCAATATTCATCAACTGATTGAGGTATAAAC AGCTTGCCTTGTCCCCGCCGGGTCACC |
| **$3'$-*nat*MX** | CGTTTATATTTTGTTTAATTTTCTTTTTCACT AATGACTCGACACTGGATGGCGGCGTTAGT ATCG |
| **$5'$-downstream1** | CGATACTAACGCCGCCATCCAGTGTCGAGT CATTAGTGAAAAAGAAAATTAAACAAAATAT AAACG |
| **$3'$-downstream1** | ACACAAAAGATAACGGCATTGATCAAC |
| Primers used for the verification (VR) of integration of the cassette in the *mpc*1 locus | |
| **$5'$-upstream1-VR** | GGTGTAAGGAAAATATTCGCATTGC |
| **$3'$-upstream1-VR** | CCGATTGGTCTTCTATAGATCCAATGG |

Table 3.3: Oligonucleotides used for the disruption of the *mpc2* gene.

| Primer | Sequence (5′ → 3′) |
| --- | --- |
| Primers used for the construction of the gene disruption cassette | |
| **5′-upstream2** | TGTAAACGCCGAGGAAAAAGTAGATC |
| **3′-upstream2** | GCTAAACAGATCTCTAGACCTAGTATCCGTA TTAGACATGCT |
| **5′-*kan*MX** | AGCATGTCTAATACGGATACTAGGTCTAGA GATCTGTTTAGC |
| **3′-*kan*MX** | GACTGTTATTCCTTATTTATTTTTCATTAAG GGTTCTCGAGAGCTCG |
| **5′-downstream2** | CGAGCTCTCGAGAACCCTTAATGAAAAATAA ATAAGGAATAACAGTC |
| **3′-downstream2** | ATACATGAACTCCATTTGAAAGAGAAAAAAA CG |
| Primers used for the verification (VR) of integration of the cassette in the *mpc*2 locus | |
| **5′-upstream2-VR** | GGAATGTATTCTAAGGGAGCCTAAAAGGCG |
| **3′-upstream2-VR** | CCCAAGAAATAGCGACCTGACAAATACCCC |

## 3.4 Growth media and chemicals

### 3.4.1 Chemicals

Agar and yeast extract for the preparation of complex medium were obtained from Difco Laboratories (Detroit, USA). All other chemicals used were of analytical grade and were obtained from: Fluka (Buchs, Austria), Sigma-Aldrich (Steinheim, Germany), Riedel-de-Haen (Seelze, Germany), Merck (Darmstadt, Germany), Acros Organics (Geel, Belgium), Grüssing (Filsum, Germany), Jena Bioscience (Jena, Germany) and Invivogen (San Diego, USA). Zymolyase-20T was obtained by Seikagaku Biobusiness (Tokyo, Japan). 99 % enriched glucose ([1-$^{13}$C]-glucose) was obtained from Cambridge Isotope Laboratories (Andover, MA, USA).

### 3.4.2 Complex medium for *S. pombe*

For the preparation of complex medium for the cultivation of *S. pombe* cells (liquid/agar cultures), the following components were used as summarized in Table 3.4.

Table 3.4: Complex Medium (YES) for *S. pombe*.

| | |
|---|---|
| Glucose | 30 g |
| Yeast Extract | 5 g |
| L-Histidine | 225 mg |
| L-Leucine | 225 mg |
| L-Lysine | 225 mg |
| Adenine | 225 mg |
| Uracil | 225 mg |

Ad 1L distilled water

Sterilize by autoclaving

For the preparation of agar plates, 2 % Difco Bacto Agar was added to liquid YES-medium prior to autoclaving

### 3.4.3 Synthetic medium for *S. pombe*

Synthetic, minimal medium was used for the cultivation of the second pre-culture and the main culture. For the preparation of 1 Liter of minimal medium (MM), the components are specified in Tables 3.5 , 3.6 , 3.7 .

Table 3.5: Vitamin stock solution (x1000).

| | |
|---|---|
| Calcium pantothenate | 1 g |
| Nicotinic acid | 10 g |
| Myoinositol | 10 g |
| Biotin | 10 mg |
| Pyridoxine-HCl | 0.5 mg |

Ad 1L distilled water
Sterilize by filtration

Table 3.6: Mineral stock solution (x10000).

| | |
|---|---|
| $H_3BO_3$ | 5 g |
| $MnSO_4 * H_2O$ | 4 g |
| $ZnSO_4 * 7H_2O$ | 4 g |
| $FeCl_2 * 4H_2O$ | 2 g |
| $Na_2MoO_4 * 2H_2O$ | 0.6 g |
| KI | 1 g |
| $CuSO_4 * 5H_2O$ | 0.4 g |
| Citric acid | 10 g |

Ad 1L distilled water
Sterilize by filtration

Table 3.7: Minimal Medium.

| | |
|---|---|
| Glucose $* H_2O$ | 17.8 g |
| $(NH_4)_2SO_4$ | 5.6 g |
| $MgSO_4 * 7H_2O$ | 1.2 g |
| NaCl | 1.2 g |
| $CaCl_2 * 2H_2O$ | 14.7 mg |
| Vitamin stock solution | 1 mL |
| Mineral stock solution | 0.1 mL |

Ad 1L distilled water; adjust pH at 5.5
Sterilize by filtration

For the needs of sterile filtration, stericup vacuum filtration systems (0.22 $\mu$m Durapore) were used for large volumes (100 - 1000 mL) and Minisart syringe filter systems for smaller volumes.

### 3.4.4   Complex medium for *E. coli*

*Escherichia coli* cells were cultivated in lysogeny broth medium (LB medium) (Sambrook et al., 1989) as illustrated in Table 3.8 and antibiotics (kanamycin or ampicillin) were added when appropriate.

Table 3.8: Medium (LB) for *E. coli*.

| | |
|---|---|
| Trypton | 10 g |
| NaCl | 10 g |
| Yeast extract | 5 g |

Ad 1L distilled water; pH 7.0
Sterilize by autoclaving

For the preparation of agar plates, 2 % agar was added prior to autoclaving whereas appropriate sterile solutions of antibiotics where added after autoclaving.

### 3.4.5   SOC medium for *E. coli*

For achieving a higher grade of transformation efficiency of *E. coli* cells, the antibiotic-free SOC-medium (Hanahan and Harbor, 1983) was used with a composition as illustrated in Table 3.9.

Table 3.9: SOC-medium for *E. coli*.

| | |
|---|---|
| Trypton | 2.0 % (w/v) |
| NaCl | 0.5 % (w/v) |
| Yeast extract | 10 mM |
| KCl | 2.5 mM |
| Glucose $*$ $H_2O$ | 20 mM |
| Ad distilled water; Sterilize by autoclaving | |
| $MgCl_2$ (sterile filtered) | 10 mM |
| $MgSO_4$ (sterile filtered) | 10 mM |

### 3.4.6 Antibiotics

For selection by means of antibiotic resistance of mutant strains, the following antibiotics were applied:

- Nourseothricin: The available stock solution had a concentration of 100 mg/mL and was applied at an end concentration of 100 $\mu$g/mL.

- Geneticin sulfate G418: The available stock solution had a concentration of 100 mg/mL and was applied at an end concentration of 200 $\mu$g/mL.

- Ampicillin sodium salt : The available stock solution had a concentration of 150 mg/mL and was applied at an end concentration of 150 $\mu$g/mL.

- Kanamycin : The available stock solution had a concentration of 50 mg/mL in 0.9 % NaCl and was applied at an end concentration of 50 $\mu$g/mL.

## 3.5 Cultivation of cells

All cultivations were carried out at 30 °C (*S. pombe*) or at 37 °C (*E. coli*) in a rotary shaker at 230 rpm and 5 cm of shaking diameter (Multitron, Infors AG, Bottmingen, Switzerland). To avoid a lack of oxygen in the culture, only 10 % of the total volume of the shake flasks was filled. Shake flasks used had 4 baffles each.

### 3.5.1 Agar plates

For the needs of inoculation or for testing transformed clones if they have gained resistance to an appropriate antibiotic, cells were cultivated at 30 °C (*S. pombe*) or 37 °C (*E. coli*) on agar plates (either complex or minimal medium, organism-specific) for approximately three to four days in the incubator (Heraeus, Hanau, Germany).

### 3.5.2 First pre-culture of *S. pombe*

Single colonies from an agar plate served as inoculum for the first pre-culture. This culture was grown overnight in a 100 mL baffled shake flask with YES medium. Then cells from the first pre-culture were harvested by centrifugation during 3 minutes at 7388 x g and 4 °C (Biofuge Stratos, Heraeus, Hanau, Germany). Afterwards, cells were resuspended in minimal medium, the $O.D_{595nm}$ was measured and an appropriate volume thereof was used according to the desired optical density of the second pre-culture. Optical density ($O.D_{595nm}$) was measured at a wavelength of 595 nm (Spectrophotometer Novaspec$^{\delta}$II, Pharmacia Biotech, Little Chalfont, UK) and was referred to $H_2O$.

### 3.5.3 Second pre-culture of *S. pombe*

This cultivation was carried out in 250 mL baffled shake flasks with minimal medium. Cells from this second pre-culture upon growing exponentially were harvested by centrifugation for 3 minutes at 7388 x g and 4 °C. The cells were consequently resuspended in minimal medium and the $O.D_{595nm}$ was measured. Again the volume to be transferred to the main culture from the second pre-culture was determined on a case-by-case approach based on measured and desired optical density values.

### 3.5.4 Main culture and sample treatment

The main culture was carried out in duplicates in 500 mL baffled shake flasks containing minimal medium that was inoculated with cells originating from the second pre-culture. In defined time intervals, a 1 mL sample was taken from each of the main cultures in order to measure its optical density at 595 nm at each time point.

The sample was then centrifuged for 5 min at 13009 x g and 4 °C (Biofuge Fresco, Heraeus, Hanau, Germany), and the supernatant was stored at -20 °C for further analysis such as quantification of organic acids and glucose.

## 3.6 Long-term storage of organisms

### 3.6.1 *S. pombe*

For preserving cells of fission yeast for months up to years, usually 1 mL from an overnight-grown culture of minimal medium medium (30 °C at 230 rpm in a rotary shaker) was mixed with 1 mL of a 60 % (v/v) glycerine solution and stored at -70 °C. For shorter time intervals, cells were stored at 4 °C, as single-cell colonies that were previously grown at 30 °C on YES agar plates in an incubator. When this was the case, agar plates were sealed with parafilm tape.

### 3.6.2 *E. coli*

For preserving *E. coli* cells, 1 mL from an overnight-grown culture in LB medium (37 °C at 230 rpm in a rotary shaker), was mixed with 1 mL of a 60 % (v/v) glycerine and stored at -70 °C. For shorter time intervals, cells were stored at 4 °C, as single-cell colonies that had previously grown at 37 °C on LB agar plates in an incubator. When this was the case, agar plates were sealed with parafilm tape.

# 3.7 Isolation and analysis of nucleic acids

## 3.7.1 Isolation of genomic DNA from *S. pombe*

Isolation of genomic DNA from *S. pombe* cells was performed based on a modified method of Hoffman et al. (Hoffman and Winston, 1987). A volume of 1.5 - 2 mL taken from an overnight culture grown in YES medium, was centrifuged for 3 min at 11084 x g (Biofuge Fresco, Heraeus, Hanau, Germany) and the supernatant was discarded. The cell pellet was washed once with 1.5 mL distilled $H_2O$ and then resuspended in 40 $\mu$L of lysis buffer as specified in Table 3.10.

Subsequently, glass beads (diameter 0.25 - 0.5 $\mu$m) were added along with 70 $\mu$L of chloroform and the cells were vortexed for 1 minute, interrupted with a 1 minute pause and then proceeded with another minute vortexing. Following a one minute pause, 40 $\mu$L of 1 x TE-buffer (Table 3.11) were added and mixed vigorously. The mixture was then centrifuged for 5 minutes at 11921 x g (Biofuge Fresco, Heraeus, Hanau, Germany) and the aqueous supernatant was transferred in a new tube. A volume of 1 mL 99 % ethanol was added to precipitate the DNA contained in the aqueous phase and then centrifuged for 3 minutes at 12568 x g (Biofuge Fresco, Heraeus, Hanau, Germany). The supernatant was discarded and the DNA-containing pellet was left to dry and then resuspended in 40 $\mu$L distilled $H_2O$.

Table 3.10: Lysis Buffer.

| | |
|---|---|
| Triton-X 100 | 1 mL |
| SDS | 0.5 g |
| NaCl | 0.3 g |
| Tris-HCl pH 8.0 | 80 mg |
| EDTA | 15 mg |

Ad 50 mL distilled water; pH 8.0
Sterilize by autoclaving

Table 3.11: 1 x TE buffer.

| | |
|---|---|
| Tris-HCl pH 8.0 | 10 mM |
| EDTA | 1 mM |

Ad distilled water; pH 8.0
Sterilize by autoclaving

### 3.7.2   Plasmid preparation

The isolation of plasmids from transformed *E. coli* cells was based on the alkaline lysis method (Birnboim and Doly, 1979) and was performed with a HiYield$^{\hat{o}}$ Plasmid Mini kit (Sud-Laborbedarf GmbH, Gauting, Germany) consisting of commercial buffers PD1, PD2, PD3, W1 and the Wash buffer.

A volume of 1.5 mL of overnight-grown cells containing the plasmids was centrifuged at 13009 x g (Biofuge Fresco, Heraeus, Hanau, Germany) for 1 minute and the supernatant was discarded. The pellet was resuspended in 200 $\mu$L PD1 buffer and afterwards another 200 $\mu$L of PD2 buffer was mixed with the cell suspension and let to incubate at room temperature for 2 minutes.

For the precipitation of proteins, 300 $\mu$L of PD3 buffer was added and the cell extract was mixed gently and centrifuged for 3 minutes at 13009 x g (Biofuge Fresco, Heraeus, Hanau, Germany). For the extraction of the plasmids, the supernatant containing the clear lysate was taken and put on a DNA-binding column. After a 30-second centrifugation the column was washed with 400 $\mu$L W1 buffer, the flow-through was discarded and finally 600 $\mu$L Wash buffer (containing ethanol) was added. After a 3-minute centrifugation at 16060 x g to dry the column matrix, the plasmid DNA was eluted with the addition of 50 $\mu$L distilled $H_2O$ and a 2-minute centrifugation at 16060 x g (Biofuge Fresco, Heraeus, Hanau, Germany).

### 3.7.3   Clean-up and extraction of DNA fragments

For the exctraction and clean-up of DNA fragments from either PCR products or excised agarose gel fragments, a NucleoSpin Gel and PCR Clean-up kit (Macherey-Nagel, Düren, Germany) was used based on a method by Vogelstein and Gillespie (Vogelstein and Gillespie, 1979).

#### 3.7.3.1   Isolation of DNA fragments from agarose gel

After the end of an electrophoretic run, single bands of interest containing DNA fragments were excised from the gel and each one was placed in a 1.5 mL tube. A volume of 200 $\mu$L NTI buffer (part of the NucleoSpin Gel and PCR Clean-up kit) per 100 mg agarose gel was added to each tube and incubated at 50 °C until the gel was completely dissolved. The dissolved gel was transferred to a NucleoSpin$^{TM}$Extract II column and was centrifuged at 11084 x g (Biofuge Fresco, Heraeus, Hanau, Germany) for 1 minute.

The flow-through was discarded and the silica membrane was washed with 700 $\mu$L NT3 buffer (part of the NucleoSpin Gel and PCR Clean-up kit) and centrifuged again at 11084 x g (Biofuge Fresco, Heraeus, Hanau, Germany) for 1

minute. The flow-through was discarded, the column dried by centrifugation at 11499 x g (Biofuge Fresco, Heraeus, Hanau, Germany) for 3 minutes and then DNA was eluted by incubating the column with 40 $\mu$L of diluted $H_2O$ at room temperature. Finally the column was centrifuged at 11084 x g (Biofuge Fresco, Heraeus, Hanau, Germany) for 1 minute and then discarded, while the purified DNA was captured as flow-through in the vial.

### 3.7.3.2 Isolation of DNA fragments from PCR mixtures

When the amplified DNA product of a PCR was known to yield a single band in an agarose gel lane, then DNA could be isolated directly from the PCR preparation. A volume of 100 $\mu$L distilled $H_2O$ was added to the PCR product along with 200 $\mu$L of the NT buffer. Finally the concentrated DNA amplified by means of PCR would be eluted with the addition of 40 $\mu$L of distilled $H_2O$.

## 3.7.4 Quantification of DNA concentration

For quantifying the DNA concentration of relevant samples, a photometer was used (Genesys 10Bio, ThermoElectron, Oberhausen, Germany) set at a wavelength of 260 nm. The purity in regards of DNA content of a sample was controlled by measuring the protein content of the sample at a wavelength of 280 nm. Subsequently a ratio of $E_{260nm}/E_{280nm}$ between 1.8 - 2.0 was assigned to a protein-free sample.

## 3.8 Polymerase chain reaction (PCR)

For the needs of DNA amplification, the so called polymerase chain reaction (PCR) was applied, executed in a thermocycler (T*gradient*, Biometra, Goettingen, Germany). For synthesizing DNA sequences a Phusion$^{TM}$High-Fidelity DNA Polymerase (Biozym Scientific GmbH, Hessisch Oldendorf, Germany) was used. The aforementioned enzyme is a modified version of the extremophile organism *Pyrococcus furiosus*, exhibiting higher extension rates and lower error rates than the native *Pfu* polymerase, possesses a $3' \rightarrow 5'$ exonuclease activity additionaly to the $5' \rightarrow 3'$ polymerase one and generates blunt-ended products. The typical composition of a single amplification reaction for amplifying a specific DNA sequence was as following in Table 3.12 :

Table 3.12: Components of a single PCR reaction used to amplify a defined DNA sequence by the action of the Phusion$^{TM}$High-Fidelity DNA Polymerase.

| Single PCR reaction components | |
|---|---|
| 10x Phusion$^{TM}$Reaction buffer | 10 $\mu$L |
| milliQ H$_2$O | 35 $\mu$L |
| dNTPs (10 mM) | 1 $\mu$L |
| DMSO | 1.5 $\mu$L |
| DNA template | 1 $\mu$L |
| 5′ primer | 0.5 $\mu$L |
| 3′ primer | 0.5 $\mu$L |
| Phusion$^{TM}$High-Fidelity DNA Polymerase | 0.5 $\mu$L |

Components were added in the order shown in order to avoid degradation of DNA caused by the $3' \rightarrow 5'$ exonuclease activity of the polymerase.

The PCR reaction for each genetic target to be amplified was initiated in a thermocycler after the addition of the polymerase. A thermocycler was programmed to execute necessary cycles as described in Table 3.13.

Table 3.13: Temperature cycles along with duration for every step during the Phusion$^{TM}$High-Fidelity DNA polymerase-catalysed DNA amplification.

| Cycle description | T [°C] | Duration | |
|---|---|---|---|
| Initial denaturation | 98 | 5 min | |
| Denaturation | 98 | 20 sec | |
| Annealing | x | 20 sec | 30 cycles |
| Elongation | 68 | 30 sec/kb | |
| Final elongation | 68 | 7 min | |
| End | 4 | ∞ | |

Ad 80 $\mu$L distilled water

The duration of the elongation step depends on the length of the sequence to be amplified, as it is noted in Table 3.13 and is polymerase-dependent. Furthermore the annealing temperature (x) depends on the length and the composition of the primers that are homologous to the flanking regions of the sequence-target and was calculated by Equation 3.1.

$$T_m[°C] = \left(69.3 + (0.41 \times GC[\%]) - \left(\frac{650}{Length[bp]}\right)\right) - 2 \qquad (3.1)$$

## 3.8.1 Overlap Extension-PCR (OE-PCR): Constructing the disruption cassette and fusion of homologous segments

The overlap extension cloning technique (Bryksin and Matsumura, 2012) for splicing at least two sequences is based on primers with a 5′-overhang that is complementary (at least 25 bp homology) to the 3′-end of the sequence to be fused with. We were able to construct the disruption cassette that would be inserted into each *S. pombe* gene-target in 5 separate PCR steps using the primers described in Tables 3.2 and 3.3 (Section 3.3, page 41). A sixth PCR would then amplify the integration cassette prior to transforming wild type cells. A general scheme describing the different fusion events and the final product being integrated by homologous recombination in a gene are illustrated in Figure 2.
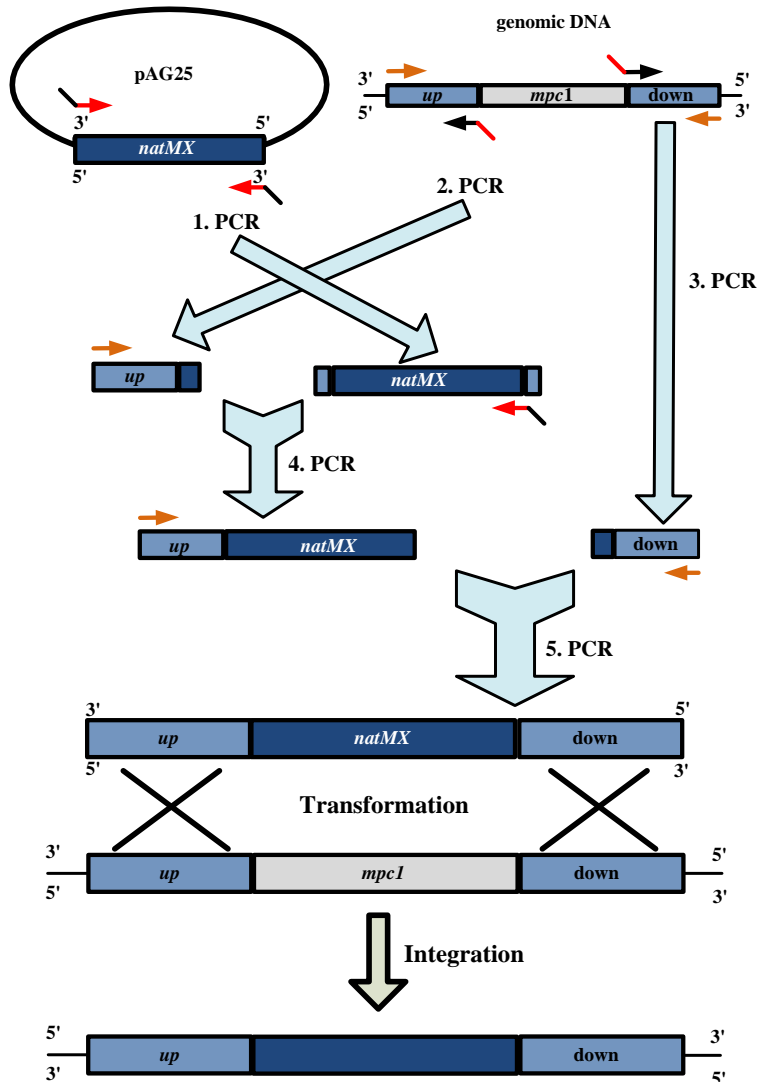
Figure 3.1: Schematic representation of the construction of the integration cassette for disrupting gene *mpc1* in *S. pombe* by means of OE-PCR.

### 3.8.2 Colony-PCR

Colony-PCR was performed in order to assess whether the disruption cassettes or the insert in general were integrated at the correct position in the genome of the target organism.

#### 3.8.2.1 Colony-PCR for *E. coli*

Single-cell colonies from transformed *E. coli* cells were taken with a sterile pipette tip and mixed with 8 $\mu$L from the reaction mix that had the composition as described in Table 3.14. Additionally single-cell colonies of transformed cells were plated on agar plates with the appropriate antibiotic marker and were incubated at 37 °C in

order to monitor growth.

Cell lysis was initiated in the thermocycler during the initial step while the thermocycler was programmed to execute necessary cycles as described in Table 3.15. The components of a reaction mix used for colony-PCR typically consisted of the JumpStart$^{TM}$ RED*Taq* ReadyMix$^{TM}$ Reaction Mix (Sigma, Steinheim, Germany), which did not possess proof-reading activity but had a high extension rate. For the examination of more than one clone a master-mix was used as illustrated in Table 3.14.

Table 3.14: A list of the components for a master-mix for the examination of 10 clones with a JumpStart$^{TM}$ RED*Taq* ReadyMix$^{TM}$-catalyzed colony-PCR.

| Colony-PCR components | |
| --- | --- |
| RED*Taq* ReadyMix$^{TM}$ | 40 $\mu$L |
| Template | x |
| Primer-Forward | 2 $\mu$L |
| Primer-Reverse | 2 $\mu$L |

Ad 80 $\mu$L distilled water

### 3.8.2.2  Colony-PCR for *S. pombe*

Initially the yeast colonies had to be lysed before performing a colony-PCR on transformed yeast clones. Single-cell colonies were picked from YES-containing plates at the presence of appropriate antibiotics. Cells were then resuspended in 20 $\mu$L of 0.02 M NaOH and vortexed for 30 seconds. Subsequently the cells were exposed to heat (99 °C) in the thermocycler for 5 minutes in order to achieve complete cell lysis.

Table 3.15: Temperature cycles along with duration for every step during the JumpStart$^{TM}$ RED*Taq* ReadyMix$^{TM}$ polymerase-catalysed DNA amplification.

| Cycle description | T [°C] | Duration | |
| --- | --- | --- | --- |
| Initial denaturation | 95 | 5 min | |
| Denaturation | 95 | 30 sec | |
| Annealing | x | 20 sec | 30 cycles |
| Elongation | 72 | 30 sec/kb | |

| | | |
|---|---|---|
| Final elongation | 72 | 7 min |
| End | 4 | ∞ |

Samples were then centrifuged at full speed for 30 seconds. The supernatant was collected and 1 $\mu$L thereof used as a template for the needs of the colony-PCR. The polymerase used was the Phusion$^{TM}$High-Fidelity DNA polymerase as described in Table 3.16 for a single clone and the cycle programming of the thermocycler was as specified in Table 3.13. The annealing temperature (x) depended on the length and the composition of the primers that are homologous to the flanking regions of the sequence-target and was calculated by Equation 3.1.

Table 3.16: Components of a single colony-PCR catalyzed by the Phusion$^{TM}$High-Fidelity DNA Polymerase used to identify positively transformed *S. pombe* cells.

| Single PCR reaction components | |
|---|---|
| 10x Phusion$^{TM}$Reaction buffer | 5 $\mu$L |
| milliQ H$_2$O | 17 $\mu$L |
| dNTPs (10 mM) | 0.5 $\mu$L |
| DMSO | 0.75 $\mu$L |
| DNA template | 0.5 $\mu$L |
| 5$'$ primer | 0.5 $\mu$L |
| 3$'$ primer | 0.5 $\mu$L |
| Phusion$^{TM}$High-Fidelity DNA Polymerase | 0.25 $\mu$L |

Components were added in order to avoid degradation of DNA caused by the $3' \to 5'$ exonuclease activity of the polymerase

## 3.9 Gel electrophoresis

The size of DNA fragments that were either direct products of a PCR or had been initially isolated as mentioned before, have been quantified by means of agarose gel electrophoresis. The stationary phase was the cross-linked agarose matrix and the mobile phase consisted of diluted (1x) TAE buffer. DNA fragments moved towards the anode of the electrophoretic chamber based on their relative charge after a 100 - 120 V voltage was applied to create an electric field for a duration of 1 hour. Prior to injecting the DNA fragments into the agarose gel, a loading dye was applied to the samples in order to stain DNA in a ratio of 1:10 of DNA to loading dye. Agarose gel was routinely prepared as a 1 % (w/v) solution of agarose in 1xTAE buffer and stored at 80 °C as a liquid. Tables 3.17 and 3.18 Illustrate the composition of a 50x-concentrated TAE buffer and that of a 10x-concentrated Orange G loading dye.

Table 3.17: 50 x TAE Buffer.

| | |
|---|---|
| Tris | 2 M |
| EDTA (100 mL; 0.5 M; pH 8.0) | 50 mM |
| Acetate (100%) | 57 $\mu$L |

Ad 1L distilled water

Table 3.18: 10 x Orange G

| | |
|---|---|
| Glycerine (50%) | 50 mL |
| EDTA (1 M; pH 8.0) | 1 mL |
| Orange G | 75 mg |

When the gel electrophoretic separation of DNA was concluded, the gel was dyed in an ethidium bromide bath for 15 minutes. After dying the gel, the DNA-ethidium bromide complex was visible with the assistance of a Transilluminator (E.A.S.Y. Plus System, Herolab, Wiesloch, Germany) that was set at an excitation of 260 - 360 nm and an emission of 590 nm. A GeneRuler$^{TM}$ 1 kb DNA Ladder was always present in the gel as a means for sizing and relative, approximate quantification of the target-DNA sequences.

# 3.10 Transformation of cells

## 3.10.1 Generating electrocompetent *E. coli* cells

An overnight culture of *E. coli* BL21-Gold(DE3) was harvested when it reached an O.D$_{600nm}$ of 0.5. Cells were centrifuged for 15 minutes at 4000 x g (Biofuge Stratos, Heraeus, Hanau, Germany) and 4 °C and were washed twice with ice-cold, sterile, demineralized H$_2$O. Then the cells were washed with ice-cold 10 % glycerine (v/v) while progressively reducing the volume from 200 mL then to 20 mL and finally to 2 mL. The cell suspension was then divided in 50 $\mu$L aliquots and stored at -70 °C.

## 3.10.2 Transformation of *E. coli*

Electrocompetent *E. coli* BL21-Gold(DE3) cells were thawed in ice and were mixed with the DNA to be inserted in an ice-cold electrotransformation cuvette. The electroporation was performed on a BioRad Gene Pulser II (Hercules, CA,USA) with settings fixed at 2.5 kV, capacity at 25 LF, resistance at 400 N and a time constant at 8-9 msec. Following the electroporation via an electric pulse, the cells were mixed with 1 mL SOC-medium in order to regenerate their membranes and were incubated at 37 °C for 1 hour. After the regeneration, the cells were spread on antibiotic-containing agar plates in duplicates and at different cell concentrations and were incubated at 37 °C.

## 3.10.3 Transformation of *S. pombe*

*S. pombe* transformation via electroporation was based on a modified version of the protocol developed by Prentice (Prentice, 1991). An overnight culture growing in minimal medium was harvested when it reached an O.D$_{595nm}$ equal to 4 and centrifuged at 7388 x g (Biofuge Stratos, Heraeus, Hanau, Germany) and 4 °C. The cell pellet was washed with sterile, ice-cold demineralized H$_2$O and then with ice-cold 1 M sorbitol.

The cells were suspended in 1 M sorbitol and 25 mM DTT were added in order to increase electroporation efficiency (Suga and Hatakeyama, 2001). The cell suspension was incubated for 15 minutes at 30 °C and 230 rpm in a rotary shaker. Incubation was followed by centrifugation and the cell pellet was resuspended in 200 $\mu$L ice-cold 1 M sorbitol. A volume of 40 $\mu$L from the cell suspension was mixed with 100 ng of the DNA to be inserted and was incubated in ice for 5 minutes.

The mixture was loaded in a sterile, ice-cold electrotransformation cuvette and the cuvette was inserted in a BioRad Gene Pulser II (Hercules, CA, USA), that was set with 2.25 kV, a capacity of 25 LF and a resistance of 200 N. Directly after elec-

troporation, a volume of 900 $\mu$L ice-cold 1 M sorbitol was given to the electroporated cells and were shortly incubated in ice. The cell suspension was finally used to inoculate a 25 mL YES-medium culture and was incubated overnight at 30 °C and 230 rpm in a rotary shaker. After a 24-hour cultivation a volume of 2 mL from the culture was harvested, washed and used to spread YES-agar plates containing the appropriate antibiotics. The plates were incubated at 30 °C.

## 3.11   Selective permeabilization of *S. pombe* cells

Exponentially growing cells ($1\times10^8$ cells/mL) were harvested and washed twice with ice-cold milliQ $H_2O$. The cell pellets were resuspended in a pH 6.8 respiratory buffer (per liter of distilled water: mannitol, 118.4 g; $MgCl_2*_6H_2O$, 1.016 g; $KH_2PO_4$, 2.18 g; imidazole, 0.68 g; lipid-free bovine serum albumine, 1 g; EGTA, 0.76 g; 100 $\mu$L final media antifoam 289) containing digitonin 0.002% (w/v).

The reaction mixture was incubated for 45 minutes at 30 °C and then centrifuged at low speed (799 x g) at 9 °C (Biofuge Stratos, Heraeus, Hanau, Germany). Cells were washed twice with digitonin-free respiratory buffer and were subjected to further analysis. Selectively permeabilized cells were always stored on ice for a maximum of 4 hours to avoid any loss of mitochondrial function and intracellular integrity.

## 3.12    Miniaturized reactor system and sampling

Mitochondrial activity of selectively permeabilized cells, was quantified in a closed PEEK (polyether ether ketone) reactor (Figure 3.2) without a gas phase. It had an inner diameter ($\varnothing$) of 15 mm and a height of 40 mm and was connected to the mass spectrometer via a membrane inlet probe projecting at the bottom of the reactor through a 14 mm x 22.5 mm opening.

The reactor was tempered (30 °C) with an integrated cooling loop ($\varnothing$ 3 mm) connected via a peristaltic pump (Alitea-XV, Hüneberg, Switzerland) to a heated circulation bath (MGW Lauda M3, Lauda-Königshofen, Germany), and temperature was monitored on-line with a sensor (Pt 1000, Mettler-Toledo GmBH, Urdorf, Switzerland) via a pH/ORP transmitter (2050e, Mettler-Toledo). Mixing was provided by a cylindrical stir bar (6 mm, $\varnothing$3 mm) which was put at the bottom of the reactor, stirred by a magnetic hotplate (Heidolph MR 3001K, Aldrich, Germany) at a speed of 400 rpm.
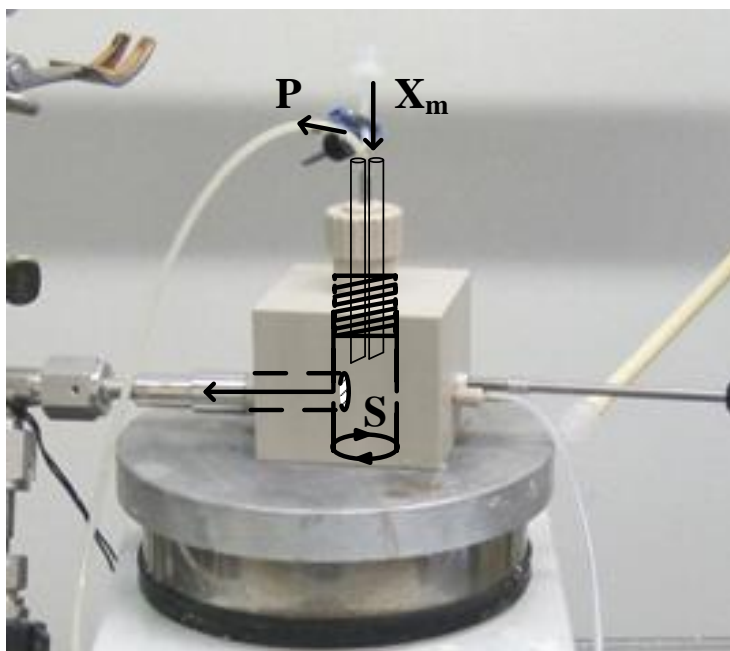


Figure 3.2: A PEEK miniaturized reactor system with the plunger on top. [S] is defined as the substrate(s) that the permeabilized cells metabolize, as [$X_m$] the concentration of permeabilized cells incubating in the mini-reactor and as [P], the various products that are eventually sampled and quantified. On the left side of the reactor the membrane inlet probe can be distinguished, which protrudes into the system. The arrow indicates the movement of gaseous analytes towards the MS. On the right side of the reactor the temperature sensor is inserted into the reactor and the inlet and outlet of the cooling loop can be distinguished.

To achieve sampling without allowing the entry of air into the reactor system, a screw type plunger was developed to act as a sealing cap of the reactor. Two stain-

less steel inlets penetrating the whole length of the plunger were integrated on top of the sealing cap, and their external entry points were attached to 50 mm long silicone tubings. With each 360° counter-clockwise rotation and downward pressure of the plunger, approximately 120 $\mu$L of reactor volume per inlet could be extracted. Usually one of the inlets served for sampling purposes and the other for injecting selectively permeabilized cells into the reactor at the beginning of each experiment. After the injection of cells, one of the inlets was sealed off with a clamp. Harvested cell samples were immediately metabolically inactivated by boiling for 3 minutes. They were then placed in ice for at least 15 minutes and were subsequently centrifuged at 13009 x g (Biofuge Fresco, Heraeus, Hanau, Germany) for 5 minutes. Supernatants were subjected to chromatographic quantification.

## 3.13   Biochemical-Analytical methods

### 3.13.1   Measurement of optical density and CDW-O.D correlation

Cell concentration was determined by measuring the optical density (O.D) of the cell culture at a specific wavelength (595 nm for *S. pombe* and 600 nm for *E. coli*) (Spectrophotometer Novaspec II, Pharmacia Biotech, Little Chalfont, UK). The spectrophotometric measurements were referred to measurements of distillate water at the specified wavelength. The measured range of optical density values that held a linear relationship to the cell concentration values was approximately between 0.05 and 0.3. When the optical density of the cell culture was higher than these values, it had to be accordingly diluted with water. The dilution was carried out in a single use 1.5 mL polystyrene-cuvette (Halbmikro-Plastibrand, Wertheim, Germany) and was always performed in duplicates on the balance (CP225 D, Sartorius, Göttingen, Germany).

Generally, when the optical density of a cell sample is known, a graph of the natural logarithm of it ln(O.D) against time can be plotted, where the slope of the exponential curve represents the growth rate ($\mu$; h$^{-1}$) of the cell culture. On the other hand, the cell dry weight (CDW) could be calculated based on the O.D values as following. A volume of 40 mL was harvested in triplicates from cultures of *S. pombe* cells growing on synthetic medium and for different O.D$_{595nm}$ values. The cell suspensions were centrifuged at 7388 x g and 4 °C for 10 minutes (Biofuge Stratos, Heraeus, Hanau, Germany) and washed twice with ice-cold distilled H$_2$O. Subsequently the cell pellets were left to dry at 80 °C until they reached a constant mass. Subsequently, the accurate mass value for each pellet was estimated gravimetrically (CP225 D, Sartorius, Göttingen, Germany). Results are depicted in Figure 3.3.
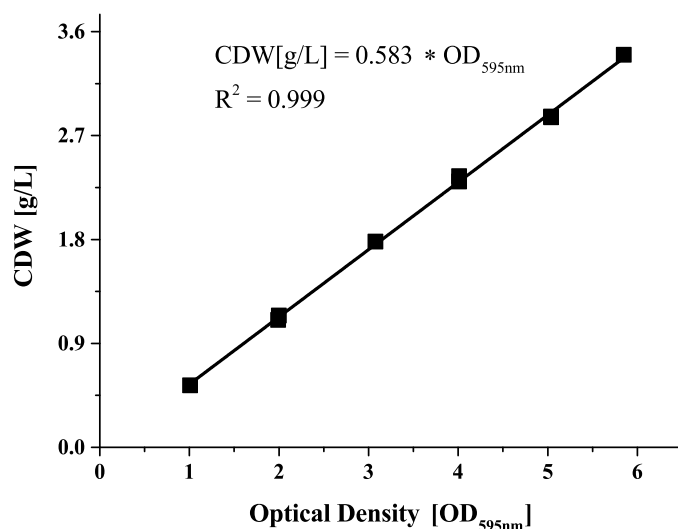
Figure 3.3: CDW (g/L) - O.D$_{595nm}$ correlation expressed as the slope of the curve CDW = $f$(O.D$_{595nm}$). Optical densities were measured separately for each sample that corresponded to the cell dry weight values for each shake flask cultivation on glucose synthetic medium and in parallel.

### 3.13.2   Memrane inlet mass spectrometer (MIMS)

The mass isotopomers for various gas species like oxygen, $CO_2$ and acetaldehyde were quantified dynamically by means of a membrane inlet mass spectrometer (Yang et al., 2006).

As mentioned before, the miniaturized reactor was connected to the MS through an inlet probe containing a semi-permeable membrane (perfluoroalkoxy alkane membrane, 25 $\mu$m, Hach-Lange GmbH, Duesseldorf, Germany). Any gas species would diffuse through the liquid phase of the reactor, sorb into, diffuse and desorb from the membrane on the MS side of the membrane. Gas transfer throughout the membrane is governed by Fick's law that predicts the change of the diffusion of flux of a gas at a steady state, as described by Equation 3.2:

$$J_i = \frac{(D \times A \times \Delta P)}{l} \tag{3.2}$$

with

J$_i$: Diffusion flux of a gas species i throughout a semi-permeable membrane

D: gas diffusion coefficient

A: membrane area

l: membrane thickness or distance

$\Delta$P: partial pressure difference

Generally, the difference of partial pressure at the vacuum MS side is very small, thus gas transfer ($J_i$) throughout the membrane is proportional to the gas concentration at the liquid phase in the well-mixed reactor. Therefore the measured signal intensities by the MS which is generated by differences of the partial pressure of different gas molecules can be directly attributed to gas concentrations in the liquid phase (Beckmann et al., 2009).

The MS operated at 120 °C and consisted of a QMA 400 quadrupole mass filter (Pfeiffer Vacuum GmbH, Asslar, Germany) and a rhenium cathode as the ion source (ionization energy, 70 eV) with a 90° secondary electron multiplier as the detector, set to 1800 V. Vacuum in the MS (working vacuum set between 3.4 - $5\times10^{-8}$ mbar) was achieved with a turbomolecular drag pumping station (TSU 261, Pfeiffer Vacuum GmbH), whereas vacuum in the membrane inlet part was generated by a second turbopump (TMU 064, Pfeiffer Vacuum GmbH). Sufficient vacuum has to be maintained in the MS throughout an analysis in order to prevent any ions generated at the rhenium cathode colliding with adjacent molecules or ions. Therefore pressure was maintained at about $10^{-8}$ mbar in order to ensure a mean free path long enough for the analysis.
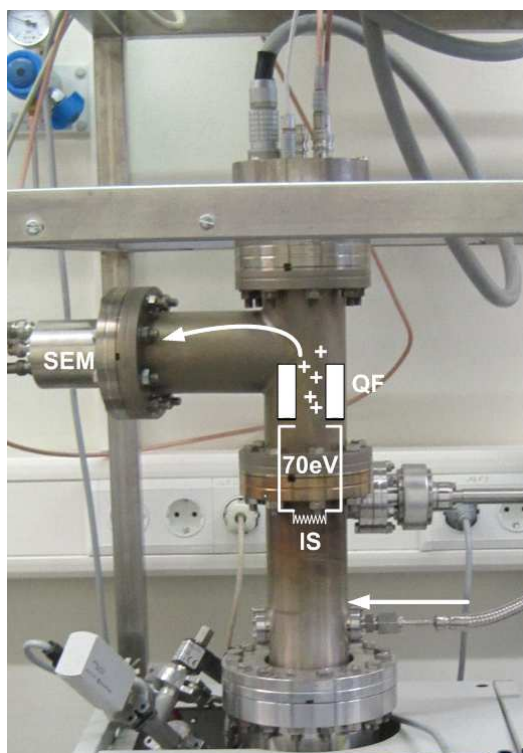


Figure 3.4: The MIMS used throughout the experiments. The arrow on the right indicates the movement of gaseous analytes towards the MIMS from the mini-reactor. The MIMS here consists of the rhenium cathode that functions as the ion source (IS), the quadropole filter (QF) and the secondary electron multiplier (SEM) that acts as detector.

Junction points between the membrane inlet and the two pumping stations consisted of metal vacuum sealings (Swagelok Company, USA) and magnetically controlled valves (DVI 005 M, Pfeiffer Vacuum GmbH). Pressure in the MS was monitored constantly with a dual gauge measurement unit (TPG 262, Pfeiffer Vacuum GmbH). Data acquisition from the MS was performed with the Quadstar 422 software (Pfeiffer Vacuum GmbH).

### 3.13.2.1   Calibrating for $O_2$

For the calibration of $O_2$ at 30 °C a slightly larger version of the aforementioned miniaturized reactor system was used. A certified gas mixture flask (Praxair NV, Oevel, Belgium) was connected via inlet to the head-space of a well-mixed (cross-shaped magnetic impeller fixed at the bottom; rotation speed of 400 rpm) reactor (polyetheretherketone; inner diameter of 30 mm and depth of 35 mm) that was tempered with an integrated cooling loop ($\varnothing$ 3 mm) connected via a peristaltic pump (Alitea-XV, Hüneberg, Switzerland) to a heated circulation bath (MGW Lauda M3, Lauda-Königshofen, Germany). The gas mixture contained a 21 % (v/v) $O_2$ and was continuously blown into the system, thus the physical solubility of $O_2$ in the liquid phase of the reactor while in equilibrium accounted for the concentration of oxygen in the gas flask. Based on Henry's law the saturation concentration of $O_2$ in the reactor ($C_{L,O_2}$) could be calculated as following :

$$P_{L,O_2} = C_{L,O_2} \times k_H \tag{3.3}$$

with

$P_{L,O_2}$: the partial pressure of $O_2$

$k_H$: Henry's coefficient for $O_2$ (856.9 (L×bar)/mol) at 30 °C

Equation 3.3 could be modified into Equation 3.4 by taking into account Raoult's law.

$$C_{L,O_2} = \frac{\left(y_{O_2} \times P_{tot}\right)}{k_H} \tag{3.4}$$

with

$y_{O_2}$: the molar fraction of $O_2$

For a total pressure $P_{tot}$ equal to 1 atm at 30 °C (corrected for the vapor pressure of $H_2O$; $P_{H_2O}$ = 0.042 atm) and for the concentration of $O_2$ in the flask corrected for the abundance of mass isotopomer $^{16}O_2$ ($m_0$ = 0.9951), Equation 3.4 could deter-

mine the concentration of solubilized $O_2$ in the reactor in g/L. When the signal was stabilized after the continuous flux of certified gas mixture into the reactor, the gas was switched to inert $N_2$ and was let to purge all other gas species out of the MIMS until all signals stabilized. The intensity for m/z = 32 under the later conditions would account for the zero point. With these two intensities a two-point calibration curve could be calculated and serve for the calculation of oxygen concentration in the mini-reactor.

### 3.13.2.2 Calibrating for $CO_2$

Before calibrating $CO_2$ it had to be considered that inorganic carbon in a liquid phase is balanced between 4 different forms throughout 3 chemical equilibria, whereas only dissolved $CO_2$ can be detected by the MIMS. Dissolved $CO_{2[aq]}$ in the liquid phase is in equilibrium with $H_2CO_3$ according to reaction 3.5 and subsequently carbonic acid with bicarbonate ($HCO_3^-$) (Reaction 3.6) and $HCO_3^-$ with carbonate ($CO_3^{2-}$) (Reaction 3.7).

$$H_2CO_3 \rightleftharpoons CO_{2[aq]} + H_2O \tag{3.5}$$

$$H_2CO_3 \rightleftharpoons HCO_3^- + H^+ \tag{3.6}$$

$$HCO_3^- \rightleftharpoons CO_3^{2-} + H^+ \tag{3.7}$$
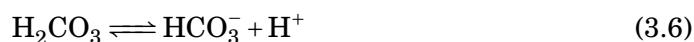
Based on these reactions, the constants for each species could be determined according to Equations 3.8, 3.9 and 3.10.

$$K'_{CO_2[aq]} = \frac{[CO_2]_{[aq]}}{[H_2CO_3]} \tag{3.8}$$

$$K'_{H_2CO_3} = \frac{[HCO_3^-] \times [H^+]}{[H_2CO_3]} \tag{3.9}$$

$$K'_2 = \frac{[CO_3^{2-}] \times [H^+]}{[HCO_3^-]} \tag{3.10}$$

Usually $[CO_{2[aq]}]$ and $[H_2CO_3]$ are represented combined as $[CO_2]$ because at equilibrium only a fraction of 1 % of $CO_2$ exists as the neutral carbonic acid. Therefore it is relevant to describe this relationship with equilibrium 3.11 and Equation 3.12.

$$CO_2 + H_2O \rightleftharpoons HCO_3^- + H^+ \tag{3.11}$$
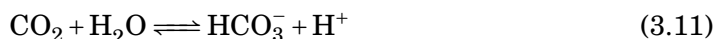
$$[CO_2] = [CO_{2[aq]}] + [H_2CO_3] \tag{3.12}$$

The dissociation constant for equilibrium 3.11 is described by Equation 3.13.

$$K_1' = \frac{[HCO_3^-] \times [H^+]}{[CO_2]} \tag{3.13}$$

Solving Equation 3.13 by combining Equations 3.8, 3.9 and 3.12 and eliminating $H_2CO_3$ generates Equation 3.14.

$$K_1' = \frac{K_{H_2CO_3}'}{K_{CO_{2[aq]}}' + 1} \tag{3.14}$$

Equation 3.14 can be further modified because $K_{CO_{2[aq]}}' \gg 1$, since the value for $K_{CO_{2[aq]}}'$ lies between 350 - 990 at 25 °C. Subsequently Equation 3.15 is generated.

$$K_1' = \frac{K_{H_2CO_3}'}{K_{CO_{2[aq]}}'} \tag{3.15}$$

In the liquid phase of the reactor the total amount of inorganic carbon would be described by the relation:

$$\Sigma CO_2 = [CO_2] + [HCO_3^-] + [CO_3^{2-}] \tag{3.16}$$

By combining Equations 3.16, 3.8 and 3.10 and solving for $[CO_2]$, Equation 3.17 is generated:

$$[CO_2] = \frac{\Sigma CO_2}{1 + \dfrac{K_1'}{[H^+]} + \dfrac{K_1'K_2'}{[H^+]^2}} \tag{3.17}$$

which can be reformulated into Equation 3.18 to take into account the pH of the liquid phase.

$$[CO_2] = \frac{\Sigma CO_2}{1 + \dfrac{K_1'}{10^{-pH}} + \dfrac{K_1'K_2'}{10^{-2pH}}} \tag{3.18}$$

A miniaturized reactor system (see Section 3.12) operating at 30 °C was filled with respiratory buffer (see Section 3.11) containing different concentrations of $K_2CO_3$. When the m/z = 44 signal corresponding to the $m_0$ mass isotopomer for $CO_2$ was stable, then 2 M HCl were added to the reactor causing a rapid decrease of the reactor's pH below a value of 2.0. As a result, all inorganic carbon was released in the form of $CO_2$ which could be detected by the MIMS. The difference between the signals before and after the addition of HCl for $CO_2$ corresponded to

each concentration of $K_2CO_3$. A standard calibration curve is depicted in Figure 3.5.
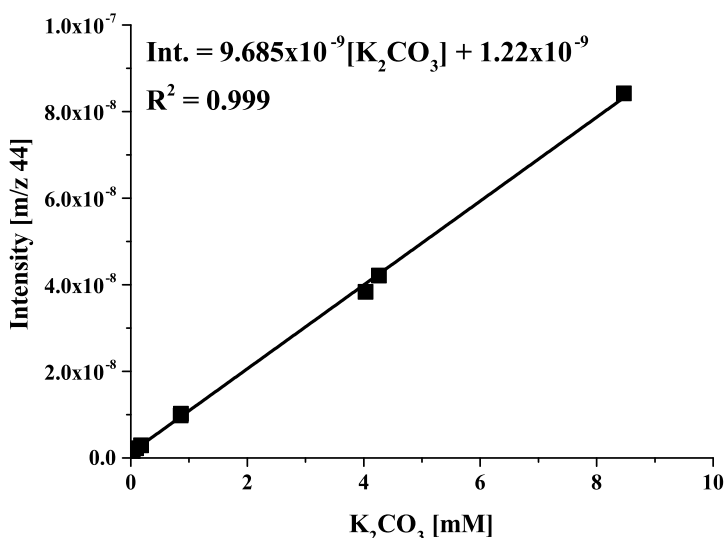


Figure 3.5: Standard calibration curve for the signal measured by the MIMS for each concentration of $K_2CO_3$ added to the reactor and treated with HCl at 30 °C.

Finally as a quality control for the sensitivity and accuracy of the MS, ratios of the measured intensities for the $CO_2$ mass isotopomers ($m/z_{44}$, $m/z_{45}$, $m/z_{46}$) were compared to the theoretical ratios that were calculated. If the difference between the measured and the theoretical ratios was less than 2 %, then the acquisition of experimental values would proceed. The theoretical values of the appropriate mass distribution vector ratios are specified with Equations 3.19 and 3.20.

$$\frac{m/z_{44}}{m/z_{45}} = \frac{^{12}C^{16}O_2}{^{13}C^{16}O_2} = \frac{0.9845}{0.0114} = 86.35 \tag{3.19}$$

$$\frac{m/z_{44}}{m/z_{46}} = \frac{^{12}C^{16}O_2}{^{12}C^{18}O^{16}O} = \frac{0.9845}{0.0041} = 240.12 \tag{3.20}$$

### 3.13.2.3   Calibrating for acetaldehyde

Calibration of a well-mixed, miniaturized reactor system tempered at 30 °C for acetaldehyde was carried out in respiratory buffer with different concentrations of 99.5 % acetaldehyde. The mass isotopomer chosen to be used for the quantification of acetaldehyde was the m/z = 43 that did not coincide with mass isotopomers of other molecules. Also it was experimentally verified that the $m/z_{44}$ mass isotopomer of $CO_2$ was far more abundant than the acetaldehyde molecule with the same mass, thus the presence of acetaldehyde did not interfere with the detection of $CO_2$. A

calibration curve was generated before each experiment, such as the one illustrated in Figure 3.6.
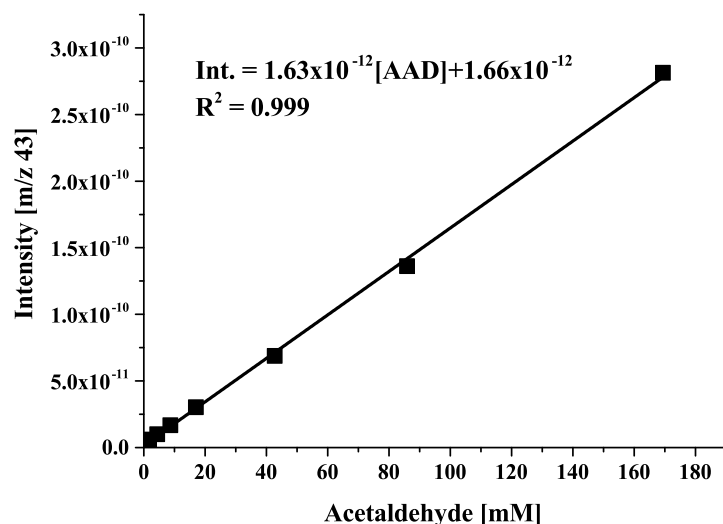


Figure 3.6: Standard calibration curve for the signal measured by the MIMS for each concentration of acetaldehyde (AAD) added to the reactor at 30 °C.

### 3.13.3 Simultaneous quantification of redox precursors, organic acids and adenosine mono-and polyphosphates.

A uHPLC system was used for the separation of various analytes found in the mitochondrial extracts after heat-inactivating selectively permeabilized cell preparations. In particular, mobile phase A consisted of 0.68 g/L TbAS (tetrabutylammonium hydrogensulfate), 1.703 g/L $K_2HPO_4$, 0.031 g/L $KH_2PO_4$, 1 % (v/v) acetonitrile and pH was set at 7.5. Mobile phase B consisted of 0.68 g/L TbAS (tetrabutylammonium hydrogensulfate), 1.703 g/L $K_2HPO_4$, 0.031 g/L $KH_2PO_4$, 40 % (v/v) acetonitrile and pH was set at 7.5.

Samples were placed in a thermostated autosampler (1290 Infinity Autosampler with FC/ALS Therm module, Agilent Technologies, California, USA) and 10 $\mu$L of sample were injected into the system. Separation was achieved through a 150 x 4.6 mm Gemini C18 column (Phenomenex, California, USA) with a 5 $\mu$m pore size, connected to a guard column (SecurityGuard Guard Cartridge System, Phenomenex, California, USA). The column was thermostated at 40 °C (Agilent 1290 TCC) and connected to a binary pump (Agilent 1290 Infinity). The elution program was as follows in Table 3.19. Flow rate was maintained at 1 mL/min and a typical run (Figure 3.7) was concluded after 50 minutes.
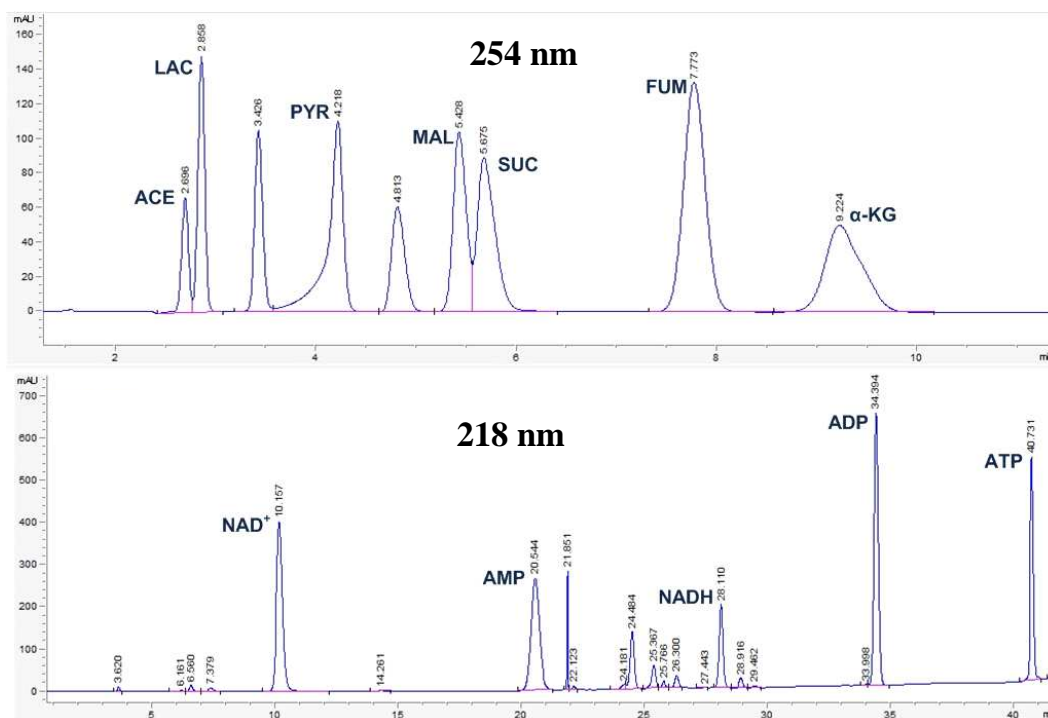
Figure 3.7: Chromatograms for analytes of standard concentrations dissolved in a 16 mM KH$_2$PO$_4$ buffer (pH 6.8) at wavelengths 254 nm and 218 nm. A typical run in the uH-PLC system allowed for separation of organic acids like acetate (ACE), lactate (LAC), pyruvate (PYR), malate (MAL), succinate (SUC), fumarate (FUM), $\alpha$-ketoglutarate ($\alpha$-KG); oxidized (NAD) and reduced (NADH) nicotinamide adenine dinucleotides; AMP, ADP and ATP (A(X)Ps). Organic acids were detected and quantified at 254 nm, redox precursors at 218 nm and A(X)Ps at 254 nm (or at 218 nm).

The thermostability of the analytes illustrated in figure 3.7 was assessed in a 16 mM KH$_2$PO$_4$ buffer, pH 6.8, where aliquotes of standard concentrations were boiled at 100 °C and for various time intervals. Organic acids and A(X)Ps were stable for 3 minutes (equal to the time duration applied for thermally deactivating the metabolism of selectively permeabilized cells). On the other hand NAD and NADH decayed at a steady rate from the initiation of their boiling and these factors were calculated and taken into account for the quantification of samples containing redox precursors.

Table 3.19: Gradient of eluent A and eluent B in the column.

| Time [min] | Eluent A [%] | Eluent B [%] |
|---|---|---|
| 0 | 100 | 0 |
| 10 | 100 | 0 |
| 30 | 70 | 30 |
| 31 | 40 | 60 |
| 37 | 100 | 0 |
| 50 | 100 | 0 |

### 3.13.4   Enzymatic quantification of ethanol

Samples were taken from *S. pombe* cells growing on synthetic medium and the supernatant was isolated in order to quantify ethanol. An ethanol enzymatic kit was employed (R-Biopharm, Darmstadt, Germany). Quantification is based on the enzymatic conversion of ethanol to acetaldehyde by the alcohol dehydrogenase activity (ADH) and of acetaldehyde to acetate by the acetaldehyde dehydrogenase activity (AcDH).

The increasing concentration of NADH, which is produced during both reactions, can be determined by an increase of the absorption at 340 nm. Typically 96-well plates were used. The increase of the absorption at 340 nm was estimated spectrophotometrically over 15 minutes to ascertain that complete ethanol had been quantitatively converted. Each plate contained a set of standards with known ethanol concentrations to determine the ethanol concentration of the samples.

### 3.13.5   Quantification of sugars and organic acids

The quantification of sugars (glucose, glycerol) and organic acids (acetate, pyruvate) from samples corresponding to cultivation supernatants was carried out by high pressure liquid chromatography (HPLC) (Kontron Instruments, Neufahrn, Germany), at 40 °C . The separation was based on each substance's affinity to the stationary phase of the column Aminex$^{TM}$HPX-87H (300 x 7.8 mm) (Biorad, Hercules, CA, USA). The elution was isocratic and the eluent was $H_2SO_4$ (7 mM) at a flow rate of 0.8 mL/min. Detection was determined by UV absorption at 210 nm for organic acids (HPLC 535, Biotek, Neufahrn, Germany). The detection of glucose and glycerine was based on the changes of the refractive index measured by

a RI detector (ERC-7515A, ERC Inc, Altegolfsheim, Regensburg, Germany). When necessary samples had to be diluted to reach the same concentration range as the standards.

### 3.13.6 Quantification of amino acids

The quantification of amino acids was conducted by means of high pressure liquid chromatography (HPLC) (Agilent 1100 Series, Agilent Technologies, Waldbronn, Germany). Supernatants obtained during a cultivation were diluted 1:10 on the balance (CP225 D, Sartorius, Göttingen, Germany) with ABU ($\alpha$-aminobutyric acid, 197.505 $\mu$M), that acted as an internal standard. The separation was carried out by a reversed phase Gemini column (Gemini 5u C18 110Å, 150 x 4,6 mm, Phenomenex, Aschaffenburg, Germany), at an operating temperature of 40 °C and a flow rate of 1 mL/min.

The stationary phase of the system was apolar (a long-chained carbohydrate), whereas the mobile phase was a polar mixture of eluent A containing a 40 mM $NaH_2PO_4$ solution (monohydrate, set pH at 7.8 with NaOH) and eluent B containing methanol, acetonitril and $H_2O$ at a proportion of 45:45:10 (v/v/v).

A gradient of these two eluents was applied to facilitate the separation of the different amino acids according to Table 3.20. Calibration was carried out with external amino acid standards diluted with ABU (1:10) on a scale. The detection of the amino acids was conducted by a fluorescence detector (Agilent, Waldbronn, Germany).

Table 3.20: Gradient of eluent A and eluent B in the column.

| Time [min] | Eluent A [%] | Eluent B [%] |
| --- | --- | --- |
| 0 | 100 | 0 |
| 41.0 | 59 | 41 |
| 46.0 | 19 | 81 |
| 46.5 | 0 | 100 |
| 49.0 | 0 | 100 |
| 49.5 | 100 | 0 |
| 52.0 | 100 | 0 |

The amino acids were subjected to a pre-column derivatisation. During derivatisation the amino acids reacted with ortho-phthaldialdehyde (OPA) and mercaptoethanol, and fluorescent derivatives were produced as illustrated in Figure 3.8. Proline could not be quantified since the OPA reagent reacts only with primary amines and it needed an additional derivatisation step with 9-fluorenylmethoxycarbonyl chloride (FMOC) to be detected by the fluorescence detector (excitation at 266 nm, emission at 305 nm). Also, cysteine and homocysteine form disulfide bonds between thiol-groups and could not be easily derivatized by OPA.

Therefore, prior to the OPA derivatization the disulfide bonds were firstly reduced with 0.5 % 2-mercaptopropionate (in 0.4 M borate buffer) and then re-oxidization was prevented by a capping reaction with iodoacetate (50 g/L iodacetate in 0.4 M borate buffer). Then the derivatized amino acids were detected (excitation at 340 nm, emission at 450 nm). The peaks were manually integrated, and the quantification was carried out based on the dilution factor with ABU and the concentration of the amino acid standards.
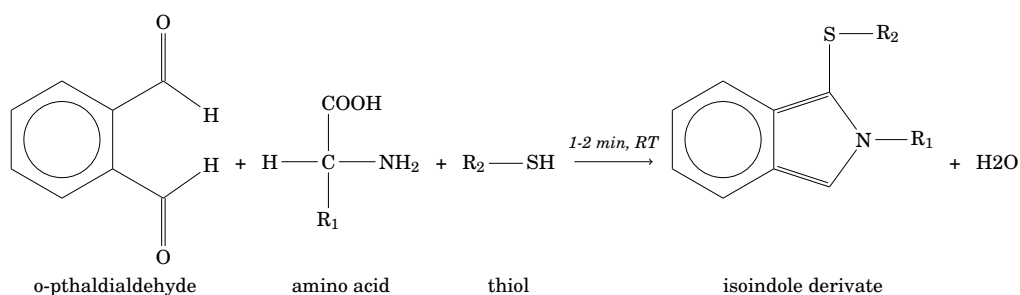


Figure 3.8: Pre-column derivatisation reaction of primary aminoacids with OPA producing fluorescent isoindole derivatives.

## 3.13.7  Total protein hydrolysate amino acid quantification

The amino acid composition of the total cell protein was based on applying different hydrolysis times (Fountoulakis and Lahm, 1998) with 6 M HCl as the hydrolysing agent at 100 °C . Post hydrolysis aminoacids were quantified by means of HPLC as described in Subsection 3.13.6. The residues that were fast cleaved from the total protein could be assessed as well as those that have retained a constant concentration after 24 hours of hydrolysis based on plots of residue concentration against time.

A sufficient number of samples were kept at 100 °C for more than 24 hours, in order to monitor the effect of evaporation on a sample that was kept in a tightly sealed vial.

### 3.13.8   Quantification of free intracellular amino acid pools

Intracellular amino acids were sampled with cold methanol quenching (Bolten and Wittmann, 2008) and quantified as described in Subsection 3.13.6. The quenching solution consisted of 10 mM HEPES, 60 % (v/v) methanol and the pH was set to 7.0. Throughout the process pre-weighed syringes and Falcon tubes were used. During the exponential growth phase at 3 different time points, 5 mL of culture was harvested from duplicate cultivations and added to 50 mL tubes containing 40 mL of the quenching solution (frozen 24 hours before at -80 °C ).

The cells were centrifuged for 7 minutes at 10016 x g (-20 °C, Biofuge Stratos, Heraeus, Hanau, Germany), the supernatant was discarded and the pellet was washed twice with 40 mL of the quenching solution while the tubes were kept in an acetone bath at a temperature of -50 °C . After the washing steps, 2 mL of boiling milliQ $H_2O$ was added to the pellet and the tubes were placed for 15 minutes in a water bath at 100 °C. The Falcon tubes were subsequently set on ice and then weighed (CP225 D, Sartorius, Göttingen, Germany). Finally, the cell extract was centrifuged for 5 minutes at 10016 x g in 15 mL tubes (-20 °C, Biofuge Stratos, Heraeus, Hanau, Germany) and 1 mL of the supernatant was taken for subsequent analysis.

### 3.13.9   Quantification of total lipid content

The estimation of the mass of the total lipids of *S. pombe* cells was based on an extraction protocol by Schneiter and Daum (Schneiter and Daum, 2006). Cells were harvested from parallel cultures during the mid-exponential growth phase in a chemically defined medium. After washing twice with 14 mL $H_2O$ (MilliQ) for 7 minutes (6793 x g, 4 °C, Biofuge Stratos, Heraeus, Hanau, Germany) the cell pellet was resuspended in 28 mL disruption buffer (50 mM sodium citrate tribasic dihydrate, 50 mM sodium phosphate dibasic, 1 M sorbitol, 28 mM $\beta$-mercaptoethanol; pH 5.6) and was incubated for 10 minutes in room temperature. After washing twice with the disruption buffer (7 minutes, 6793 x g, 4 °C, Biofuge Stratos, Heraeus, Hanau, Germany) 28 mL of the zymolyase buffer (1 g/L zymolyase-20T in the disruption buffer) was added to the pellet in order to digest the cell wall. Samples were then incubated for 30 minutes at 30 °C. After centrifuging at low speed (10 minutes, 1698 x g, 4 °C, Biofuge Stratos, Heraeus, Hanau, Germany) the cell pellet was washed twice with ice-cold 1 M sorbitol solution.

In order to achieve cell lysis, 10 mL $H_2O$ (MilliQ) were added to the protoplast pellet, samples were then vortexed and centrifuged for 30 minutes at the highest speed (4 °C, Biofuge Stratos, Heraeus, Hanau, Germany). The supernatant was discarded and 10 mL methanol was added to the pellet which was resuspended and

centrifuged again at the highest speed (4 °C, Biofuge Stratos, Heraeus, Hanau, Germany). Chloroform (20 mL) was added to the methanol-treated pellet to achieve a 2:1 (v/v) of chloroform/methanol ratio and the suspension was transferred to glass flasks and was shaken for 1 hour at room temperature. The extract was then transferred to a 250 mL glass beaker and 10 mL of 0.034 % $MgCl_2$ was added followed by a 10-minute stirring. The extract was transferred to glass vials and centrifuged at 1137 x g (5 minutes, 4 °C, Labofuge 400 R, Thermo Scientific, Germany). The upper aqueous phase was aspirated and the organic phase containing the lipids was washed with 3 mL 2 N KCl/methanol (4:1 (v/v)) and was again centrifuged at 1137 x g (5 minutes, 4 °C, Labofuge 400 R, Thermo Scientific, Germany). The upper aqueous phase was aspirated along with the protein boundary phase that was formed and 3 mL of artificial upper phase (chloroform/methanol/$H_2O$, 3:48:47 (v/v/v)) was added and the extract was centrifuged at 1137 x g (5 minutes, 4 °C, Labofuge 400 R, Thermo Scientific, Germany). The final step of adding 3 mL of artificial upper phase was repeated until all the protein boundary phase was removed and became clear. Finally the organic phase was transferred in a pre-weighed glass beaker and was let to evaporate under a fume hood. Following the complete evaporation of the solvents the mass of the total lipid extract was quantified gravimetrically.

### 3.13.10  Quantification of intracellular *in vivo* carbon fluxes

#### 3.13.10.1  Protein hydrolysis and derivatization for GC/MS quantification

Wild type *S. pombe* cells were grown on chemically defined medium with [1-$^{13}$C]-glucose as the sole carbon source. The starting optical density (measured at 595 nm) of the main culture was between 0.02 - 0.05. The cell biomass in the beginning was low in order to minimize the effect of naturally-labeled carbon stored in the initial population of cells used as inoculum for the main culture. Cells were harvested and centrifuged (5 minutes, 13009 x g, 4 °C, Biofuge Fresco, Heraeus, Hanau, Germany) when they reached their exponential growth phase. Each sample's O.D$_{595nm}$ was determined in order to calculate the CDW.

The cell pellet was washed twice with $H_2O$ (MilliQ) and then the protein hydrolysis was initiated with the application of 6 M HCl at 100 °C for 24 hours. After letting the samples cool down at room temperature, they were neutralized by the addition of 6 M NaOH. Consequently the neutralised samples were filtered (Ultrafree-MC Centrifugal Filter Devices, pore size 0.22 $\mu$m, Amicon, Bioseparations, Bedford, USA) and centrifuged (5 minutes, 13009 x g, 4 °C, Biofuge Fresco, Heraeus, Hanau, Germany) in order to remove cell debris. The hydrolysates were then lyophilised (Lyovac GT2, GEA Lyophil GmbH, Hürth, Germany) overnight and thereafter the derivatization agent was applied. The lyophilized cell extracts were

dissolved in 50 $\mu$L dimethylformamide (DMF) containing 0.1 % pyridine followed by the addition of 50 $\mu$L of the derivatisation agent N-methyl-N-t-butyldimethylsilyl-trifluoroacetamide (MBDSTFA, Macherey and Nagel, Düren, Germany) and incubated for 30 min at 80 °C. The incubation with MBDSTFA led to the silylation of all functional groups ($-OH, -COOH, -NH_2, =NH, -SH$) of proteinogenic amino acids to the corresponding t-butyldimethylsilyl (TBDMS) derivates (Driouch et al., 2012) as it is illustrated in Figure 3.9. The derivates were therefore more stable and volatile, which was important for the subsequent GC/MS analysis.
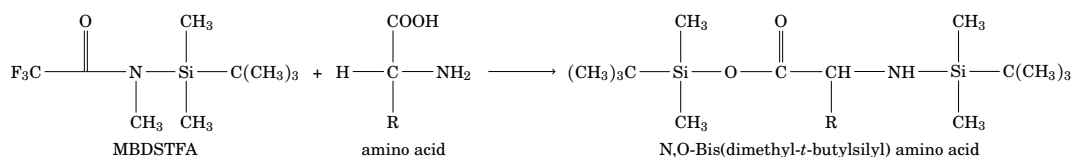


Figure 3.9: Reaction of an amino acid with N-methyl-N-t-butyldimethylsilyltrifluoroacetamide (MBDSTFA) towards the formation of the corresponding t-butyldimethylsilyl (TBDMS) derivate.

The samples containing the derivatives were centrifuged (15 min, 13009 x g, 4 °C, Biofuge Fresco, Heraeus, Hanau, Germany) in order to remove any salts being formed after the neutralisation reaction. The supernatant of each sample was then transferred to a glass vial and was analysed by means of GC/MS.

### 3.13.10.2 Quantification of labeled metabolites by GC/MS

The GC/MS instrument used in the current work was a HP 6890 GC gas chromatographer with a Mass Selective Detector 5973 (Hewlett Packard, Paolo Alto, California, USA). Separation of amino acids was carried out with a 60 m x 0.2 mm I.D. fused silica HP-5ms column (Agilent Technologies, Waldbronn, Germany) and a helium carrier gas flow rate of 0.7 mL/min. The separation in the gas chromatograph was based on the following gradient: 120 °C for 5 min, increase of the temperature at a rate of 4 °C/min until it reached 270 °C and then increase at a rate of 20 °C/min until it reached 320 °C. The inlet had a temperature of 300 °C, whereas the interface and the quadrupole had a temperature of 320 °C. The sample volume injected was always 1 $\mu$L through a split/splitless injector in spitless mode. Full scan mass spectra were generated (30-600 amu) at a speed of 9 scans/second and a -70 eV electron beam was used for electron impact ion formation.

During ionisation in the mass spectrometer, the primary ions generated fragment ions, each one of them possessing a characteristic mass to charge (m/z) ratio. The identification of each amino acid was done according to the retention time during separation and the fragment ions they possessed at SCAN-mode over a mass

to charge region of 150 - 650 m/z. For the calculation of the mass isotopomers of an amino acid, the [M-57]-fragments were measured in the SIM-mode (Selected Ion Monitoring), since these fragments contain the whole of the carbon backbone of the amino acid and have a high intensity. For isoleucine the fragments measured were the [M-159]-fragments, since it was hard to determine from the respective [M-57]-fragments whether they had lost (during ionisation) a butyl group from the amino acid side chain or from the derivatisation reagent, as in both cases the [M-57]-fragments yielded the same mass. The fragments taken into account along with their precursors and the carbon atoms they contain, are summarized in Table 3.21.

Table 3.21: Ion clusters of MBDSTFA-derivatised proteinogenic amino acids along with their biosynthetic precursors and the corresponding carbon atoms that they have in common.

| Monoisotopic m/z | C-atoms | Precursor molecule |
|---|---|---|
| ala260 | 1,2,3 | PYR |
| ala232 | 2,3 | PYR |
| gly246 | 1,2 | G3P |
| val288 | 1,2,3,4,5 | PYR |
| val260 | 2,3,4,5 | PYR |
| ile200 | 2,3,4,5,6 | PYR |
| ser390 | 1,2,3 | G3P |
| ser362 | 2,3 | G3P |
| thr376 | 2,3,4 | OAA |
| thr404 | 1,2,3,4 | OAA |
| phe336 | 1,2,3,4,5,6,7,8,9 | PEP+E4P |
| phe302 | 1,2 | PEP+E4P |
| phe234 | 2,3,4,5,6,7,8,9 | PEP+E4P |
| asp418 | 1,2,3,4 | OAA |
| glu432 | 1,2,3,4,5 | $\alpha$-KG |

### 3.13.10.3   Automatic integration and isotope correction of GC/MS data

The GC/MS data sets that were obtained in SIM-mode, were integrated in order to measure the mass isotopomers of every amino acid and trehalose. The integration was executed by MATLAB (R2010b, R2012b, The MathWorks Inc., Nattick, MA, USA) based programme which was developed by Prof. Elmar Heinzle. Also the measured mass isotopomers were corrected for the occurrence of natural isotopes (Wittmann and Heinzle, 1999; Yang et al., 2009).

### 3.13.10.4   Metabolic flux analysis

In order to quantify the intracellular *in vivo* activities of metabolic pathways, the metabolic flux analysis approach was applied based on $^{13}$C labelling data. The mathematical models describing *S. pombe* metabolism consisted of the glycolysis, the pentose phosphate pathway (PPP), the anaplerotic reactions, the tricarboxylic acid cycle (TCA) and ethanol biosynthesis. Moreover transport reactions between pools in the cytosol and the mitochondria were taken into account. Specifically the transport reactions between the two compartments were those of pyruvate, acetyl-CoA, malic acid and oxaloacetate. Additionally the pathways leading to the formation of pyruvate, ethanol, glycerine and biomass were taken into account.

The mathematical modelling of central metabolism was based on the experimentally assessed mass distribution vectors of proteinogenic amino acids (see Appendix) along with the standard deviation of the measurements. The execution of the modelling process also required as input data the glucose uptake rate and the specific rate for biomass, pyruvate, glycerine and ethanol formation as well as the anabolic demand of metabolic precursors that led to biomass formation.

The anabolic demand of central metabolic precursors for *S. pombe* was based partially on this work as well as on literature data on *S. cerevisiae*. In order to normalise the anabolic demand on glucose uptake, the value of the anabolic demand for metabolic precursors (in mmol$_{precursor}$/g$_{CDW}$) was multiplied with the biomass yield coefficient ($Y_{X/S}$; g$_{CDW}$/mmol$_{glucose}$). The data sets consisting of measured mass distribution vectors from two parallel shake flask cultivations on labeled glucose were combined in order to estimate the carbon fluxes. The metabolic flux analysis was carried out using the software XFluxGate (versions XFG2010 and XFG2016), developed by Tae Hoon Yang (Yang et al., 2008) and executed by MATLAB (R2010b, R2012b, The MathWorks Inc., Nattick, MA, USA). The modelling process employed cumomer balance equations (Wiechert et al., 1999) and a decomposition algorithm based on the elementary metabolite unit (EMU) platform (Antoniewicz et al., 2007) a *S. pombe*-specific metabolic network and a hybrid optimization algorithm that led to the computation of the fluxes after 100 Monte Carlo simulations.

### 3.13.11 Quantification of *in vitro* enzymatic activities

#### 3.13.11.1 Cell disruption

Exponentially growing *S. pombe* cells were harvested ($1x10^8$ cells/mL) and washed twice with milliQ $H_2O$ (5 min, 4 °C, 7388 x g, Biofuge Stratos, Heraeus, Hanau, Germany). The cell pellets were washed twice with ice-cold disruption buffer (100 mM potassium phosphate, 2 mM $MgCl_2$, 1 mM DTT, pH 7.5) and were resuspended in 4 mL/(g wet cell weight) of disruption buffer at the presence of protease inhibitors (1 tablet per 10 mL disruption buffer) (cOmplete mini Protease Inhibitor Coctail, Roche, Mannheim, Germany). Dithiothreitol was always added fresh. Cell extraction was performed on ice in an ultrasonic disintegrator (MSE, Soniprep 150, London, UK) with 6 cycles in total and each cycle consisting of 20 microns amplitude bursts of a 30 seconds duration followed by a minute pause and at the presence of 0.25 - 0.5 mm glass beads. Cell debris were removed by centrifugation (5 min, 4 °C, 7388 x g, Biofuge Stratos, Heraeus, Hanau, Germany) and the supernatant was collected for further analysis of the specific enzymatic activities and for the quantification of the protein content.

#### 3.13.11.2 Protein content quantification

In order to quantify the protein content of the cell extracts on a colorimetric basis, the Bradford Assay was used, with reference to standards of bovine serum albumine (BSA). The quantification was based on the shift of the absorption maximum of the reagent from 465 nm to 595 nm, due to the binding of the Coomasie brilliant blue reagent to proteins in an acidic environment.

The Bradford reagent (phosphoric acid, methanol, Coomassie brilliant blue) obtained from Biorad$^{TM}$ was diluted 1:5 with $H_2O$ and was then used for the protein content quantification. The quantification was performed by mixing 1 mL of the diluted Bradford reagent along with 20 $\mu$L of the diluted cell extract in a 1.5 mL polystyrol cuvette (Halbmikro-Plastibrand, Wertheim, Germany), incubating the mixture for a duration of 20 minutes and measuring the absorption at 595 nm. The photometer used was a Spectronic Unicam Helios $\alpha$ (Spectronic Analytical Instruments, West Yorkshire, UK) and zeroed with blank samples containing milliQ $H_2O$.

#### 3.13.11.3 *In vitro* enzyme activities

The principle of quantifying *in vitro* enzymatic activities lied on the spectrophotometric quantification of the turnover of NAD or NADP to NADH or NADPH respectively at a wavelength of 340 nm and at a temperature of 30 °C. The relative changes of absorption was therefore indicative of the synthesis of reduced or oxi-

dized cofactors. More precisely, based on the Lambert-Beer law the relative change of the concentration of the absorbing species (NAD(P)H) over time would be proportional to the relative change of absorption at a wavelength of 340 nm over time. Thus, Equation 3.21 formulates this proportionality.

All reactions were carried out in a 1 mL final volume at 30 °C with a 50 $\mu$L cell extract being added. When necessary, extracts were diluted with reaction buffer and negative controls were created by substituting either the substrate or the cell extract with $H_2O$ (milliQ). The photometer used was a Spectronic Unicam Helios $\alpha$ (Spectronic Analytical Instruments, West Yorkshire, UK) set at 340 nm and zeroed with blank samples containing $H_2O$ (milliQ).

$$\frac{dA}{dt} = \varepsilon_{NAD(P)H} \times \frac{dC}{dt} \times d \tag{3.21}$$

with

$\frac{dA}{dt}$: the rate of absorption ($s^{-1}$)

$\varepsilon_{NAD(P)H}$: molar extinction coefficient (6.22 L/(cm×mol))

$\frac{dC}{dt}$: the rate of change of concentration (mM/s)

d: cuvette thickness (cm)

### 3.13.11.4  Alcohol dehydrogenase assay

The alcohol dehydrogenase activity catalyses the oxidation of ethanol and the formation of acetaldehyde with the parallel reduction of NAD. The assay was carried out in an appropriate reaction buffer (50 mM Glycine-KOH, pH 9.0) with 100 mM ethanol and 1 mM NAD as the starting substrates (Postma et al., 1989) in a total volume of 1 mL.

### 3.13.11.5  Malic enzyme assay

Malic enzyme catalyses the reverse reaction of malate decarboxylation towards the synthesis of pyruvate with the simultaneous reduction of a redox precursor. Both NAD and NADP were tested for *S. pombe* as reducing equivalents, in order to confirm which redox precursor participated in the reaction. The reaction was carried out in an appropriate buffer (100 mM Tris-HCl, 10 mM $MgCl_2*_6H_2O$, 2 mM NAD or NADP; pH 7.5) and the reaction was initiated with the addition of 20 mM L-malate in a total volume of 1 mL.

### 3.13.11.6 Acetaldehyde dehydrogenase assay

Acetaldehyde dehydrogenase catalyses the oxidation of acetaldehyde to acetate. The reaction was carried out in an appropriate buffer (100 mM potassium phosphate, 15 mM pyrazole, 0.4 mM DTT, 10 mM KCl; pH 8.0) with 100 mM acetaldehyde initiating the reaction (Postma et al., 1989) in a total volume of 1 mL. To measure the activity of both NAD- and NADP-dependent acetaldehyde dehydrogenase isozymes, either 0.4 mM NAD or NADP were used respectively.

### 3.13.11.7 Pyruvate carboxylase assay

Pyruvate carboxylase catalyses the ATP-dependent fixation of $CO_2$ to pyruvate and the formation of oxaloacetate. In order to measure the absorption of NADH photometrically, the pyruvate carboxylase reaction was coupled to the malate dehydrogenase activity. Acetyl-CoA was also present in order to efficiently inhibit any pyruvate dehydrogenase complex activity. The reaction was carried out in an appropriate buffer (100 mM Tris-HCl, 7.5 mM $MgSO_4*_7H_2O$, 0.1 mM Acetyl-CoA, 20 mM $K_2CO_3$, 12 U/ml Malate-DH, 0.15 mM NADH; pH 7.8) and was initiated with the addition of 10 mM pyruvate and 4 mM ATP (de Jong-Gubbels et al., 1996).

## 3.13.12 Measurement of dissolved $O_2$ in shake flasks

In order to quantify dissolved $O_2$ in unbaffled shake flasks, a shake flask reader (Presens GmbH, Regensburg, Germany) was employed that readily fitted in the rotary shaker. Unbaffled flasks contained sensor spots that were fixed at the bottom. The principle of the measurement was that the dye of the spots was excited by the shake flask reader thus the luminescence half-time was detected. The oxygen partial pressure inside the flasks correlated with the luminescence half-time and was converted by the software to [%] dissolved oxygen. Prior to each measurement and for each flask and tray position, a calibration was performed with sodium sulfite. In short, the 100 % dissolved $O_2$ value corresponded to that of the medium used each time and the 0 % dissolved $O_2$ value to that when sodium sulfite was added which exhausted $O_2$ from the medium.

A second parameter needed to be extracted to eventually calculate oxygen concentrations in mol/L was the volumetric mass-transfer coefficient $k_L a$. Oxygen was exhausted from an open 50 mL unbaffled shake flasks in a rotary shaker at 30 °C by using a solution containing 1 % (w/v) sodium sulfite, 0.9 % NaCl, 0.1 mM $CoCl_2 \cdot 6H_2O$ and 0.5 % (v/v) of 1:10 diluted antifoam 289. Dissolved oxygen was continuously measured by a shake flask reader as mentioned above and at different shake speed rates (in rpm). From the increase of dissolved oxygen in such a medium the $k_L a$ was calculated based on Equation 3.22.

$$\frac{d[O_2]_L}{dt} = k_L a \times ([O_2]_L^\star - [O_2]_L) \qquad (3.22)$$

with

$[O_2]_L$: dissolved oxygen concentration (mmol/L)

$[O2]_L^*$: saturated oxygen concentration (mmol/L)

$k_L a$: volumetric mass-transfer coefficient ($h^{-1}$)

Experimental values of dissolved oxygen were used as input data along with Equation 3.22 for simulating and solving for the actual $k_L a$ with the help of the software Berkeley-Madonna based on the best fit of the experimental data on the simulated dynamic evolution of dissolved $O_2$. Finally, for converting dissolved $O_2$ values to oxygen concentration it was assumed that the saturated oxygen concentration at 30 °C was 0.235 mmol/L.

# 3.14 Calculation of physiological parameters

Rates of substrate uptake and product formation (either for intact cells or selectively permeabilized cells), as well as appropriate yields were employed in order to describe and characterize in an absolute quantitative manner a cultivation on minimal medium or the metabolism of respiratory substrates by digitonin-permeabilized cells and draw conclusions upon comparing different strains between them.

## 3.14.1 Specific substrate consumption rate

The specific substrate uptake rate $q_S$ (mmol/(g CDW×h)) was defined as the time related change of the substrate concentration and was calculated by dividing the change of the substrate concentration over time (dS/dt in mmol/(L×h)) by the average biomass concentration (in g/L) according to Equation 3.23.

$$q_S \left( mmol/(g\ CDW {\times} h) \right) = \frac{dS}{dt} \times \frac{1}{X} \qquad (3.23)$$

## 3.14.2 Specific product formation rate

The specific product formation rate $q_P$ (mmol/(g CDW×h)) was defined as the change of the product concentration over time (dP/dt in mmol/(L×h)) and was calculated by dividing this amount by the average biomass concentration (in g/L) according to Equation 3.24.

$$q_P \left( mmol/(g\ CDW {\times} h) \right) = \frac{dP}{dt} \times \frac{1}{X} \qquad (3.24)$$

## 3.14.3 Biomass yield coefficient

The biomass yield coefficient $Y_{X/S}$ (g CDW/mmol), was calculated by dividing the change of the biomass concentration produced (dX/dt in g CDW/(L×h)) by the change of the substrate concentration consumed [dS/dt in mmol/(L×h)) according to Equation 3.25 and graphically illustrated as the slope of the curve $\varphi$ ° in Figure 3.10.

$$Y_{X/S} \left( g\ CDW/mmol \right) = \frac{dX}{dS} \qquad (3.25)$$

## 3.14.4 Product yield coefficient

The product yield coefficient $Y_{P/S}$ (mol/mol), was calculated by dividing the change in product being formed (dP/dt in mmol/(L×h)) by the change in substrate (dS/dt in

mmol/(L×h)) being consumed according to Equation 3.26 and graphically illustrated as the slope of the curve $\vartheta$ ° in Figure 3.10.

$$Y_{P/S}\ (mol/mol) = \frac{dP}{dS} \tag{3.26}$$
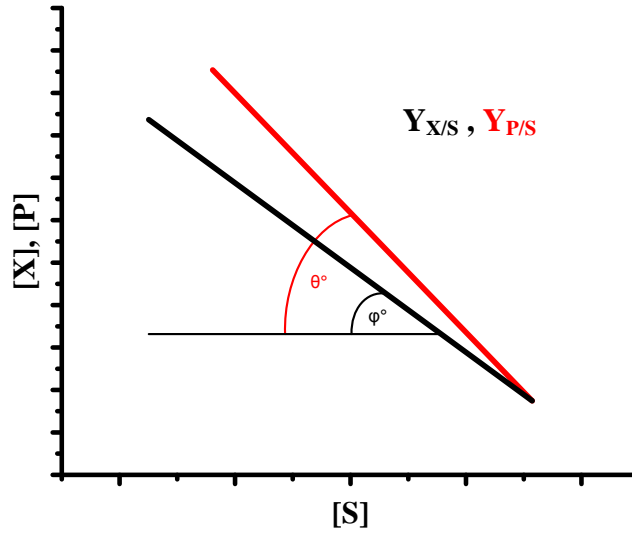


Figure 3.10: Graphical illustration of calculating biomass ($Y_{X/S}$) and product ($Y_{P/S}$) yields during the uptake of substrate [S].

# Chapter 4

# Results and Discussion

## 4.1 Succinate uptake and oxidation in *Schizosaccharomyces pombe* mitochondria

Succinate, as a mitochondrial respiration substrate, was used in conditions where respiration was either activated by ADP or not. In yeast, succinate is transported through the outer and inner mitochondrial membranes where it further serves as a substrate for the succinate dehydrogenase in the mitochondrial matrix. However, up to now no specific mitochondrial transporter has been identified in *S. pombe*.

In general, yeast cells depend on two systems to import succinate. One of them is the dicarboxylate carrier protein (Palmieri et al., 1996), exchanging a dicarboxylate (succinate or malate) for inorganic phosphate, while the other is the succinate-fumarate antiporter (Palmieri et al., 1997). Yeast cells with no succinate-fumarate antiporter or a dicarboxylate carrier are not able to grow on either acetate or ethanol (Fernfindez et al., 1994; Palmieri et al., 1997). It has been reported that mitochondria harvested from *S. pombe* cells grown on glucose are able to oxidize succinate although with a low respiratory control ratio (RCR) (Heslot et al., 1970). Elsewhere it was shown that isolated *S. pombe* mitochondria exhibited no significant increase of the respiration rate when ADP was added in the presence of succinate (Jault et al., 1994). Considerable respiration was only observed when additionally to succinate other carboxylates, like glutamate or pyruvate, where added to the substrate mixture (Labaille et al., 1977; Moore et al., 1992; Jault et al., 1994).

Obviously succinate can be oxidized by *S. pombe* mitochondria *in vivo* but the question remains how this process proceeds *in situ* when succinate is the sole respiratory substrate. In our studies selectively permeabilized *S. pombe* cells were suspended in a suitable buffer in a miniaturized reactor online with a membrane inlet mass spectrometer. This allowed the dynamic quantification of mitochondrial respiration as well as to rapid sampling from the reactor system accompanied by

heat inactivation of the metabolism. We subsequently extended this approach to an open system as well, by employing unbaffled flasks with optical quantification of dissolved oxygen. Samples from both systems were quantified by means of a gradient-elution HPLC method developed for measuring redox cofactors, organic acids and adenosine nucleotides.

### 4.1.1 Selectively permeabilized *S. pombe* cells contain mitochondria that are well coupled and intact

Mitochondria that are prepared for an *in situ* analysis have to retain functionality of their transporter proteins and of the respiratory chain. A first prerequisite towards functional mitochondria is to possess non-damaged outer and inner membranes, where transporters are anchored. The integrity of the mitochondrial membranes was ensured by developing a suitable buffer that was used throughout all respiratory analyses and achieved to mimic the intracellular environment. A quality control for mitochondrial functionality established over 50 years ago is the respiratory control ratio (RCR).

Table 4.1 summarizes various RCR values from a literature meta-analysis for various organisms, isolated mitochondria or selectively permeabilized cells (various permeabilizing agents) and for complex II oxidation.

Table 4.1: Respiratory Control Ratios (RCR) associated with complex II oxidation (succinate as the main respiratory substrate) for a variety of organisms and source of mitochondrial preparations (isolated mitochondria or permeabilized cells). Respiratory substrates: SUC, succinate; GLU, glutamate; ROT, rotenone. IM corresponds to the method of yielding isolated mitochondria and PERM on the one yielding selectively permeabilized cells.

| Organism/Organ | Substrate | RCR | Method | Source |
|---|---|---|---|---|
| *S. pombe* | SUC | 1.80 | IM | (Heslot et al., 1970) |
| *S. carlbergensis* | SUC | 1.40-1.70 | IM | (Ohnishi et al., 1966) |
| *S. pombe* | SUC + GLU | 1.49-2.10 | IM | (Moore et al., 1992) |
| *S. pombe* | SUC | 1.09 | IM | (Jault et al., 1994) |
| *S. pombe* | SUC + PYR | 2.40-3.40 | IM | (Jault et al., 1994) |
| Chick heart | SUC | 2.40 | IM | (Toth et al., 1990) |
| *S. cerevisiae* | SUC | 2.60 | IM | (Pallotta, 2012) |
| Striatal cells | SUC + ROT | 3.20 | PERM | (Milakovic and Johnson, 2005) |
| Potato tubers | SUC | ~4.0 | IM | (Affourtit et al., 2001) |
| Muscle cells | SUC + ROT | ~6.0 | PERM | (Salabei et al., 2014) |

| | | | | |
|---|---|---|---|---|
| *S. cerevisiae* | SUC | 3.34 | PERM | (Avéret et al., 1998) |
| *S. cerevisiae* | SUC | 2.18 | IM | (Avéret et al., 1998) |
| Castor beans | SUC | 2.30 | IM | (Chappell and Beevers, 1983) |
| Mung beans | SUC | 2.0-3.0 | IM | (Phillips and Williams, 1973) |
| Mouse liver | SUC | > 4.5 | IM | (Gonzalvez et al., 2005) |
| *S. cerevisiae* | SUC | 5.10 | IM | (Gonzalvez et al., 2005) |
| Tumor cells | SUC + ROT | 9.60 | IM | (Moreadith and Fiskum, 1984) |
| Tumor cells | SUC + ROT | 7.0 | PERM | (Moreadith and Fiskum, 1984) |
| Rat liver | SUC | 4.2 | IM | (Lemasters et al., 1984) |

The RCR is defined as the ratio of the ADP-stimulated respiration (state 3) to the basal respiration in the absence of ADP (state 4) when one or more oxidative substrates are present and typically it holds a value of at least 2. Illustrated in Figure 4.1 are two typical experiments in the closed reactor system where mitochondria respired significantly faster at the presence of succinate when ADP was additionally present.
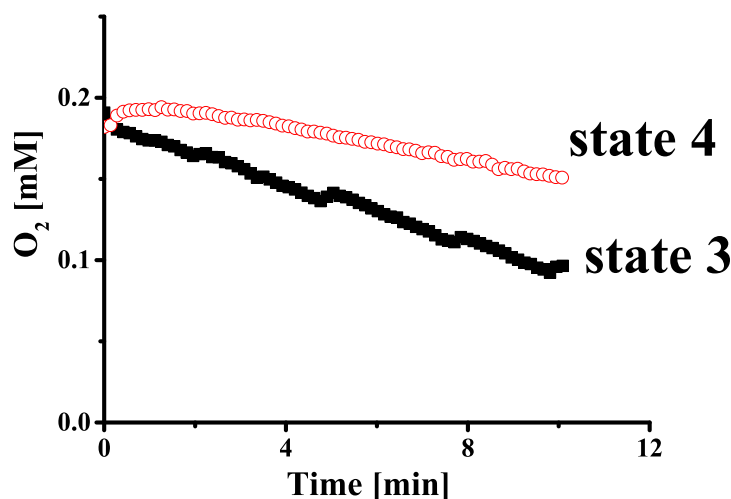


Figure 4.1: Evolution of oxygen concentration versus time in the reactor system for *S. pombe* digitonin-permeabilized cells in the presence of 5 mM succinate in respiratory buffer (pH 6.8) at 30 °C. State 3 respiration (■) was initiated with the addition of 0.5 mM ADP, while there was no ADP present during state 4 respiration (○). Exponentially growing cells were harvested from the same culture and after digitonin-permeabilization they were used at a final reactor concentration of 2.19 g/L (state 3) and 1.88 g/L (state 4).

On average from triplicate experiments for the closed system, state 4 respiration was described by a rate of 0.004 ± 0.001 mM/min (normalized rate equal to 1.37 ± 0.15 nmol/(mg CDW×min)) and state 3 respiration by a rate of 0.011 ± 0.004 mM/min (normalized rate equal to 4.73 ± 0.26 nmol/(mg CDW×min)). In general rates were calculated from the first 4 minutes of respiration where the rate was constant over time. Subsequently, the RCR was calculated from each preparation with or without the addition of ADP to be 3.37. The RCR as the ratio of respiration rates expressed in mM/min is a dimensionless number. When comparing the RCR value acquired by experiments in the closed reactor to the values indicated in Table 4.1 for succinate oxidation, it is apparent that the quality of mitochondria yielded was high in terms of functionality and membrane integrity.

In order to further strengthen our findings another quality control was applied to examine the intactness of *S. pombe* mitochondria after digitonin-permeabilization. A saturating concentration of cytochrome $c$ (10 $\mu$M) was added to mitochondria that were oxidizing succinate in the presence of ADP. In the case that the external mitochondrial membrane was damaged from either a harsh permeabilization process or the usage of an unsuitable respiration buffer, the oxygen uptake would increase upon the addition of cytochrome $c$. Mitochondria with damaged outer mitochondrial membranes exhibit leakage of cytochrome $c$ from the mitochondrial intermembrane space and as a direct result thereof a decreased respiratory capacity compared to structurally intact mitochondria. Both the RCR and the use of cytochrome $c$ are controls of the permeabilization method that are integral for establishing the quality of the subsequent analysis of mitochondrial function.

Permeabilized cells treated with cytochrome $c$ in the closed reactor system exhibited a respiration rate of 0.011 ± 0.000 mM/min. Mitochondrial preparations yielded from the same cell cultures and at comparable cell concentrations without the addition of cytochrome $c$ were characterized by a respiration rate of 0.010 ± 0.000 mM/min. The difference in the respiration rates of 7.6 % with and without the addition of cytochrome $c$ accounts for a loss of mitochondrial integrity during the permeabilization procedure which is minimal and similar to that of isolated *S. pombe* mitochondria as described in the literature (Moore et al., 1992).

### 4.1.2 Adenosine nucleotide dynamics in a closed and an open system

Up to now in this study all experimental results concerning the qualitative control of intactness of mitochondria were generated in the closed reactor system. However the mitochondrial uptake of succinate and the formation of energy in the form of ATP were studied in two systems: a closed reactor and an open system. Both

functioned complementary to each other for extracting physiological information from respiring mitochondria. In the closed, sealed system the gas phase was absent and in the unsealed, unbaffled flask, namely the open system, oxygen diffused freely from the gas to the liquid phase.

A typical experiment, regardless of the system used, consisted of adding between 7-12 mg of digitonin-permeabilized cells to the respiration buffer which contained 5 mM succinate and 0.5 mM ADP. In order to attribute any ATP produced to the mitochondrial activity of ATP synthase solely (Avéret et al., 1998) (Kawamata et al., 2010), Ap5A (P1,P5-di(adenosine-5')pentaphosphate) was present at a 1:50 ratio to ADP (Ap5A : ADP) (Feldhaus et al., 1975) (Clémençon et al., 2011) in order to abolish any adenylate kinase activity that is located in the mitochondrial intermembrane space (IMS). It was validated that selectively permeabilized cells at the presence of only ADP and Ap5A, did neither respire nor synthesize ATP, confirming that the adenylate kinase, located at the IMS, was inhibited. Furthermore, in the presence of ADP solely, no hydrolysis of this adenosine nucleotide took place towards the formation of AMP.

A series of experiments with the miniaturized reactor were performed for a longer period until $O_2$ was exhausted. Here, samples were rapidly spun down at a low speed (799 x g, 4 °C) (Figures 4.2.A, C & E) to separate permeabilized cells from supernatants without damaging the mitochondria. In this case, adenosine nucleotides exclusively stemmed from the extramitochondrial space. In the experiments of Figures 4.2.B, D & F, metabolism was inactivated after sampling by heat and then the samples were centrifuged. The adenosine species quantified represented the total pool of adenosine nucleotides (A(X)P) in the mitochondria and in the extramitochondrial space. In all experiments involving the closed reactor, where a gas phase did not exist, the concentration of dissolved oxygen could be directly measured via the membrane inlet mass spectrometer (MIMS) by recording the intensity of the m/z=32 isotopomer over time.

As illustrated in Figures 4.2.A & B for the closed reactor system, ADP and $O_2$ were consumed and ATP was produced in both cases as long as $O_2$ was available. Mitochondrial metabolism operated at steady state as can be concluded from the linear relationship (Figure 4.2.D) between ATP, ADP and oxygen concentrations in the case where oxygen was not limiting (Deshpande et al., 2009). Steady state kinetics were also observed for extramitochondrial ATP at an oxygen concentration between 0.05 and 0.15 mM in the series of experiments where oxygen was eventually exhausted. The relation between extramitochondrial ADP and oxygen was not linear. An initial faster decrease at high oxygen concentration could be caused by an initial accumulation of ADP in the mitochondrial matrix. In such a closed system, after a period of time the adenosine nucleotide pools entered a stationary

phase, even when oxygen continued to be consumed at a steady rate until exhausted (Figure 4.2.C) after 20-25 minutes. During the short duration experiment (without $O_2$ exhaustion) in the closed reactor the steady state rates of ADP elimination and ATP accumulation as well as the yields of ADP and ATP to $O_2$ consumed could be graphically calculated (Figures 4.2.C & D). The $Y_{ADP/O_2}$ was equal to 1.04 ± 0.20 mol/mol and the $Y_{ATP/O_2}$ was equal to 1.12 ± 0.04 mol/mol. Accordingly, the net ADP elimination rate was calculated to be 0.008 ± 0.003 mM/min (5.05 ± 0.92 nmol/(mg CDW×min)) and the net ATP formation rate was 0.009 ± 0.000 mM/min (5.4 ± 0.14 nmol/(mg CDW×min)).
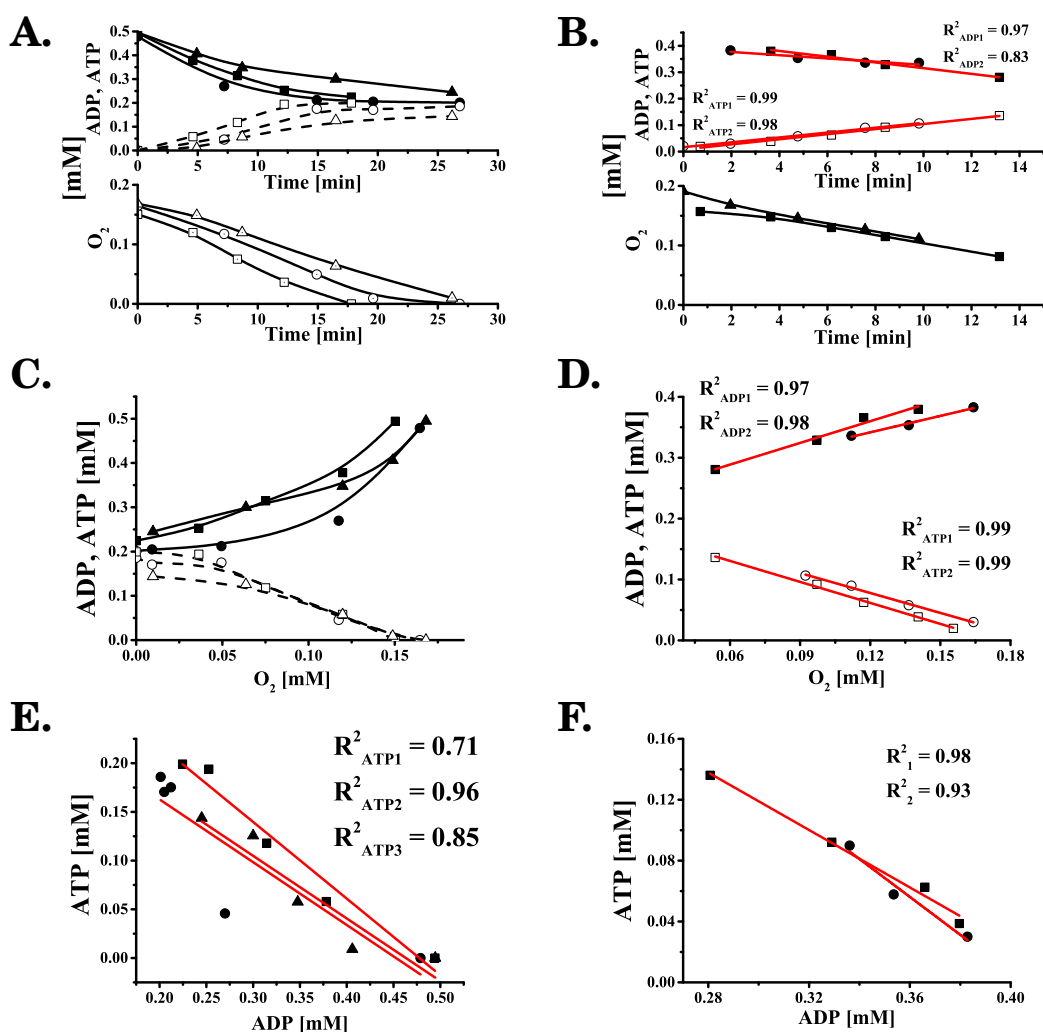
Figure 4.2: Oxidative phosphorylation with succinate (5 mM) as a substrate for experiments conducted in the closed reactor system with and without the eventual exhaustion of oxygen upon addition of succinate (5 mM) and ADP (0.5 mM) to digitonin-permeabilized cells at 30 °C. Experiment with eventual exhaustion of oxygen [A]. Points represent ADP and ATP pools of extra-mitochondrial origin. ADP ((■), (♦) and (▲)) and ATP concentrations ((□), (◊) and (△)) represented as a function of time for three independent experiments. Average cell concentration = $2.38 \pm 0.20$ g/L. Experiment [B] with state-3 repiration prior to oxygen depletion. ADP ((■) and (•)) and ATP concentrations ((□) and (○)) as a function of time for two independent experiments. Samples represent total (intra-and extra-mitochondrial) pools of ATP and ADP yielded by heat-inactivated whole suspensions. Yield plot [C] using data of [A]. Yield plot [D] using data of [B]. Ratio [E] of the concentration of ATP to ADP for data from [A] ((■), (•) and (▲)). Ratio [F] of the concentration of ATP to ADP for data from [B] ((■) and (•)). Average cell concentration = $1.43 \pm 0.14$ g/L. Red line indicates each curve of the regression analysis along with the $R^2$.

Another characteristic that could be described concerns the overall ATP to ADP stoichiometry which also entails the phosphorylation of ADP towards ATP during state 3 respiration by the mitochondrial ATP synthase. Any mitochondrial Sal1p activity, catalyzing the transport of ATP and to some extent of ADP, could be ig-

nored since its activity is highly dependent on the presence of $Ca^{2+}$ (Traba et al., 2008). In the respiratory buffer used here, $Ca^{2+}$ was not added. Instead EGTA was present, which as a strong chelating agent can complex with $Ca^{2+}$ and can inhibit the ATP-Mg/Pi carrier (Joyalt and Aprilles, 1992). Therefore the transport of adenosine nucleotides in and out of the mitochondria could be attributed solely on the adenine nucleotide translocator (ANT), which is docked on the inner mitochondrial membrane. In the initial experiments with the miniaturized reactor, where oxygen was finally exhausted, ATP/ADP ratios of 0.69 ± 0.08 mol/mol where obtained (Figure 4.2.E). The same ratio (ATP/ADP) for the steady state system corresponded to the sum of the intra- and extramitochondrial pool and was equal to 1.09 ± 0.21 mol/mol which was very close to the 1:1 stoichiometry between adenosine nucleotides as expected (Vignais, 1976; Klingenberg, 2008). The difference between the extramitochondrial ATP/ADP from the total ATP/ADP ratio and the deviation of the former from the 1:1 stoichiometry was most likely caused by the accumulation of ADP in the mitochondria. Therefore in subsequent experiments thermal inactivation of the metabolism post-sampling was preferred as it yielded qualitatively better results, e.g. a linear relation between nucleotides and oxygen, with higher accuracy and smaller standard deviations.

Both adenosine nucleotides (ADP and ATP) leveled off and ADP was not completely exhausted by respiring mitochondria. The question arose whether these observations could be replicated or not in a system where oxygen supply would not be limiting as in the closed reactor system. Would the yield of adenosine nucleotides on oxygen change or remain the same?
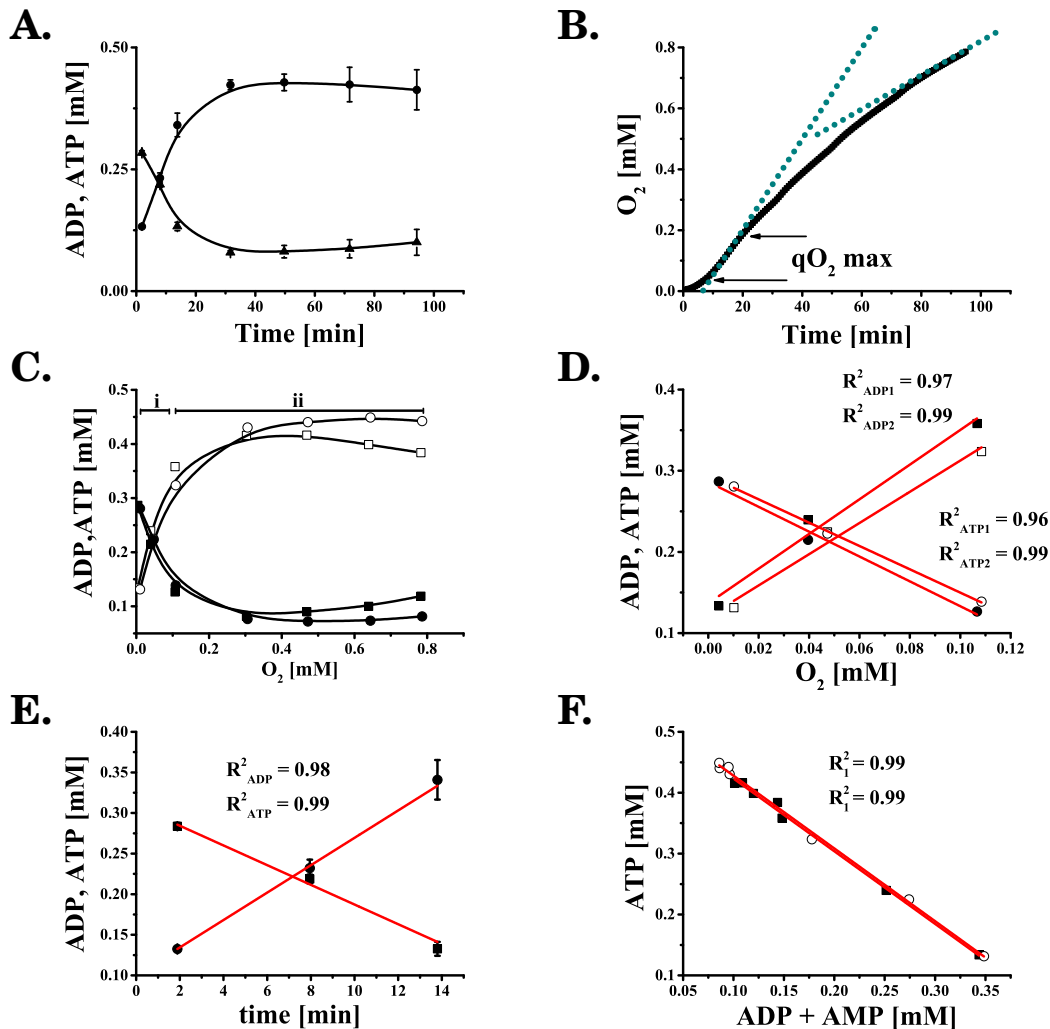
Figure 4.3: Oxidative phosphorylation with succinate (5 mM) as a substrate for experiments conducted in the open system with a continuous supply of oxygen upon addition of succinate (5 mM) and ADP (0.5 mM) to digitonin-permeabilized cells at 30 °C. Average concentrations of ADP (▲) and ATP (•) [A] represented as a function of time for two independent experiments over time. Evolution [B] of integrated oxygen consumption over time (■) for two independent experiments. Blue dotted lines represent calculated respiration rates for the time duration where they are linear and identical to the actual curve. Yield plot [C] using data of [A] and [B] for ATP ((□) and (○)) and ADP ((■) and (•)) for phases (i) and (ii). Yield plot [D] using data of phase (i) from [C] for ADP ((■) and (□)) and ATP ((•) and (○)). Evolution [E] of average concentration of ATP (■) and ADP (•) over time for phase (i) from [C]. Ratio [F] of the concentration of ATP to the sum of ADP and AMP ((■) and (•)). Average cell concentration = $1.58 \pm 0.06$ g/L. Red line indicates each curve of the regression analysis along with the $R^2$.

Therefore identical experiments as in the closed reactor were repeated in an open system, i.e. a shake flask, where oxygen was constantly supplied. Both adenosine nucleotides, ADP and ATP, were initially changing proportionally to the oxygen consumed but eventually leveled off (Figures 4.3.A & C). The one defined as phase (i) (Figure 4.3.D) was characterized from the net ATP formation and ADP elimina-

tion respectively being linearly proportional to oxygen consumption. The rates of ADP elimination and ATP formation where calculated from the steady state curves of phase (i) (Figure 4.3.C) and where equal to 0.013 ± 0.001 mM/min (specific rate equal to 7.8 ± 0.71 nmol/(mg CDW×min) when normalized for the cell concentration in the flask) and to 0.017 ± 0.002 mM/min (specific rate equal to 10.75 ± 1.20 nmol/(mg CDW×min)) respectively. Oxygen uptake initially lagged as illustrated in Figure 4.3.B, and then obtained a maximum consumption rate which was constant for the 10-20 minutes time frame as calculated from the regression analysis of the curve (dashed line, $R^2$ = 0.996).

The maximum oxygen uptake rate ($q_{O_2,max}$) was 0.013 ± 0.001 mM/min and the specific rate when normalized for the cell concentration in the flasks was equal to 8.05 ± 0.15 nmol/(mg CDW×min) for parallel experiments. Oxygen is illustrated graphically as a quantity that seems to accumulate over time instead of being up-taken but this is only due to the fact that it derives from the integration of the experimentally measured oxygen uptake rate ($\int$OUR). During the phase where the concentrations of ADP and ATP changed proportionally to oxygen, the $Y_{ADP/O_2}$ and $Y_{ATP/O_2}$ where determined graphically as illustrated in Figure 4.3.D. The $Y_{ADP/O_2}$ was equal to 1.48 ± 0.07 mol/mol and the $Y_{ATP/O_2}$ was equal to 2.03 ± 0.15 mol/mol.

From the above it was evident that when the net synthesis of ATP and the net elimination of ADP reached their maximum rates, the calculated oxygen uptake rate ($q_{O_2,max}$) reached also its highest value. Phase (i) coincided with state 3 respiration where both the respiratory chain and the ATP synthase functioned in their maximum capacity. The open system shared a common characteristic with the closed system, with the net pools of ADP and ATP gradually leveled off even with continuous $O_2$ consumption. This phase (ii) was also characterized by decreasing oxygen consumption rates. In the end of the experiments in the open system (Figure 4.3.B) the calculated oxygen consumption rate was reduced 2.23-fold compared to the maximum rate it reached during state 3 (phase (i)). Combining these results it can be easily shown that mitochondria gradually switched from state 3 respiration to uncoupled state 4 respiration, with lower oxygen consumption rates and subsequently lower rates for the mitochondrial metabolism of adenosine nucleotides.

For both the closed and the open system, the fact that adenosine nucleotide pools reached a stationary phase was attributed to ATP-utilizing enzymatic activities outside of the mitochondria. In such a scenario, ATP could be potentially hydrolysed by two categories of enzymes, ATPases and apyrases (Komoszynski and Wojtczak, 1996). The ATPase enzymatic activity (EC 3.6.1.3), which targets ATP with high specificity, hydrolyses it into ADP and orthophosphate. The other category of enzymes, that of apyrases (EC 3.6.1.5), can hydrolyse ATP or ADP towards AMP and orthophosphate. Experiments with digitonin-permeabilized cells in the presence

of ADP or ATP solely, exhibited no ADP degradation (no presence of AMP) for the former, whereas ATP alone could be hydrolysed to ADP. Such ATPase and apyrase activities could be at a degree part of a substrate cycle along with the ATP synthase of the mitochondrial matrix. ATP could serve as a substrate for the ATPase in the cytosol and re-feed ADP to the adenosine nucleotide translocator (ANT) therefore explaining why adenosine nucleotide pools eventually reached constant levels.

The mitochondrial ATP synthase could not reverse its activity and hydrolyse ATP instead of phosphorylating ADP. Normally such an event is accompanied by the inability of mitochondria to respire (Metelkin et al., 2009), which was not the case for ADP-energized permeabilized cells respiring on succinate in the closed or the open system. In the open system, the ATP to ADP ratio of 1.38 ± 0.04 mol/mol indicated that the net synthesis of ATP exceeded the 1:1 stoichiometry. Closer examination revealed that AMP was present in the initially obtained samples at a concentration equivalent to 11.9 % of the total concentration of adenosine nucleotides (AXN) and was subsequently eliminated at levels below the detection limit (5 $\mu$M). This amount of AMP could not have originated from the cytosol, since cells were washed after permeabilization, thus eliminating such a source. Nevertheless, when correcting for the aforementioned amount of AMP, the ATP/(sum of AMP and ADP) ratio during state 3 respiration was 1.19 ± 0.001. This ratio is statistically identical to the ADP/ATP ratio yielded from the closed system during state 3 respiration, where no AMP was detected. The source of AMP in these initial samples could not have been the adenylate kinase residing in the IMS, since it was inhibited by the Ap5A.

Previously, yields of the adenosine nucleotides on consumed oxygen where calculated for both the open and the closed system. From the $Y_{ATP/O_2}$, we can calculate the P/O ratio as the amount of ATP synthesized by the ATP synthase per unit of oxygen. The P/O ratio for the reactor was 0.56 ± 0.021, whereas the P/O ratio of the open system was 1.01 ± 0.008. The theoretical, mechanistic P/O ratio on succinate is calculated based on the following assumptions that are common for *S. cerevisiae* and *S. pombe*. Firstly it is assumed that the ATP synthase is pumping 10 protons for each 3 ATP molecules (10/3 H$^+$/ATP) synthesized (Hinkle, 2005; Ferguson, 2010) based on one rotation of the $C_{10}$-ring rotor of the yeast ATP synthase. Secondly that only complexes III (2 H$^+$) and IV (4 H$^+$) are pumping protons (6 H$^+$/2e$^-$ = H$^+$/O). Thirdly, that the transfer of ATP to the cytosol except for the exchange of ATP for ADP by the ANT, also demands an additional proton due to the symport of a phosphate and a proton by the mitochondrial phospate carrier into the mitochondrial matrix. Therefore the theoretical P/O for *S. pombe* respiring on succinate would be 6/[10/(3+1)] $\simeq$ 1.38, thus lower than the P/O ratio for mammalian mitochondria which is $\simeq$ 1.64 (Watt et al., 2010).

Our experimentally calculated P/O ratios were significantly lower than the theoretical stoichiometry which links mitochondrial ATP synthesis to the amount of oxygen consumed from the respiratory chain. The activity of ATP hydrolysing enzymes in the extramitochondrial space and the fact that the ADP was never totally exhausted by the mitochondria led us to the conclusion that the P/O ratio inferred experimentally was other than the mechanistic ratio of phosphorylating mitochondria, therefore any comparison would be pointless. The limitation of not being able to calculate the P/O when ADP is not being completely consumed by selectively permeabilized cells has been an issue previously described as well (Salabei et al., 2014). Also the issue of competing activities for ATP and ADP outside of the mitochondria has been raised in the past as well with Kawamata (Kawamata et al., 2010) arguing that the use of selectively permeabilized cells may entail exactly this caveat compared to isolated mitochondria, due to the activity of $Na^+/K^+$ ATPases, endoplasmic $Ca^{2+}$ ATPases, phosphorylases, phosphatases and kinases. The possibility of our mitochondrial preparations containing dysfunctional respiratory chains or damaged membranes causing a drop in the P/O was excluded due to the high RCR values obtained and the impermeability of cytochrome *c* to the IMS.

### 4.1.3 Succinate uptake and its metabolism from mitochondria

During the ADP-driven oxidation of succinate there is a cascade of events that are triggered by the entry of this dicarboxylate into the mitochondrial matrix where the succinate dehydrogenase resides. Therefore it is important to quantify dynamically not only the uptake of succinate but also to determine which TCA cycle steps are further activated. By identifying products of the succinate metabolism we can verify which enzymatic activities participate and to which extent. Another point of interest is whether and in which degree the substrate's entry and flow in the mitochondria are connected to oxidative phosphorylation.

We were not able to quantify succinate uptake in the closed system due to the short exposure time with associated low conversions. During this time the relative difference of succinate concentration was too small to allow a meaningful calculation of the specific uptake rate of succinate. This limitation was overcome by quantifying succinate in the open system, where typically an experiment had a duration of 90 minutes. In this system succinate, fumarate and malate were quantified simultaneously. When oxidative phosphorylation was active, succinate entered into the mitochondrial matrix and was oxidized by the membrane-bound succinate dehydrogenase. At the same time fumarate was synthesized and subsequently malate.
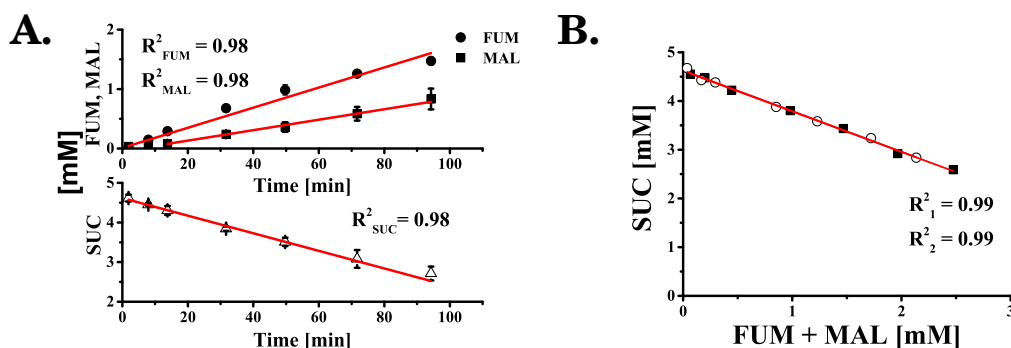
Figure 4.4: Evolution [A] of average concentration of fumarate (•), malate (■) and succinate (△). Ratio [B] of the concentration of succinate to the sum of fumarate and malate for two independent experiments ((■) and (○)). Average cell concentration = 1.58 ± 0.06 g/L. Red line indicates each curve of the regression analysis along with the $R^2$.

As illustrated in Figure 4.3.B, oxygen uptake rate reached its maximum at about 20 minutes while the pool size of ATP reached a constant value. During the whole period of sampling (90 minutes) the succinate uptake rate (Figure 4.4.A, empty triangle), was 0.021 ± 0.002 mM/min (specific succinate uptake rate equal to $q_{SUC}$ = 13.07 ± 0.59 nmol/(mg CDW×min)). Accordingly, for the same time period the fumarate synthesis rate was 0.016 ± 0.000 mM/min (specific fumarate production rate equal to $q_{FUM}$ = 10.2 ± 0.14 nmol/(mg CDW×min)) as illustrated in Figure 4.4.A (filled circle). In the beginning, malate concentrations were below the detection limit (50 $\mu$M) due to the necessary compromise of diluting (1:5) the samples that were obtained. Malate concentration started to rise after about 10 min (Figure 4.4.A, filled square). The rate of malate formation was 0.010 ± 0.002 mM/min (specific malate production rate equal to $q_{MAL}$ = 6.06 ± 1.19 nmol/(mg CDW×min)). Plotting the concentration of succinate versus the sum of malate and fumarate resulted in a linear relationship (Figure 4.4.B) between them.

The molar yield was calculated from the slope of the linear regression from the plot of Figure 4.4.B and was equal to 0.834 ± 0.003 mol/mol. This value was clearly below the 1:1 molar ratio that was theoretically expected between succinate as a substrate and the sum of its products, fumarate and malate. An explanation for this would be that succinate accumulated in the IMS prior to its transfer through the IMM and to the succinate dehydrogenase activity in the mitochondrial matrix. Furthermore, malate was considered to be the end product of the oxidation of succinate in the mitochondrial matrix. In principle malate could be used as a substrate for the formation of oxaloacetate. This could be possible if a catalytic amount of NAD was present intramitochondrially but it would lead to the decline of the uptake/elimination rate of succinate during malate formation since oxaloacetate is a potent inhibitor of the succinate dehydrogenase (Huang et al., 2006). There are examples of adding glutamate to isolated *S. pombe* mitochondria while having suc-

cinate present, in order to remove oxaloacetate from the system (Moore et al., 1992) and to protect the activity of the succinate dehydrogenase. However in our system, after heating the extracts post-sampling the amount of oxaloacetate present would be converted to pyruvate. We could not detect any pyruvate under the current conditions although the theoretical amount of oxaloacetate converted to pyruvate in the samples would be over the detection limit for pyruvate (10 $\mu$M).

Based on the data available, we cannot localize whether malate synthesis by fumarase took place either in the mitochondrial matrix and/or the cytosol. It was verified that both malate and fumarate were present in the extra-mitochondrial space from samples where mitochondria were separated from the supernatant without applying heat-inactivation after sampling. Therefore either malate or fumarate had to be transported out of the mitochondrial matrix to serve as substrates for the fumarase. One of these carboxylic acids had to be present in the cytosol as we confirmed that malate and fumarate where interconverted to each other when added separately to selectively permeabilized cells. Also such a scenario would further support the molar ratio of succinate to the sum of fumarate and malate being <1.

### 4.1.4 Succinate is transported actively into the mitochondrial matrix

To test the hypothesis whether the transport of succinate is governed by a mitochondrial transporter or not, succinate uptake was monitored in the open system with phenylsuccinate present along with succinate in equimolar quantities. Phenylsuccinate is a dicarboxylate structural analogue of succinate and a competitive inhibitor of succinate transporters from mammalian cells to yeast. It has an inhibitory effect on succinate transporters of rat liver cells (Palmieri et al., 1971), on the *S. cerevisiae* dicarboxylate carrier protein (Lançar-Benba et al., 1996; Palmieri et al., 1996) and the *S. cerevisiae* succinate-fumarate antiporter (Palmieri et al., 1997). Additionally, phenylsuccinate does not permeate the inner mitochondrial membrane and cannot act as a substrate of the succinate dehydrogenase (Phillips and Williams, 1973).

As illustrated in Figures 4.5.A & B, there was a 35 % inhibition of succinate elimination ($q_{SUC,PHESUC}$ = 0.013 ± 0.003 mM/min), namely of succinate uptake and a 51 % decrease of the oxygen uptake rate ($q_{O_2,PHESUC}$ = 0.006 ± 0.002 mM/min). In Figure 4.5.B the dashed blue lines for both experiments represent the slope of the line from which the maximum oxygen uptake rates were determined ($qO_2$ max). These rates were used for the comparison to the maximum respiration rates for experiments in the open system without the addition of the inhibitor phenylsuccinate. Inhibiting the transport of succinate into the mitochondria reduced oxygen uptake due to the lower availability of $FADH_2$ being produced by the succinate dehydroge-

nase.

Net fumarate and malate formation in both compartments (cytosol and mitochondrial matrix) was also decreased compared to the non inhibited mitochondrial preparations that were yielded by identical cultures. Net fumarate formation was reduced by an average of 38 % compared to the non-inhibited system. Malate begun to be detectable in the samples (detection limit: 50 $\mu$M) after a duration of 30 min of selectively permeabilized cells respiring on succinate. The high degree of inhibition that phenylsuccinate introduced to the metabolism and oxidation of succinate by the permeabilized cells, could only be possible if succinate was transferred actively by a carrier protein to the mitochondrial matrix.
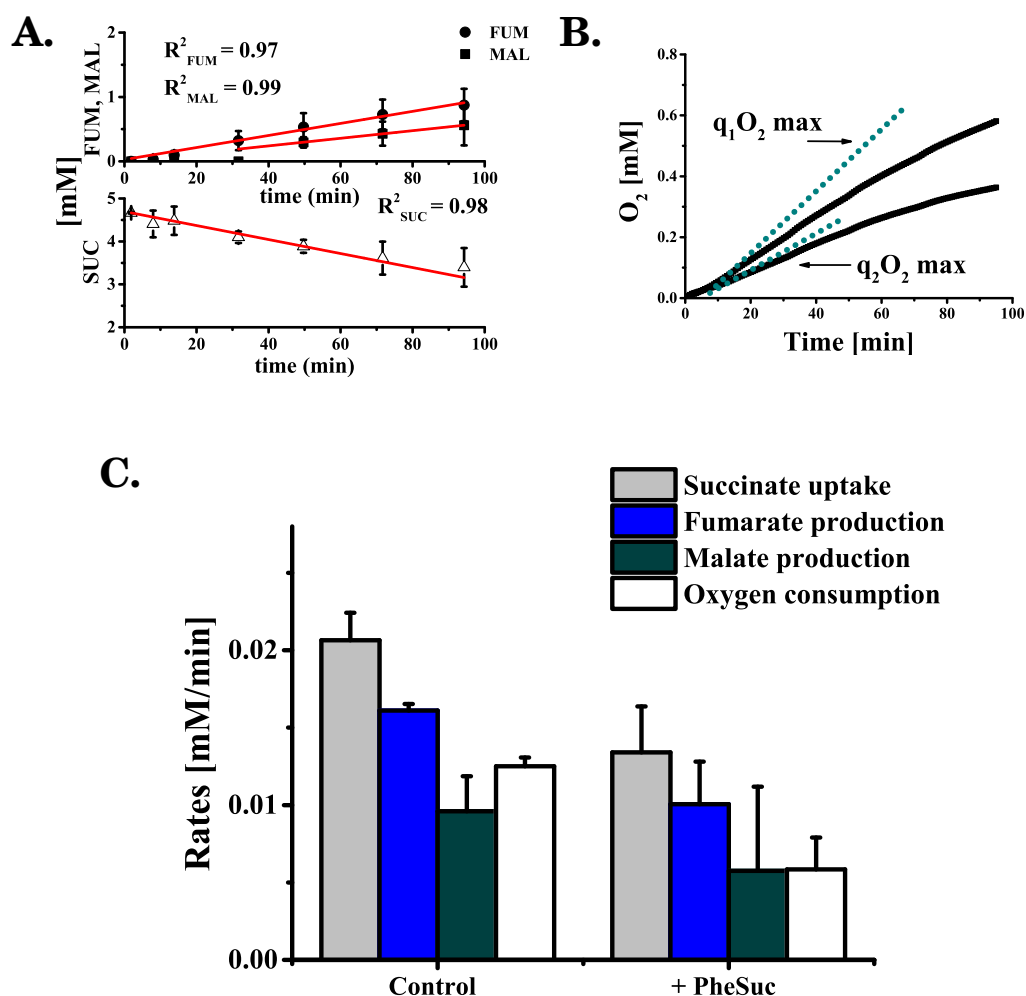
Figure 4.5: Succinate uptake, product formation and mitochondrial respiration in the presence of the inhibitor phenylsuccinate (5 mM) in the open system. Evolution [A] of average concentration of fumarate (•), malate (■) and succinate (△ for two independent experiments. Red line indicates the curve of the regression analysis along with the $R^2$. Evolution [B] of integrated oxygen consumption over time ((■) and (•). Blue dotted lines indicate the slope of the line for each experiment from which the maximum respiration rate was calculated ($q_1O_2$ max and $q_2O_2$). Average cell concentration = 1.46 ± 0.18 g/L. Comparison [C] of calculated rates between experiments untreated and treated with the inhibitor phenylsuccinate for the same system.

Experiments with equimolar concentrations of phenylsuccinate and succinate added to isolated castor bean mitochondria inhibited succinate oxidation at 50 % (Phillips and Williams, 1973) and uptake of succinate in at 51 % (Chappell and Beevers, 1983). In liposomes, the reconstituted yeast dicarboxylate carrier protein was inhibited at 60 % upon phenylsuccinate addition (Palmieri et al., 1996) whereas similarly the reconstituted succinate-fumarate antiporter showed 79 % inhibition.

However, based on these results we could not definitely distinguish whether only

a dicarboxylate carrier protein or a succinate-fumarate antiporter (or a combination thereof) were active in *S. pombe* permeabilized cells. Moreover it remains an open question whether the *S. pombe* importer of succinate or another transporter further catalyzed the efflux of malate as well. The succinate-fumarate antiporter would demand the presence of fumarate intramitochondrially in order to be exchanged for cytosolic succinate. Fumarate however, was not detected in extracts of selectively permeabilized cells when succinate was not added to the reaction mix. Based on these findings alone we could not rule out the scenario incorporating an initial activation of succinate influx alone which subsequently triggered a succinate-fumarate antiporter activity.

It was proposed that in *S. cerevisiae* the dicarboxylate carrier protein (Dicp) and the succinate-fumarate carrier (Sfcp) actually connected the synthesis of succinate in the cytosol to the mitochondrial succinate dehydrogenase due to the activity of the glyoxylate cycle (Palmieri et al., 1999c). Nonetheless, *S. pombe* cells lack a functional glyoxylate shunt as isocitrate lyase and malate synthase do not exist (Tsai et al., 1987; de Jong-Gubbels et al., 1996). The ratio of succinate to molecular oxygen (yield of uptaken succinate on consumed oxygen) remained unaffected by the addition of phenylsuccinate. The ratios were $2.36 \pm 0.2$ mol/mol in the absence of phenylsuccinate and $2.67 \pm 0.35$ mol/mol when phenylsuccinate was supplied to the system during succinate oxidation by ADP-activated mitochondria (see $Y_{SUC/O_2}$ in Figures 4.6.A & B). Such a finding suggests that the inhibitor had an influence primarily on the kinetics of active succinate transport and not on the integrity of the mitochondrial membranes, the number of enzymatic reactions taking place or the efficiency of the respiratory chain transporting electrons and pumping protons.
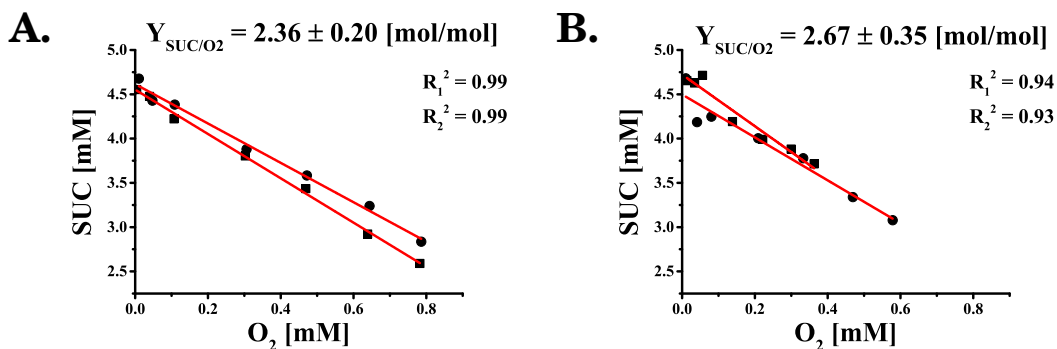


Figure 4.6: Yield of succinate on the integrated oxygen consumed by mitochondria untreated [A] and treated [B] with the inhibitor phenylsuccinate for two independent experiments ((■) and (●)). Red line indicates each curve of the regression analysis along with the $R^2$. Conditions identical to the ones described in Figures 4.4 and 4.5.

The absence of a predicted protein sequence acting as a succinate mitochondrial carrier in databases like PomBase or the lack of experimental evidence about such a structure being docked on the inner membrane of *S. pombe* mitochondria does not exclude the possibility of an existing protein with a similar functionality to either the yeast Sfcp or Dicp that remains elusive (see Figure 4.7).
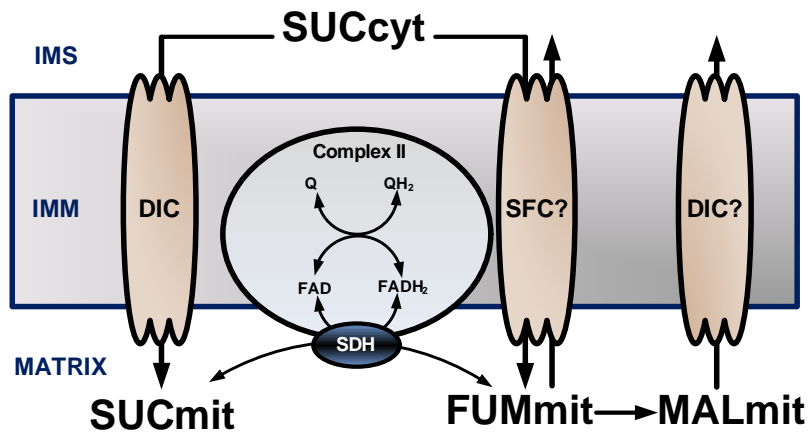


Figure 4.7: Hypothetical succinate uptake by *S. pombe* mitochondria. Succinate is oxidized by succinate dehydrogenase (SDH) to yield fumarate which then is converted to malate by fumarate hydratase. Mitochondrial transporters illustrated here: DIC: dicarboxylate carrier protein; SFC: succinate/fumarate antiporter. The cytosolic compartment is merged with the IMS and the IMS is separated from the mitochondrial matrix by the inner mitochondrial membrane (IMM).

## 4.2 Oxidation of NADH in *Scizosaccharomyces pombe* mitochondria

So far the approach of dynamically quantifying mitochondrial transport and bioenergetics was applied only during succinate oxidation. This consisted of the uptake of succinate via a transport mechanism and the subsequent oxidation of the substrate by the complex II of the respiratory chain. The closed reactor system, helped validate that digitonin selectively permeabilized only the cell membrane of *S. pombe* cells which subsequently retained their mitochondrial functionality and integrity. The open flask system complemented the aforementioned results with elucidating the manner of succinate transfer from the cytosol to the mitochondrial matrix by utilizing a mitochondrial transporter-specific inhibitor. Nonetheless, the question arose how *S. pombe* mitochondria would behave in the presence of respiratory substrates that would be oxidized at sites of the respiratory chain other than the complex II succinate dehydrogenase. The simplest respiratory substrate candidate for answering such a question is NADH.

Redox cofactors, NAD and NADH, play a pivotal role in cellular homeostasis and growth and are central substrates for a plethora of reactions (>200 in *S. cerevisiae* (Vemuri et al., 2007)). The intracellular concentration of the sum of NAD and NADH in *S. cerevisiae* have been reported to be 1 mM and is strongly compartmentalized (Bakker et al., 2001) based on the carbon source consumed. For example during growth on glucose yeast cells generate NADH from enzymes of the glycolysis in the cytosol and from enzymes of the TCA cycle in the mitochondrial matrix. On the other hand, during lactate oxidation, NADH is produced exclusively in the mitochondria (Bakker et al., 2001), most propably by the matrix-localized D-lactate dehydrogenase Dld2p (Pallotta, 2012). This D-lactate dehydrogenase should not be confused with the Dld1p isoform which is docked on the external side of the IMM directing electrons towards cytochrome *c* (oxidized by complex IV) (Mourier et al., 2008). All the other dehydrogenases docked on the mitochondrial intermembrane space side of the IMM direct electrons to the ubiquinone pool (oxidized by complex III) such as the NADH (Nde1p and Nde2p) and glycerol 3-phosphate (Gut2p) dehydrogenases that are docked on the IMM (Bakker et al., 2001).

Typically, when NADH is externally supplied to isolated mitochondria or permeabilized cells of yeast origin, it serves as a substrate for the external NADH dehydrogenase docked on the inner mitochondrial membrane (IMM) facing the mitochondrial intermembrane space (IMS) (Bradshaw and Pfeiffer, 2006). These mitochondrial dehydrogenases substitute for the mammalian complex I. Mitochondria of *S. pombe* origin do not possess a mammalian-like, proton-pumping, rotenone-

sensitive complex I, exactly as *S. cerevisiae* mitochondria. An exception is the obligate aerobic yeast *Yarrowia lipolytica* that possesses a 35-subunit complex I (Kerscher et al., 2002) with the capacity to pump protons, quite similar to its mammalian counterpart. The loss of complex I from *Y. lipolytica* leads to cell death which can be averted with the expression of an alternative NADH:ubiquinone oxidoreductase (Mourier and Larsson, 2011) like the one located in yeast mitochondria. It is widely accepted that mammalian cells do not possess an external NADH dehydrogenase activity docked on the IMM and rely on shuttle mechanisms to re-oxidize NADH in the cytosol (Dawson, 1979; Luttik et al., 1998). However mitochondria from pigeon heart (Rasmussen and Rasmussen, 1985) and rat heart cells (Nohl and Schönheit, 1996; Oliveira et al., 2000) have exhibited such an external NADH-dehydrogenase activity that was however not coupled to ADP phosphorylation in the mitochondrial matrix.

After NADH is oxidized, the generated electrons are subsequently channeled towards the ubiquinone pool, throughout the respiratory chain (complexes III and IV) creating a proton gradient that is eventually driving the ATP synthase (complex V) for the formation of metabolic energy in the form of ATP in the mitochondrial matrix. We have seen that *S. cerevisiae* possesses two external NADH dehydrogenases (Nde1p and Nde2p) (Luttik et al., 1998) as well as an internal one (Ndi1p) facing the mitochondrial matrix side. Sequence homology analysis has predicted that *S. pombe* possesses only two mitochondrial NADH dehydrogenases, expressed by sequences *nde1* (SPBC947.15c) and *nde2* (SPAC3A11.07) that are homologous to the external *S. cerevisiae* dehydrogenase-coding genes *NDE1* and *NDE2* and internal yeast dehydrogenase coding gene *NDI1*. However there exist no experimental data on *S. pombe* that could provide information whether the predicted mitochondrial NADH dehydrogenases are localized on the inner mitochondrial membrane facing the mitochondrial matrix side and/or facing the IMS side (cytosolic side).

### 4.2.1 Oxidation of exogenous NADH and NAD-linked substrates

#### 4.2.1.1 Respiration on externally supplied NADH

The activity of mitochondria from selectively permeabilized *S. pombe* cells was monitored respirometrically in the sealed, reactor system. NADH was externally supplied with an initial concentration of 1 mM in the presence or absence of ADP (0.5 mM) (state 3 and state 4 respiration respectively) and the RCR could be calculated.
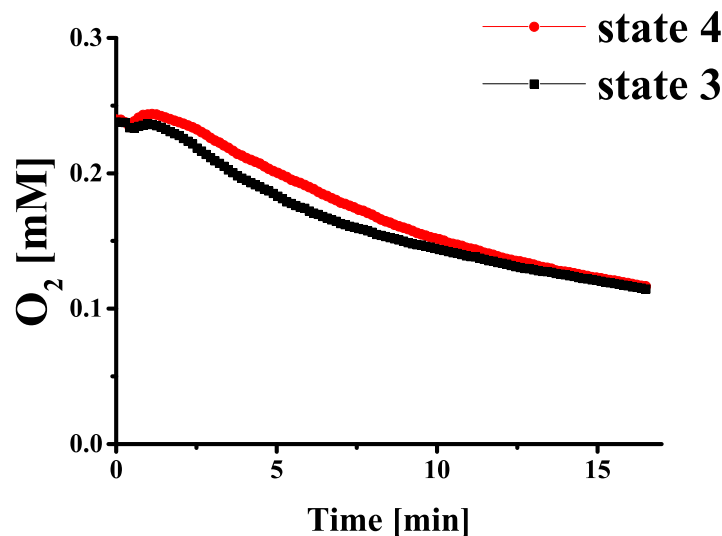
Figure 4.8: Evolution of oxygen concentration in the closed reactor system for *S. pombe* digitonin-permeabilized cells (yielded from the same culture) in the presence of 1 mM NADH in respiratory buffer (pH 6.8) at 30 °C. State 3 respiration (■) was initiated with the addition of 0.5 mM ADP, while there was no ADP present during state 4 respiration (•)). Exponentially growing cells were harvested from parallel cultivations and after digitonin-permeabilization they were used at a final reactor concentration of 2.30 ± 0.06 g/L (state 3) and 2.29 ± 0.10 g/L (state 4).

As it is evident from Figure 4.8, mitochondria in selectively permeabilized cells were respiring in the presence of NADH but when ADP was subsequently added to the reaction mix the respiration rate did not increase significantly. After the exogenous supply of a saturating concentration of NADH and ADP, mitochondria respired with a rate of 0.015 ± 0.000 mM/min (specific respiration rate = 6.51 ± 0.15 nmol/(mg CDW×min)) whereas the oxygen uptake rate during state 4 respiration was 0.012 ± 0.001 mM/min (specific respiration rate = 4.99 ± 0.12 nmol/(mg CDW×min)). Both rates were calculated from the first 4 minutes of respiration where the rate reached its maximum value and was constant over time. Therefore the calculated RCR inferred from the ratio of the oxygen rate during state 3 respiration to that during state 4 respiration was 1.30.

These results agree with previous findings on *S. pombe* isolated mitochondria that oxidized externally added NADH at a rate 1.25-fold faster than in the absence of ADP (Crichton et al., 2007) (RCR = 1.25). Other RCR values for *S. pombe* isolated mitochondria that oxidized exogenous NADH were in the range of 2.8 - 3.2 (Jault et al., 1994). Similar results for the RCR (RCR = 2.1) were obtained as well when the uncoupler carbonyl cyanide m-chlorophenyl hydrazone (CCCP) (that allows the respiration rate to reach its maximum value) was added to NADH-oxidizing mitochondria during ADP-driven respiration (Heslot et al., 1970). Concerning the oxidation of externally added NADH an RCR value of 2.8 was reported for isolated mi-

tochondria from *S. cerevisiae* cells (Avéret et al., 1998). Isolated mitochondria from *Saccharomyces carlsbergensis* oxidized NADH and exhibited a RCR in the range of 3.0 - 3.6 (Ohnishi et al., 1966).

An RCR value below 2 is usually attributed to a lack of coupling between the flow of electrons throughout the respiratory chain on one side and the pumping of protons from the respiratory complexes and subsequently the formation of ATP on the other side (Kuznetsov et al., 2008). Loss of intactness of the outer mitochondrial membrane as a cause for uncoupling could be excluded since the permeabilization method described here, yielded mitochondria that possessed intact outer mitochondrial membranes in a reproducible manner. On the other hand, it would be expected that state 3 respiration during oxidation of exogenous NADH (Figure 4.8) would be characterized by a much higher rate than that on succinate (Figure 4.1). In the existing literature about *S. pombe* mitochondria, state 3 respiration on NADH was reported to be 2 - 14 times higher than that on succinate (Heslot et al., 1970; Moore et al., 1992; Jault et al., 1994). However the ADP-activated respiration rate on NADH observed here was only slightly higher that that on succinate ($q_{O_2,SUC}$ = 0.011 ± 0.004 mM/min versus $q_{O_2,NADH}$ = 0.015 ± 0.000 mM/min).

Furthermore, the comparison of state 4 respiration rates between the two substrates showed significant differences, with the rate on NADH being 2.8-fold higher than that on succinate. It was speculated that varying proton leak was the cause of the high NADH-driven state 4 respiration. With the term "active proton leak" a process is defined where energy is wasted by an active dehydrogenase under non-phosphorylating conditions (Mourier et al., 2009). In such cases the proton motive force is decreased and the inner mitochondrial membrane conductance for protons is increased, thus leading to a proton leak when ADP is absent. In general the mechanism of proton leak along with that of proton slip are used to decrease the reactive oxygen species (ROS) production (Postmus et al., 2011) which can harm mitochondrial homeostasis.

In general, the rate at which yeast mitochondria oxidize exogenous NADH via the external NADH-dehydrogenase activity alone does not reflect the total oxidative capacity of these organelles when more dehydrogenases are functioning (usually activated with a combination of respiratory substrates). NADH can only be targeted by the external NADH-dehydrogenase (IMS-facing) due to the fact that the inner mitochondrial membrane is impermeable to NADH, thus reduced pyridine nucleotides can not access the NADH-dehydrogenase facing the mitochondrial matrix side (Van Urk et al., 1989). It is important to note that although it was believed that the inner mitochondrial membrane is a barrier for both NAD and NADH (based on the analysis of *S. carlsbergensis* (von Jagow and Klingenberg, 1970)), this was proven to be slightly different for *S. cerevisiae* mitochondria. In *S. cerevisiae* trans-

membrane mitochondrial transporters allow the transfer of NAD from the cytosol to the mitochondrial matrix. Ndt1p, which was confused with the mitochondrial pyruvate carrier in the past (Hildyard and Halestrap, 2003b) and Ndt2p (Agrimi et al., 2011; Todisco et al., 2006) are responsible for the direct uptake of cytosol-synthesized NAD in *S. cerevisiae* mitochondria. The existence of mammalian counterparts has not yet been confirmed (Stein and Imai, 2012). NAD in yeast can not be synthesized *de novo* in the mitochondria and is transported either unidirectionally or is exchanged for mitochondrial (d)AMP, (d)GMP (Palmieri et al., 2006). In *S. pombe* such a mitochondrial transporter is predicted to exist encoded by the gene *yea6* (SPAC227.03c) which exhibits homology to the *S. cerevisiae* genes *NDT1* and *NDT2*.

To summarize, exogenous NADH oxidation resulted in uncoupling of respiration, although mitochondria were structurally intact. The observed high active proton leak is indicated by the high state 4 respiration rate. Thus, there was an apparent limitation during NADH oxidation and the question that arose was whether this limitation was connected with the fact that only the IMM-docked, external NADH dehydrogenase was active.

### 4.2.1.2 Respiration on NAD-linked substrates

Therefore the next step was to examine whether the aforementioned limitation could be abolished. The strategy applied was instead of providing exogenous NADH, create the conditions for the *in situ* synthesis of NADH from NAD in the cytosol by NAD-dependent dehydrogenases. At the same time any NADH-linked organic acids present could enter the mitochondria and further serve as substrates in the mitochondrial matrix for the production of NADH. The target would be activating the oxidation of exogenous and endogenous NADH simultaneously, therefore theoretically functioning at maximum total oxidizing capacity. At the same time the participation of cytosolic dehydrogenases might reveal the collaboration of cytosolic enzymes with elements of the mitochondrial respiratory chain, such as the external NADH-dehydrogenase, in the form of metabolite channeling. Could respiring *S. pombe* mitochondria exhibit under such conditions better respiratory coupling than on exogenous NADH alone? The NAD-linked substrates chosen were malate and glutamate in equimolar amounts along with saturating concentrations of NAD.

When malate and glutamate are supplied to the external side of mitochondria in digitonin-permeabilized cells the following reactions may take place as summarized in Figure 4.9. Malate and NAD can act as substrates for the cytosolic malic enzyme (Mae2p) and lead to the formation of NADH, $CO_2$ and pyruvate. From there, pyruvate may be decarboxylated to form $CO_2$ and acetaldehyde, it can be carboxylated and form oxaloacetate in the ATP-consuming pyruvate carboxylating direction or it

can finally enter the mitochondria, where it is oxidized by the pyruvate dehydrogenase complex (metabolism of malate and pyruvate covered in subsequent parts). According to global protein localization studies in *S. pombe* there is not any cytosolic malate dehydrogenase activity present (Matsuyama et al., 2006). Also, as mentioned in previous parts, NAD can be actively transported from the cytosol to the mitochondrial matrix were it could be further reduced and oxidized if the appropriate carboxylates are present.
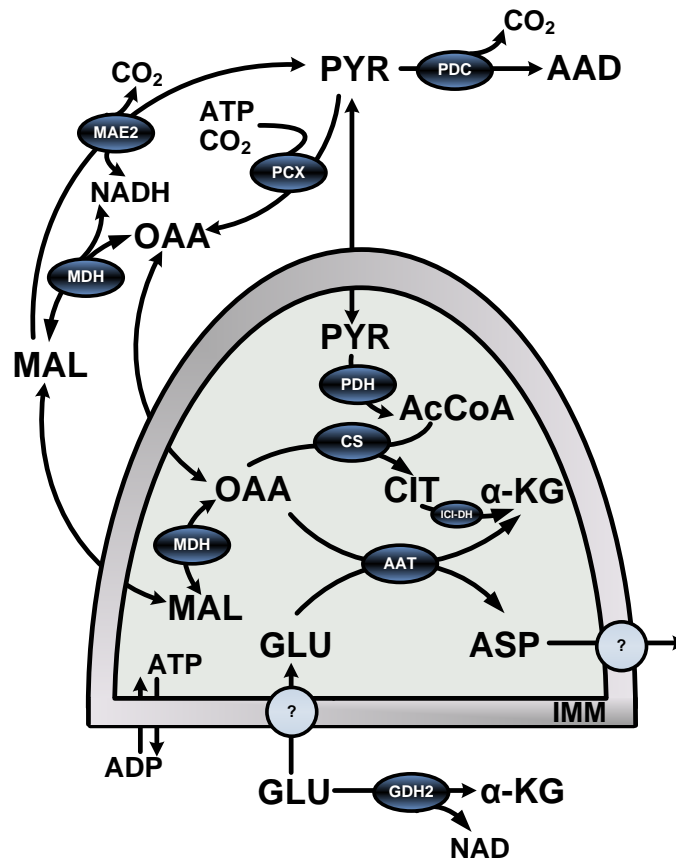


Figure 4.9: General reaction scheme for all reactions activated in the cytosol and the mitochondrial matrix (separated by the IMM) when glutamate, malate and NAD are supplied to selectively permeabilized cells. Reactions that may participate in recycling NAD are illustrated for the cytosol. The antiporter activity transferring aspartate and glutamate out of and into the mitochondrial matrix is only speculative, therefore illustrated with a question mark. The outer mitochondrial membrane is omitted. Enzymes illustrated here are: MAE2, malic enzyme; PCX, pyruvate carboxylase; PDC, pyruvate decarboxylase; AAT, aspartate aminotransferasee; PDH, pyruvate dehydrogenase complex; MDH, malate dehydrogenase; CS, citrate synthase.

At the same time, in the presence of glutamate, NAD can be reduced at another site in the cytosol, namely at the NAD-specific glutamate dehydrogenase, Gdh2p, producing $\alpha$-ketoglutarate and $NH_4^+$. In previous studies glutamate was additionally added with succinate to isolated, respiring *S. pombe* mitochondria (Moore

et al., 1992), in order to prevent oxaloacetate being accumulated (by removing it). Nonetheless, in our study, glutamate was added in order to activate the cytosolic Gdh2p as mentioned before and synthesize NAD. Transporting glutamate into mitochondria would require a membrane protein like the *S. cerevisiae* Agc1p, that acts as a uniport for glutamate and as an antiporter for glutamate and aspartate. Such a protein, which is also a part of the aspartate-malate shuttle (Bakker et al., 2001; Satrustegui et al., 2007) is not known to exist in *S. pombe*. This was supported further by comparing the amino acid sequence of Agc1p of *S. cerevisiae* versus the protein database for *S. pombe*, which did not reveal any suitable candidate. The *S. pombe* protein that had the highest homology (35 %) to Agc1p was the 2-oxoadipate and $\alpha$-ketoglutarate transmembrane transporter (SPAC328.09).

Based on the aforementioned annotated *S. pombe* sequences with predicted functionality and topology there are no data concerning the existence of a *S. pombe* mitochondrial malate-aspartate shuttle, although both cytosolic and mitochondrial aspartate aminotransferases (SPAC10F6.13c and SPBC725.01 respectively) are predicted to exist.
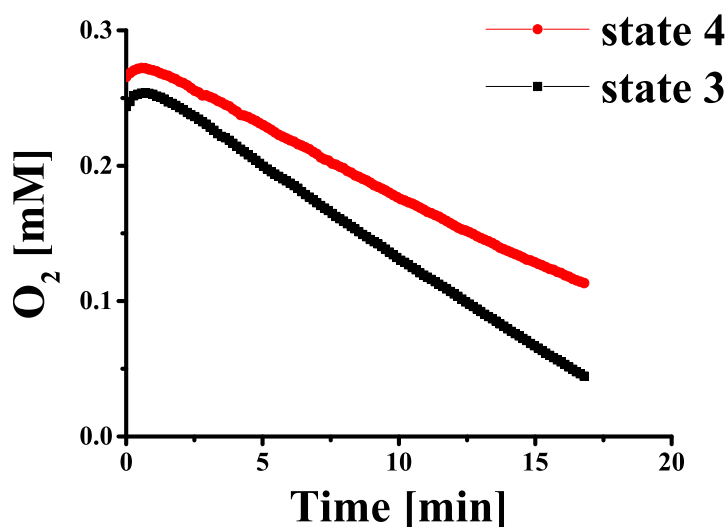


Figure 4.10: Evolution of oxygen concentration in the closed reactor system for *S. pombe* digitonin-permeabilized cells (yielded from the same culture) in the presence of 2.5 mM malate, 2.5 mM glutamate and 1 mM NAD in respiratory buffer (pH 6.8) at 30 °C. State 3 respiration (■) was initiated with the addition of 0.5 mM ADP, while there was no ADP present during state 4 respiration (●). Exponentially growing cells were harvested from parallel cultivations and after digitonin-permeabilization were used at a final reactor concentration of 3.39 ± 0.18 g/L (state 3) and 3.37 ± 0.18 g/L (state 4).

Based on Figure 4.10 it can be directly illustrated that the limitation that was described during exogenous NADH oxidation persisted under these conditions as well. During state 3 respiration, in the presence of ADP, the respiration rate was

$0.014 \pm 0.000$ mM/min (specific rate $q_{O_2}$ = $4.04 \pm 0.25$ nmol/(mg CDW×min)). Mitochondrial preparations in non-phosphorylating conditions exhibited a specific respiration rate of $0.010 \pm 0.000$ mM/min (specific rate $q_{O_2}$ = $2.99 \pm 0.01$ nmol/(mg CDW×min)). All experiments were performed in duplicates with cells obtained from parallel cultivations growing exponentially. Both rates were calculated from the first 4 minutes of respiration where the rate reached its maximum value and was constant over time. Based on the ratio of state 3 respiration to state 4 respiration we could calculate an RCR of 1.4, indicative of a poor coupling.

A closer examination revealed that $CO_2$ was synthesized due to the presence of malate, indicative of at least the activation of the malic enzyme functioning in the decarboxylating direction. At the same time there was no acetaldehyde being detected by the MIMS, which is the product of the pyruvate decarboxylase reaction using pyruvate as a substrate. A propable explanation is the fact that there was a low degree of metabolite channeling between the cytosolic malic enzyme and the pyruvate decarboxylase enzyme. Pyruvate formed from the malic enzyme would be released in the bulk phase of the synthetic cytosolic medium where it would be diluted and not be accessible to the pyruvate decarboxylase enzymatic activity. At phosphorylating and non-phosphorylating conditions the ratio of $CO_2$ to $O_2$ was $1.96 \pm 0.38$ mol/mol and $2.17 \pm 0.14$ mol/mol respectively. The addition of ADP did not influence the production of $CO_2$ and it affected the respiration rate of the mitochondria only slightly.

The observation that ADP did not activate *S. pombe* mitochondria in the presence of NAD-linked substrates (RCR should normally be $\geq$2) could be a result of a limitation for NADH uptake occurring at the outer mitochondrial membrane. Such a limitation, similar to what was observed with the exogenous supply of NADH, would be indicative of NADH being not easily accessible to the external NADH-dehydrogenase docked on the inner mitochondrial membrane and facing the mitochondrial intermembrane space. Such an obstacle could also explain why the specific respiration rates during phosphorylating conditions (state 3) with exogenous NADH or NAD-linked substrates were not significantly higher than the one during succinate oxidation. Therefore, the questions that arose from these observations were:

1. Is there a way to by-pass the limitation of NADH transport at the OMM?

2. Would this by-pass fully activate mitochondrial respiration?

3. Would such an approach lead to overcoming the high state 4 respiration observed mostly for NADH-oxidizing conditions with poor RCRs, indicative of highly active proton leak?

The prime regulator of the communication between the cytosol and the intramitochondrial matrix is the voltage-dependent anion-selective channel (VDAC) or porin. The VDAC is an unselective transporter docked on the outer mitochondrial membrane (OMM) capable of transporting carboxylates, adenosine nucleotides, anions, cations and $Ca^{2+}$ and is capable of complexing with other proteins (Shoshan-Barmatz et al., 2006). Positive or negative membrane potentials close the porin, while in the open state it allows the transfer of molecules up to 5 kDa in size (Lemasters and Holmuhamedov, 2006). Another metabolite highly regulating the closure of the VDAC is actually NADH and not NAD, and this behaviour of NADH has been highly conserved in fungi and *S. cerevisiae* and mammalian cells (Zizi et al., 1994).

The VDAC in mammalian cells has been implicated with regulating apoptosis by releasing pro-apoptotic proteins from the IMS and by being targeted by pro- and antiapoptotic proteins ($Bcl_2$ family of proteins) in mammalian cells (Shoshan-Barmatz et al., 2006). Furthermore in yeast, the VDAC is proposed to regulate the opening of the yeast mitochondrial unspecific channel (YMUC) also known as yeast permeability transition pore (yPTP), a pore of the inner mitochondrial membrane allowing for the transport of metabolites of 1.1 kDa size between the mitochondrial matrix and the IMS (Gutiérrez-Aguilar et al., 2007). The interaction of pores of the OMM (VDAC), the IMM (YMUC) and NADH transport and oxidation has been shown with the respiration-induced YMUC being inhibited by externally added NAD (Bradshaw and Pfeiffer, 2006) to swollen mitochondria, stopping the loss of mitochondrial NAD(H) to the cytosol (Bradshaw and Pfeiffer, 2013).

### 4.2.2 Oxidation of *in situ* formed NADH and proof for metabolite channeling and microcompartmentation

VDACs are highly conserved throughout species like fungi, plants and animals (Colombini, 2004), show voltage dependence by changing conductivity when membrane potential changes and are selective for anions (Lee et al., 1998). Elements of the cytoskeleton are bound on them as well as cytosolic hexokinases in order to be in close proximity to ATP produced in the mitochondria (Mannella, 1998; Adams et al., 1991).

VDACs are also presumed to associate with the ANT (docked in the inner mitochondrial membrane) in heart (Brdiczka et al., 2006) cells. In mammalian cells mitochondrial hexokinases bind with the VDAC on the outer mitochondrial membrane and form a functional complex along with the ANT and the ATP synthase that recycles ADP and protects from ROS and pro-apoptotic factors (Wilson, 1997; Bryson et al., 2002; Seixas et al., 2004; Gall et al., 2011) although in yeast something similar has not been reported so far (Robey and Hay, 2006).

In yeast there are two isoforms for the outer mitochondrial membrane VDAC encoded by genes *POR1* and *POR2*, whereas only the protein Por1p is able to form a barrel-like channel allowing the passage of non-charged molecules with a size up to 5000 Da (Lemasters and Holmuhamedov, 2006) through the membrane. Strains containing VDAC-coding gene deletions were still able to grow (Blachly-Dyson et al., 1997), showing that other proteins, like Tom-40 (Kmita and Budzinska, 2000), may fullfill their transporter role as well (Mannella, 1998). Although the mammalian VDAC has been postulated to be a part of the initiation of apoptosis due to its complexing with the ANT and the permeability transition pore, it has been proven that this is not the case in *S. cerevisiae* (Colombini, 2004; Gross et al., 2000).

It was proposed for the first time for *S. cerevisiae* (Avéret et al., 1998) that a major controlling point for the mitochondrial respiration on NADH was the passage of this redox precursor from the cytosol to the IMS through the VDAC. At the same time a novel characteristic of selectively permeabilized cells was revealed that was absent from isolated mitochondria. Permeabilized yeast cells possessed an always closed porin whereas isolated mitochondria an always open porin. The state of the porin-mediated diffusion of metabolites was thought to be extended not only on the passage of NADH to the IMS but also on the diffusion of other large metabolites like ADP (Avéret et al., 1998). It was later proven that the porin did not function in a general, non-specific open-close mode, but rather was metabolite-specific and was implicated in the channeling of NADH from cytosolic dehydrogenases to the external mitochondrial NADH dehydrogenase (Avéret et al., 2002).

If this is the case for *S. pombe* as well, then any NADH formed from a dehydrogenase associated in the cytosol with the VDAC could pass into the IMS (general scheme illustrated in Figure 4.11). There NADH could be oxidized at the external NADH dehydrogenase, its oxidized form could serve as a substrate for the adenine nucleotide translocator and pass into the mitochondrial matrix to be used by other reactions or be reduced by the internal NADH dehydrogenase. At the same time any produced protons could fuel the ATP synthase docked on the IMM.
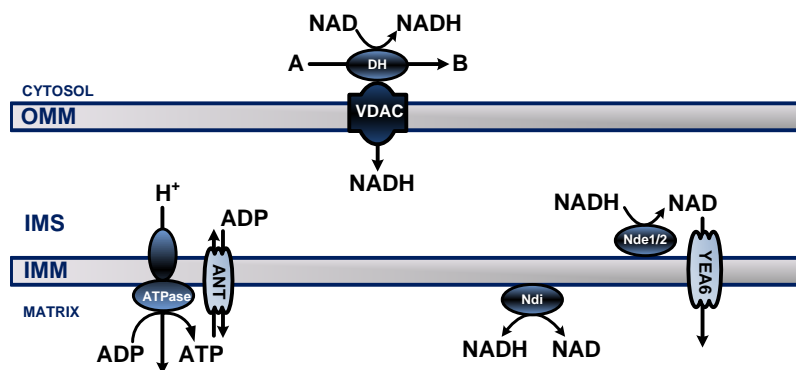
Figure 4.11: General reaction scheme for a hypothetical cytosolic dehydrogenase (DH) associated with the VDAC and allowing for the passage of the produced NADH into the IMS. Enzymes illustrated here are: NDE1/2, external mitochondrial NADH dehydrogenases; NDI, internal mitochondrial NADH dehydrogenases; ATPase, mitochondrial matrix ATP synthase. The mitochondrial transporters docked on the OMM and IMM are: VDAC, voltage-dependent anion channel or porin; ANT, adenine nucleotide translocator; YEA6, NAD transporter. The cytosolic compartment (CYT) is separated from the IMS by the outer mitochondrial membrane (OMM) and the IMS from the mitochondrial matrix by the inner mitochondrial membrane (IMM).

#### 4.2.2.1   Obtaining coupled respiration on *in situ* formed NADH

The experimental conditions consisted of digitonin-permeabilized *S. pombe* cells, suspended in the synthetic cytosol-mimicking medium along with fructose 1,6-bis-phosphate (10 mM) and NAD (2 mM). As with the studies that comprised exogenous NADH supply and malate and pyruvate as respiratory substrates, metabolism was monitored in the closed reactor system at 30 °C.

The NAD-reducing enzymatic activity selected to be activated was the glyceraldehyde 3-phosphate dehydrogenase (GA3P-DH) which is localized in the cytosol. Glyceraldehyde 3-phosphate dehydrogenase along with other enzymes of the glycolysis are known to be associated with the outer mitochondrial membrane. It is part of a metabolon characterized in plants like *A. thaliana* (Graham et al., 2007) and in yeast. More specifically in yeast, the GA3P-DH structure has been found to strongly associate with aldolase and enolase along with the ANT and the OMM porin and with elements of the mitochondrial matrix ATP synthase along other proteins (Brandina et al., 2006). Up to now there have not been any studies conducted concerning the aforementioned kind of metabolic configuration and microcompartmentation in *S. pombe*.

As it is illustrated in Figure 4.12 during *in situ* NADH generation from the cytosolic GA3P-DH, ADP-driven oxygen consumption (state 3) slowed down after 5 minutes. Mitochondria respiring in the presence of ADP (Figure 4.12), eventually

switched from state 3 respiration to a slower respiration rate (equal to 0.004 ± 0.000 mM/min) close to the respiration rate observed in the absence of ADP, until $O_2$ in the reactor was completely depleted. During non-phosphorylating conditions (state 4) with NAD present, respiration was kept lower than state 4 respiration during the oxidation of exogenous NADH and NAD-linked substrates. More specifically the state 4 respiration rate was 0.006 ± 0.002 mM/min (specific respiration rate = 2.93 ± 0.17 nmol/(mg CDW×min)). Compared to other state 4 specific respiration rates it was 1.7-fold lower than that during NAD-linked substrate oxidation and 2-fold lower than during exogenous NADH oxidation. The initial sharp decrease of the dissolved oxygen concentration in the closed system during ADP-driven oxidation of *in situ* formed NADH (state 3) was characterized by a respiration rate of 0.027 ± 0.005 mM/min (specific respiration rate = 10.75 ± 2.23 nmol/(mg CDW×min)). The RCR inferred from the ratio of state 3 to state 4 respiration from separate experiments with and without the presence of ADP was calculated to be 3.7.

The integrity of the outer mitochondrial membrane was also assessed with the exogenous supply of cytochrome *c* (10 μM) in separate experiments. In this case, state 3 respiration without the addition of cytochrome *c* was 0.034 ± 0.001 mM/min (average cell concentration in reactor = 2.37 ± 0.11 g/L) and in the presence of cytochrome *c*, state 3 respiration was 0.038 ± 0.001 mM/min (average cell concentration in reactor = 2.37 ± 0.12 g/L). Therefore the outer mitochondrial membrane was intact at a percentage of 87.3 %, since the state 3 respiration rate in the presence of cytochrome *c* was 12.7 % higher than that without its addition.
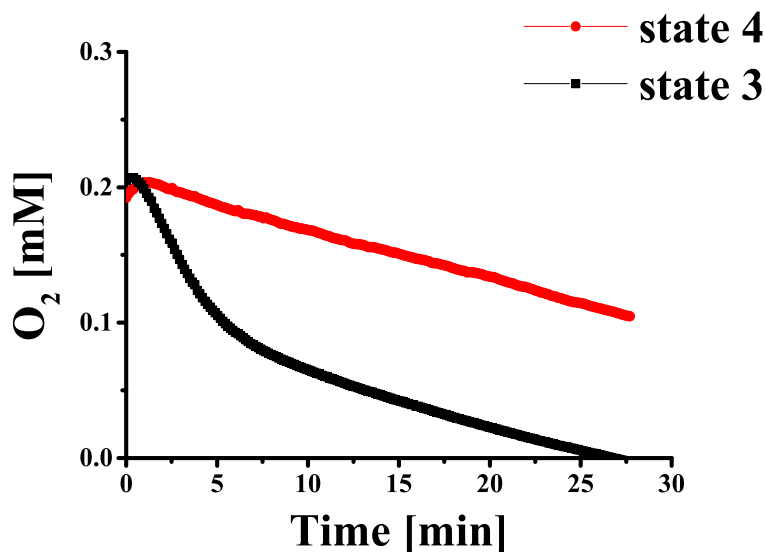
Figure 4.12:  Consumption of oxygen in the reactor system for *S. pombe* digitonin-permeabilized cells (yielded from the same culture) in the presence of 10 mM fructose 1,6-bisphosphate and 2 mM NAD in respiratory buffer (pH 6.8) at 30 °C. State 3 respiration (■) was initiated with the addition of 2 mM ADP, while there was no ADP present during state 4 respiration (●). Exponentially growing cells were harvested from parallel cultivations and after digitonin-permeabilization were used in duplicates at a final reactor concentration of 2.55 ± 0.08 g/L (state 3) and 2.45 ± 0.00 g/L (state 4).

The excellent coupling of respiration as presented here was able to minimize the proton leak during state 4 respiration and was a direct result of using the proper NADH-forming system in the cytosol. The *S. cerevisiae* glyceraldehyde 3-phosphate dehydrogenase enzyme has been known to control the influx of NADH through the outer mitochondrial membrane by channeling this metabolite through the porin (VDAC) directly to the IMS and the vicinity of the NADH-dehydrogenase (Avéret et al., 2002). However it was claimed that any NADH-forming dehydrogenases in the cytosol could efficiently participate in channeling NADH into the IMS. Our results direct towards a different interpretation of this phenomenon.

The poor coupling of mitochondrial respiration to ADP phosphorylation that was yielded in *S. pombe* when malate and glutamate were supplied as substrates supports the point that a generalization of the substrate channeling can not be plausible. These findings support that not all cytosolic dehydrogenases are either docked on the cytosolic side of the outer mitochondrial membrane or can lead to the opening of the porin. Furthermore this degree of association of the total activity of cytosolic glycolytic enzymes with the mitochondria can differ between organisms (Brandina et al., 2006). Therefore, it is highly likely that there exists an evolutionary divergence of the spatial organization and association of enzymes with membrane transporters based on different metabolic needs. A straightforward advantage of enzymes and transporters of the mitochondria to cooperate through metabolite chan-

neling would be a higher degree of a substrate being efficiently utilized in conditions where its availability is limited.

### 4.2.2.2 Nucleotide phosphate dynamics and the P/O ratio

To better understand how the aforementioned kind of metabolite channeling functioned in *S. pombe*, the dynamics of coupling NADH oxidation to the production of ATP during state 3 respiration was elucidated. In order to do so, the evolution of ATP/ADP interconversion over time and their corresponding yields on oxygen were quantified.

**A.**

**B.**

**C.**
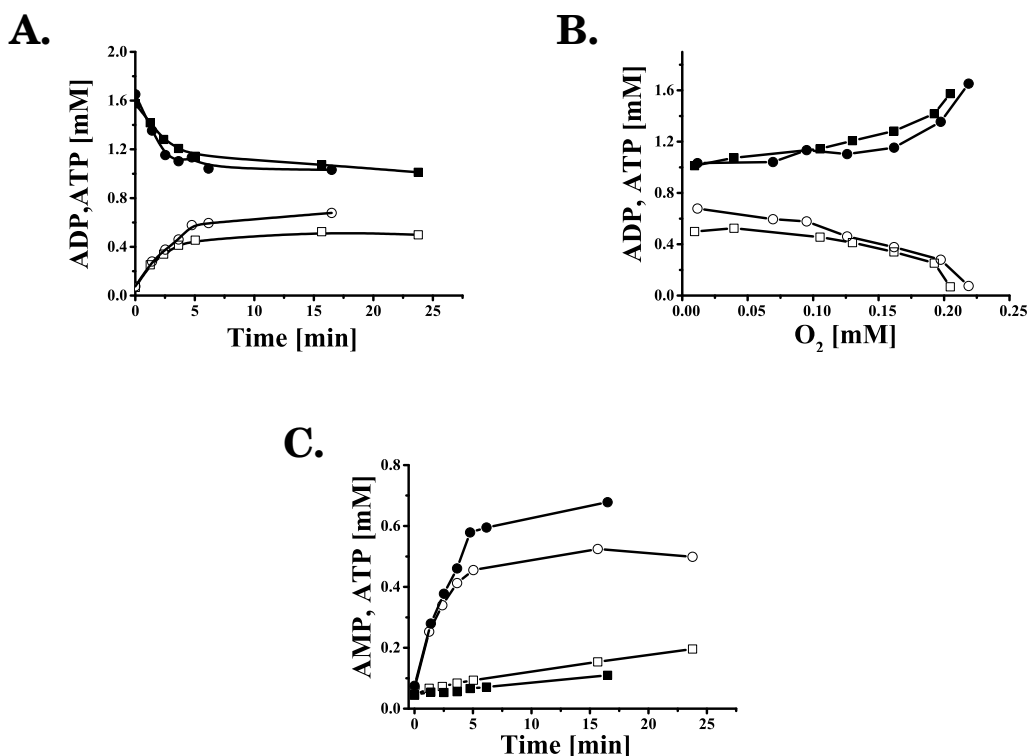
Figure 4.13: Metabolism of ADP ((■) and (●)) and ATP ((□) and (○)) [A] and their relationship [B] to the concentration of oxygen in the sealed reactor. Comparison of the net production [C] of ATP ((●) and (○)) and AMP ((■) and (□)) over time. Substrate composition, concentrations and experimental setup detailed in Figure 4.12.

As it is illustrated in Figures 4.13.A & B both ADP and ATP were eliminated and formed respectively at maximum rates coinciding with the respiratory chain functioning at a maximum rate. Subsequently, the leveling off of both adenosine nucleotides occurred when the respiration rate was reduced to a value approximating that of state 4 respiration.

The net elimination and formation rates for ADP and ATP respectively, before their concentrations leveled off, were $0.07 \pm 0.01$ mM/min (specific rate $q_{ADP} = 26.3 \pm 1.1$ nmol/(mg CDW×min)) and $0.09 \pm 0.00$ mM/min (specific rate $q_{ATP} = 35.5 \pm$

0.4 nmol/(mg CDW×min)). The same behaviour, where these two adenosine derivatives reached total formation and elimination rates of zero after some time, was observed during succinate oxidation as well. This phenomenon seems to be a general characteristic of selectively permeabilized *S. pombe* cells during respiration pointing towards the activity of extramitochondrial ATP hydrolysing enzymatic activities participating along with the ATP synthase in a substrate cycle. With the *in situ* formation of NADH and its oxidation, 5 minutes later the cells respired at a decreased rate compared to the initial maximum rate of oxygen uptake, approximating a value similar to state 4 respiration. However this decrease can only be partially attributed to the uncoupling of respiration from ADP phosphorylation into the mitochondria, when mitochondria transition from state 3 respiration to state 4. Our findings presented ADP-consuming mitochondria which in the presence of succinate had a constant respiration rate even when adenosine nucleotides eventually leveled off. Therefore, we claim that when the maximum mitochondrial respiration rate reaches state 4, adenosine nucleotide levels level off but the opposite claim can not be held true in all cases (succinate oxidation).
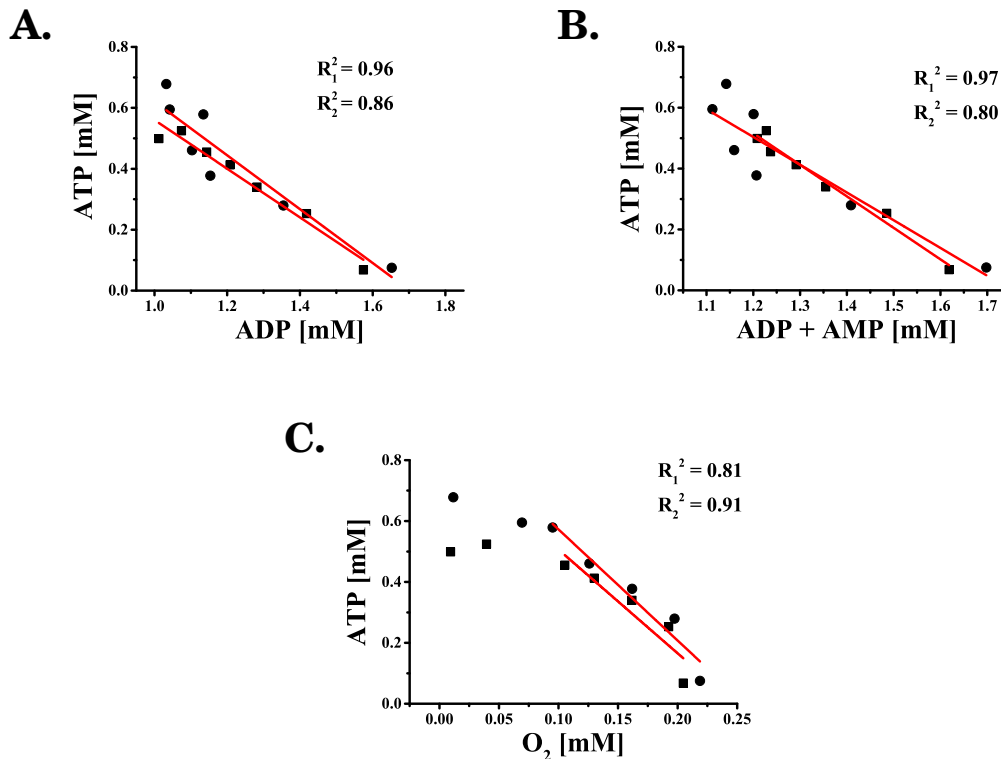


Figure 4.14: Ratio [A] of the concentration of ATP to ADP ((■) and (●). Ratio [B] of ATP to the sum of ADP and AMP ((■) and (●) for duplicate experiments). Relationship [C] of the net formation of ATP to the amount of oxygen being consumed. Substrate composition, concentrations and experimental setup detailed in Figure 4.12. Red line indicates each curve of the regression analysis along with each $R^2$.

During NADH-oxidation there were also enzymatic activities interconverting adenosine nucleotides other than the ATP synthase as was evident by the continuous formation of AMP (in comparison to ATP formation over time, Figure 4.13.C). Thus, the activity of ATP or ADP hydrolysing activities in the cytosol could be confirmed by the presence of AMP.

By illustrating graphically ATP as a function of ADP as depicted in Figure 4.14.A for two independent measurements in the closed reactor system, a ratio of ATP/ADP of 0.84 ± 0.06 mol/mol was calculated. When the net production of AMP was taken into account, the ratio of ATP/(sum of AMP and ADP) was equal to 0.97 ± 0.09 mol/mol (Figure 4.14.B). It was hypothesized that cytosolic ADP was exchanged for mitochondrial ATP by the ANT and in the mitochondrial matrix it served as a substrate for the formation of ATP by the ATP synthase. Subsequently the ATP in the cytosol could be hydrolysed to ADP and/or to ADP and AMP or ADP instead could be directly hydrolysed to AMP under these conditions. A general scheme for this scenario is illustrated in Figure 4.15.
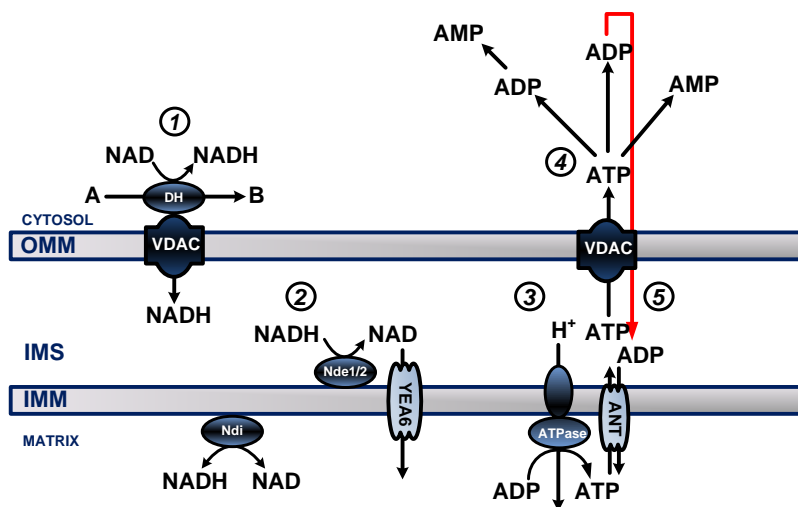


Figure 4.15: General reaction scheme for the fate of mitochondrially produced ATP during the oxidation of *in situ* formed NADH. 1. NADH is formed; 2. NADH is oxidized; 3. ATP is formed in the mitochondrial matrix 4. ATP is metabolized in the cytosol; 5. ADP re-enters the mitochondrial matrix. Enzymes illustrated here are: DH, cytosolic dehydrogenase oxidizing A to B; NDE1/2, external mitochondrial NADH dehydrogenases; NDI, internal mitochondrial NADH dehydrogenases; ATPase, mitochondrial matrix ATP synthase. The mitochondrial transporters docked on the OMM and IMM are: VDAC, voltage-dependent anion channel or porin; ANT, adenine nucleotide translocator; YEA6, NAD transporter. The cytosolic compartment (CYT) is separated from the IMS by the outer mitochondrial membrane (OMM) and the IMS from the mitochondrial matrix by the inner mitochondrial membrane (IMM).

The P/O ratio was calculated and compared to the theoretical P/O value, in order to examine mitochondrial bioenergetics and the extent of mitochondrial and

cytosolic ATP formation. In previous parts it was mentioned that the theoretical P/O ratio for succinate as a respiratory substrate for the yeast ATP synthase pumping 10 protons for each 3 ATP molecules synthesized and for complexes III and IV transporting electrons would be 6/(10/3+1) $\simeq$ 1.38. As there is no proton-pumping complex I in yeast, the theoretical P/O ratio on NADH will be identical to the one on succinate. The experimental P/O ratio during NADH (*in situ* formed) oxidation was calculated in a similar fashion as for succinate oxidation and was inferred from the ATP/$O_2$ which was equal to 3.53 $\pm$ 0.17 mol/mol (P/O = (ATP/$O_2$)/2 = 1.76 $\pm$ 0.09) (Figure 4.14.C).

This ratio was higher than the P/O ratio expected from the theoretical stoichiometry of protons moved through the respiratory chain and ATP molecules synthesized by the ATP synthase. This could be caused by a source of ATP formation different than the mitochondrial one. The NADH generation in the cytosol via the glyceraldehyde 3-phosphate dehydrogenase, could have activated kinases located downstream from this enzyme in the presence of ADP (phosphoglycerate kinase and pyruvate kinase), thus generating additional ATP in the cytosol. Therefore the increased P/O ratio compared to the theoretical one can be attributed to the fraction of non-mitochondrial ATP formation due to glycolytic enzymes activated downstream of the glyceraldehyde 3-phosphate dehydrogenase. However no 3-phosphoglycerate, PEP, pyruvate or acetaldehyde were detected chromatographically in the mitochondrial extracts.

### 4.2.2.3 The dynamics of *in situ*-formed NADH oxidation by selectively permeabilized cells

The next step towards characterizing respiration and mitochondrial metabolism under the aforementioned conditions (*in situ* formed NADH) was to monitor the evolution of the NADH concentration over time. First of all it was assessed that during state 4 respiration experiments without ADP being added to the reaction mixture, no NADH was formed. This was indicative of no other NAD-reducing reaction being active when NAD was present in the cytosol along with fructose 1,6-bisphosphate.

Illustrated in Figure 4.16.A is the evolution of NADH concentration profile over time during ADP-driven respiration. NADH was formed rapidly by the glyceraldehyde 3-phosphate dehydrogenase in the cytosol and then was continuously transported through the outer mitochondrial membrane into the IMS. There NADH was oxidized by the external NADH dehydrogenase (Nde1/2p) (see Figure 4.11). Therefore, since samples represent total cell extracts per time point, the steady state kinetics represent the sum of: i. NADH oxidation in the mitochondrial intermembrane space and ii. NAD reduction in the cytosol by the glyceraldehyde 3-phosphate

dehydrogenase.

The time point where NADH was completely exhausted coincided with the mitochondria transitioning from state 3 maximum respiration to the reduced and uncoupled state 4 respiration and the characteristic leveling off for ADP and ATP. After this point, NADH could not be detected, with the lower detection limit lying between 5-10 $\mu$M. The net rate of NADH elimination due to oxidation was 0.016 ± 0.001 mM/min (specific rate of NADH oxidation $q_{NADH}$ = 6.35 ± 0.81 nmol/(mg CDW×min)).
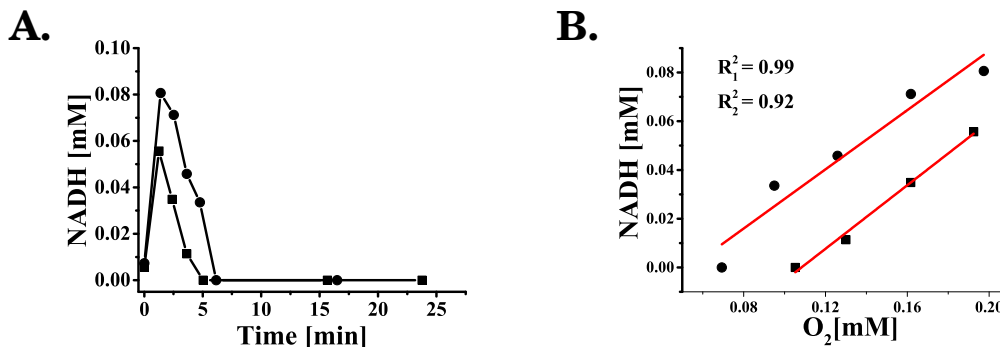


Figure 4.16: Digitonin-permeabilized *S. pombe* cells respired in the closed, reactor system with the supply of 10 mM fructose 1,6-bisphosphate, 2 mM NAD and 2 mM ADP. Results represent two independent experiments ((■) and (•)). Evolution [A] of NADH over time. Molar yield [B] of NADH on oxygen that was consumed by the mitochondria in the reactor. Red line indicates the curve of the regression analysis along with the $R^2$.

Another characteristic of respiring mitochondria during state 3 respiration was the yield of total NADH on oxygen as exhibited in Figure 4.16.B. The $Y_{NADH/O_2}$ was 0.63 ± 0.03 mol/mol. The theoretical $Y_{NADH/O_2}$ if NADH would only be oxidized (equation 4.1) from the mitochondria would be equal to $Y_{NADH/O_2}$ = 2.

$$NADH + \tfrac{1}{2}O_2 \rightleftharpoons NAD + 2H^+ + 2e^- \qquad (4.1)$$
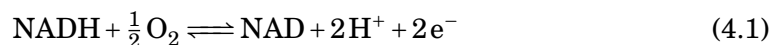
However, the experimental yield illustrated here encompasses NADH being simultaneously synthesized due to the activity of the glyceraldehyde 3-phosphate dehydrogenase as well. Therefore the molar yield of NADH on $O_2$ can not be equal to 2. To summarize, although oxygen was consumed with a maximum rate in the first 5 minutes, NADH was initially synthesized with a higher rate than being oxidized and was then swiftly consumed with a higher rate leading to its depletion after 5 minutes.

### 4.2.2.4 Quality control of the chromatographic quantification of adenosine nucleotides and redox precursors

After the quantification of adenosine nucleotides and redox cofactors, the sum of the concentration for each pool was plotted versus the duration of each experiment. The adenosine nucleotide pool was represented by the sum of AMP, ADP and ATP throughout a typical experiment (Figure 4.17.A). The redox cofactor pool was represented in a simmilar manner by the sum of NAD and NADH (Figure 4.17.B). These results were used as a quality control for the HPLC quantification of the aforementioned pools in order to follow the interconversion of an initially added substrate to its products. Any reduction of the initial concentration of the substrate has to be recovered as an equal increase in the concentration of newly formed products in the end. Therefore the sum of the products and substrates concentrations has to be constant over time.

**A.**

**B.**
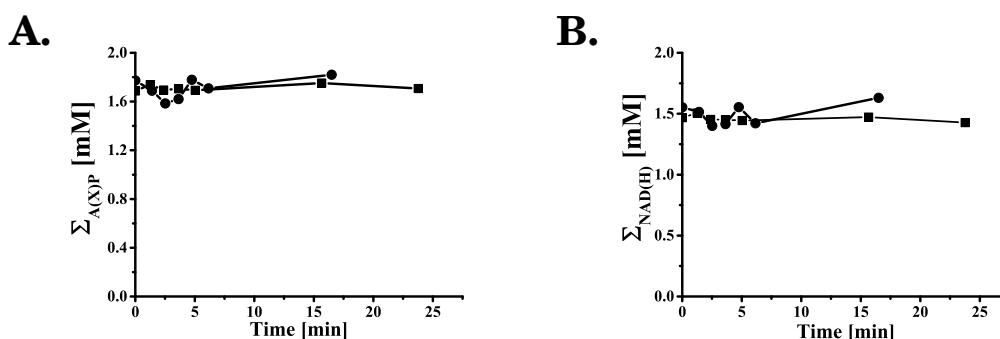


Figure 4.17: Sum of the concentration of adenosine nucleotides $\Sigma_{A(X)P}$ [A] and sum of the concentration of redox precursors $\Sigma_{NAD(H)}$ [B] during duplicate experiments ((■) and (●)) with selectively permeabilized cells harvested from parallel cultivations. Experimental setup detailed in Figure 4.12.

## 4.2.3 Metabolite channeling through the porin of the outer mitochondrial membrane

The strategies employed so far in order to elucidate the oxidation of NADH throughout the respiratory chain of *S. pombe* mitochondria are summarized in Figure 4.18. When NADH was supplied exogenously (Figure 4.18.A) or was generated in the cytosol by dehydrogenases (malic enzyme, possibly a cytosolic malate dehydrogenase and glutamate dehydrogenase) together with the supply of malate, glutamate and NAD (Figure 4.18.B), the mitochondrial oxidation of NADH was limited. One of the interesting implications of NADH oxidation was the fact that the respiratory efficiency of mitochondria increased when NADH was formed from NAD in the cytosol by employing a main glycolytic enzyme (GA3P-DH) (Figure 4.18.C). This was predominantly exhibited by a higher rate of ADP-activated respiration, an ef-

ficient coupling between respiration and ADP phosphorylation (high RCR) and the decrease of the proton leak (lower state 4 respiration).

It was hypothesized that a porin structure, namely the VDAC (voltage-dependent anion channel, POR1 in Figure 4.18.C), may play a role as mediator in bridging elements of the cytosol and the IMS. The core of this hypothesis entails the functional association of cytosolic enzymes with the OMM via the VDAC allowing for respiratory substrates like NADH to be efficiently channeled towards the sites of mitochondrial oxidation in the IMS. Therefore the next step was to verify whether the elimination of the outer mitochondrial membrane porin would have any influence on NADH oxidation during the *in situ* NADH formation in the cytosol by the glyceraldehyde 3-phosphate dehydrogenase. This is schematically illustrated with Figure 4.18.D.

To answer whether the outer mitochondrial membrane porin is implicated in metabolite channeling, specifically of NADH, a porin-deficient *S. pombe* mutant was examined. More specifically, the porin sequence based on homology is predicted to be SPAC1635.01, and its expression product is homologous to the Por1p and Por2p of *S. cerevisiae* and the VDAC1, VDAC2 and VDAC3 proteins of *H. sapiens*. A *S. pombe* VDAC deletion mutant was provided by Bioneer with the genotype orf4Δ: kanMX4 *ade6*-M216 *ura4*-D18 *leu1*-32. The mutant strain grew in glucose minimal medium containing 250 mg/L of adenosine, uracil, leucine along with 200 μg/L of the antibiotic geneticin G418. When cells reached the mid-exponential growth phase, they were harvested and selectively permeabilized with digitonin exactly as with wild type *S. pombe* cells in previous respiration studies.
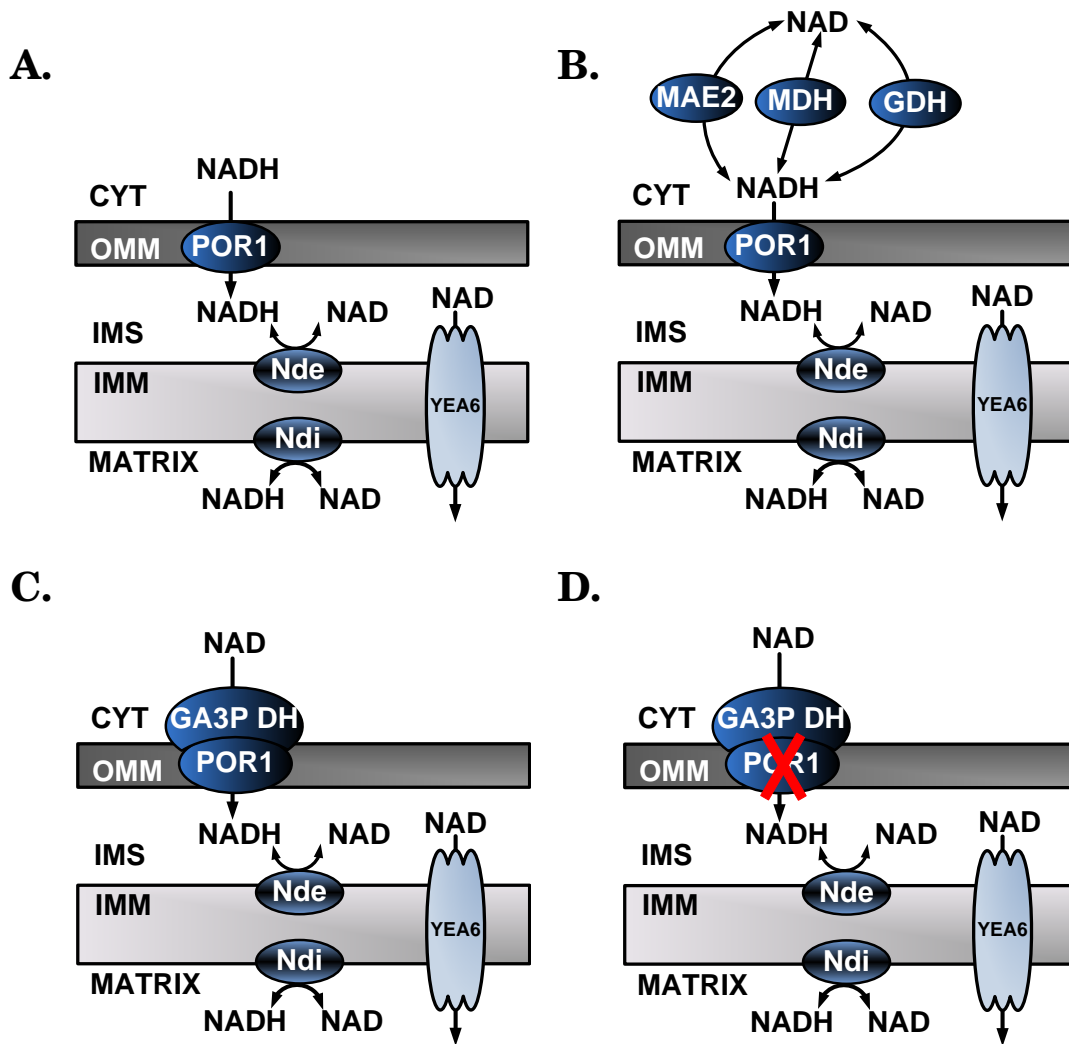
Figure 4.18: Summary of all scenarios experimentally examined where NADH was the main respiratory substrate. [A] Supply of 1 mM NADH in the cytosol. [B] Supply of 2.5 mM malate and glutamate along with 1 mM NAD. [C] Supply of 2 mM of NAD and 2 mM ADP along with 10 mM fructose 1,6-bisphosphate. [D] Supply of 2 mM of NAD and 2 mM ADP along with 10 mM fructose 1,6-bisphosphate in selectively permeabilized *S. pombe por1Δ* cells. Enzymes and transporters illustrated here are: MAE2, malic enzyme; MDH: malate dehydrogenase; GDH: glutamate dehydrogenase; NDE: external NADH dehydrogenase; NDI: internal NADH dehydrogenase; YEA6: mitochondrial NAD transporter; POR1: the OMM porin or VDAC. The cytosolic compartment (CYT) is separated from the IMS by the outer mitochondrial membrane (OMM) and the IMS from the mitochondrial matrix by the inner mitochondrial membrane (IMM).

As it is illustrated in Figure 4.19 the deletion of the gene coding for VDAC, led to a significant impairment of mitochondrial respiration under ADP-activated conditions. Respiration of mitochondria derived from the mutant cells, was reduced 6-fold compared to the wild type with a respiration rate of $0.005 \pm 0.001$ mM/min (specific respiration rate $q_{O_2} = 1.84 \pm 0.23$ nmol/(mg CDW×min)).
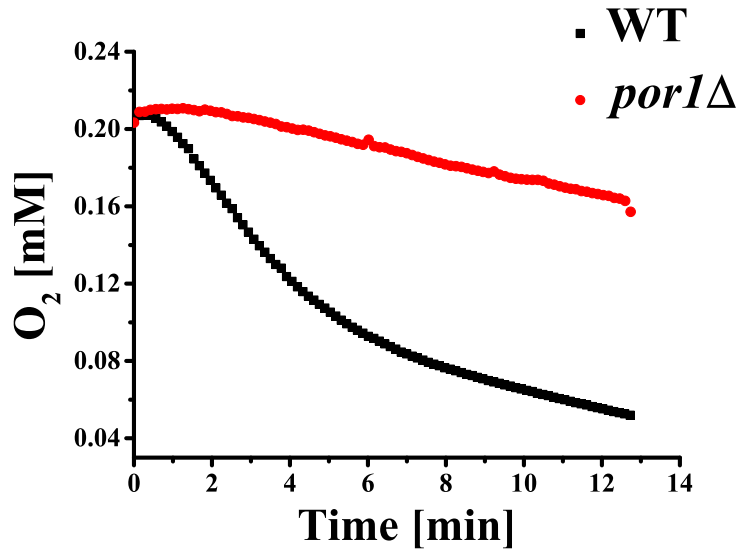
Figure 4.19: Evolution of oxygen concentration in the sealed reactor system over time for digitonin-permeabilized cells in the presence of 10 mM fructose 1,6-bisphosphate, 2 mM NAD and 2 mM ADP in respiratory buffer. Comparison between a typical mitochondrial respiration experiment with wild type *S. pombe* cells (■) and porin-deficient *S. pombe por1Δ* cells (•). Average final cell concentration in reactor for duplicate experiments with the aforementioned conditions: Wild type = 2.55 ± 0.08 g/L, *por1Δ* = 2.49 ± 0.01 g/L.

At the same time, as it is illustrated in Figure 4.20.A, NADH was accumulated initially while oxygen was consumed. NADH was not rapidly oxidized in the mitochondria as it was the case with the wild type *S. pombe* mitochondria because of the non-functioning VDAC. The absence of a functional porin on the OMM led to the loss of metabolite channeling of NADH from the glyceraldehyde 3-phosphate dehydrogenase in the cytosol to the IMS, thus failing to support a high respiratory capacity.

After some point, NADH did not accumulate any more. Both the accumulation and stationary phases of NADH can be explained as follows. NADH was in the beginning continuously formed by the glyceraldehyde 3-phosphate dehydrogenase at a rate faster with which it was eventually diffused into and oxidized by the mitochondria, due to the absence of a functional porin. Therefore, the lack of functional metabolite channeling led to NADH being accumulated initially in the cytosol. Subsequently, after the accumulation of NADH came a phase where its levels remained constant. This can be attributed in a small extent to NADH oxidation in the IMS on one hand and on the presence of NADH and ATP on the other hand. Both NADH and ATP can act as competitive inhibitors of the glyceraldehyde 3-phosphate dehydrogenase therefore increasing its $K_m$-value for NAD (Aithal et al., 1985) and slowing down the NADH formation rate.
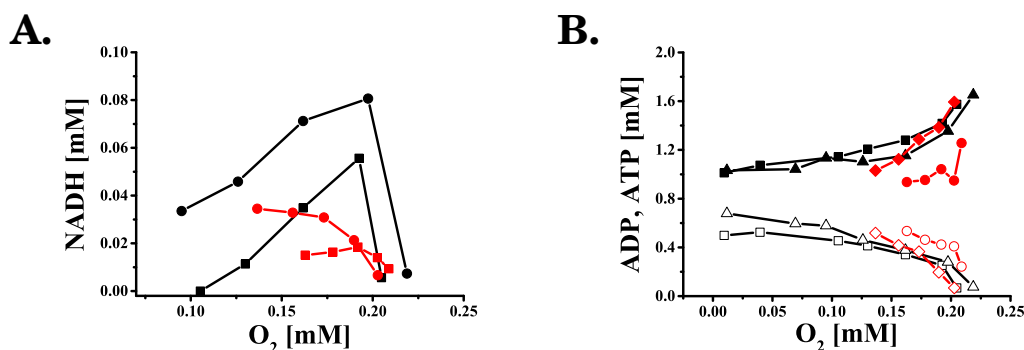
Figure 4.20: Relationship [A] between produced NADH and uptaken $O_2$ for the wild type (($\blacksquare$) and ($\bullet$)) and for strain *por1*$\Delta$ (($\color{red}\blacksquare$) and ($\color{red}\bullet$)) during duplicate experiments in the sealed reactor. Comparison [B] of ADP consumed during $O_2$ uptake by permeabilized wild type cells (($\blacksquare$) and ($\blacktriangle$)) and by the *por1*$\Delta$ strain (($\color{red}\bullet$) and ($\color{red}\blacklozenge$)). Comparison of ATP synthesized during $O_2$ uptake by permeabilized wild type cells (($\square$) and ($\triangle$)) and by the *por1*$\Delta$ strain (($\color{red}\circ$) and ($\color{red}\diamond$)). Wild type = $2.55 \pm 0.08$ g/L, *por1*$\Delta$ = $2.49 \pm 0.01$ g/L.

The adenosine nucleotide yields also changed for the *por1*$\Delta$ strain ($Y_{ADP/O_2}$ and $Y_{ATP/O_2}$) compared to wild type cells (Figure 4.20.B). The $Y_{ADP/O_2}$ for the *por1*$\Delta$ strain was $6.54 \pm 2.41$ mol/mol (compared to $3.93 \pm 0.05$ mol/mol for the wild type) and the $Y_{ATP/O_2}$ was $5.91 \pm 1.08$ mol/mol (compared to $3.53 \pm 0.17$ mol/mol for the wild type). These findings for mitochondria that lack an OMM porin show that while the only point of the metabolism perturbed was the passage of NADH to the IMS and to its oxidation site it increased the cost on oxygen for the uptake and interconversion of ADP and ATP at the ATP synthase site, as was shown with the higher yields for ADP and ATP on oxygen.

The comparison of ADP and ATP uptake and synthesis rates respectively for the wild type and porin-deficient mitochondria in nmol/(mg CDW×min), further supported the aforementioned findings (Figure 4.21). The rates were calculated for the beginning of each experiment (initial 4 - 5 minutes), where it was assumed that mitochondria functioned at their maximum capacity during ADP-driven, state 3 respiration. The net elimination and formation rates for ADP and ATP respectively for strain *por1*$\Delta$, before their concentrations leveled off, were $0.05 \pm 0.01$ mM/min (specific rate $q_{ADP} = 18.3 \pm 2.2$ nmol/(mg CDW×min)) and $0.04 \pm 0.01$ mM/min (specific rate $q_{ATP} = 15.8 \pm 3.7$ nmol/(mg CDW×min)).

Evidently, the absence of the mitochondrial outer membrane porin had an effect on the rate that the ANT and the ATP synthase functioned due to the limited availability of NADH in the IMS. Therefore as it was described previously, the state 3 respiration rate could not reach its maximum capacity due to a limited supply of electrons from NADH, affecting the speed of the end-step of the respiratory chain as well. This further illustrates the interplay between elements of the mitochondrial membrane that facilitate metabolite transport and enzymes located either in the

cytosolic or in the mitochondrial side.
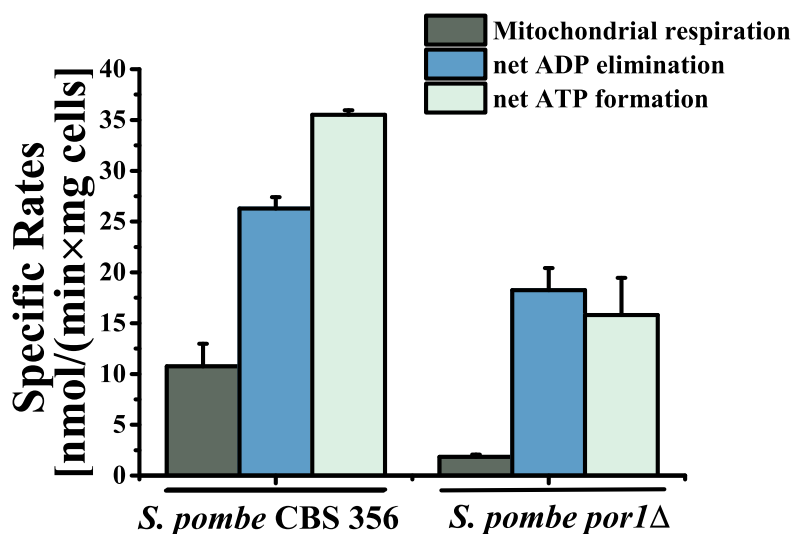


Figure 4.21: A comparison between the specific rates for oxygen and ADP uptake and ATP synthesis nmol/(mg CDW×min) for the *S. pombe* wild type cells (CBS 356) and the porin-deficient *S. pombe* Δ*por* cells. Experiments were conducted in duplicates in the closed, reactor system at 30 °C in the presence of 10 mM fructose 1,6-bisphosphate, 2 mM NAD and 2 mM ADP in respiratory buffer.

Conclusively, these data strongly support the fact that just supplying exogenous NADH to mitochondria does not lead them to consume oxygen efficiently with a high RCR. It is therefore necessary to connect the NADH supply to the external NADH-dehydrogenase in the IMS with the precursor's synthesis in the cytosol via the porin structure of the OMM. Such an approach was succesfully employed when NADH was formed *in situ* in the cytosol with NAD as a substrate by the NAD-dependent glyceraldehyde 3-phosphate dehydrogenase activity. Furthermore, by comparing mitochondrial function (respiration, energy formation, substrate uptake) of the mutant *S. pombe* strain to the one derived from the wild type *S. pombe*, it is clear that the porin-coding sequence, SPAC1635.01, is the one that expresses the OMM-porin structure, which is of central importance for metabolite channeling of substrates from the cytosol to the IMS. Thus, it was illustrated that by employing selectively permeabilized cells with well coupled, intact mitochondria that respire in a sealed mini-reactor it is possible to identify the function of a mitochondrial transporter-coding gene.

# 4.3 The entry of pyruvate into fission yeast mitochondria

Pyruvate is one of the most highly participating intermediate in a plethora of metabolic reactions. This three-carbon carboxylate functions mainly as a substrate in mitochondria for the formation of acetyl-CoA, as the precursor for the biosynthesis of the branched chained amino acids (leucine, valine, isoleucine) and participates in the synthesis of lipoic acid, an important precursor for various multienzymatic complexes like the pyruvate dehydrongenase complex (Pronk et al., 1996; Schonauer et al., 2009).

Moreover pyruvate holds a central position at the cytosol-mitochondria interface, since the cytosolic pyruvate node serves as the main entry point of carbon flux from the glycolysis into the TCA cycle via the mitochondrial pyruvate transport system. Simultaneously under appropriate growth conditions the pyruvate node branches towards the ethanol biosynthetic pathway in the cytosol and towards the anaplerotic reactions connecting pyruvate to oxaloacetate and malate. It is therefore clear that this node where fluxes converge and diverge at the cytosol-mitochondria interface can play a regulatory role influencing the fermentative and respirative metabolism which govern the Crabtree effect.
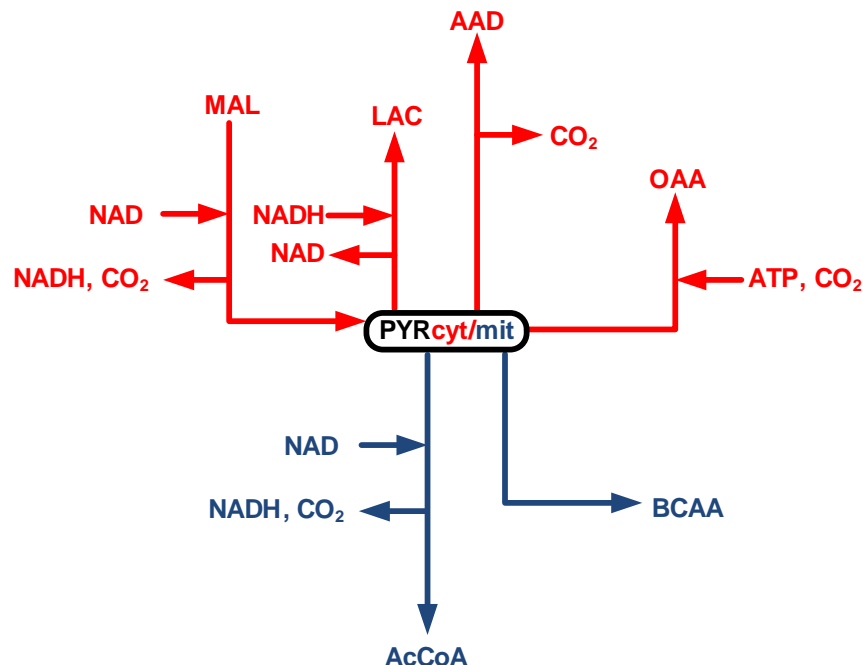


Figure 4.22: A generalized depiction of the fate of the pyruvate pool in the cytosol (red-colored reactions) and mitochondria (blue-colored reactions) interface. PYR: pyruvate; MAL: malate; LAC: L-lactate; AAD: acetaldehyde; OAA: oxaloacetate; AcCoA: acetyl-CoA; BCAA: branched chain amino acids.

In mammalian cells the glycolytic flux at the pyruvate node splits into either the formation of lactate in the cytosol and/or is uptaken by mitochondria where it is oxidized. The major enzymatic activities of the central metabolism that are bound to pyruvate can be organized into the cytosol- and mitochondria-located ones, as illustrated in Figure 4.22. Starting from the left, the *S. pombe* malic enzyme (expressed by gene sequence *mae2*) is located solely in the cytosol and is NAD-dependent and responsible for the oxidative decarboxylation of L-malate to pyruvate and $CO_2$ (Viljoen et al., 1994, 1999). According to the PomBase database and based on sequence homology a further malic enzyme has been predicted to exist, localized in the mitochondrial matrix and encoded by gene sequence SPAC750.08c, although no experimental information exists to support its mitochondrial localization.

A probable L-lactate dehydrogenase has been predicted to exist in the cytosol (gene sequence SPAC186.08c) and a D-lactate dehydrogenase (SPBC713.03) in mitochondria, however direct experimental data on their activity do not exist. It is only known that D-lactate and L-lactate do not support growth of intact *S. pombe* cells, are not oxidized by isolated mitochondria and L-lactate can be oxidized in the cytosol solely (higher oxidation when cells are grown aerobically on glycerol instead on glucose) (Heslot et al., 1970). The occurence of intracellular lactate was only observed in engineered *S. pombe* cells possessing a malolactic enzyme from *L. lactis* (Ansanay et al., 1996).

The next cytosolic enzyme connected to the pyruvate node, is also the first step of the cytosolic ethanol biosynthesis in *S. pombe*, namely the pyruvate decarboxylase activity. The products are acetaldehyde and $CO_2$. The predicted protein coding sequences, based on the PomBase database, are SPAC13A11.06, SPAC186.09, SPAC1F8.07c and SPAC3G9.11c. In *S. cerevisiae* there are 3 isozymes functioning as pyruvate decarboxylases with Pdc1p the major one (Pronk et al., 1996) and the enzyme itself is a tetramer. Finally, another enzymatic activity connected to cytosolic pyruvate is the pyruvate carboxylase, encoded by *pyr1*. The enzyme is part of the anaplerosis and catalyses the ATP-dependent carboxylation of pyruvate towards the synthesis of oxaloacetate in the cytosol.

In the mitochondrial matrix, pyruvate can act as substrate for the synthesis of branched chain amino acids (BCAA-leucine, valine, isoleucine) and also be decarboxylated by the pyruvate dehydrogenase complex forming NADH and acetyl-CoA. The *pda1* gene is predicted to encode the *S. pombe* pyruvate dehydrogenase E1 component alpha subunit which is part of the multimeric complex linking glycolysis to the TCA cycle. In *S. cerevisiae* the first step catalyzed by this enzyme of the pyduvate dehydrogenase complex yields an active aldehyde, which is also an early substrate for the biosynthesis of leucine and valine (Pronk et al., 1996).

The mitochondrial transporter system for pyruvate is of considerable importance, controlling the rate of its entry into the mitochondrial matrix where it is oxidized and thus participates in energy formation on one hand and in the fueling of the TCA cycle with carbon on the other. The gene sequences coding for the mitochondrial pyruvate carrier (MPC) proteins have been unearthed only recently providing some insight on the structure, function and regulation of this transporter system (Herzig et al., 2012; Bricker et al., 2012). In *S. cerevisiae* the transporter was found to form a 150 kDa oligomeric heterocomplex consisting of proteins Mpc1p (or Mpc3p depending on the presence of lactate) and Mpc2p, anchored on the IMM (inner mitochondrial membrane) with Mpc2p more likely being the major structural subunit. The function of the *S. pombe* MPC during pyruvate metabolism will be covered in detail in subsequent parts.

### 4.3.1 Quantifying *in vivo* carbon fluxes at the pyruvate node

As it was described in previous parts, the cytosolic pyruvate pool is the point of the respirofermentative metabolism of glucose where the glycolytic flux converges and then diverges towards anaplerosis, the mitochondria and the ethanol biosynthetic pathway. However before assessing how pyruvate is utilized by mitochondria *in situ*, it is important to obtain a snapshot of the *in vivo* fluxes of carbon throughout the central metabolism during growth on glucose in batch cultivations.

This snapshot or carbon flux map can reveal the degree in which the pyruvate flux is split at the cytosol-mitochondria interface and provide us with which fluxes mark entry or exit points of intermediates in or out of mitochondria respectively. Furthermore, this approach entails conditions where cells grow exponentially with glucose as a substrate, which are the identical conditions of growth for cells used for *in situ* studies after digitonin-permeabilization has been applied. Metabolic flux analysis has already been applied in engineered *S. pombe* cells growing in chemostat cultures containing glucose and glucose/acetate mixtures, where the effect of secreted proteins on the central metabolism was studied (Klein et al., 2014).

#### 4.3.1.1 Setting up the metabolic network

The metabolic network on which the flux analysis was based on, consisted of the glycolysis, the pentose phosphate pathway, the TCA cycle and the fermentative pathway towards ethanol production. Additionally other metabolic pathways taken into account were the anaplerotic reaction of pyruvate to oxaloacetate catalysed by the pyruvate carboxylase and all fluxes that led from central metabolism intermediates to the formation of proteinogenic amino acids, that were eventually incorporated into cellular biomass.

Establishing which reactions were used for constructing the *S. pombe* metabolic network was based on published experimental data on the enzymatic activities of the central metabolism and their topology, predicted from the PomBase database and the reconstructed genome-scale metabolic network of *S. pombe* SpoMBEL 1693 (Sohn et al., 2012). Also previous models based on *S. cerevisiae* were used as a guide due to the similarities between the two yeast systems. Nonetheless there are some profound differences between the metabolism of the two organisms, that will be covered in subsequent parts (see Appendix, Table 1 for central metabolism model).

**Glycolysis.**   The entry of glucose into the cytosol follows the irreversible phosphorylation catalysed by the phosphoglucomutase activity and then the reversible isomerization by the glucose 6-phosphate isomerase. The latter reaction was defined as the first step into the metabolic network. Five reactions followed -four of them irreversible and one reversible (triosephosphate isomerase)- marking the flow of glucose 6-phosphate into pyruvate in the cytosolic compartment. The flow was diverted towards covering the anabolic demand for lipids, carbohydrates, proteins and nucleotides at the glucose 6-phosphate (G6P), glyceraldehyde 3-phosphate (GA3P), 3-phosphoglycerate (3PG), phosphoenolpyruvate (PEP) and pyruvate (PYR) nodes. Two products of the glycolytic pathway were exported from the cells, namely glycerine and pyruvate, as confirmed by their quantification in the supernatant of growing (with glucose as the carbon source) *S. pombe* cells.

**Pentose phosphate pathway.**   At the glucose 6-phosphate node, the carbon flux was diverted into the pentose phosphate pathway (PPP) with the first step being irreversibly catalysed by the glucose 6-phosphate dehydrogenase. All reactions leading from glucose 6-phosphate to the 5-carbon containing metabolites (ribulose 5-phosphate, xylulose 5-phosphate and ribose 5-phosphate) were summed into one irreversible decarboxylation reaction and the aforementioned metabolites into one metabolite pool with the name pentose 5-phosphate. Members of the pentose 5-phosphate pool share a common carbon skeleton and therefore have the same carbon labeling pattern. The reversible reactions of the PPP were catalysed by the transaldolase and transketolase activities stemming from the pentose 5-phosphate pool. Anabolic fluxes towards the formation of nucleotides and amino acids were diverted from the pentose 5-phosphate pool and the erythrose 4-phosphate.

**Ethanol biosynthetic pathway.**   At the cytosolic pyruvate node, pyruvate was decarboxylated by the pyruvate decarboxylase producing $CO_2$ and acetaldehyde. Acetaldehyde could then lead either to the formation of acetate (and subsequently to acetyl-CoA) and to ethanol. All reactions were considered to be irreversible and

ethanol was defined as a metabolite that could be exported to the extracellular environment along with pyruvate and glycerine that were mentioned above. The contribution of acetyl-CoA to lipid biosynthesis was also taken into account.

**Anaplerosis.** Two irreversible reactions were grouped together as anaplerotic with pyruvate occuring as a metabolite in both pathways. The first one was the pyruvate decarboxylating reaction of pyruvate towards oxaloacetate (OAA) and the other one the cytosolic NAD-dependent malic enzyme. The *in vitro* enzymatic activity of malic enzyme was quantified and it was established that there is no enzymatic activity with NADP as the redox precursor. The cytosolic malic enzyme (Mae2p), encoded by gene *mae2* (Viljoen et al., 1994), can function in the decarboxylating direction towards the reduction of NAD and replenishment of the cytosolic pyruvate pool. The cytosolic OAA pool was further connected with the cellular demand for protein synthesis. It has been verified that the gluconeogenic enzyme PEP-carboxykinase does not exist in *S. pombe* cell extracts (de Jong-Gubbels et al., 1996).

**TCA cycle.** The mitochondria were the focal point of the quantification of the *in vivo* fluxes of the *S. pombe* central metabolism and the compartment where the TCA cycle was active. The entry points of carbon into the TCA cycle were based on the existing knowledge about mitochondrial membrane transporters that were extensively described in the introductory part of this work. These points connected the cytosolic pools of pyruvate, oxaloacetate, malate and acetyl-CoA to their mitochondrial counterparts. Oxaloacetate could be transferred preferentially by the Oac1p transporter (expressed by the predicted sequence SPAC139.02c) and to a lesser extent by the citrate transporter, similar to *S. cerevisiae* that possesses the citrate transporter Yhm2p (Castegna et al., 2010b).

Oxaloacetate transfer throughout the mitochondria was considered to be occurring in both directions. During the setup of the metabolic network it was hypothesized that pyruvate can be actively transported through the inner mitochondrial membrane, assuming that the mitochondrial pyruvate carrier proteins exist in *S. pombe*. The mechanism of mitochondrial pyruvate uptake was a matter of debate (Hildyard and Halestrap, 2003b; Todisco et al., 2006), until the genetic sequence for such a transport mechanism was identified in 2012 for *Drosophila*, humans and *S. cerevisiae* (Bricker et al., 2012; Herzig et al., 2012). Concerning *S. pombe* such a mechanism has not been yet identified, while in the PomBase database two mitochondrial pyruvate carriers are predicted to exist (Mpc1p and Mpc2p) encoded by sequences SPCC1235.11 and SPAC24B11.09 respectively.

As for malate, its efflux from the mitochondria was considered to take place as

well, even if it is up to now unknown whether a dicarboxylate carrier protein exists that could facilitate such a transfer in *S. pombe*. In previous parts of this work (see Section 4.1) it was discussed how a mitochondrial transport system for malate may actually exist in *S. pombe* as well. The import of acetyl-CoA into the mitochondria is not resolved in *S. pombe* but it was inferred during the reconstruction of its metabolic network that such a shuttle system for the indirect carnitine-dependent transfer of acetyl-CoA has to exist. Although there are no sequences homologous to the carnitine-dependent acetyl-CoA transferases of *S. cerevisiae* (*CAT2*, *YAT1*, *YAT2*) (Sohn et al., 2012), the *S. pombe ort1* sequence showed homology to the *S. cerevisiae CRC1* gene which expresses a carnitine transporter and is part of the carnitine-dependent transfer mechanism of acetyl-CoA from peroxisomes to mitochondria during fatty acid beta-oxidation.

In total, six reactions comprised the TCA cycle with only the fumarase activity being reversible. The citrate and isocitrate pools were lumped together due to identical carbon labeling. Fluxes stemmed from oxaloacetate, $\alpha$-ketoglutarate, pyruvate and acetyl-CoA towards meeting the cellular anabolic demands for biomass formation. Based on the PomBase database, there are isocitrate dehydrogenase isoforms predicted to have specificity for either NAD (Idh1p/Idh2p) or NADP (Idp1p), with either mitochondrial and/or cytosolic localization. The $\alpha$-ketoglutarate dehydrogenase is predicted to be encoded by genes SPBC3H7.03c and *kgd2* (*e1* and *e2* components of the enzymatic complex respectively). During the construction of the metabolic network the $\alpha$-ketoglutarate dehydrogenase was lumped together with the also mitochondrially localised succinyl-CoA ligase. The end-products of both reactions are $CO_2$, NADH and succinyl-CoA.

The last reactions of the TCA cycle which are also localized in the mitochondrial compartment, were the succinate dehydrogenase complex which yielded fumarate and $FADH_2$, the fumarase activity (Fum1p) which formed malate and finally the NAD-dependent malate dehydrogenase (Mdh1p) catalysing the formation of OAA. The rotational symmetry of the carbon skeleton of succinate was also taken into account for carbon transfer. The Fum1p is predicted to exist both in the cytosol and in the mitochondrial matrix.

### 4.3.1.2 Calculating the cellular anabolic demand for biomass

The next part focuses on the calculation of the amount of precursor molecules needed based on the actual cellular demands for amino acids, nucleotides, lipids and carbohydrates during growth on glucose in batch cultures. These data could be then used as input for the calculation of the *in vivo* fluxes that comprise the central metabolic pathways upon glucose uptake.

Since a high percentage (30-50 %) of yeast biomass consists of biosynthesized

proteins (de Jong-Gubbels et al., 1996), it was of importance to exactly quantify the amino acid composition of the total cellular protein fraction. Firstly, amino acid biosynthesis and localization of such pathways were incorporated into the metabolic network. Some amino acids were defined as being derived by precursor molecules (pyruvate and oxaloacetate) and relevant aminotransferases residing in both the cytosolic and the mitochondrial compartment, whereas others (valine and glutamate biosynthesis) were localized in the mitochondria.

All proteinogenic amino acids were quantified, in order to subsequently calculate the precursor demand needed for their biosynthesis in *S. pombe*. This precursor demand was then integrated in the model used for the Matlab-based quantification of the *in vivo* carbon fluxes. The results for all amino acids that were quantified and normalized for the biomass concentration are depicted in Table 4.3. The experimental results yielded here for each amino acid were compared to literature data from *S. cerevisiae* (Forster et al., 2003) to illustrate the similarities between the two organisms concerning amino acid biosynthesis and as a quality control step to ensure that the experimentally quantified values did not deviate from physiological values.

The typical protocol for the amino acid quantification of protein hydrolysates requires the acidic boiling at 100 °C for a duration of 24 h. However acidic hydrolysis can lead to an underestimation of sensitive amino acids after 24 h. First of all glutamine and asparagine are completely hydrolyzed to glutamate and aspartate respectively, cysteine can not be determined, serine and threonine have partial losses of 5-10% and tryptophan is completely destroyed after 24 h (reviewed in (Fountoulakis and Lahm, 1998)).

Table 4.3: Amino acid composition of the *S. pombe* total protein hydrolysate during exponential growth (pseudo steady state) with glucose as substrate during batch cultivation in shake flasks. Experimental results are compared to data from *S. cerevisiae* yielded on similar conditions that were used for the genome-scale reconstruction of its metabolic network (Forster et al., 2003). n.d denotes non determined amino acids. Glutamate and glutamine are summed together as GluX and aspartate and asparagine are summed as well as AspX. Along with the experimental data, the stoichiometric demand for central metabolism intermediates is illustrated as well for each amino acid. PYR: pyruvate; $\alpha$-KG: $\alpha$-ketoglutarate; OAA: oxaloacetate; 3PG: 3-phosphoglycerate; R5P: ribose 5-phosphate; EryP: erythrose 4-phosphate.

| | Amino acid content | | |
|---|---|---|---|
| Amino acid | *S. pombe* | *S. cerevisiae* | Precursor demand |
| | mmol/(g CDW) | mmol/(g CDW) | |
| Alanine | $0.444 \pm 0.034$ | 0.459 | $1 \times \text{PYR}_{mit,cyt}$ |
| Arginine | $0.248 \pm 0.016$ | 0.161 | $1 \times \alpha\text{-KG}$ |
| AspX | $0.478 \pm 0.048$ | 0.4 | $1 \times \text{OAA}$ |
| Cysteine | n.d | 0.006 | $1 \times \text{3PG}$ |
| GluX | $0.554 \pm 0.045$ | 0.407 | $1 \times \alpha\text{-KG}$ |
| Glycine | $0.379 \pm 0.019$ | 0.29 | $1 \times \text{3PG}$ |
| Histidine | $0.077 \pm 0.005$ | 0.066 | $1 \times \text{R5P}$ |
| Isoleucine | $0.149 \pm 0.013$ | 0.193 | $1 \times \text{PYR}_{mit}, 1 \times \text{OAA}_{cyt}$ |
| Leucine | $0.277 \pm 0.022$ | 0.296 | $2 \times \text{PYR}_{mit}, 1 \times \text{AcCoA}$ |
| Lysine | $0.314 \pm 0.014$ | 0.286 | $1 \times \alpha\text{-KG}$ |
| Methionine | $0.031 \pm 0.005$ | 0.051 | $1 \times \text{OAA}$ |
| Phenylalanine | $0.159 \pm 0.009$ | 0.134 | $1 \times \text{EryP}, 2 \times \text{PEP}$ |
| Proline | $0.167 \pm 0.001$ | 0.165 | $1 \times \alpha\text{-KG}$ |
| Serine | n.d | 0.185 | $1 \times \text{3PG}$ |
| Threonine | $0.241 \pm 0.019$ | 0.191 | $1 \times \text{OAA}$ |
| Tryptophan | $0.01 \pm 0.002$ | 0.028 | $1 \times \text{3PG}, 1 \times \text{EryP}, 1 \times \text{PEP}$ |
| Tyrosine | $0.144 \pm 0.008$ | 0.101 | $1 \times \text{EryP}, 2 \times \text{PEP}$ |
| Valine | $0.22 \pm 0.018$ | 0.265 | $2 \times \text{PYR}_{mit}$ |

Table 4.4: Stoichiometric demand for energy, redox cofactor molecules, $NH_3$, $CO_2$ and molecular sulfur needed for the biosynthesis of each proteinogenic amino acid that consisted part of the cellular biomass. Values were adapted from (Schneider, 2011).

| Amino acid | ATP | NADPH | NADH | $NH_3$ | $CO_2$ | S |
|---|---|---|---|---|---|---|
| Alanine | 0 | -1 | 0 | -1 | 0 | 0 |
| Arginine | -7 | -4 | 1 | -4 | 0 | 0 |
| Asparagine | -3 | -1 | 0 | -2 | 0 | 0 |
| Aspartate | 0 | -1 | 0 | -1 | 0 | 0 |
| Cysteine | -4 | -5 | 1 | -1 | 0 | -1 |
| Glutamine | -1 | -1 | 0 | -2 | 0 | 0 |
| Glutamate | 0 | -1 | 0 | -1 | 0 | 0 |
| Glycine | 0 | -1 | 1 | -1 | 1 | 0 |
| Histidine | -6 | -1 | 3 | -3 | -1 | 0 |
| Leucine | 0 | -2 | 1 | -1 | 0 | 0 |
| Isoleucine | -2 | -5 | 0 | -1 | 0 | 0 |
| Lysine | -2 | -4 | 2 | -2 | 0 | 0 |
| Methionine | -7 | -8 | 0 | -1 | -1 | -1 |
| Phenylalanine | -1 | -2 | 0 | -1 | 0 | 0 |
| Proline | -1 | -3 | 0 | -1 | 0 | 0 |
| Serine | 0 | -1 | 1 | -1 | 0 | 0 |
| Threonine | -2 | -3 | 0 | -1 | 0 | 0 |
| Tryptophan | -5 | -3 | 2 | -2 | 0 | 0 |
| Tyrosine | -1 | -2 | 1 | -1 | 0 | 0 |
| Valine | 0 | -2 | 0 | -1 | 0 | 0 |

Therefore we applied a series of hydrolysis times during a 24 h duration in order to recover the concentration of sensitive amino acids with as minimized losses as possible. It was verified that under 24 h each sample's volume remained constant, whereas during a more prolonged incubation (up to 129 h) there was significant volume loss. This approach is illustrated with two examples of the sensitive methionine and non-sensitive alanine in Figures 4.23.A & B respectively. Each amino acid concentration either leveled off (e.g. alanine) or reached a maximum value before decomposing after 24 h (e.g. methionine).

**A.**



**B.**
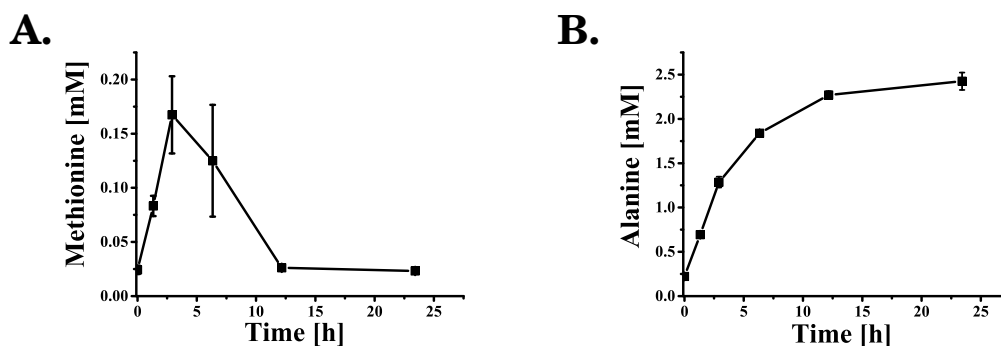


Figure 4.23: Examples for the acid hydrolysis of the *S. pombe* total protein at different time intervals at 100 °C. Quantification of the sensitive methionine [A] and of the more stable alanine [B] over time. Acid hydrolysis was performed in triplicates.

Table 4.4 combined with Table 4.3 illustrate specifically the metabolic cost for synthesizing every single amino acid in the cell that add up to the protein fraction (determined to be 0.502 g/(g CDW)) of the biomass. As metabolic cost here we define the stoichiometric demand for each one of the central metabolism intermediates/precursors (pyruvate, $\alpha$-ketoglutarate, oxaloacetate, 3-phosphoglycerate, glycerine 3-phosphate, ribose-5-phosphate, erythrose 4-phosphate and acetyl-CoA) along with energy (ATP), redox cofactors (NAD(P)H), $CO_2$, $NH_3$ and S.

The protein fraction was only a part of the sum of biopolymers that comprise the cellular biomass. Therefore, the molar fraction per gram of biomass was calculated for each metabolic precursor, energy and redox cofactors. The total amount of lipids was quantified gravimetrically (0.096 g/(g CDW)) using the Folch protocol and the stoichiometric demand for precursors for lipid biosynthesis was adapted from *S. cerevisiae* (Schneider, 2011). The amount of carbohydrates and nucleotides were adapted from *S. pombe*-specific data from the existing literature (Sohn et al., 2012). As a result a detailed analysis of the amount of metabolic intermediates, cofactors and energy needed for each biomass component (in mmol/(g CDW)) was calculated as illustrated in Table 4.5 and was integrated in the model that was used to quantify the *in vivo* fluxes. The sum of all biopolymers that led to the formation of biomass (based on the aforementioned quantification of total protein hydrolysate, lipids, DNA/RNA etc.) was depicted as a mass balance and can be summarized in Equation 4.2 with the sum of the components being 0.984 g/(g CDW) with the ash content not taken into account (usually 4 % CDW (Gombert et al., 2001)).

$$0.502 \, Protein + 0.108 \, DNA/RNA + 0.096 \, Lipids + 0.28 \, Carbohydrates \rightarrow Biomass$$

$$(4.2)$$
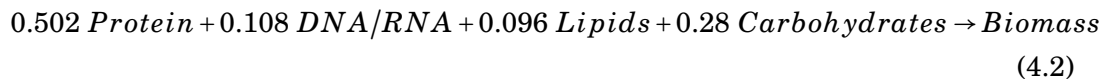
Table 4.5: Anabolic demand for central metabolism intermediates, redox cofactors and energy for the biosynthesis of proteins, lipids, nucleotides (DNA/RNA) and carbohydrates (in mmol/(g CDW)).

| Precursor | Protein | Lipid | Nucleotides | Carbohydrates | **SUM** |
|---|---|---|---|---|---|
| Glucose 6-P | 0 | 0.027 | 0 | 1.556 | 1.582 |
| Acetyl-CoA | 0.591 | 2.603 | 0 | 0 | 3.194 |
| $\alpha$-ketoglutarate | 1.283 | 0 | 0 | 0 | 1.283 |
| Erythrose 4-P | 0.313 | 0 | 0 | 0 | 0.313 |
| 3-phosphoglycerate | 0.379 | 0.043 | 0.166 | 0 | 0.588 |
| Glycerine 3-P | 0 | 0.105 | 0 | 0 | 0.105 |
| PEP | 0.616 | 0.043 | 0.166 | 0 | 0.616 |
| Pyruvate | 1.587 | 0 | 0 | 0 | 1.587 |
| Ribose 5-P | 0.087 | 0 | 0.166 | 0 | 0.253 |
| OAA | 0.899 | 0 | 0 | 0 | 0.899 |
| *NAD* | 1.927 | 0.013 | 0.499 | 0 | 2.440 |
| *NADPH* | 8.027 | 4.061 | 0.152 | 0 | 12.239 |
| *ATP* | 4.343 | 2.357 | 1.448 | 0 | 8.148 |

### 4.3.1.3  Taking into account the extracellular fluxes

As it was mentioned in previous parts, in order to calculate the *in vivo* fluxes it is important to enter the experimentally assayed extracellular fluxes to the existing model. These export fluxes connected intracellular to extracellular pool of metabolites that were secreted and quantified in supernatants taken from *S. pombe* cells growing on [1-$^{13}$C]-glucose at a metabolic steady state in batch cultures. The metabolites in question were ethanol as a final product of the biosynthetic pathway, glycerine from the upper part of glycolysis and pyruvate. Furthermore, in order to simulate the *in vivo* fluxes, the measured fluxes for these extracellular metabolites were used as input. The experimentally assayed product yields for ethanol on glucose from 4 independent experiments was 1.52 ± 0.26 mol/mol, the yield of pyruvate on glucose from 6 independent experiments was 0.0049 ± 0.0011 mol/mol and the product yield of glycerine on glucose from 6 independent experiments was 0.137 ± 0.004 mol/mol. The biomass yield on glucose from 6 independent experiments was 0.019 ± 0.003 (g CDW)/mmol.

#### 4.3.1.4 Quality control and validation of $^{13}$C-based flux analysis

The measured intensities (GC/MS-based) of MBDSTFA-derivatized amino acid fragments (m/z ratio of the [M-57] mass fragment) are the basis for the estimation of the labeling distribution of carbon in proteinogenic amino acids (Wittmann and Heinzle, 1999, 2001). This information consists of the experimental mass isotopomer distribution vectors (mdv) yielded from parallel batch cultivations with [1-$^{13}$C]-labeled glucose in shake flasks. At this point it is important to note that this study focused not only on yielding mdvs of high quality but also cover as many positional isotopomers as possible (Christensen and Nielsen, 1999). Therefore 15 positional isotopomers were assessed in order to cover fully the distribution of carbon labeling in as much proteinogenic amino acid as possible.

Each GC/MS measurement was validated for accuracy and sensitivity (Wittmann et al., 2002) by comparing the measured $I_{M+1/M0}$ mass isotopomer ratio to the theoretical one based on the molecular composition of each positional isotopomer. A measurement met these qualitative criteria when the difference between the theoretical and measured $I_{M+1/M0}$ was below 2 %. Mass isotopomers were then corrected for the presence of naturally occuring isotopes (C, H, O, N, Si, S) (Van Winden et al., 2002; Wittmann and Heinzle, 1999; Yang et al., 2008) before being used as input for the calculation of *in vivo* carbon fluxes throughout the central metabolism.

Two further qualitative criteria were employed. The first was establishing if an isotopic steady state was achieved during sampling from *S. pombe* batch cultures growing on [1-$^{13}$C]-glucose. The second criterion was assessing the degree of fitting of the measured mdv for each proteinogenic amino acid to the simulated mdv generated during the stochastic simulations. The experimental error, that was generated between measured mdv datasets from different cell cultures was also calculated.

**Isotopic and metabolic steady state.** Typical metabolic flux analysis, as presented in this work, is conducted when cells reach a metabolic and isotopic steady state during growth on $^{13}C$-glucose. By isotopic steady state we define the saturation of the carbon skeleton of metabolites with a stable labeling pattern (Gombert et al., 2001; Driouch et al., 2012). The metabolic steady state on the other hand is characterized by time invariable metabolite concentrations (dC/dt = 0), where biomass and product formation yields on the substrate are constant as well as the metabolic fluxes. The metabolic steady state can be reached in batch cultivations during the exponential growth phase where the specific growth rate is constant over time (Deshpande et al., 2009). When these criteria are met, then central metabolism can be mapped by quantifying the carbon labeling of intracellular metabolites and by measuring the extracellular fluxes.

To ensure that metabolic steady state was reached, the specific growth rate of

all batch cultures containing labeled glucose was monitored and compared to a control batch culture containing naturally labeled glucose. All cultures grew with a constant growth rate not deviating from the specific growth rate ($\mu$ = 0.2 h$^{-1}$) of *S. pombe* cells growing in shake flask cultures. It is crucial to establish when the introduction of isotope labeling in a system that is operating at metabolic steady state reaches equilibrium and an isotopic steady state (illustrated in Figure 4.24).

During an isotopic steady state, the estimated carbon fluxes can be regarded as representative for a strain under focus over the whole cultivation period (Becker et al., 2008). To determine the labeling pattern, samples of different cell dry weight (CDW) were obtained from parallel batch cultivations with [1-$^{13}$C]-labeled glucose at different time points during the exponential growth phase. Then the relative fractions of mass isotopomers of various proteinogenic amino acids were determined. The relative fractions chosen were the $m_0$ (non labeled amino acid), the $m_1$ (single carbon labeled amino acid) and the $m_2$ (double carbon labeled amino acid). The proteinogenic amino acids represent various points of the metabolic network in order to examine whether the samples were representative of an isotopic steady state.
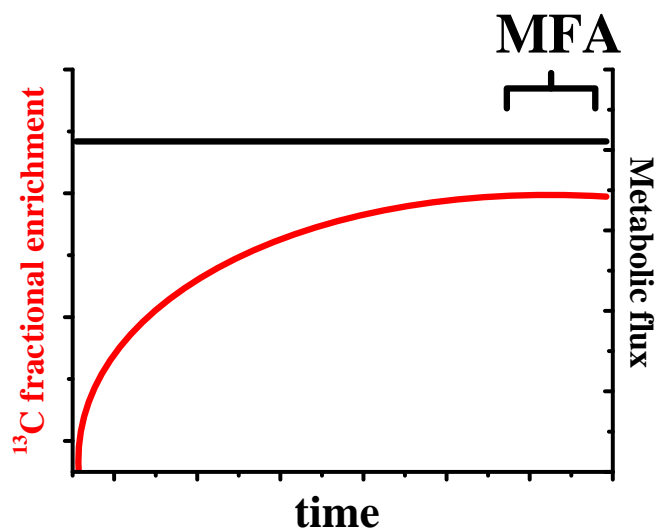


Figure 4.24: Achieving metabolic and isotopic steady state for conducting metabolic flux analysis (MFA).

As it is illustrated in Figure 4.25 the labeling of various mass isotopomers was maintained at constant levels for different biomass concentrations, thus the isotopic steady state was achieved. For simplicity only 7 mass isotopomers (ala260, gly246, ser390, glu432, val288, thr404 and phe336) are illustrated here.
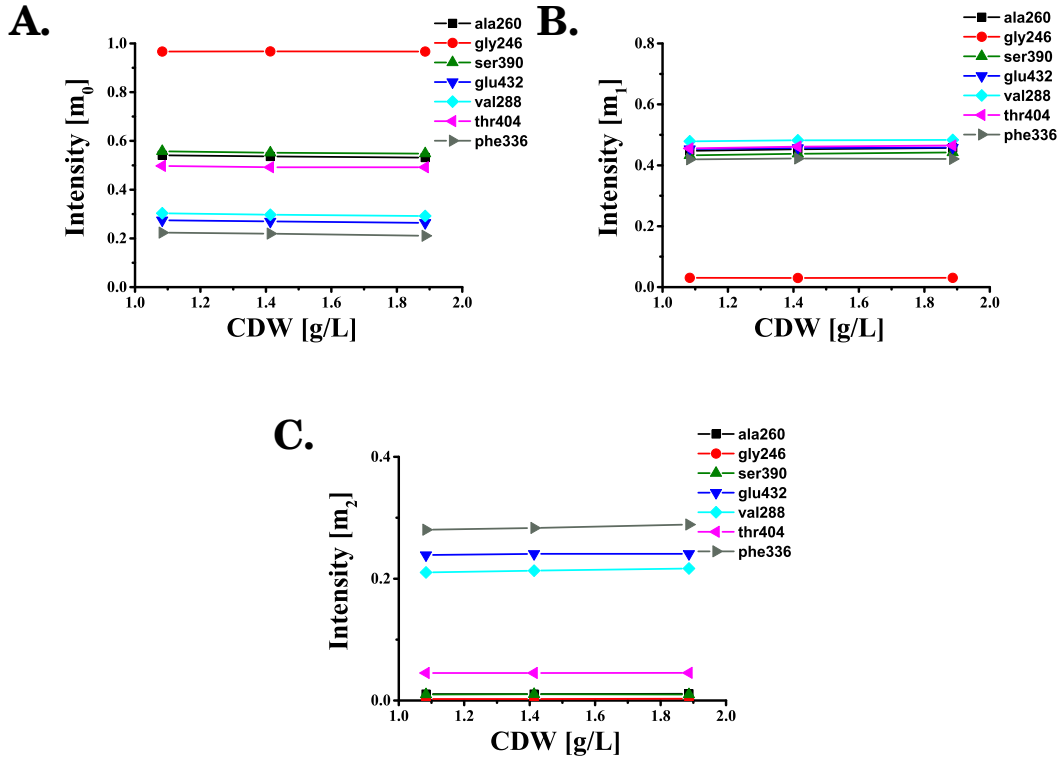
Figure 4.25: Fraction of mass isotopomers $m_0$ (non labeled) [A], $m_1$ (single labeled) [B], $m_2$ (double labeled) [C] of proteinogenic amino acids alanine (ala260), glycine (gly246), serine (ser390), glutamate (glu432), valine (val288), threonine (thr404) and phenylalanine (phe336) from protein hydrolysates harvested at CDW concentrations 1.08 g/L, 1.41 g/L and 1.89 g/L for wild type *S. pombe* cells grown on [1-$^{13}$C]-glucose during the exponential growth phase in one of the parallel batch cultures.

**Comparison of calculated and simulated mdvs.**   It is important for the simulated and experimental mass distributions to have the minimum deviation possible between them.  When the deviation is minimal then it is ascertained that the metabolic network we have set up, approximates best the *in vivo* metabolic rate of the cell based on the labeling distributions and the extracellular fluxes that have been measured. Prior to this comparison, the various measured mdv datasets yielded from parallel cultivations were examined for their mean error propagation. This statistical term allows us to assess the error that may be generated and accumulated in the measured mdvs due to instrument limitations such as the precision of measurement.  The mean error propagation (in [%]) (Equation 4.3) between experimental values for mass distribution vectors is calculated as the mean value of the square root of the sum of squared deviations for each mass distribution vector.

$$\text{experimental error} = \sqrt{\sigma_1{}^2 + \sigma_2{}^2} \tag{4.3}$$

The values $\sigma_1$ and $\sigma_2$ refer to the standard deviations for mass distributions

from the first and the second cultivation respectively for each proteinogenic amino acid that was assessed. The mean error propagation was calculated to be 0.26 % which allowed us to be certain for the measurement precision.

It was mentioned in previous parts, that the measured mdv datasets were used as input for simulating mdvs by a Matlab-based software. The linear fitting of simulated to measured mdvs was used as a measure of the quality of the performed simulations and is illustrated in Figure 4.26. The calculated correlation coefficient ($R^2$) here is indicative of the fact that the simulated datasets did not deviate from the measured ones. Therefore it can be concluded that the metabolic network used as input for the calculation of carbon labeling distribution reflects the *in vivo* cellular metabolism.
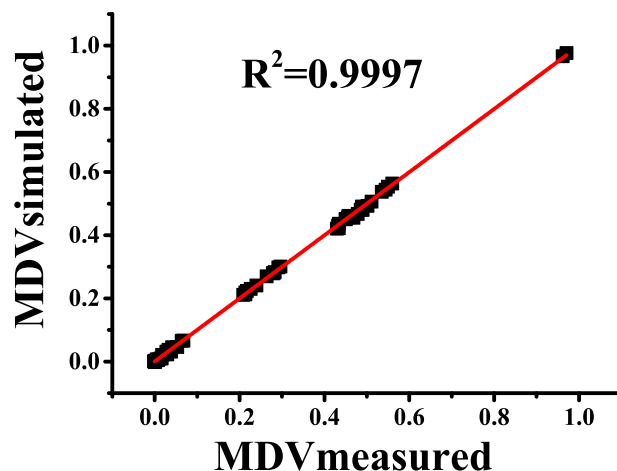


Figure 4.26: Linear fit (red line) between the mass distribution vectors obtained by GC/MS measurements (MDV measured) and the mass distribution vectors obtained by stochastic simulations (MDV simulated) for the cultivation of wild type *S. pombe* on [1-$^{13}$C]-labeled glucose. $R^2$ presented on the graph is the squared correlation coefficient.

#### 4.3.1.5  *In vivo* carbon fluxes

When all steps were fulfilled, the intracellular flux distribution of carbon stemming from uptaken glucose was calculated. The intracellular fluxes depicted in Figure 4.27 represent relative fluxes to the glucose uptake which has been set with a relative flux of 100 %. The intracellular fluxes were calculated after 100 Monte Carlo simulations on a Matlab-based software incorporating an algorithm developed by Yang et al. (Yang et al., 2008) and were based on intervals for 95 % confidence (see Appendix). The external metabolites that were secreted and quantified in the extracellular space during steady state were ethanol, pyruvate and glycerine. As it will be shown in subsequent parts of this work acetate started accumulating in the

extracellular space only during the stationary phase, when glucose was depleted, therefore was not taken into account as a secreted metabolite.

As we have seen, the intracellular metabolism was quantified during the exponential growth phase with glucose as a substrate. Under these conditions *S. pombe*, like *S. cerevisiae*, exhibits a respirofermentative metabolism due to the fact that it belongs to the Crabtree-positive yeasts (Urk et al., 1990; de Jong-Gubbels et al., 1996). Crabtree-positive yeasts (in the presence of a non-limiting concentration of glucose and $O_2$) exhibit a high glycolytic flux, and increased carbon flow towards ethanol production (fermentative pathway) and a partial repression of the TCA cycle (Christen and Sauer, 2011) and of mitochondrial respiration. Therefore it was of interest to examine during exponential growth the *in vivo* flux partitioning at the pyruvate node between the flux towards ethanol and the one towards the mitochondria through the mitochondrial pyruvate dehydrogenase complex and towards anaplerosis. In this way we could capture a snapshot of the metabolism at the mitochondria-cytosol interface during the onset of respirofermentative metabolism and quantify the actual carbon flux through the TCA cycle

As it is evident from the flux map of Figure 4.27, the split ratio ($\Phi_{PPP}$) (defined according to Equation 4.4 (Wittmann and Heinzle, 2001) with $v$ as the reaction rate/metabolic flux) between the glycolysis and the oxidative part of the PPP (pentose phosphate pathway) had a value of 0.084. The *S. pombe* split ratio did not differ largely from the split ratio ($\Phi_{PPP}$ = 0.094) of wild type *S. cerevisiae* cells growing on glucose in batch cultures (Schneider, 2011).

$$\Phi_{PPP} = \frac{v_{PPP}}{v_{PPP} + v_{Glycolysis}} \tag{4.4}$$

The production rate of NADPH via the first steps of the PPP (glucose 6-phosphate dehydrogenase and gluconate 6-phosphate dehydrogenase) during respirofermentative metabolism was 1.72 mmol/(g CDW×h), when taking into account the specific glucose uptake rate ($q_{glucose}$ = 10.51 ± 1.49 mmol/(g CDW × h) from 6 independent experiments). Since the cytosolic malic enzyme of *S. pombe* is NAD-dependent (Osothsilp and Subden, 1986; Viljoen et al., 1994) and not NADP-dependent (as in *S. cerevisiae*), the major contributor of NADPH was the oxidative part of the PPP.

NADH in the cytosol was mainly oxidized at the biosynthetic pathway of the major metabolic by-product, ethanol. Subsequently NAD could be reduced at the cytoplasmic glyceraldehyde-3-phosphate-dehydrogenase, setting cytosolic NADH available again for oxidation among others by the mitochondria. The biosynthesis of ethanol with a relative flux of 151.9 % (15.96 mmol/(g CDW×h)) was in good agreement with the rate of 14.99 ± 3.38 mmol/(g CDW×h) (acquired from 4 independent experiments) which was experimentally quantified in batch cultures of exponen-

tially growing cells on glucose (shown in subsequent parts of this work). During the respirofermentative metabolism of *S. pombe*, the major loss of carbon from the central metabolism (almost 50 % of uptaken glucose) was due to ethanol formation during the exponential growth phase. Also, the high capacity of the fermentative pathway under these conditions was in stark contrast to the low carbon flux that entered the mitochondria.

The carbon flux entering the mitochondria could be divided between three major transport events as defined by the metabolic network on which the flux analysis was based. The first entry flux was the one directed to the mitochondrial pool of acetyl-CoA. Based on labeling information, the fluxes from cytosolic pyruvate and from the cytosolic acetyl-CoA (synthesized from acetate in the cytosol) towards the mitochondrial acetyl-CoA could be distinguished from each other. Furthermore, the quantification of the labeling of isoleucine and valine (with 2-oxoisovalerate as an intermediate) led to the calculation of the fluxes from the mitochondrial pool of pyruvate towards the formation of these two BCAAs.

However, even under such conditions, the carbon flux from pyruvate into the mitochondrial matrix through the MPC machinery compared to the flux towards ethanol in the cytosol was far smaller, indicative of the repression of the TCA cycle activity under the Crabtree effect. In Crabtree-positive yeasts like *S. cerevisiae* two of the metabolic adaptations indicative of the Crabtree effect are an overexpressed pyruvate decarboxylase (facilitating a high flux into the ethanol biosynthetic pathway) and at the same time a transcriptional down-regulation of the pyruvate dehydrogenase complex (Diaz-Ruiz et al., 2011). These traits are also shared by cancer cells where the Warburg effect (similar to the yeast Crabtree effect) is active and pyruvate is diverted towards lactate biosynthesis in the cytosol and at the same time both the entry through the MPC and its metabolism by the PDH complex are significantly reduced (Schell et al., 2014a; Szlosarek et al., 2014; Kesten et al., 2015; Rampelt and Laan, 2015).

It was assumed that the transport of acetyl-CoA from the cytosol to the mitochondrial matrix was mediated by an carnitine/acylcarnitine translocator, since the mitochondrial inner membrane is impermeable to acyl moieties (Palmieri et al., 2000). In *S. cerevisiae*, the Crc1p transporter exchanges acetylcarnitine for free L-carnitine from the mitochondria (Palmieri et al., 1999a). In *S. cerevisiae* the Crc1p is in interplay with other enzymes related to carnitine and acetyl-CoA. Acetylcarnitine is generated in the peroxisomes by Cat2p during fatty acid oxidation (Choudhary et al., 2014), whereas during oxidation of ethanol and conversion of acetate to acetyl-CoA, the Yat1p protein (located at the outer mitochondrial membrane) transfers the acetyl group to L-carnitine (Palmieri et al., 1999a). The *S. cerevisiae* *CRC1*, *CAT2* and *YAT1* genes exhibit no homology to any *S. pombe* genes, thus this

indirect acetyl-CoA transport mechanism through the mitochondrial membranes remains unknown for the fission yeast.

Another point of carbon transport between the cytosol and the mitochondrial matrix as ilustrated in the flux map of Figure 4.27 was the transporter of oxaloacetate. Pyruvate was carboxylated with a relative flux of 9.0 % with the consumption of ATP, via the cytosolic pyruvate carboxylase, to form oxaloacetate which then entered the mitochondria with a flux of 7.4 %, namely 0.78 mmol/(g CDW×h). The *S. pombe* oxaloacetate carrier protein (Oac1p) has been predicted on a genetic level (SPAC139.02c) but has been not biochemically characterized. In *S. cerevisiae* this transporter was identified, expressed in *E. coli* and reconstituted in liposomes (Palmieri et al., 1999b). It has been postulated that the *S. cerevisiae* oxaloacetate transporter catalyzes the symport of the carboxylate (either influx or efflux) along with a proton, thus depends on the transmembrane pH gradient and therefore the proton motive force of the cell (Palmieri et al., 2006).

Based on the flux analysis, malate in the cytosol is connected to the mitochondrial pool catalyzed by a transport reaction. As seen in previous parts that covered the *in situ* succinate uptake by mitochondria, malate was eventually present in the extramitochondrial space. Although no biochemical or genetic data exist about the occurrence of a *S. pombe* Dicp that could catalyse such a transport event, it seems plausible also from the perspective of flux distributions that a transport mechanism for dicarboxylates may be active in *S. pombe* as in *S. cerevisiae*. During the setup of the metabolic network on which the flux analysis was based, it was assumed that only one mitochondrial malate dehydrogenase exists (localized in the mitochondrial matrix). The *mdh1* sequence of *S. pombe* has been found to encode an integral protein of the inner mitochondrial membrane (Matsuyama et al., 2006) based on localization studies of the protein products of cloned ORFs from *S. pombe*. The cytosolic pools for malate and oxaloacetate could be differentiated from each others as well as the fluxes stemming from their mitochondrial counterparts. Thus based on the snapshot of the *in vivo* fluxes at the anaplerosis, the cytosolic NAD-dependent malic enzyme was part of a cycle. More specifically, carbon fluxes were directed from pyruvate to oxaloacetate, which was then imported to the mitochondria as previously described. In the TCA cycle malate was produced and exported from the mitochondria with a flux of 5.1 % to the cytosol. There it was subsequently decarboxylated, with the simultaneous reduction of NAD, to form pyruvate, thus closing the cycle. The net effect of this cycle was the transfer of reduced NADH in the cytosol and the hydrolysis of ATP.

Although fluxes at the pyruvate node could be resolved, we could not identify (based on these results alone) the nature of a mitochondrial pyruvate transport mechanism. Even if the *S. pombe* mitochondrial pyruvate transport mechanism

exists, the role of each one of the predicted subunits of the transporter (subunits Mpc1p and Mpc2p; inferred from homology to *S. cerevisiae*) would be unknown during mitochondrial pyruvate uptake. Moreover, with MFA alone we cannot explore the relationship between oxidative phosphorylation and the mitochondrial pyruvate uptake. Mitochondrial pyruvate also acts as a respiratory substrate as it can be metabolized at the pyruvate dehydrogenase complex and yield NADH which can subsequently serve as electron donor for the respiratory chain.

Therefore the next steps would involve the identification of the mitochondrial pyruvate transfer machinery in *S. pombe* and its role (as a whole and of its subunits separately) in central carbon metabolism, physiology and mitochondrial function. For the analysis of the mitochondrial function, selectively permeabilized cells were employed with intact and functional mitochondria and pyruvate as the main respirative subtrate under suitable conditions.
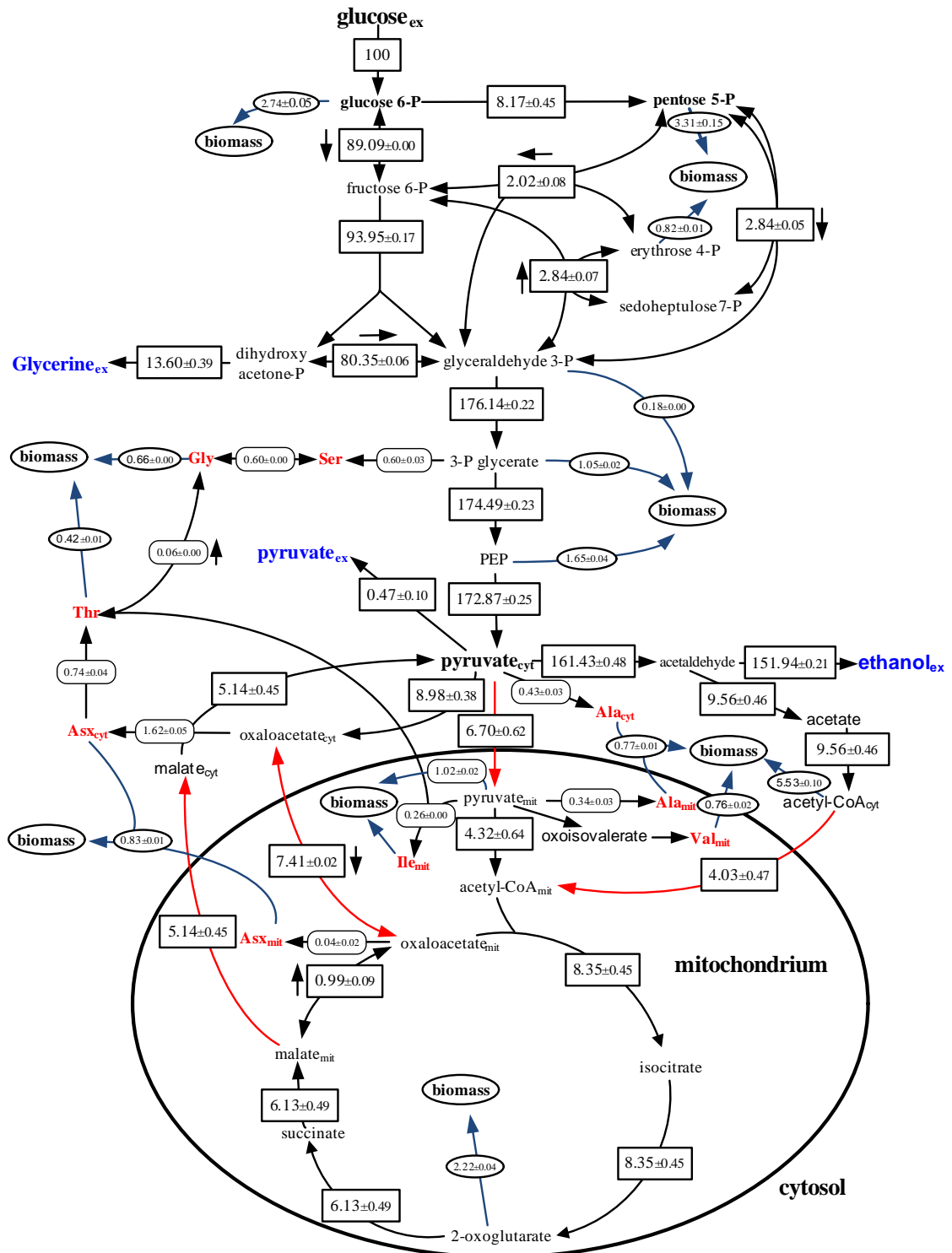
Figure 4.27: Flux map of *S. pombe* CBS 356 parallel batch cultivations, with [1-$^{13}$C]-glucose as the carbon source, where relative carbon fluxes are illustrated based on a 100 % glucose uptake rate (glucose$_{ex}$), standardized for an experimentally measured q$_{glucose}$ = 10.51 ± 1.49 mmol/(g CDW × h) from 6 independent experiments. Blue arrows denote biosynthetic precursor fluxes towards biomass formation, red arrows account for transport fluxes between the cytosol and the mitochondria and black arrows refer to *in vivo* fluxes between metabolic intermediates.

### 4.3.2  *In situ* mitochondrial respiration on pyruvate

The *in vivo* fluxes around the pyruvate node may capture a snapshot of the partition of carbon flow at this point but can not provide a clear picture of the entry of pyruvate into the mitochondrial matrix. Therefore the *in situ* approach was applied in order to establish the mechanism of mitochondrial pyruvate metabolism and the metabolic pathways implicated. Selectively permeabilized cells were suspended in a synthetic buffer, while pyruvate along with other respiratory substrates were supplied directly on the external side of the outer mitochondrial membrane.

The first step was to examine whether there was any mitochondrial activity with only pyruvate present. Intact *S. pombe* mitochondria were barely respiring with exogenous pyruvate as the sole respiratory substrate as it is evident from Figures 4.28A & B. This is especially evident when comparing this rate to the background oxygen elimination rate from the reactor into the MIMS in the presence of buffer without any cells. Therefore the synthetic respiratory buffer was supplemented with malate additionaly to pyruvate in order to examine whether the mitochondria would exhibit any activity. As it has been mentioned in previous parts, it is unknown whether there exists a mitochondrial dicarboxylate carrier capable to transfer malate into the mitochondrial matrix. The presence of malate in the extramitochondrial space along with pyruvate significantly increased the activity of the mitochondrial respiratory chain compared to pyruvate alone. With both substrates the respiratory rate was $0.007 \pm 0.001$ mM/min (specific respiration rate $q_{O_2} = 2.33 \pm 0.75$ nmol/(mg CDW$\times$min)).

Reports on isolated mitochondria from *S. pombe* oxidizing the combination of malate and pyruvate have been so far contradictory. A study by Heslot et al. (Heslot et al., 1970) claimed that mitochondria would not respire significantly in the presence of the aforementioned substrates while Jault et al. (Jault et al., 1994) exhibited results with mitochondria respiring on these substrates at a high rate and the RCR reaching a value of 4.

**A.**



**B.**
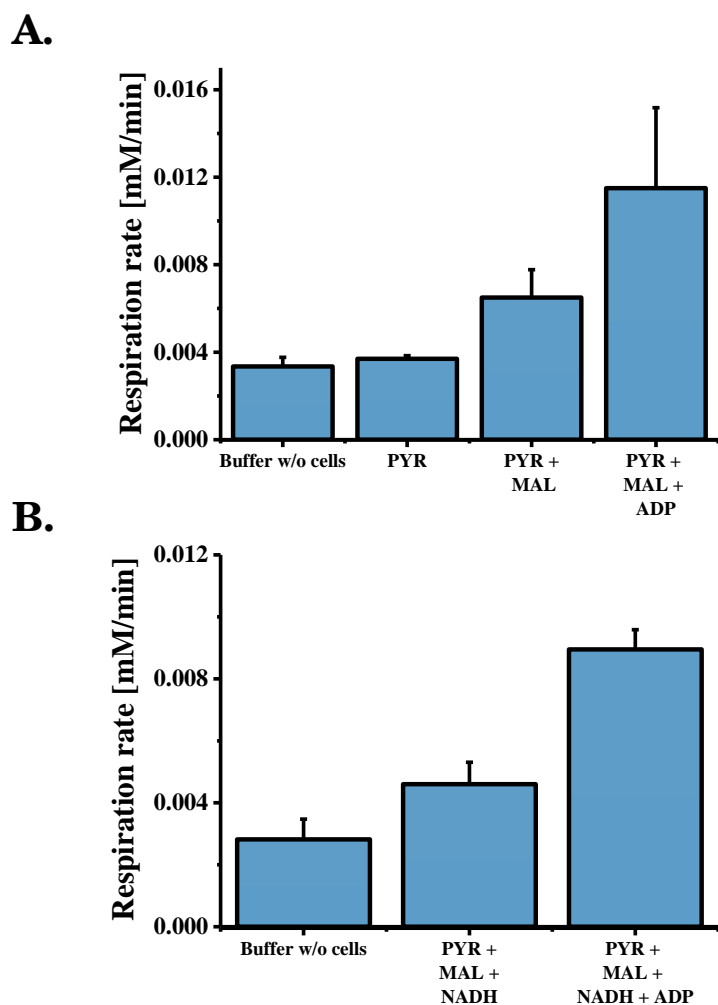


Figure 4.28: Mitochondrial respiration rate (as average value along with standard deviation for duplicates) in the sealed mini-reactor at 30°C with digitonin-permeabilized wild type *S. pombe* cells. The substrates used were pyruvate (PYR; 5 mM), L-malate (MAL; 3 mM), ADP (0.5 mM), NADH (0.25 mM). Cell concentration: [A] = 2.84 ± 0.36 g/L, [B] = 1.59 ± 0.28 g/L

The ADP-activated respiration in the presence of malate and pyruvate had a rate of 0.012 ± 0.004 mM/min (specific respiration rate $q_{O_2}$ = 3.99 ± 0.78 nmol/(mg CDW×min)), with an RCR of 1.71. Therefore it was concluded that intact mitochondria were also respiring in the presence of pyruvate and malate, although with a very poor coupling of oxidation to phosphorylation.

When malate can be transported into the mitochondrial matrix, it can be oxidized by the malate dehydrogenase to form oxaloacetate which can then form citrate together with acetyl-CoA. Pyruvate is converted into acetyl-CoA in the mitochondrial matrix by the pyruvate dehydrogenase complex with the parallel reduction of NAD and the production of $CO_2$. The accumulation of NADH and acetyl-CoA in the matrix may lead to the competitive inhibition of the pyruvate dehydrogenase complex (Pronk et al., 1996).

The next step towards finding the optimal substrate combination that could adequately energize mitochondria while supporting the uptake of pyruvate, involved the addition of NADH along with pyruvate and malate. The supply of NADH in the extramitochondrial space ensures that it will be oxidized in the intermitochondrial membrane space by the external NADH dehydrogenase and that NAD will pass into the mitochondrial matrix. NAD is an important cofactor for the activity of the pyruvate dehydrogenase complex which utilizes pyruvate to form acetyl-CoA. Although the reduced form (NADH) is inhibitory for the pyruvate dehydrogenase complex it can not permeate the inner mitochondrial membrane. Therefore in the beginning of the experiments the exogenous supply of NADH can not influence the activity of the pyruvate dehydrogenase complex. The use of NADH is further justified as following. The focus in this part is not to specifically quantify the activity of the respiratory chain or its various complexes by using either NAD-linked substrates, NADH or FADH$_2$. The focus of this part of this work is rather set on :

1. Identifying the mitochondrial pyruvate carrier (MPC) in *S. pombe*.

2. Characterize the function of the MPC components under conditions that mimic as closely as possible the physiological ones during an active respirofermentative metabolism on glucose as it was described with the $^{13}$C-based flux analysis.

3. Quantify the extent at which a loss of function (either completely or partially) of the MPC machinery influences the metabolism at the pyruvate node in either the cytosolic or the matrix side of the mitochondria.
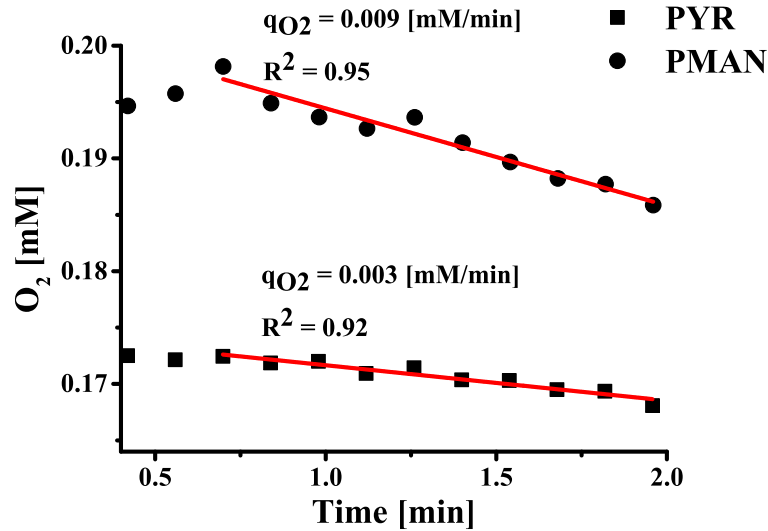
Figure 4.29: Example of the calculation of the respiration rate for one experiment with selectively permeabilized *S. pombe* cells in cytosol-mimicking buffer containing pyruvate, malate, NADH and ADP (PMAN; cell concentration = 1.80 g/L) or pyruvate (PYR; cell concentration = 3.10 g/L). Experiments conducted in a sealed reactor at 30 °C. Red line indicates each curve of the regression analysis along with the $R^2$.

The respiration rate with the additional supply of NADH to malate and pyruvate was $0.005 \pm 0.001$ mM/min (specific respiration rate $q_{O_2} = 2.97 \pm 0.96$ nmol/(mg CDW×min)) whereas the ADP-driven respiration along with pyruvate, malate and NADH had a rate of $0.009 \pm 0.001$ mM/min (specific respiration rate $q_{O_2} = 5.74 \pm 1.40$ nmol/(mg CDW×min)) (PMAN curve from Figure 4.29.B). The calculated RCR was 1.93, slightly better than the RCR yielded without the addition of NADH to the ADP-activated mitochondria in the presence of malate and pyruvate. Interestingly, the ADP-driven specific respiration rate with pyruvate, malate and NADH was not significantly higher than the specific respiration rate on NADH and ADP ($q_{O_2} = 6.51 \pm 0.15$ nmol/(mg CDW×min)) as it was described in previous parts.

This can be explained partially by the increasing presence of acetaldehyde as a product of the first step of the fermentative pathway in the cytosol catalysed by the pyruvate decarboxylase. Acetaldehyde which can freely permeate the mitochondrial membranes, was shown to have little effect on the P/O ratio at concentrations under 3-5 mM and an inhibitory effect on NAD-linked respiration, specifically for rat liver mitochondria (Cederbaum et al., 1974). Acetaldehyde in yeast is reported to have an inhibitory effect on respiration at concentrations higher than 12.5 mM (Carlsen et al., 1991). Physiologically, fermenting yeasts may accumulate intracellularly higher amounts of acetaldehyde than these measured in the extracellular environment, thus reaching intracellular concentrations approximating levels at 0.33 g/L (7.5 mM) (Aranda and del Olmo, 2004; Stanley and Pamment, 1993). Ac-

etaldehyde at concentrations above 0.5 g/L led to growth arrest in *S. cerevisiae* cultures, while concentrations below 0.05 g/L had no effect whatsoever (Stanley et al., 1993).

From combining the results of the metabolic map that resulted from the $^{13}$C-flux analysis and the selection of pyruvate, malate and NADH as the respiratory substrates for the *in situ* studies, a theoretical model was constructed as illustrated in Figure 4.30 (cytosol and IMS lumped together as one compartment). This will be the metabolic network of reference for subsequent analysis using selectively permeabilized cells. Nevertheless, after choosing the aforementioned substrate combination as suitable for the analysis of the PMC machinery, the next step would be to identify the genes expressing the components of this mitochondrial machinery. Therefore as next followed the construction of knock-out mutants lacking the predicted gene sequences coding for Mpc1p, Mpc2p and the combination thereof.
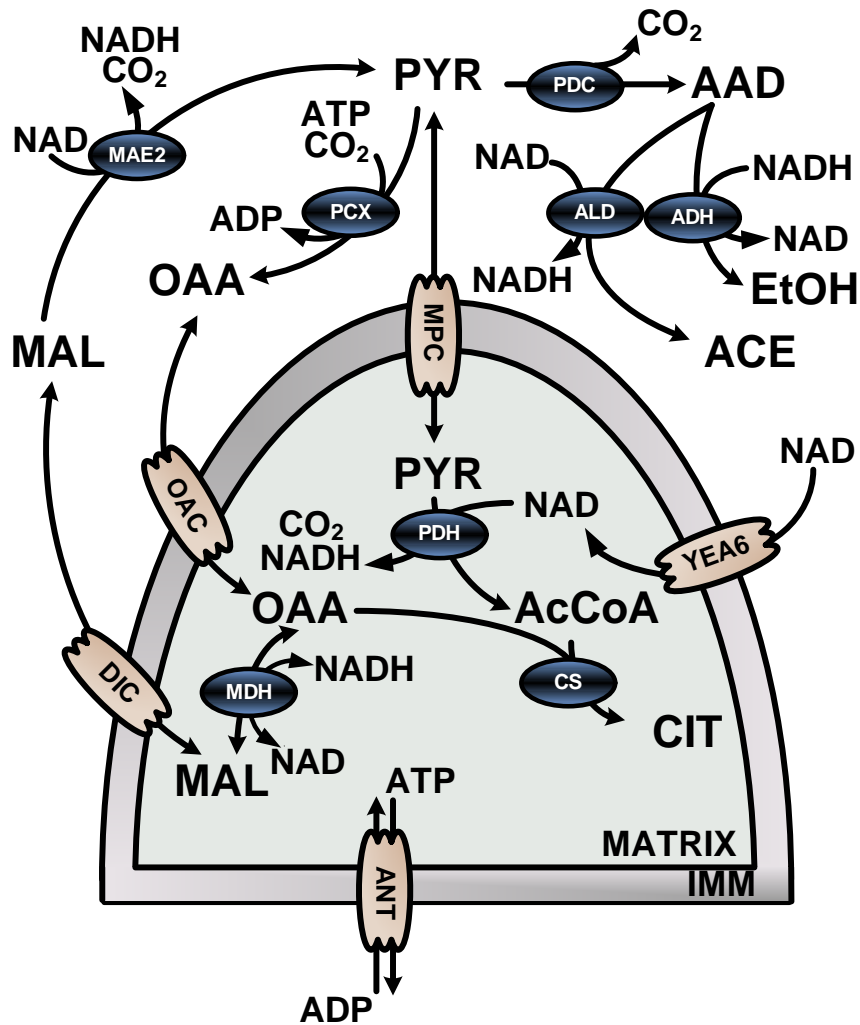
Figure 4.30: Theoretical model of active metabolic pathways at the pyruvate node when digitonin-permeabilized *S. pombe* cells are supplied with pyruvate (PYR), malate (MAL), NADH and ADP (at the cytosol-mitochondria boundary region). Products that may occur are oxaloacetate (OAA), $CO_2$, NAD, acetaldehyde (AAD), ethanol (EtOH), acetate (ACE), acetyl-CoA (AcCoA), citrate (CIT). In reactions only the product forms of the cofactor pairs NAD/NADH and ADP/ATP are depicted. The outer mitochondrial membrane is omitted. Enzymes illustrated here are: MAE2, malic enzyme; PCX, pyruvate carboxylase; PDC, pyruvate decarboxylase; ADH, Alcohol dehydrogenase; ALD, aldehyde dehydrogenase; PDH, pyruvate dehydrogenase complex; MDH, malate dehydrogenase; CS, citrate synthase. The mitochondrial transporters docked on the inner mitochondrial membrane (IMM) are: OAC, oxaloacetate transporter; DIC, hypothetical dicarboxylate carrier; ANT, adenine nucleotide translocator; YEA6, NAD transporter; MPC, mitochondrial pyruvate carrier.

### 4.3.3 Construction of *S. pombe* strains that lack a mitochondrial pyruvate transporter

For the needs of constructing *S. pombe* mutant cells lacking a mitochondrial pyruvate carrier system, the sequences encoding Mpc1p and Mpc2p were identified based on amino acid homology to their *S. cerevisiae*, *A thaliana* and *H. sapiens* counterparts (Bricker et al., 2012; Herzig et al., 2012).

These sequences are SPCC1235.11 encoding Mpc1p and SPAC24B11.09 encoding Mpc2p. Both sequences are also referred in the PomBase database as predicted to encode Mpc1p and Mpc2p respectively in *S. pombe*. Since it has been reported that Mpc1p and Mpc2p form heterodimeric complexes in *S. cerevisiae* (Bender et al., 2015), a *S. pombe* strain combining both the *mpc1* and *mpc2* gene deletions had to be constructed additionally to the single gene deletion strains. Interestingly there was no indication based on sequence homology that a sequence exists in *S. pombe*, that encodes the *mpc3* sequence, which is part of the MPC system in *S. cerevisiae* under specific conditions, as will be discussed in subsequent parts of this work.

The protein product of the *S. pombe* gene *mpc1* was aligned versus the MPC1 proteins of human, yeast and *A. thaliana* origin (Figure 4.31). The two transmembrane helices that are conserved throughout MPC1 subunits, were also present in the *S. pombe* amino acid sequence at positions 31 - 52 and 60 - 82. The corresponding transmembrane helices were located at positions 23 - 45 and 55 - 77 for *S. cerevisiae*, at positions 21 - 41 and 53 - 71 for *H. sapiens* and at positions 20 - 36 and 44 - 61 for *A. thaliana*. An identical approach was carried out for the gene product of the *S. pombe* sequence *mpc2* yielding the alignment of the Mpc2p amino acid sequence of *S. pombe* versus these sequences from *S. cerevisiae*, *H. sapiens* and *A. thaliana* (Figure 4.32). Again here a high degree of sequence conservation was observed and all three transmembrane helices that are typical for Mpc2p were identified for *S. pombe* at positions 19 - 35, 50 - 66 and 72 - 94. The corresponding transmembrane helices were located at positions 23 - 39, 55 - 71 and 75 - 91 for *S. cerevisiae*, at positions 41 - 61, 73 - 90 and 96 - 115 for *H. sapiens* and at positions 19 - 35, 51 - 67 and 74 - 90 for *A. thaliana*.

Only recently the NRGA1 protein of *A. thaliana* was identified as part of the MPC machinery in plants and was shown to exhibit high homology to the atMPC2 sequence (see Q949R9 sequence of Figure 4.32) (Li et al., 2014). Furthermore NRGA1 was presumed to form functional complexes with the *A. thaliana* MPC1 (atMPC1) and participate in the mitochondrial pyruvate transport and in the regulation of K$^+$ and ion channels. The existence of 5 genes coding for members of the MPC family in *A. thaliana* show that at least in this plant other proteins may form functional complexes with core subunits of the MPC machinery.

```
sp|P53157|MPC1_YEAST    ......MSQPVQRAAAARSFLQKYINKETLKYIFTT    29
sp|Q9Y5U8|MPC1_HUMAN    ......MAGALVRKAA.DYVR...SKDFRDYLMST    25
sp|O74847|MPC1_SCHPO    MNASEKLSQKAAQSVTRRFITWLKSPDFRKYLCST    35
sp|Q949R9|MPC1_ARATH    ......MATSRFQAFLNSPIG..........PKTT    19
consensus               ......maq.r.raaarsfig...skdfrkyl.tT


sp|P53157|MPC1_YEAST    HFWGPVSNFGIPIAAIYDLKKDPTLISGPMTFALV    64
sp|Q9Y5U8|MPC1_HUMAN    HFWGPVANWGLPIAAINDMKKSPEIISGRMTFALC    60
sp|O74847|MPC1_SCHPO    HFWGPLSNFGIPIAAILDLKKDPRLISGRMTGALI    70
sp|Q949R9|MPC1_ARATH    HFWGPIANWGFVAAGLVDMQKPPEMISGNMSSAMC    54
consensus               HFWGPvaN.Gipiaai.D.kKdPelISGrMtfAlc


sp|P53157|MPC1_YEAST    TYSGVFMKYALSVSPKNYLLFGCHLINETAQLAQG    99
sp|Q9Y5U8|MPC1_HUMAN    CYSLTFMRFAYKVQPRNWLLFACHATNEVAQLIQG    95
sp|O74847|MPC1_SCHPO    LYSSVFMRYAWMVSPRNYLLLGCHAFNTTVQTAQG   105
sp|Q949R9|MPC1_ARATH    VYSALFMRFAWMVQPRNYLLLACHASNETVQLYQL    89
consensus               cYSavFMryAwmV.PrNyLL.aCHa.NetaQlaQg


sp|P53157|MPC1_YEAST    YRFLKYTYFTTDEEKKALDKEWKEKEKTGKQ....   130
sp|Q9Y5U8|MPC1_HUMAN    GRLIKH................EMTKTASA....   109
sp|O74847|MPC1_SCHPO    IRFVNFWYGKEGASKQSVFENIMQAAKHPESGTRQ   140
sp|Q949R9|MPC1_ARATH    SRWARAQGYLSSK........KEEEKPSQ.....   110
consensus               .Rf.k..y.....k......ke.eKta......


sp|P53157|MPC1_YEAST    .    130
sp|Q9Y5U8|MPC1_HUMAN    .    109
sp|O74847|MPC1_SCHPO    K    141
sp|Q949R9|MPC1_ARATH    .    110
consensus               .
```

|  |  |
|---|---|
| X | non conserved |
| X | similar |
| X | ≥50% conserved |
| X | ≥80% conserved |

Figure 4.31: Alignment of multiple amino acid sequences of the MPC subunit Mpc1p for the organisms *S. cerevisiae* (UniProtKB accession number: P53157), *H. sapiens* (UniProtKB accession number: Q9Y5U8), *S. pombe* (UniProtKB accession number: O74847) and *A. thaliana* (UniProtKB accession number: Q949R9). The consensus illustrates in capital letters the amino acids that have over 80 % degree of conservation in all of the aforementioned organisms. For the alignment of the protein sequences the TeXshade macro package for LaTeXwas used (Beitz, 2000).

```
sp|O95563|MPC2_HUMAN   MSAAGARGLRATYHRLLDKVELMLPEKLRPLYNHP    35
sp|Q8L7H8|MPC2_ARATH   ......................MATSKLQALWNHP    13
sp|Q09896|MPC2_SCHPO   ......................MFRAGFKRFWNHP    13
sp|P38857|MPC2_YEAST   .................MSTSSVRFAFRRFWQSE    17
consensus              ......................m.r.k.rr.wnhp


sp|O95563|MPC2_HUMAN   AGPRTVFFWAPIMKWGLVCAGLADMARPAEKLSTA    70
sp|Q8L7H8|MPC2_ARATH   AGPKTIHFWAPTFKWGISIANIADFQKPPENISYL    48
sp|Q09896|MPC2_SCHPO   AGPKTVHFWAPAMKWTLVLSGIGDYARSPEYLSIR    48
sp|P38857|MPC2_YEAST   TGPKTVHFWAPTLKWGLVFAGFSDMKRPVEKISGA    52
consensus              aGPkTvhFWAPtmKWglv.agiaDmarppEk.Sya


sp|O95563|MPC2_HUMAN   QSAVLMATGFIWSRYSLVIIPKNWSLFAVNFFVGA   105
sp|Q8L7H8|MPC2_ARATH   QQIAVTCTGMIWCRCSTIITPKNWNLFSVNVAMAA    83
sp|Q09896|MPC2_SCHPO   QYAALCATGAIWTRWSLIVRPKNYFNATVNFFLAI    83
sp|P38857|MPC2_YEAST   QNLSLLSTALIWTRWSFVIKPRNILLASVNSFLCL    87
consensus              Q.aalcaTg.IWtRwSl.i.PkNw.lasVNfflaa


sp|O95563|MPC2_HUMAN   AGASQLFRIWRYNQELK...AKAHK..........   127
sp|Q8L7H8|MPC2_ARATH   TGIYQLTRKIKYDYVSE...AEAAVEIEG......   109
sp|Q09896|MPC2_SCHPO   VGAVQVSRILVYQRQQKRITAQSEQRTELARSLAA   118
sp|P38857|MPC2_YEAST   TAGYQLGRIANYRIRNGDSISQLCSYILSGADESK   122
consensus              tgayQl.Ri..Y....k...aqa...ie.ga....


sp|O95563|MPC2_HUMAN   .......   127
sp|Q8L7H8|MPC2_ARATH   .......   109
sp|Q09896|MPC2_SCHPO   .......   118
sp|P38857|MPC2_YEAST   KEITTGR   129
consensus              .......
```

X   non conserved
X   similar
X   ≥50% conserved
X   ≥80% conserved

Figure 4.32: Alignment of multiple amino acid sequences of the MPC subunit Mpc2p for the organisms *S. cerevisiae* (UniProtKB accession number: P38857), *H. sapiens* (UniProtKB accession number: O95563), *S. pombe* (UniProtKB accession number: Q09896) and *A. thaliana* (UniProtKB accession number: Q8L7H8). The consensus illustrates in capital letters the amino acids that have over 80 % degree of conservation in all of the aforementioned organisms. For the alignment of the protein sequences the TeXshade macro package for LATEXwas used (Beitz, 2000).

Based on sequence homology, the construction of the deletion strains would employ the introduction of an integration cassette containing a gene coding for antibiotic resistance, with flanking regions homologous to the target gene to be deleted. Then by homologous recombination, the gene conferring antibiotic resistance could

replace the target sequence and integrate into the *S. pombe* wild type genome. Strains that have successfully incorporated the marker gene at the specific position of the genome could be verified with primers inside the integration cassette and primers outside this region. Such strains could be easily selected from single cell colonies growing in the presence of the antibiotic of interest.

An important organism-specific prerequisite for using this PCR-mediated gene disruption method, was to construct the disruption cassette with long flanking regions homologous to the sequence target in the genome. Homologous flanking regions of a length of 300-500 bp (Krawchuk and Wahls, 1999) were constructed upstream and downstream from the antibiotic resistance marker, in order to increase the possibility of successful disruption. Thus, non-homologous recombination events at random places in the genome (Kaur et al., 1997; Decottignies et al., 2003; Bähler et al., 1998) can be avoided by not using short flanking homologous regions as in *S. cerevisiae*.

### 4.3.3.1 Constructing the *S. pombe mpc1*Δ*::NatMX* strain

The integration cassette for deleting sequence *mpc1*, consisted of a 358 bp upstream flanking region, a 1261 bp long region containing the *natMX* marker (Hentges et al., 2005) and a 428 bp downstream flanking region. Both high-homology flanking regions were PCR-amplified with the *S. pombe* genome as template, while the *natMX* sequence was amplified from the pAG25 plasmid (Goldstein and McCusker, 1999). The *natMX* sequence confers nourseothricin resistance (in the presence of a final concentration of 100 $\mu$g/mL nourseothricin).

The integration cassette was constructed in two subsequent PCR steps. The first one yielded a 1561 bp upstream flanking sequence-*natMX* construct and the final step the complete 1923 bp final cassette. The single components and their combination that led to the final PCR product are illustrated in Figure 4.33.

Figure 4.33: Gel electrophoresis of the upstream (lane 1) and downstream flanking (lane 3) sequences and of the *natMX* cassette (lane 2) used for the construction of the final integration cassette (lane 6) for the PCR-mediated disruption of the *S. pombe mpc1* sequence. The GeneRuler$^{\text{TM}}$ 1 kb DNA marker is illustrated as M.

After the transformation of *S. pombe* CBS 356 cells with the integration cassette, single-cell colonies that incorporated the cassette into their genome, grew on complex medium agar plates in the presence of nourseothricin. Colonies were picked and subjected to colony-PCR with external primers this time, in order to verify the successful disruption of the target gene. PCR-amplified fragments from wild type and deletion mutant cells are exhibited in Figure 4.34.A. Mutants carrying the integration cassette exhibited a DNA fragment of a 2175 bp (lane 4) length with the external primers. Wild type cells when PCR-amplified with the same pair of primers exhibited a 2589 bp (lane 1) long DNA fragment, indicative of the intact *mpc1* sequence.

As an additional control, DNA stemming from wild type and mutant cells were subjected to PCR-amplification with the internal pair of primers. This is illustrated in Figure 4.34.B, with the amplified sequence from the wild type having a length of 2337 bp (lane 1), while the sequence from the mutant had a length of 1923 bp (lane 2). The integration cassette was PCR-amplified with the pair of internal primers and its characteristic band at the 1923 bp height (lane 3) is exhibited exactly next to the band from the mutant cell.

Figure 4.34: Colony PCR for establishing which transformant had successfully integrated the 5′ *upstream flanking sequence-natMX*-3′*downstream flanking sequence*. The GeneRuler™ 1 kb DNA marker is illustrated as M. [A] PCR-amplification utilizing the pair of external primers for: genomic DNA from wild type *S. pombe* (lane 1), the integration cassette as a negative control (lane 2), clones 1-7 (lanes 3-9). [B] PCR-amplification utilizing the pair of internal primers for: genomic DNA from wild type *S. pombe* (lane 1), clone 2 from gel [A] (lane 2), the integration cassette as a positive control (lane 3).

#### 4.3.3.2   Constructing the *S. pombe mpc2*Δ::*kanMX* strain

For constructing the *S. pombe mpc2*Δ::*kanMX* strain the same approach was followed as for the replacement of the *mpc1* gene with the antibiotic marker.

The integration cassette for deleting sequence *mpc2*, consisted of a 422 bp upstream flanking region, a 1518 bp long region containing the *kanMX* marker (Hentges et al., 2005) and a 422 bp downstream flanking region (Figure 4.35). Both high-homology flanking regions were PCR-amplified with the *S. pombe* genome as template, while the *kanMX* sequence was amplified from the pUG-6 plasmid (Güldener et al., 1996). The *kanMX* sequence confers geneticin G418 resistance (in the presence of a final concentration of 200 $\mu$g/mL geneticin G418).

The success of transformation of wild type cells with the integration cassette was determined via colony-PCR of single cell colonies growing in the presence of geneticin on complex medium agar plates. Verification of the mutants was done with primers that were external to the ORF of the gene to be replaced. This is illustrated with the gel in Figure 4.35.B, where various clones were subjected to colony-PCR with external primers (lanes 2-10) and were compared against the wild type gene locus (lane 1, 3764 bp length) amplified with the same pair of primers. The clone of lane 3 (band at 2367 bp length) was subsequently used for the construction of the double knockout mutant as well.
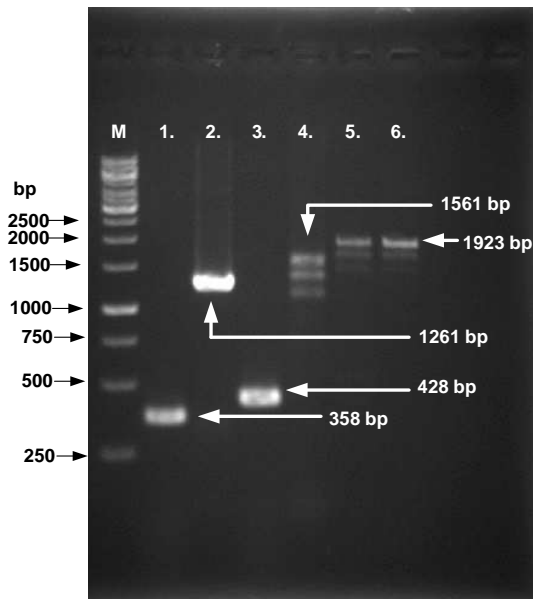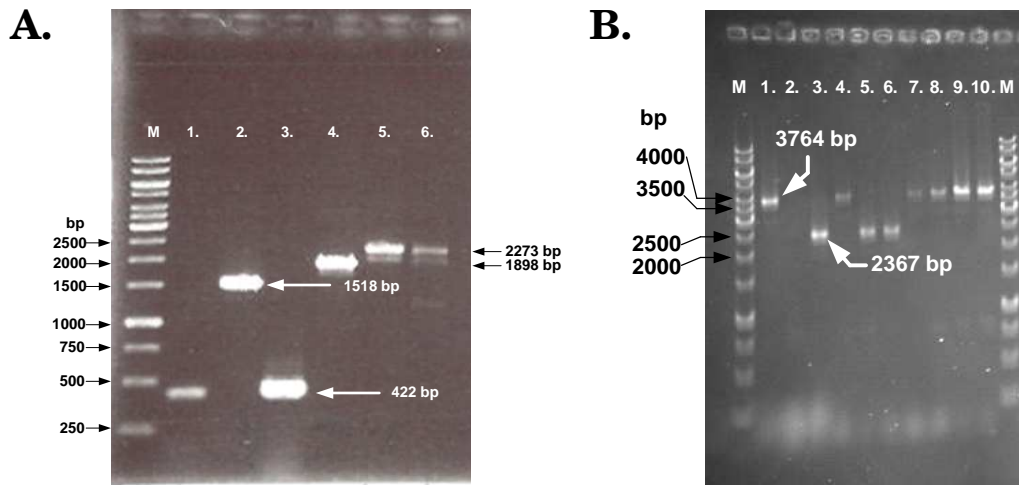
Figure 4.35: [A] Gel electrophoresis of the upstream (lane 1) and downstream flanking (lane 3) sequences and of the *kanMX* cassette (lane 2) used for the construction of the final integration cassette (lane 5) for the PCR-mediated disruption of the *S. pombe mpc2* sequence. [B] Colony PCR for establishing which transformant had successfully integrated the 5′ *upstream flanking sequence-kanMX-3′downstream flanking sequence*. PCR-amplification was used with the pair of external primers for: genomic DNA from wild type *S. pombe* (lane 1), clones 1-9 (lanes 2-10). The GeneRuler™ 1 kb DNA marker is illustrated as M.

### 4.3.3.3 Constructing the *S. pombe mpc1Δ::NatMX,mpc2Δ::kanMX* strain

The double knockout mutant was constructed by transforming the *mpc2Δ* strain with the integration cassette that was used for constructing the *mpc1Δ::NatMX* allele. Any mutant that would have its *mpc1* and *mpc2* genes deleted would be resistant to nourseothricin and geneticin as well. The success of the gene replacement with the integration cassette was verified with external primers for both gene loci.

Clones growing in the presence of nourseothricin and geneticin were subjected to colony-PCR with the pair of external primers used for the verification of the successful construction of the *mpc1Δ::NatMX* allele. In Figure 4.36 this is illustrated with clones (lanes 2-9) compared to the sequence PCR-amplified from the wild type genome (lane 1). A 2175 bp band was characteristic of the successful deletion of the *mpc1* gene, whereas the PCR-amplification of the same region from the wild type genome exhibited a 2589 bp band (see lane 1).
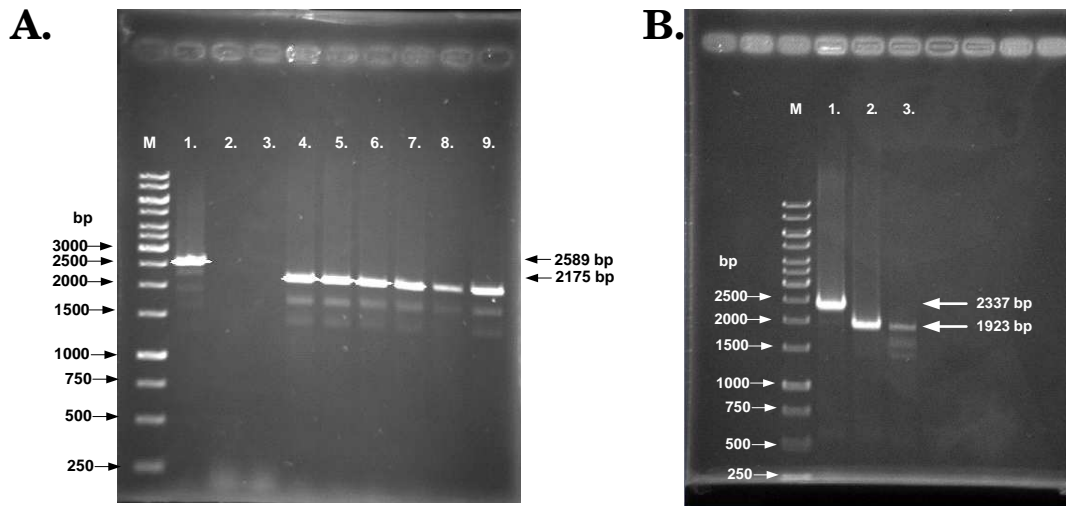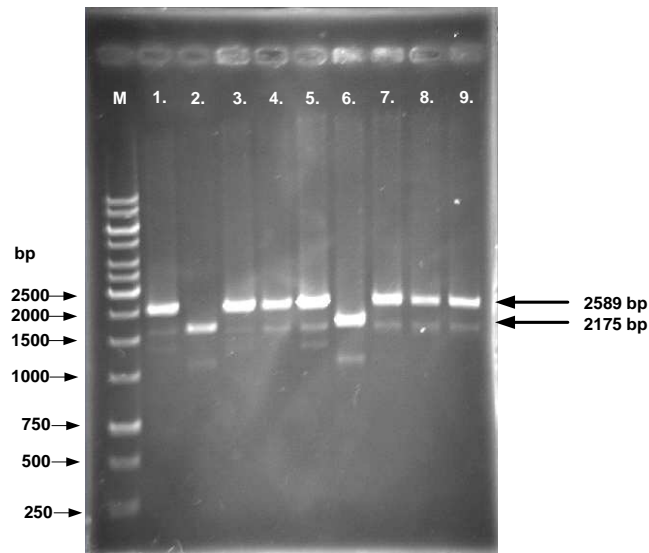
Figure 4.36: Colony PCR for establishing which transformant had successfully integrated the 5′ *upstream flanking sequence-natMX-3′ downstream flanking sequence*. PCR-amplification was used with the pair of external primers for: genomic DNA from wild type *S. pombe* (lane 1), clones 1-8 (lanes 2-9). The GeneRuler™ 1 kb DNA marker is illustrated as M.

Finally, all generated strains were compared with each other for the *mpc1* and *mpc2* loci in the same gels, in order to further strengthen our findings qualitatively (Figure 4.37.A for the *mpc1* locus and Figure 4.37.B for the *mpc2* locus).
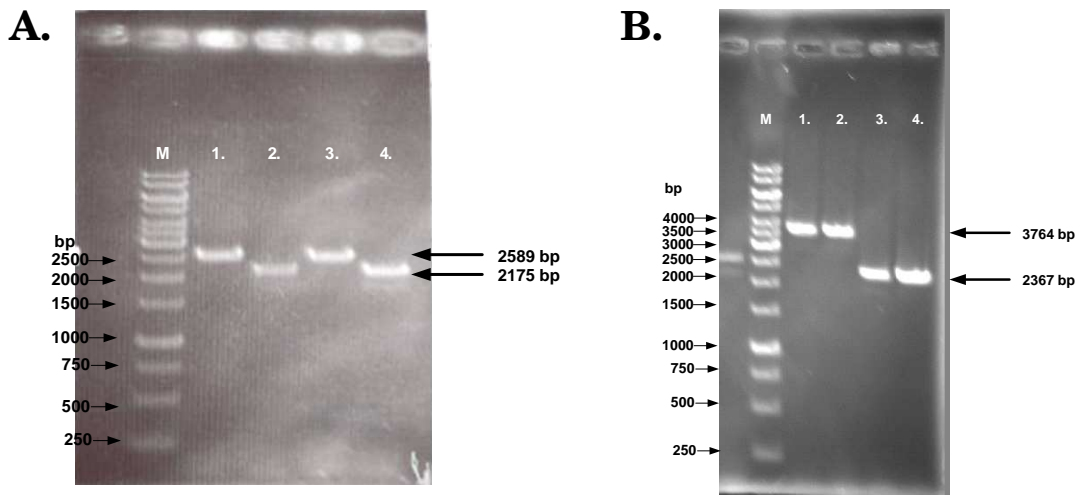


Figure 4.37: Colony-PCR for comparing the wild type cells (lane 1) and clones *mpc1*Δ (lane 2), *mpc2*Δ (lane 3), *mpc1*Δ*mpc2*Δ (lane 4) for the size of the *mpc1* [A] and the *mpc2* [B] locus with the use of the appropriate external primers each time.

### 4.3.4 Physiology of *S. pombe* mutant cells with a defective MPC machinery

This part focuses on the physiologic characterization of the deletion mutants and the subsequent comparison of the latter to the wild type *S. pombe* CBS 356 cells during exponential growth on glucose in shake flask cultivations. As it has been described in previous parts, cells growing exponentially in shake flasks, possess a constant specific growth rate where a metabolic steady state is reached (Deshpande et al., 2009). Under such conditions the yield coefficient of biomass on the given substrate is constant as proven by the linear relationship between the biomass and the substrate concentration during exponential growth. The same linear relationship applies for the concentrations for all metabolites quantified in the extracellular space (in this case pyruvate, ethanol, acetate and glycerol). Subsequently all yield coefficients calculated during metabolic steady state are constant. The slope of the linear curve of the concentration of two metabolites plotted against each other equals to the constant yield coefficient.

Up to now there has not been a systematic and comparative characterization of growth, substrate uptake and product formation of yeast cells carrying either single or multiple deletions of the genes encoding the MPC during the exponential growth phase in a chemically defined medium.

Since the discovery of the components of the yeast MPC system (Bricker et al., 2012; Herzig et al., 2012) , *S. cerevisiae* mutants were usually assayed for growth with spot assays (Bricker et al., 2012; Herzig et al., 2012), in shake flask cultures (Bender et al., 2015) or in well plates (Herzig et al., 2012; Timón-Gómez et al., 2013) on minimal media supplemented with amino acids. However such studies did not assess in an absolute quantitative manner the uptake of the substrate and subsequent synthesis of metabolic products that were secreted in the extracellular space. One study (Orlandi et al., 2014) focused only on the *S. cerevisiae mpc1*Δ strain and on metabolite levels mainly during a period of 3 days after the diauxic shift (post glucose depletion). Characteristically, there was only one sampling point from the exponential growth phase. Bricker et al. (Bricker et al., 2012) quantified intracellular pyruvate levels, acetyl-CoA and CoA pools for various *S. cerevisiae* strains (wild type, *mpc1*Δ, *mpc2*Δ, *mpc1*Δ*mpc2*Δ), but illustrated only the relative abundance of these pools.

In this study the parameters that were assessed quantitatively were the specific growth rate ($\mu$) of the cells, the specific glucose uptake rate ($q_S$) and the biomass ($Y_{X/S}$) and product yields ($Y_{P/S}$) on glucose during the pseudo steady state of the exponential growth phase in batch cultivations. The metabolic products that were secreted in the extracellular space and subsequently quantified were pyruvate, ac-

etate, ethanol and glycerine. Ethanol and acetate in specific are strongly connected with the pyruvate node and with the respirofermentative metabolism.

The minimal medium in this study was supplemented with the appropriate antibiotics (nourseothricin for *mpc1*Δ: 100 µg/L; geneticin G418 for *mpc2*Δ: 200 µg/L: both antibiotics for the double mutant strain) and the branched-chain amino acids leucine, valine, isoleucine in order to support the growth of the deletion mutants. It was verified that without the amino acid supplements in shake flask cultivations none of the mutant strains could grow on the glucose minimal medium. Similarly, *S. cerevisiae* cells lacking Mpc1p, Mpc2p and the combination thereof, exhibited a strong growth defect on a glucose medium lacking leucine (Bricker et al., 2012) verified by a spot assay. In a different study by Herzig et al. (Herzig et al., 2012) the *MPC1*Δ strain grew as fast as the wild type and reached the same final cell concentration when the SD (synthetic defined) medium was supplemented with valine and leucine. Similar growth defects were reported for *S. cerevisiae* mutant strains *MPC1*Δ and *MPC2*Δ growing in the absence of valine in SD medium (Timón-Gómez et al., 2013).
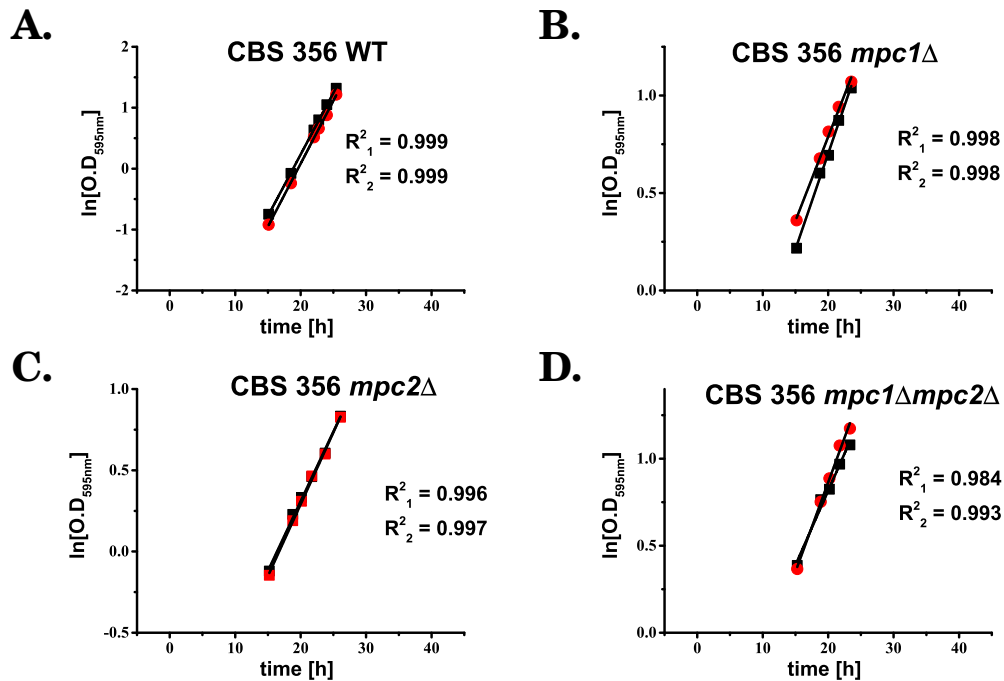


Figure 4.38: Exponential growth in parallel batch cultivations for [A] CBS 356, [B] *mpc1*Δ, [C] *mpc2*Δ and [D] *mpc1*Δ*mpc2*Δ in ((■) and (●)) in a chemically defined medium (supplemented with valine, leucine, isoleucine and appropriate antibiotics for supporting the growth of the mutant strains). Black lines represent the linear regression between the ln[O.D$_{595nm}$] and time with $R^2$ representing the goodness-of-fit of the linear regression for each one of the parallel cultivations.
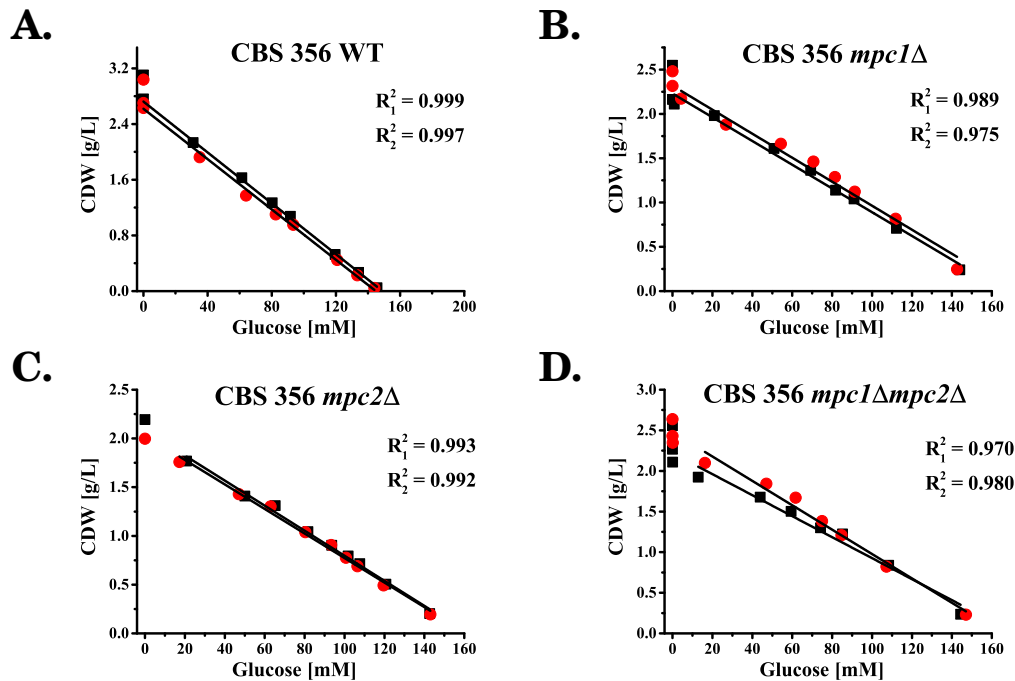
Figure 4.39: Graphical illustration of the linear relationship between the CDW and glucose concentration during the exponential growth phase for [A] CBS 356, [B] *mpc1Δ*, [C] *mpc2Δ* and [D] *mpc1Δmpc2Δ* in parallel cultivations ((■) and (●)) in a chemically defined medium (supplemented with valine, leucine, isoleucine for the growth of the mutant strains). Black line indicates each curve of the regression analysis along with the $R^2$.

Table 4.6: A comparison between the various strains for the specific growth rates ($\mu$) and the glucose uptake rate ($q_S$). These are mean values along with their standard deviations from two parallel cultivations for each strain during the exponential growth phase.

| coefficient [unit] | CBS 356 (WT) | *mpc1Δ* | *mpc2Δ* | *mpc1Δmpc2Δ* |
|---|---|---|---|---|
| $\mu$ [$h^{-1}$] | 0.204 ± 0.002 | 0.083 ± 0.009 | 0.082 ± 0.002 | 0.080 ± 0.007 |
| $q_S$ [mmol/(g CDW×h)] | 11.53 ± 0.69 | 5.76 ± 0.65 | 5.84 ± 0.21 | 5.19 ± 0.06 |

As it is illustrated in Figures 4.38 and 4.39, the rates for growth (linear relationship between $\ln[\text{O.D}_{595nm}]$ and time) and glucose uptake (linear relationship between glucose concentration and time) were constant during the exponential growth phase in shake flask cultivations for all strains.

The gene deletions had a profound effect on growth and led to a lower capacity to utilise glucose from the cultivation medium, as shown by the lower glucose uptake rates (Table 4.6). The rates of growth and of glucose uptake (which is also an indicator of cellular activity) were affected in a similar manner, indicative of a constant yield of biomass on glucose. Growth exhibited a 40 % reduction compared to the wild

165

type cells in all mutant strains independent of the gene deletion or deletions that were introduced. This is an initial indication that either the partial or the complete loss of components of the MPC transport system severely impaired growth to the same extent even in the presence of the amino acid supplements (valine, leucine, isoleucine).



Figure 4.40: Graphical illustration of the linear relationship between the extracellular concentration of pyruvate and glucose concentration during the exponential growth phase for [A] CBS 356, [B] *mpc1Δ*, [C] *mpc2Δ* and [D] *mpc1Δmpc2Δ* in parallel cultivations ((■) and (●)) in a chemically defined medium (supplemented with valine, leucine, isoleucine for the growth of the mutant strains). Black line indicates each curve of the regression analysis along with the $R^2$.

Table 4.7: A comparison between the various strains for the pyruvate yield on glucose ($Y_{PYR/GLC}$). These are mean values along with their standard deviations from two parallel cultivations for each strain during the exponential growth phase.

| coefficient [unit] | CBS 356 (WT) | *mpc1Δ* | *mpc2Δ* | *mpc1Δmpc2Δ* |
|---|---|---|---|---|
| $Y_{PYR/GLC}$ [mol/mol] | $0.006 \pm 0.000$ | $0.015 \pm 0.002$ | $0.019 \pm 0.001$ | $0.018 \pm 0.001$ |

Extracellular pyruvate concentrations were quantified and illustrated as a function of the consumed glucose in Figure 4.40 during the exponential growth phase. The curve for each plot accounts for the constant yield of pyruvate secreted in the extracellular space on consumed glucose ($Y_{PYR/GLC}$) (summarized in Table 4.7).

The striking difference between the wild type and the mutant cells were the accumulation of pyruvate in the extracellular space. The yield of pyruvate on glucose increased 3-fold in all deletion mutants compared to the wild type. Taking into account the specific growth rate for each strain, the pyruvate production rate increased from a value of $0.073 \pm 0.006$ mmol/(g CDW×h) for the wild type to values ranging from $0.088 \pm 0.019$ mmol/(g CDW×h) for *mpc1Δ* to $0.111 \pm 0.007$ mmol/(g CDW×h) for *mpc2Δ* and $0.094 \pm 0.004$ mmol/(g CDW×h) for *mpc1Δmpc2Δ*. This is a strong indication of a bottleneck created downstream from pyruvate at the MPC machinery. The same phenomenon was verified for pyruvate in *S. cerevisiae* when such deletions were introduced in the cells (Bricker et al., 2012; Orlandi et al., 2014). The deletion of either or both components of the MPC machinery in *S. pombe* clearly blocked the entry of carbon into the mitochondria at the pyruvate node and the accumulated pyruvate in the cytosol was instead secreted to the extracellular space. Furthermore, the activities of the pyruvate-consuming reactions at the cytosol (pyruvate carboxylase and pyruvate decarboxylase) could not compensate for the overflow of this metabolite.



Figure 4.41: Graphical illustration of the linear relationship between the extracellular concentration of acetate and glucose concentration during the exponential growth phase for [A] CBS 356, [B] *mpc1Δ*, [C] *mpc2Δ* and [D] *mpc1Δmpc2Δ* in parallel cultivations ((■) and (●)) in a chemically defined medium (supplemented with valine, leucine, isoleucine for the growth of the mutant strains). Black line indicates each curve of the regression analysis along with the $R^2$.

Table 4.8: A comparison between the various strains for the acetate yield on glucose ($Y_{ACE/GLC}$). These are mean values along with their standard deviations from two parallel cultivations for each strain during the exponential growth phase. n.e non existing.

| coefficient [unit] | CBS 356 (WT) | *mpc1Δ* | *mpc2Δ* | *mpc1Δmpc2Δ* |
|---|---|---|---|---|
| $Y_{ACE/GLC}$ [mol/mol] | n.e | 0.045 ± 0.005 | 0.071 ± 0.005 | 0.052 ± 0.002 |

The next metabolite that was affected by the metabolic bottleneck at the pyruvate node was acetate (see Figure 4.41), with the constant yields of acetate on glucose presented in Table 4.8.

Acetate is synthesized by the acetaldehyde dehydrogenase enzyme which is located downstream from the pyruvate decarboxylase followed by the reduction of NAD(P). During the consumption of glucose by wild type cells in shake flask cultures, the main overflow metabolite is ethanol and to some extent acetate, due to the Crabtree effect. As it is illustrated in Figure 4.41.A for wild type cells, acetate begun to accumulate after glucose was completely depleted and prior to that point its concentration was below the detection limits.

However this was not the case for the deletion mutants (Figures 4.41.B, C & D). There was a constant accumulation of acetate, when the concentration of glucose in the medium was less than 120 mM during the exponential growth phase. Apparently the increased flux of carbon into the fermentative pathway led to enzymes reaching their maximum capacity. A perfect candidate is the acetyl-CoA synthetase which is a cytosolic enzyme and catalyses the conversion of acetate into acetyl-CoA. Normally this enzyme is induced by high ethanol concentrations in *S. cerevisiae*, in order to support ethanol oxidation but this is not the case in glucose-limited cultures of *S. pombe* (de Jong-Gubbels et al., 1996). Therefore this part of the fermentative pathway could not accommodate for the higher intracellular availability of pyruvate and begun accumulating acetate as well. The highest yield for acetate on glucose was observed for strain *mpc2Δ* (Figure 4.41.C) followed by yields similar between them for strains *mpc1Δ* and *mpc1Δmpc2Δ* (Figures 4.41.B & D respectively). Interpreting this difference between the MPC-deficient mutants of acetate yields points towards the fact that the elimination of the subunits of the MPC machinery can create varying phenotypes, depending on which subunit is deleted.
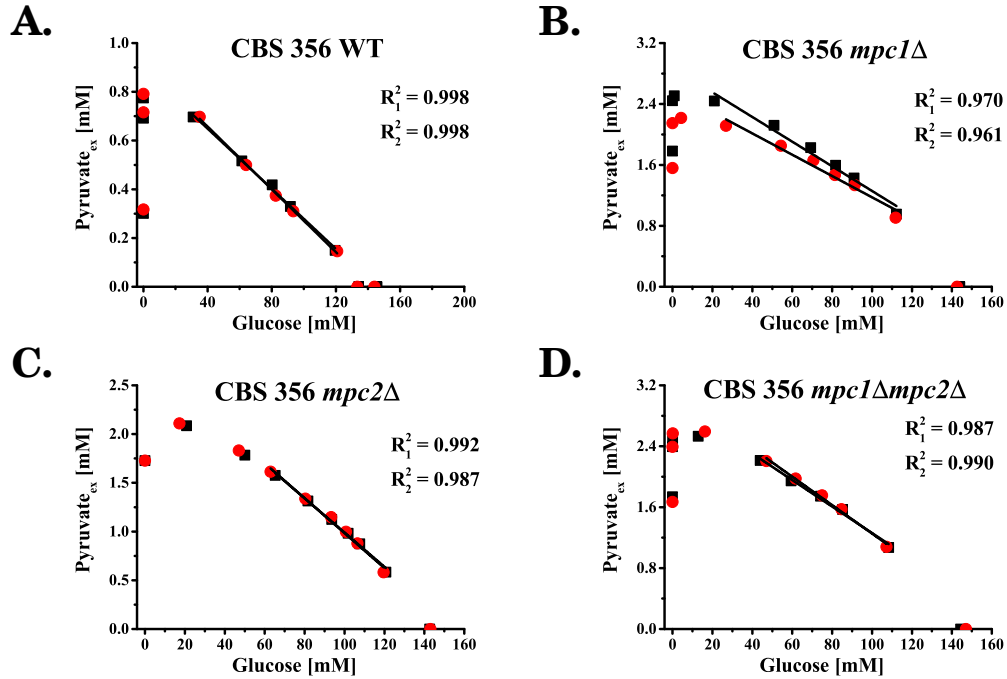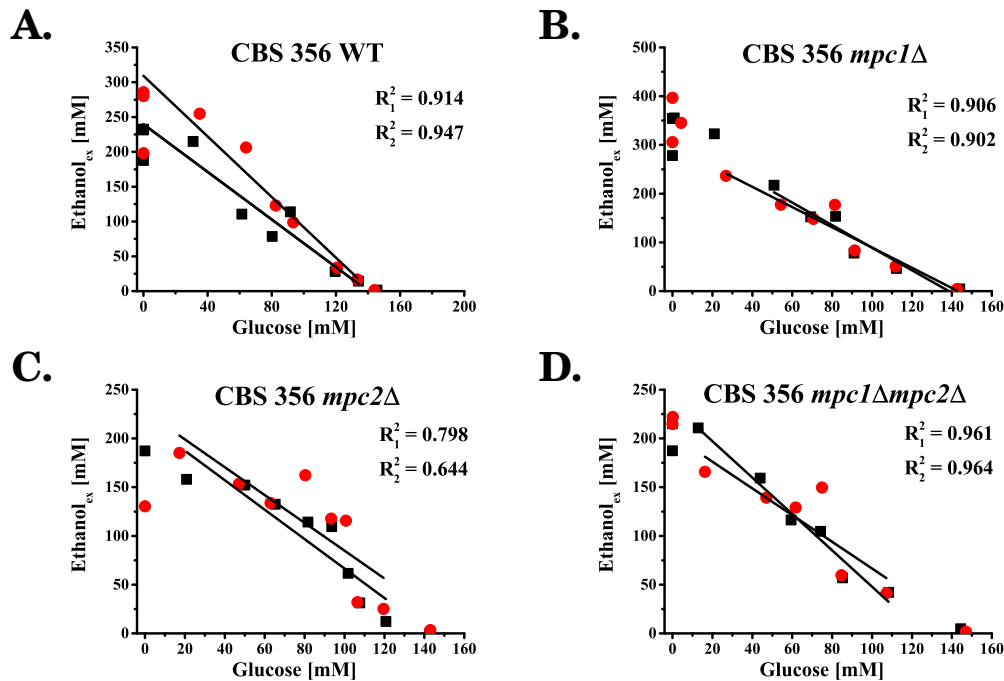
Figure 4.42: Graphical illustration of the linear relationship between the extracellular concentration of ethanol and glucose concentration during the exponential growth phase for [A] CBS 356, [B] *mpc1Δ*, [C] *mpc2Δ* and [D] *mpc1Δmpc2Δ* in parallel cultivations ((■) and (●)) in a chemically defined medium (supplemented with valine, leucine, isoleucine for the growth of the mutant strains). Black line indicates each curve of the regression analysis along with the $R^2$.

Table 4.9: A comparison between the various strains for the ethanol yield on glucose ($Y_{EtOH/GLC}$). These are mean values along with their standard deviations from two parallel cultivations for each strain during the exponential growth phase.

| coefficient [unit] | CBS 356 (WT) | *mpc1Δ* | *mpc2Δ* | *mpc1Δmpc2Δ* |
|---|---|---|---|---|
| $Y_{EtOH/GLC}$ [mol/mol] | 1.94 ± 0.33 | 2.20 ± 0.17 | 1.47 ± 0.06 | 1.62 ± 0.35 |

At the same time ethanol yields (Table 4.9) on glucose were also affected by the introduction of perturbations at the MPC machinery in the mutant strains. However the quantification of ethanol was not as precise as the quantification of the other metabolites, as can be observed by the high deviation between measured values. Therefore, the comparison of ethanol yields is mostly qualitative between the various strains. The lowest yield was observed for strain *mpc2Δ* (Figure 4.42.C), whereas the yield was comparable to the wild type for strains *mpc1Δ* and *mpc1Δmpc2Δ* (Figures 4.42.B & D).
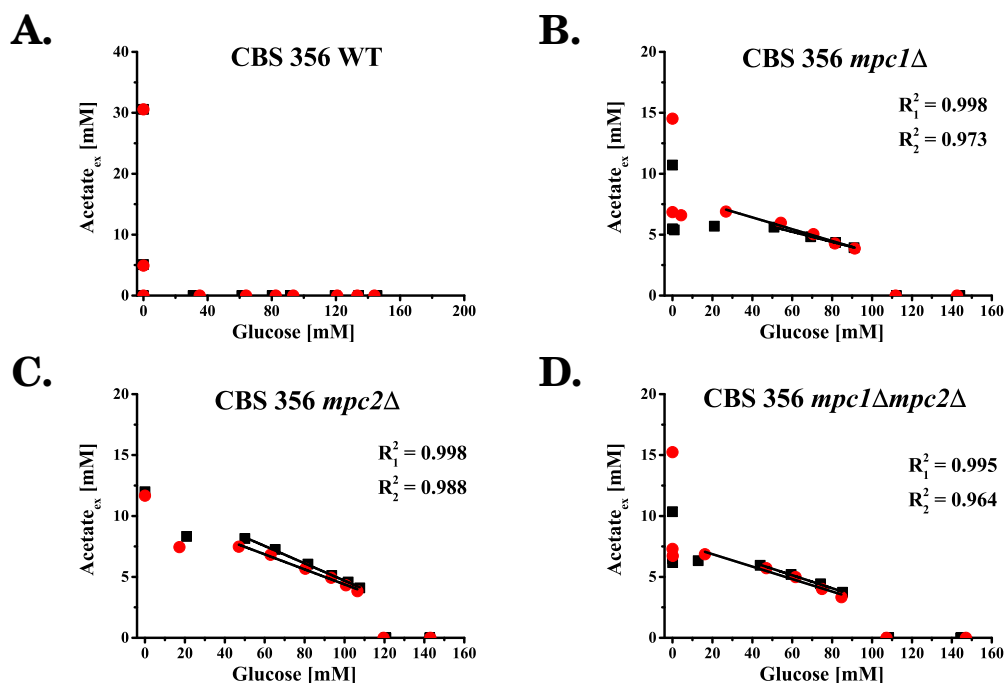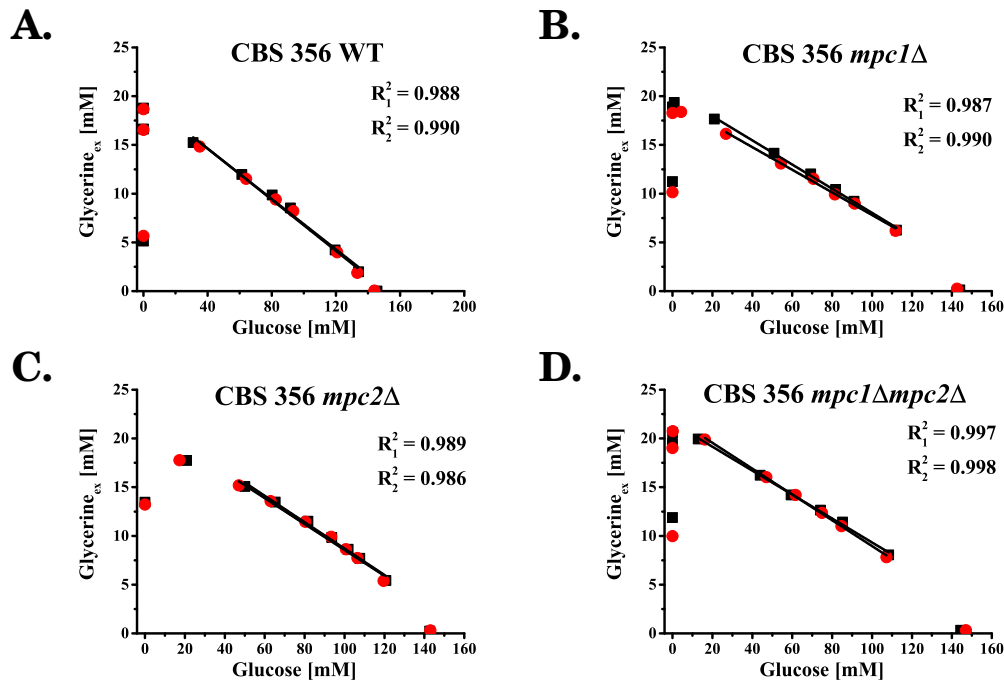
Figure 4.43: Graphical illustration of the linear relationship between the extracellular concentration of glycerine and glucose concentration during the exponential growth phase for [A] CBS 356, [B] $\Delta mpc1$, [C] $\Delta mpc2$ and [D] $\Delta mpc1\Delta mpc2$ in parallel cultivations (($\blacksquare$) and ($\bullet$)) in a chemically defined medium (supplemented with valine, leucine, isoleucine for the growth of the mutant strains). Black line indicates each curve of the regression analysis along with the $R^2$.

Table 4.10: A comparison between the various strains for the glycerine yield on glucose ($Y_{GLYC/GLC}$). These are mean values along with their standard deviations from two parallel cultivations for each strain during the exponential growth phase.

| coefficient [unit] | CBS 356 (WT) | $mpc1\Delta$ | $mpc2\Delta$ | $mpc1\Delta mpc2\Delta$ |
|---|---|---|---|---|
| $Y_{GLYC/GLC}$ [mol/mol] | $0.135 \pm 0.002$ | $0.120 \pm 0.005$ | $0.134 \pm 0.002$ | $0.128 \pm 0.007$ |

Finally glycerine was the last metabolite of the central metabolism that was secreted in the extracellular space and was quantified in supernatants from growing cells on glucose. Glycerine is a metabolic product of the upper part of the glycolysis and is synthesized in two steps. Firstly dihydroxyacetone phosphate (DHAP) is reduced to glycerol 3-phosphate by glycerol 3-phosphate dehydrogenase which is then dephosphorylated by glycerol 3-phosphatase to yield glycerine. Overall formation rates were reduced in all mutant strains in a similar manner (see Figure 4.44 in mmol/(g CDW×h) for rates) due to the decrease in the uptake of glucose. However, the molar yield of glycerine on glucose was maintained unchanged in all strains (Table 4.10). This result further supports the point that the perturbations in the MPC

machinery affected only the lower part of the glycolysis around the pyruvate node, mainly leading to a redistribution of fluxes in the ethanol and acetate biosynthetic pathways.

The fermentative pathway is one of the directions that the glycolytic flux follows after reaching pyruvate. Based on the aforementioned results, the accumulation of pyruvate at the cytosol due to a defect mitochondrial transport caused a comparable growth defect in all mutant strains, however the secretion of acetate, pyruvate and ethanol varied between the mutant strains, depending on which subunit of the MPC was deleted (see Figure 4.44 for a comparison of the product formation and substrate uptake rates).
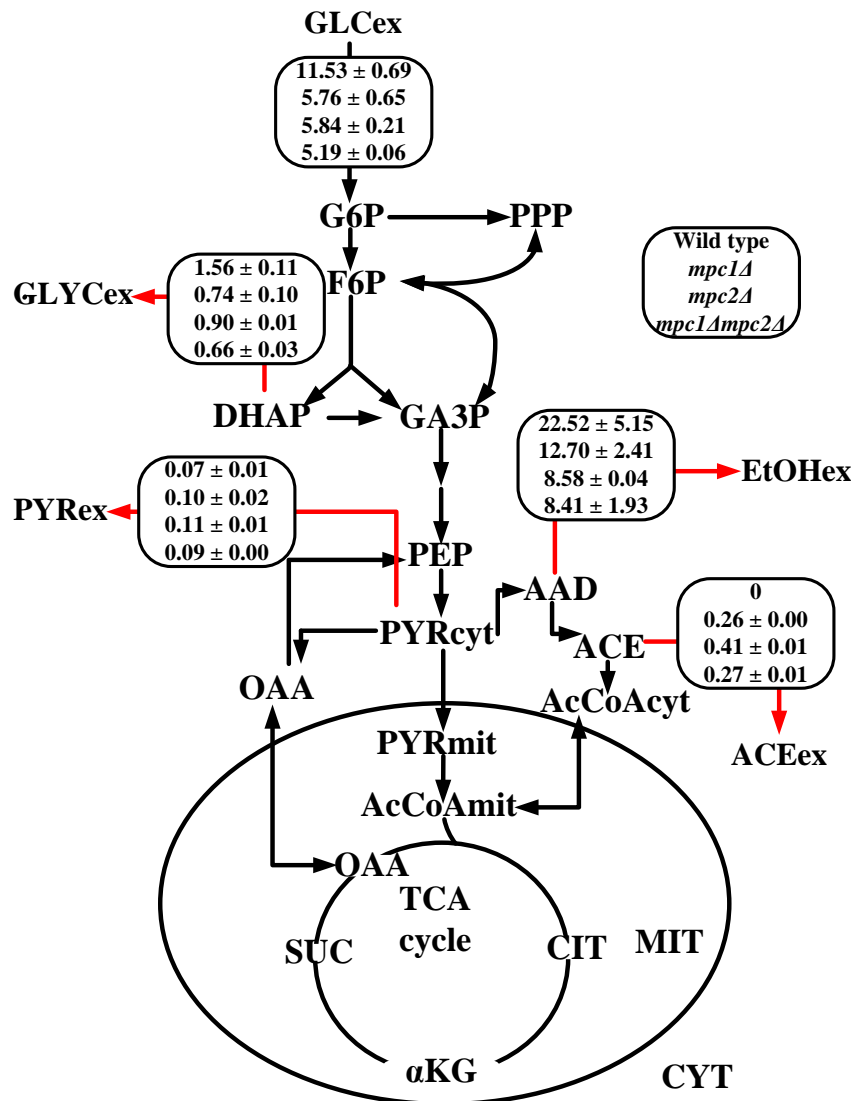


Figure 4.44: Comparison of glucose uptake rates and product formation rates (mmol/(g CDW×h)) for secreted glycerine, ethanol, pyruvate and acetate during steady state for strains (values from top to bottom) CBS 356 (WT), *mpc1Δ*, *mpc2Δ* and *mpc1Δmpc2Δ*.

Therefore, we can conclude that the metabolic network at the cytosol-mitochondria interface exhibited a varying degree of plasticity and robustness, by increasing or decreasing carbon fluxes away from pyruvate and towards acetate and ethanol biosynthesis.

Another point drawn was that even in the presence of branched-chain amino acids (BCAA: leucine, valine, isoleucine) that could theoretically enter the mitochondria and be catabolized to yield acetyl-CoA and fuel the TCA cycle, it was the absence of a fully functional MPC and the overflow of pyruvate in the cytosol that caused not only a redistribution of fluxes at the pyruvate node but also a decrease in growth and biomass formation. Therefore we could postulate that the MPC plays a more central role in regulating not only the influx of pyruvate into the mitochondrial matrix to fuel the TCA cycle and the respiratory chain, but also the lower glycolysis and the fermentative pathway as part of a larger metabolon in connection with cytosolic enzymes. The role of the MPC as a regulator is even more pronounced when comparing these results with the *in vivo* fluxes calculated from the $^{13}$C-flux analysis, where the actual flux of pyruvate entering the mitochondrial matrix is only a very small fraction of the pyruvate flux that is diverted towards ethanol and acetate biosynthesis during respirofermentative growth on glucose.

It is unknown based on these results alone, how the carbon fluxes were redistributed at the anaplerotic pathway connecting cytosolic pyruvate to malate and oxaloacetate. In principle an excess of cytosolic pyruvate could be converted into oxaloacetate by the pyruvate carboxylase which would subsequently enter the mitochondrial matrix via the Oacp to yield acetyl-CoA. Therefore it could be expected that the anaplerotic pathway was also up- or downregulated in a varying manner in the mutant strains, comparable to the changes observed in the fermentative pathway. This will be further examined with targeted *in situ* studies with pyruvate as a respiratory substrate in subsequent parts of this work.

### 4.3.5 *In situ* metabolism of pyruvate by *S. pombe* cells with a defective MPC machinery

In this section, wild type cells and mutants with an impaired mitochondrial pyruvate transporter system, were further examined *in situ*. In previous parts of this work it has been exhibited how intact mitochondria of selectively permeabilized cells respired in the presence of FADH$_2$-linked substrates (succinate) and cytosolic NADH (exogenously supplied or *in situ* generated). This time the central respiratory substrate would be pyruvate based on the rationale which was covered in section 4.3.2, with NADH and malate as respiratory co-substrates. The setup for comparing the wild type strain to strains deficient for the transporter proteins

Mpc1p, Mpc2p and the combination thereof was based on monitoring the elimination of pyruvate in the cytosol and the mitochondria in the presence of NADH and malate under ADP-phosphorylating conditions.

However caution should be taken when interpreting the behavior of an isolated set of metabolic pathways in a configuration utilizing selectively permeabilized cells. Phenomena, that are observed in *in situ* systems, can differ from the *in vivo* physiology. The level of regulation present in living cells, can not be reconstructed fully *in situ* and the multitude of metabolites that are physiologically present are missing as well as the cascade of events that they may be regulating. Nevertheless, an *in situ* system may prove itself rather helpful for illustrating the extent of the inherent metabolic robustness when genetic perturbations are introduced into a system and identify active pathways that were impossible to discern with physiological studies alone. Such an approach was applied here by activating selectively a reduced metabolic system, when these genetic perturbations were present in a defined genetic background. The reduced metabolic system refers to the inherent advantage of *in situ* approaches, in which, based on which exogenous substrates are supplied, only the reactions that are capable of using them are activated. At the same time information can be gained on mitochondrial bioenergetics, the NAD/NADH balance and the activity of mitochondrial transporters.

### 4.3.5.1  Production of $CO_2$ and acetaldehyde by wild type mitochondria in the presence of pyruvate

Mitochondria of wild type cells respiring in the presence of pyruvate (with the oxygen uptake profiles covered in Section 4.3.2) were further assessed on their capacity to form $CO_2$ and acetaldehyde. The continuous quantification of acetaldehyde was conducted by the spectrometrical analysis of the gas molecules with a signal of m/z = 43 detected by the MIMS.

Pyruvate decarboxylase in yeast exhibits cooperativity (Pronk et al., 1996; Baburina et al., 1998) for pyruvate and substrate activation with its activity described by sigmoidal kinetics as opposed to the procaryotic *Zymomonas mobilis* Pdcp which shows Michaelis-Menten kinetics and does not require substrate activation (simpler metabolic regulation) (Stevenson et al., 2008). In *S. cerevisiae* there are 6 genes expressing this tetramer protein with Pdc1p, Pdc5p and Pdc6p having catalytic activities which are markedly higher than the PDC activity of Crabtree-negative yeasts like *Komagataella pastoris* (Agarwal et al., 2013).

It was unknown whether the aldehyde and alcohol dehydrogenases were active in *S. pombe* under the applied experimental conditions as acetate and ethanol could not be detected chromatographically or by the MIMS respectively. In preliminary experiments with mitochondria oxidizing solely pyruvate, $CO_2$ was produced along

with acetaldehyde. Therefore, it was ascertained that the pyruvate decarboxylase was always active in the cytosol when pyruvate was present.

**Wild type mitochondria in the presence of pyruvate and malate.** Theoretically, since the gene deletions introduced in *S. pombe* cells were connected with the mitochondrial pyruvate entry and not with the cytosolic Pdcp activity and because of the fact that all permeabilized cells are exposed to identical concentrations of exogenous pyruvate, therefore the acetaldehyde formation rate *in situ* should not differ between the wild type and the mutant cells. However our experimental results revealed differences between the mutant strains and the wild type.

This was made initially evident with the acetaldehyde and $CO_2$ formation profiles that were generated when using a pyruvate medium, then a pyruvate medium supplemented with malate and finally a medium additionally supplemented with ADP (oxygen uptake for these conditions summarized in Figure 4.28.A). Figure 4.45 illustrates in a comparative manner the formation profiles for $CO_2$ (values summarized in Table 4.11) and acetaldehyde for the mini-reactor that were based on the m/z = 44 and m/z = 43 signals respectively and were detected continuously by the MIMS for the permeabilized wild type cells. Experiments were conducted in duplicates and it was ensured that the digitonin-permeabilized cell concentrations that were used throughout the different conditions was the same.
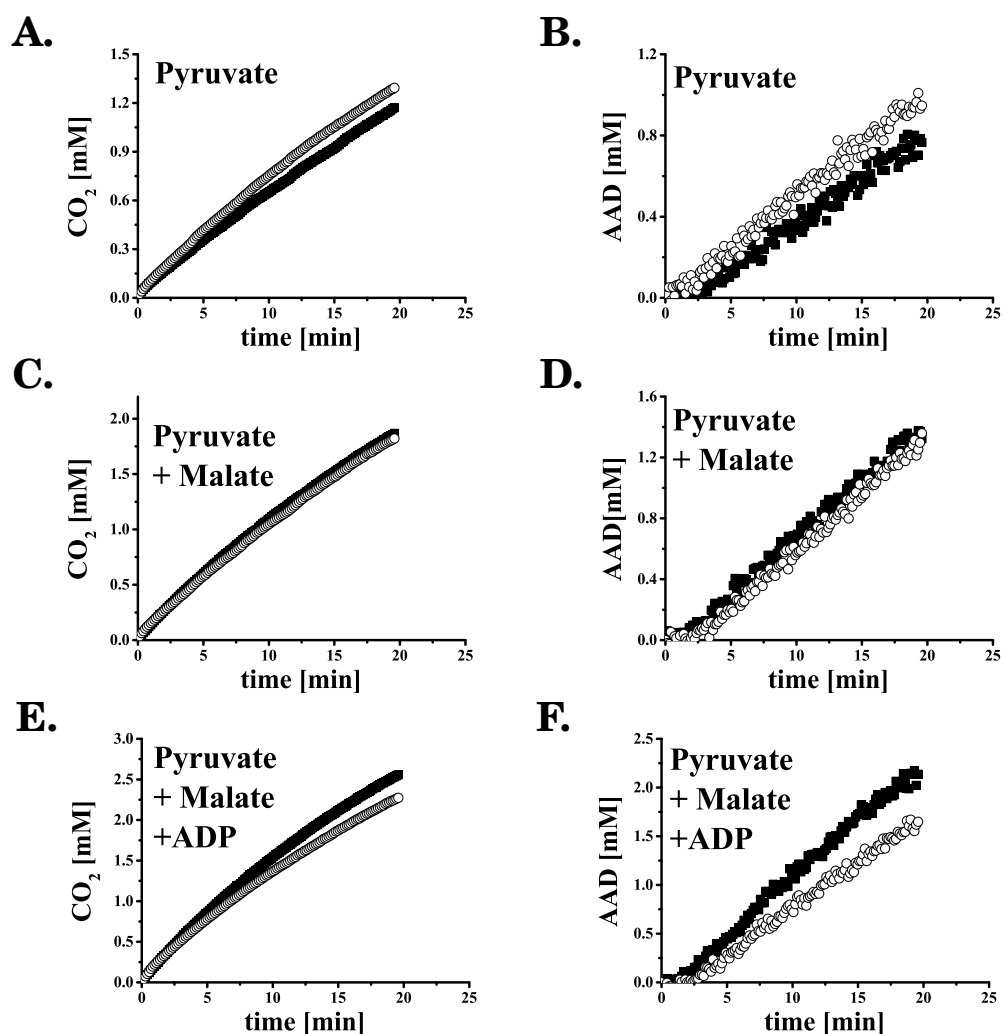
Figure 4.45: Continuous quantification of $CO_2$ ([A], [C] and [E]) and acetaldehyde (AAD) ([B], [D] and [F]) concentrations over time in the sealed mini-reactor, tempered at 30 °C for different substrate combinations. Digitonin-permeabilized cells of wild type *S. pombe* were subjected to initial concentrations of the following oxidative substrates: (PYR; 5 mM), L-malate (MAL; 3 mM) and ADP (0.5 mM). Experiments were conducted in duplicates ((■) and (○)) and with identical cell concentrations (2.84 ± 0.36 g/L) yielded from parallel growing batch cultivations in minimal growth media.

Table 4.11: A comparison of the *in situ* $CO_2$ specific production rate ($q_{CO_2}$) of wild type digitonin-permeabilized cells respiring in the presence of pyruvate, pyruvate + malate and pyruvate + malate + ADP in the sealed reactor. These are mean values along with their standard deviations from two independent experiments. Cells (cell concentration = 2.84 ± 0.36 g/L) yielded from parallel growing batch cultivations in minimal growth media.

| coefficient [unit] | Pyruvate | Pyruvate + Malate | Pyruvate + Malate + ADP |
|---|---|---|---|
| $q_{CO_2}$ [nmol/(mg CDW×min)] | 28.98 ± 1.12 | 44.74 ± 6.99 | 63.91 ± 10.95 |

It was mentioned previously that the formation of these two gases was a first indication of a functional Pdcp in the cytosol of selectively permeabilized cells. Nevertheless, this semi-quantitative comparison revealed something else as well. The amount of $CO_2$ generated by digitonin-permeabilized cells, increased when malate was present in the reaction mix. This increase was even more pronounced when the mitochondrial respiratory chain was further activated with the addition of ADP. Such a surge in the amount of $CO_2$ formed was indicative of an additional decarboxylating activity being active apart from the acetaldehyde-forming pyruvate decarboxylase in the cytosol. This source would be the mitochondrial pyruvate dehydrogenase complex, where $CO_2$ is generated by the combined activities of the E1, E2 and E3 catalytic subunits of the mitochondrial pyruvate dehydrogenase complex (Pronk et al., 1996).

The oscillating nature of the detected acetaldehyde concentration in the mini-reactor did not allow for an absolute calculation of its formation rate. Therefore the concentrations of $CO_2$ and acetaldehyde were plotted against each other and compared for the various conditions as illustrated in Figure 4.46. The data from the duplicate experiments agreed with each other for each condition. From Figures 4.46.A & B it is evident that along with the increase of $CO_2$ the formation of acetaldehyde also increased.
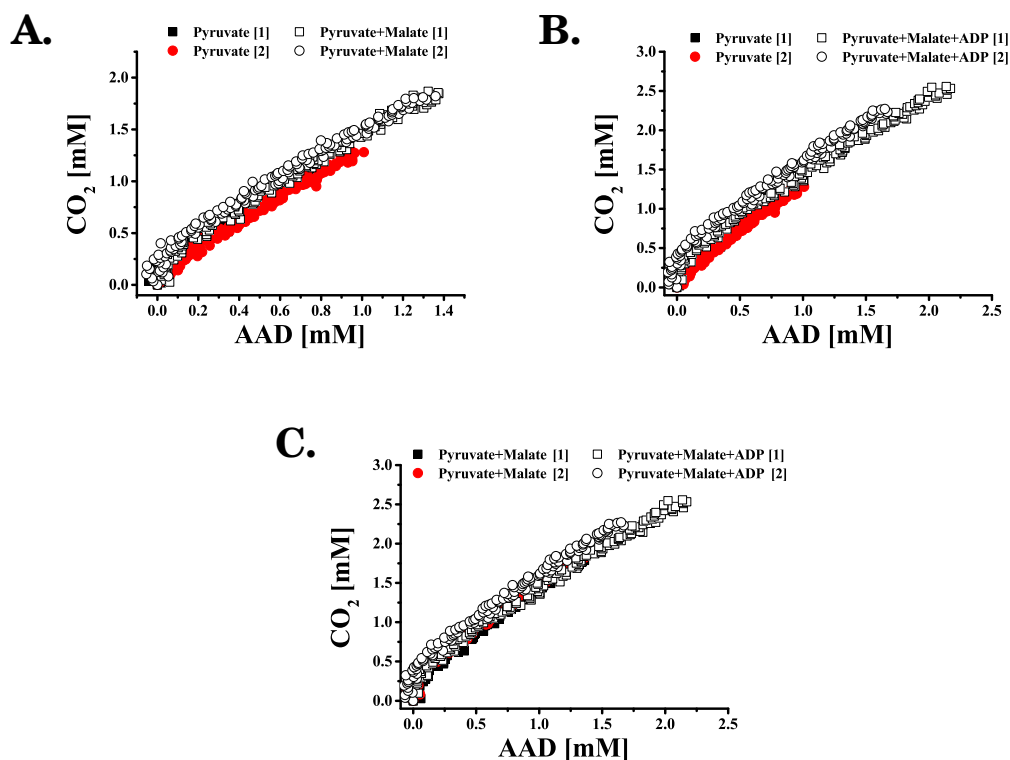


Figure 4.46: The concentration of produced $CO_2$ against the concentration of acetaldehyde being formed in the sealed reactor for various conditions with digitonin-permeabilized wild type cells. Conditions identical to the experiments described in Figure 4.45.

176

Theoretically, accepting the sole existence of a cytosolic pyruvate decarboxylase as predicted, we would have expected an increase in $CO_2$ formation (in addition due to an active pyruvate dehydrogenase complex) but not an increase in acetaldehyde formation. However this was not the case when malate and malate along with ADP were present additionally to pyruvate in the reaction mix. Therefore two scenarios could be plausible.

The first scenario explaining the simultaneous increase of $CO_2$ and acetaldehyde concentration in the reactor would have to do with the addition of malate and ADP causing an upregulation of the cytosolic pyruvate decarboxylase. However this scenario could not be plausible since the cytosolic malic enzyme could not have produced pyruvate in the cytosol in the aforementioned experimental conditions due to NAD being absent as a precursor (*S. pombe* NAD-dependent malic enzyme). Thus, there was no increased pyruvate availability that could support a higher acetaldehyde formation. Furthermore there is no evidence that malate can act as a positive regulator of the pyruvate decarboxylase activity in the cytosolic compartment. The second scenario includes a mitochondrial pyruvate decarboxylase activity generating acetaldehyde along with $CO_2$.

Concerning the mitochondrially localized pyruvate decarboxylase scenario the following points could be made. The addition of malate and ADP along with pyruvate into the mini-reactor would activate the mitochondria and increase the flow of pyruvate through the mitochondrial pyruvate carrier. Subsequently pyruvate in the mitochondrial matrix would either serve as a substrate for the E1$\alpha$ subunit of the pyruvate dehydrogenase complex or be decarboxylated to yield acetaldehyde by the hypothesized mitochondrial pyruvate decarboxylase. Such an event would explain why the slope of the curve for each condition for Figures 4.46.A-C almost overlapped with each other even when the absolute quantities of acetaldehyde and $CO_2$ increased.

It is known that in yeast there is a metabolic by-pass (oxidation of pyruvate is diverted away from the mitochondrial pyruvate dehydrogenase, Figure 4.47) which was hypothesized to involve the decarboxylation of pyruvate in the cytosol by the pyruvate decarboxylase and the diffusion of acetaldehyde in the mitochondrial matrix where it could be oxidized to form acetate by the activity of the mitochondrial aldehyde dehydrogenase (Boubekeur et al., 1999; Rigoulet et al., 2004). This pathway should not be confused with the cytosolic pyruvate dehydrogenase by-pass (Remize et al., 2000).

In *S. pombe* the following proteins-members of the ethanol biosynthetic pathway are predicted to exist in the mitochondrial matrix; the aldehyde dehydrogenase (Adh4p) and the alcohol dehydrogenase (Atd1p). However, as mentioned in previous parts, it is unclear whether *S. pombe* possesses a mitochondrial pyruvate

decarboxylase and the results illustrated here up to this point can not clearly prove the existence of such an activity. Cell fractionation and subsequent purification of the pyruvate decarboxylase activity from *S. cerevisiae* revealed that this enzyme is a soluble one with 97.3 % of its activity localized in the S fraction and the 2.33 % of its total activity in the mitochondrial fraction (fraction $P_1$) (Urk et al., 1989). It was however claimed by Van Urk et al.,(Urk et al., 1989), that the cytosolic enzyme contaminated the mitochondrial fraction because this fraction was not further purified.
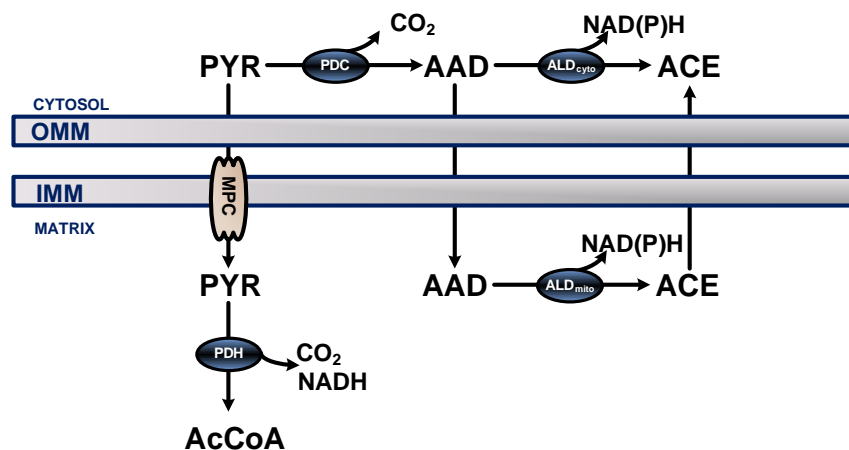


Figure 4.47: The hypothesized pyruvate dehydrogenase bypass in *S. pombe*. Products that may occur from pyruvate (PYR) metabolism here are $CO_2$, acetaldehyde (AAD), acetate (ACE) and acetyl-CoA (AcCoA). Enzymes illustrated here are: PDC, pyruvate decarboxylase; ALD(mitochondrial-cytosolic), aldehyde dehydrogenase; PDH, pyruvate dehydrogenase complex. The mitochondrial transporter docked on the inner mitochondrial membrane (IMM) for pyruvate is the MPC. OMM is the outer mitochondrial membrane.

A third scenario on interpreting the aforementioned results could in principle take into account the increasing activity of the MPC when switching from pyruvate to pyruvate and malate as respiratory substrates and eventually to pyruvate, malate and ADP. In such a case an increased flux of pyruvate through the MPC (increase of respiration as a marker of mitochondrial activity and import of pyruvate) would have an effect on the activity of the cytosolic Pdcp (this scenario does not employ the presence of a mitochondrial Pdcp). Thus, the Pdcp activity in the cytosol would be controlled and regulated by the mitochondrial pyruvate carrier.

Conclusively, the following questions stem from the aforementioned points. Can the introduction of genetic perturbations at the level of the mitochondrial pyruvate transport system reveal more about the enzymatic activities around the pyruvate node? Would the loss of pyruvate transfer across the mitochondrial inner membrane have an effect on the formation of acetaldehyde in total and reveal whether a mitochondrial pyruvate decarboxylase exists or the cytosolic activity of this enzyme is regulated by the MPC?

### 4.3.5.2 Comparative analysis of $CO_2$ and acetaldehyde production in wild type and mutant cell mitochondria in cytosol-mimicking conditions

We proceeded with examining in a comparative manner the uptake of pyruvate in the presence of malate, ADP and NADH from the mitochondria of digitonin-permeabilized wild type cells and of the *mpc1Δ*, *mpc2Δ* and *mpc1Δmpc2Δ* knockout strains. In this cytosol-mimicking environment the first parameters under examination were the kinetics of the produced gases, $CO_2$ and acetaldehyde. In subsequent parts the uptake of oxygen and pyruvate as well as the uptake of NADH and the formation of metabolic energy in the form of ATP will be covered.

Firstly, digitonin-permeabilized wild type *S. pombe* cells were compared to each other in the presence and abscence of ADP-driven respiration with pyruvate, malate and NADH as the respiratory substrates. After it was verified that indeed the addition of ADP led to a higher respiratory rate (see Figure 4.28.B), with state 3 respiration being 2-fold higher than state 4 respiration, acetaldehyde formation was examined for all strains.
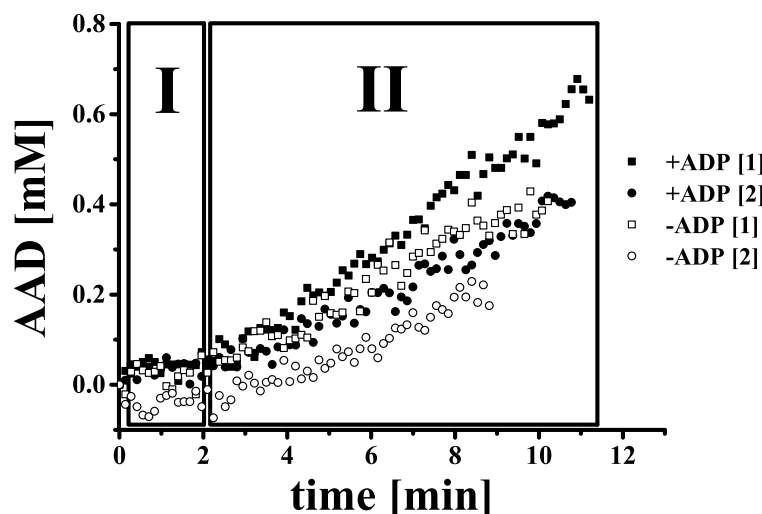


Figure 4.48: Evolution of the concentration of acetaldehyde over time in the mini-reactor based on the m/z=43 signal detected by the MIMS. Permeabilized wild type cells were subjected to a pyruvate + malate + ADP substrate combination ((■) and (●)) and to a pyruvate + malate substrate combination ((□) and (○)) in duplicates and at 30 °C. The initial concentrations of the substrates were: pyruvate (PYR; 5 mM), L-malate (MAL; 3 mM), ADP (0.5 mM) and NADH (0.25 mM). Average cell concentration = 1.59 ± 0.28 g/L.

As it is illustrated in Figure 4.48 for wild type mitochondria respiring in the presence of pyruvate, malate and NADH with and without ADP, acetaldehyde (AAD) formation could be divided in two phases (phases I and II). In phase I acetaldehyde

formation lagged up to the 2 minute timepoint and it started being detectable in the reactor environment for the rest of the experiment's duration.
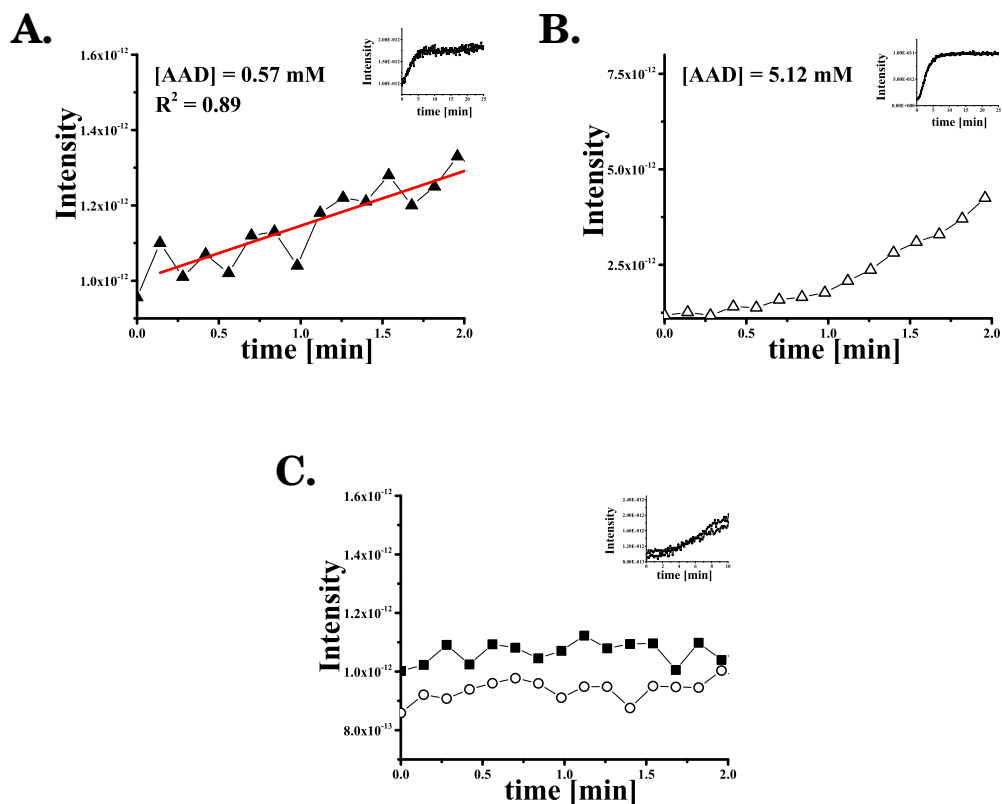


Figure 4.49: Relationship between the m/z = 43 intensity detected by the MIMS and time in the sealed reactor for: a low concentration acetaldehyde standard solution (0.57 mM) (▲) (figure A), a high concentration acetaldehyde standard solution (5.12 mM) (△) (figure B) and acetaldehyde being formed by wild type digitonin-permeabilized cells (for duplicate experiments (■) and (○)) in the presence of pyruvate, malate, NADH and ADP (figure C). Red line indicates the curve of the regression analysis along with the $R^2$. Plots in the upper right corner illustrate the curve form during the whole duration of a measurement (intensity versus time).

The response time of the MIMS was compared for detecting a low (0.5 mM) and a high (5 mM) acetaldehyde concentration in identical conditions (temperature and buffer composition). The high acetaldehyde concentration was set at 5 mM, since in the *in situ* system this would be the maximum theoretical concentration yielded by the complete conversion of an initial concentration of 5 mM of pyruvate by the pyruvate decarboxylase. These plots were then compared to the actual signal intensity for acetaldehyde produced by respiring cells in the presence of pyruvate, malate, ADP and NADH. As it can be illustrated, for a standard solution with a low acetaldehyde concentration (Figure 4.49.A) for the first two minutes, the signal was linearly proportional to time and eventually reached its saturation point. For the standard solution with a high acetaldehyde concentration (Figure 4.49.B), the

relationship between signal intensity and time was described by a sigmoidal curve eventually reaching its saturation point. On the other hand, the detected signal of acetaldehyde being formed in the *in situ* system (Figure 4.49.C) lagged under the two minutes mark and was detectable beyond that point.
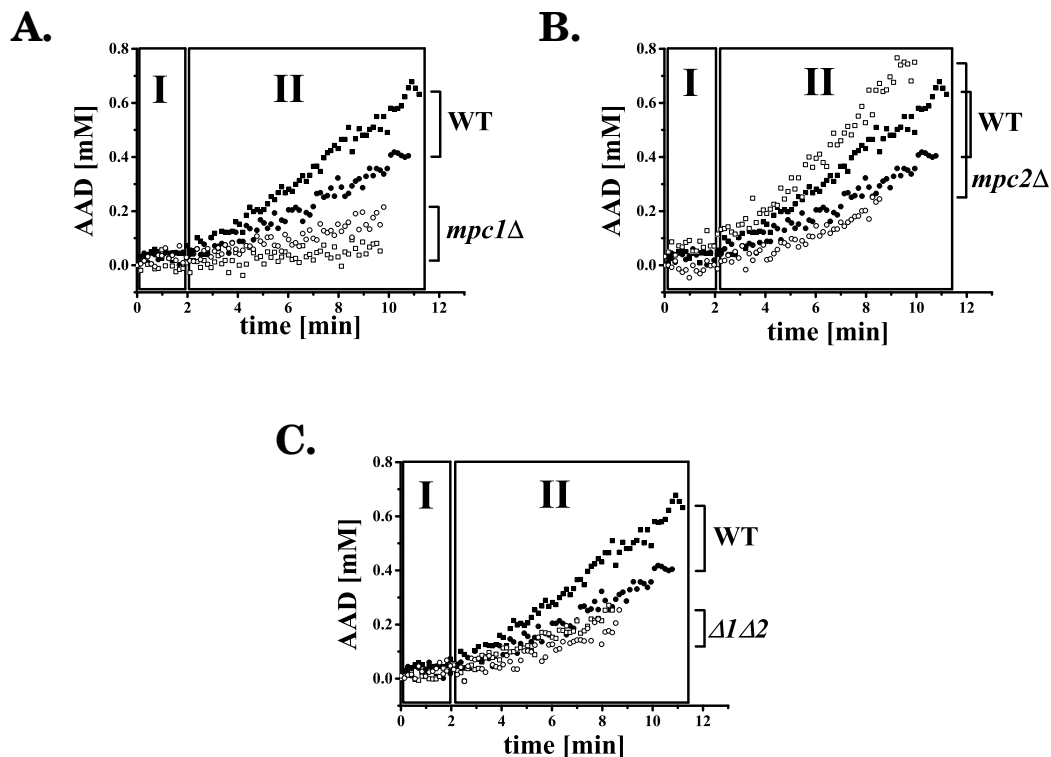


Figure 4.50: Evolution of the concentration of acetaldehyde over time in the mini-reactor for all selectively permeabilized mutant strains ((□) and (○)) compared to the wild type ((■) and (●)). Double knockout *mpc1Δmpc2Δ* depicted as *Δ1Δ2*. Conditions identical to these described in Figure 4.48. Average cell concentration : WT = 1.59 ± 0.28 g/L, *mpc1Δ* = 1.37 ± 0.07 g/L, *mpc2Δ* = 1.94 ± 0.01 g/L, *mpc1Δmpc2Δ* = 1.49 ± 0.01 g/L.

According to our findings (Figure 4.48) the presence of ADP compared to the absence of ADP led to slightly elevated acetaldehyde formation. However during ADP-activated respiration (substrates: pyruvate, malate, NADH and ADP) the MPC-deficient strains did not behave the same with the permeabilized wild type cells regarding acetaldehyde accumulation as it would be expected. Mitochondria deficient for the Mpc1p subunit of the mitochondrial pyruvate carrier (Figure 4.50.A) exhibited the largest degree of acetaldehyde formation impairment when compared to wild type permeabilized cells for the same cell concentration and substrates concentration.

During phase II and compared to the wild type, the acetaldehyde formation of the *mpc1Δ* strain was barely detectable. It was excluded as a possibility that the mini-reactor environment caused a decrease of the pyruvate decarboxylase activity. The pH range in the reactor was monitored and was between pH 6.7 - 6.8 in all

experiments with either the wild type or the mutant strains. At this pH range the pyruvate decarboxylase shows optimum activity (pH 6.0 - 6.6) (Stevenson et al., 2008). Also the initial pyruvate concentration (5 mM) was higher than the $K_m$ value reported for the native *S. cerevisiae* enzyme (1 - 3 mM) (Hübner et al., 1978; Pronk et al., 1996).

The other two mutant strains harboring mitochondrial pyruvate import deficiencies exhibited different acetaldehyde accumulation profiles compared to the *mpc1Δ* strain. Specifically, as illustrated in Figure 4.50.B, when selectively permeabilized cells of the *mpc2Δ* strain were subjected to the same conditions as the wild type strain, acetaldehyde formation was rather similar to the wild type. At the same time the double knockout mutant (Figure 4.50.C) exhibited an acetaldehyde accumulation profile only slightly decreased as compared to wild type permeabilized cells.

Concerning acetaldehyde formation it would have been expected that initially the differences between the knockout strains would have been minimal, since the genetic perturbations were affecting the pyruvate entry into the mitochondrial matrix and not the decarboxylation of pyruvate in the cytosol. Therefore, these results led us to examine further more physiological parameters stemming from the oxidation of pyruvate by *S. pombe* mitochondria, in order to characterize the role that each structural subunit of the MPC played alone and in combination with each other. Most importantly, these results combined lower the possibility for the presence of a mitochondrial pyruvate decarboxylase activity, as it was hypothesized in previous parts of this work. If this scenario was true, then the acetaldehyde levels reached in the mini-reactor by the mutant strains would never be equal or higher than these of the wild type permeabilized cells.

Since the discovery of the genes expressing the MPC subunits in yeast little is known on how the subunit makeup of the import machinery affects its function (Rampelt and Laan, 2015). The only information known is that the Mpc1p in *S. cerevisiae* forms a heterodimeric complex docked on the inner mitochondrial membrane with either Mpc2p or Mpc3p (Herzig et al., 2012) bound on Mpc1p (Bricker et al., 2012) depending on growth conditions (respiratory or fermentative growth) (Bender et al., 2015).

Based on the acetaldehyde formation over time, two phases (phase I and II) could be distinguished as discussed in previous parts. The next step was to examine the production of $CO_2$ during these two phases and compare it between the permeabilized wild type cells and the MPC-deficient mutant strains.
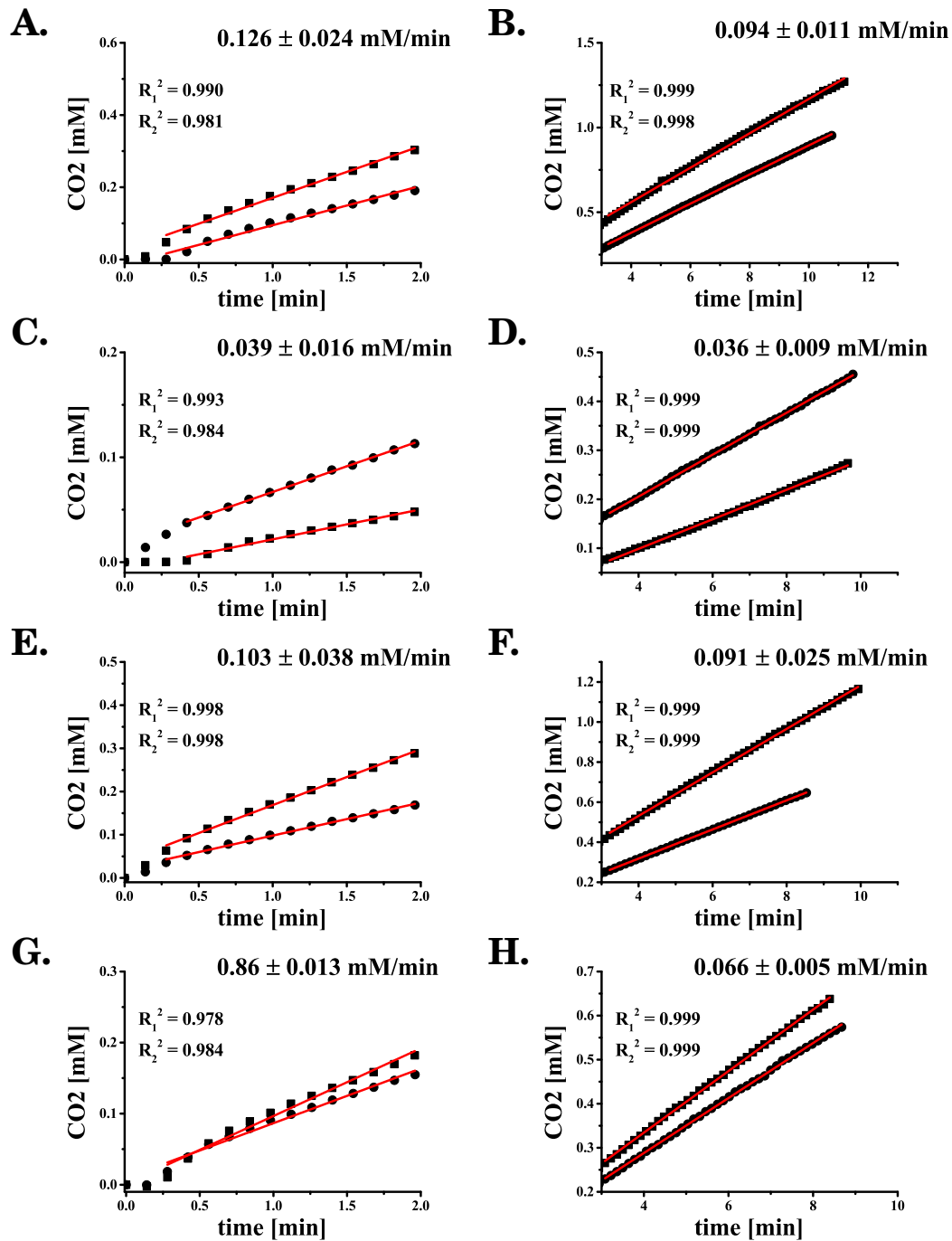
**Figure 4.51:** Evolution of $CO_2$ over time in a mini-reactor with digitonin-permeabilized cells. Plots of the left column depict phase I during the early stages of an experiment and the right column phase II, for the remaining of an experiment's duration. Figures [A]-[B] representative of the wild type, Figures [C]-[D] of the *mpc1Δ* strain, Figures [E]-[F] of the *mpc2Δ* strain and Figures [G]-[H] of the *mpc1Δmpc2Δ* strain. Conditions summarized in Figures 4.48 and 4.50 with average cell concentration : WT = 1.59 ± 0.28 g/L, *mpc1Δ* = 1.37 ± 0.07 g/L, *mpc2Δ* = 1.94 ± 0.01 g/L, *mpc1Δmpc2Δ* = 1.49 ± 0.01 g/L.. Duplicate experiments illustrated accordingly (■) and (●). Red line indicates each curve of the regression analysis along with the $R^2$.

Table 4.12: A comparison between the specific $CO_2$ formation rate ($q_{CO_2}$) for all digitonin-permeabilized strains in the presence of pyruvate, malate, NADH and ADP in the sealed reactor. These are mean values along with their standard deviations from two experiments conducted with cells yielded from parallel cultivations.

| $q_{CO_2}$ [nmol/(mg CDW×min)] | CBS 356 (WT) | *mpc1Δ* | *mpc2Δ* | *mpc1Δmpc2Δ* |
|---|---|---|---|---|
| Phase I | 81.7 ± 29.6 | 28.5 ± 11.9 | 53.0 ± 19.6 | 57.6 ± 8.4 |
| Phase II | 60.3 ± 17.5 | 26.8 ± 7.9 | 46.7 ± 13.3 | 44.2 ± 3.2 |

As illustrated in Figure 4.51.A for wild type digitonin-permeabilized cells, during the initial phase where no acetaldehyde was detectable in the mini-reactor environment, $CO_2$ formation was linear over time reaching a maximum formation rate of $q_{CO_2}$ = 0.126 ± 0.024 mM/min. This rate was later reduced in phase II by 25 % compared to the rate of phase I (Figure 4.51.B).

It is known that the mitochondrial pyruvate dehydrogenase complex and the pyruvate decarboxylase compete for pyruvate (Van Hoek et al., 1998) with the dehydrogenase complex possessing a lower $K_m$ value than the Pdcp. The aforementioned difference in $CO_2$ formation during phase I and II could be indicative of $CO_2$ production being fuelled predominantly by the pyruvate dehydrogenase complex during the initial 2 minutes that characterized phase I. However the continuous production of $CO_2$ and the abscence of acetaldehyde during phase I did not mean necessarily that the acetaldehyde- and $CO_2$-forming pyruvate decarboxylase was not functioning at all during the first two minutes.

Therefore, taking into account $CO_2$ production during these two phases, the abscence of acetaldehyde during phase I could be attributed to the enzyme (Pdcp) being active in equilibrium. In such a case the net formation of acetaldehyde would be equal to its net uptake by enzymes downstream of the Pdcp such as the aldehyde dehydrogenase and the ethanol dehydrogenase, making acetaldehyde non-detectable during phase I. Both dehydrogenases downstream from the Pdcp activity are known to function simultaneously (Kesten et al., 2015). The accumulation (also described as formation in previous parts) of acetaldehyde during phase II could be attributed on a bottleneck downstream of the Pdcp, leading to acetaldehyde accumulating in the mini-reactor environment.

With these points accounted for and in order to examine the correlation between pyruvate transport and *in situ* metabolism, the kinetics of $CO_2$ for the mutant strains were also analyzed (See Table 4.12 for specific $CO_2$ production rates for

all strains in nmol/(mg CDW×min)).

As it is illustrated in Table 4.12 for strain $\Delta mpc1$, the specific rates of $CO_2$ formation were almost identical in both phases and did not change significantly during the transition from one phase to another as it was observed for the wild type. However this rate was reduced by 65.1 % during phase I and by 55.6 % during phase II compared to the permeabilized wild type cells for the same phases (comparison between specific production rates in nmol/(mg CDW×min)). The continuous synthesis of $CO_2$ along with the almost diminished accumulation of acetaldehyde could mean two things. Firstly, that the pyruvate entry into the mitochondria was severely impaired leading to the absence of substrate to activate the mitochondrial pyruvate dehydrogenase complex, which also encompasses a decarboxylase activity producing $CO_2$ in the mitochondrial matrix. Without pyruvate, the pyruvate dehydrogenase could not function at the capacity exhibited by the wild type, thus generated less $CO_2$. Secondly, that the cytosolic pyruvate decarboxylase activity was reduced as a direct effect from the elimination of the Mpc1p subunit. This low capacity of the *in situ* system to generate $CO_2$ further supported the data from the physiological studies of strain *mpc1Δ* in previous parts, where pyruvate accumulated in the cytosol and was secreted in the extracellular environment due to the mitochondrial pyruvate transport deficiency.

Examining the *in situ* $CO_2$ formation kinetics for the *mpc2Δ* strain revealed a different behavior compared to that of the *mpc1Δ* strain. The specific formation rate for $CO_2$ was reduced at 35.1 % for phase I and at 22.7 % for phase II compared to the wild type (in nmol/(mg CDW×min)) (Figures 4.51.E & F). The decrease of the $CO_2$ rate was not as pronounced as it was for strain *mpc1Δ*. This finding accompanied by the fact that acetaldehyde accumulated in digitonin-permeabilized *mpc2Δ* cells in a similar manner to the wild type, pointed towards the assumption that the Mpc2p subunit played a different role than the Mpc1p subunit in *S. pombe* mitochondria.

On the other hand, the double knockout exhibited a 29.5 % and a 26.7 % decrease for phases I and II respectively for its specific $CO_2$ formation rate compared to the wild type (Figures 4.51.G & H). These results along with the acetaldehyde formation profile for the double knockout strain place the capacity to generate $CO_2$ and acetaldehyde for this *in situ* system (deficient for both transport proteins) in between the Mpc1p- and Mpc2p-deficient systems.

In summary, the aforementioned findings are more evident with the graphical illustration of the $CO_2$ and acetaldehyde concentration plotted against each other in Figure 4.52 for all mutant strains in comparison to the wild type system and for the same measurement duration. The introduction of the *mpc1* deletion caused the largest decrease on the simultaneous generation of acetaldehyde and $CO_2$ whereas the deletion of gene *mpc2* had a less profound effect than expected.
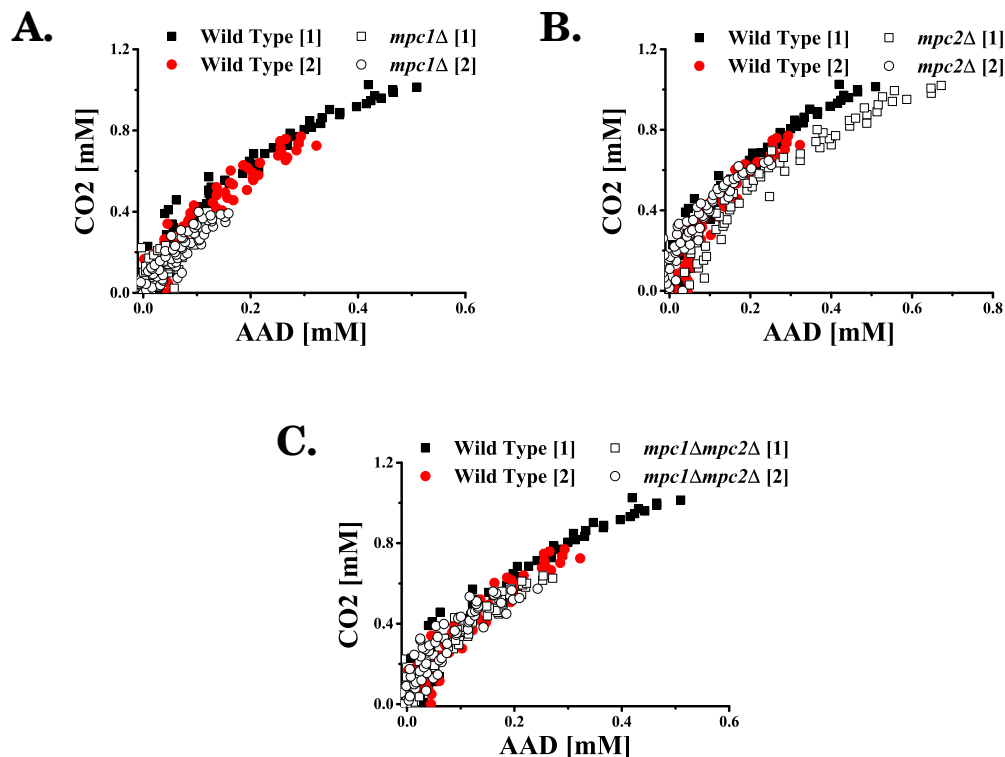
Figure 4.52: Dynamic evolution of the $CO_2$ concentration versus the acetaldehyde concentration for experiments performed in the closed system at 30 °C and for a duration of approximately 8.5 minutes. In each plot the wild type was compared versus digitonin-permeabilized cells from the *mpc1Δ* strain [A], the *mpc2Δ* strain [B] and the *mpc1Δmpc2Δ* strain [C]. Conditions summarized in Figures 4.48 and 4.50.

Taking these results into account along with the fact that the elimination of either or both of the pyruvate transporter subunits (genetic and physiological data supporting their absence covered in previous parts), exhibited a differentiated activity of $CO_2$- and acetaldehyde-forming pathways in the cytosol. This kind of diverse behaviour depending on which subunit was inactive could not be described by experiments conducted in the past with isolated mitochondria, where the interaction between the mitochondrial compartment and the cytosolic metabolic pathways was absent. For example the mitochondrial activity expressed as pyruvate import in isolated mitochondria from single yeast knockouts for genes *mpc1* and *mpc3* was close to zero (Herzig et al., 2012). Such experiments although helpful in order to discern the presence or absence of a transporter can not provide proof of the relative interaction of each transporter or transporter subunits with their adjacent metabolic pathways in the cytosol. In order to further elaborate on the mechanism of interaction of the two separate subunits of the MPC with the anaplerotic and the fermentative pathways and mitochondrial function, pyruvate uptake and mitochondrial respiration were assessed.

### 4.3.5.3 Pyruvate metabolism by selectively permeabilized *S. pombe* mutant cells

Since the discovery of the transporter proteins comprising the MPC machinery, the analysis of the uptake of pyruvate from mitochondria in *S. cerevisiae* was conducted solely with the use of isolated mitochondria and $^{14}$C-pyruvate as the substrate. Bricker et al., (Bricker et al., 2012) analysed isolated yeast mitochondria lacking the Mpc1p subunit yielded by cells growing in raffinose medium. Herzig et al., (Herzig et al., 2012) extended and supplemented the analysis on yeast mitochondria lacking the Mpc3p, Mpc2p subunits and the combination thereof from cells growing on lactate media. In all the above cases import of pyruvate was eliminated except of mitochondria from the Mpc2p-deficient strain growing on non-fermentative media (lactate). This discrepancy was explained by Bender et al., (Bender et al., 2015) who exhibited that cells growing on fermentative substrates (glucose) expressed the Mpc1pMpc2p complex while cells growing under respiratory conditions (glycerol medium) expressed the Mpc1pMpc3p complex in order to facilitate pyruvate uptake. Again this was exhibited with isolated mitochondria importing $^{14}$C-pyruvate. Only just recently pyruvate metabolism by the MPC machinery has been studied *in vivo* and dynamically based on a method employing a biosensor (Compan et al., 2015)

Although the aforementioned approach utilizing isolated mitochondria is helpful in order to identify whether a transporter is able to import a $^{14}$C-labeled substrate, an *in situ* system would be more appropriate, since the intracellular architecture is unaffected by the permeabilization process (Salabei et al., 2014). Therefore with this study it is the first time where pyruvate metabolism and import is examined in selectively permeabilized cells with a focus on the interplay of the MPC subunits with the mitochondrial matrix and the cytosol.

Samples were taken in regular intervals from selectively permeabilized cells incubated in the presence of pyruvate, malate, NADH and ADP in the sealed minireactor. All conditions were kept constant for all strains, as well as the permeabilized cell concentration in the mini-reactor. The samples were immediately boiled at 100 °C in order to stop the metabolism, disrupt the cells and release the mitochondrial content. Pyruvate was quantified chromatographically and pyruvate elimination consisted not only of the uptake by the MPC machinery but also its metabolism in the mitochondrial matrix by the pyruvate dehydrogenase complex and in the cytosol by the cumulative action of the pyruvate decarboxylase, pyruvate carboxylase and malic enzyme activities. Also it was assumed that pyruvate was eliminated in one phase and not in two, as it was the case for gases quantified directly in the mini-reactor by the MIMS. Due to the longer time intervals needed

to obtain samples containing pyruvate the time resolution was less than with the MIMS.

**A.**

0.114 ± 0.025 mM/min

$R_1^2 = 0.970$
$R_2^2 = 0.983$

PYR [mM]

time [min]

**B.**

0.025 ± 0.001 mM/min

$R_1^2 = 0.789$
$R_2^2 = 0.940$

PYR [mM]

time [min]

**C.**

0.100 ± 0.001 mM/min

$R_1^2 = 0.960$
$R_2^2 = 0.922$

PYR [mM]

time [min]

**D.**

0.092 ± 0.00 mM/min

$R_1^2 = 0.938$
$R_2^2 = 0.833$

PYR [mM]

time [min]
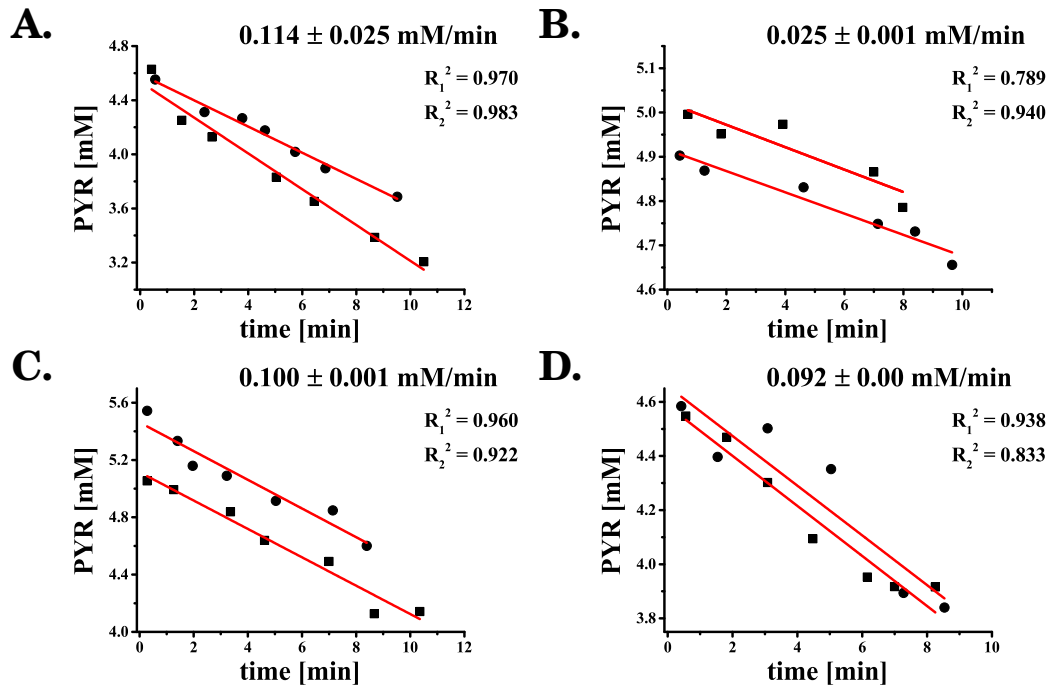
Figure 4.53: Metabolism of pyruvate over time for experiments performed in the closed system at 30 °C . Figure [A] refers to the wild type digitonin-permeabilized cells, Figure [B] to cells from the *mpc1Δ* strain, Figure [C] to cells from the *mpc2Δ* strain and Figure [D] to cells from *mpc1Δmpc2Δ* strain. Conditions summarized in Figure 4.48. Red line indicates each curve of the regression analysis along with the $R^2$.

Table 4.13: A comparison between the specific pyruvate elimination rate ($q_{PYR}$) for all digitonin-permeabilized strains in the presence of pyruvate, malate, NADH and ADP in the sealed reactor. These are mean values along with their standard deviations from two experiments conducted with cells yielded from parallel cultivations.

| $q_{PYR}$ [nmol/(mg CDW×min)] | CBS 356 (WT) | *mpc1Δ* | *mpc2Δ* | *mpc1Δmpc2Δ* |
|---|---|---|---|---|
| Phase I and Phase II | 74.3 ± 28.9 | 18.0 ± 0.2 | 51.2 ± 0.1 | 61.7 ± 0.1 |

Figure 4.53 illustrates the aforementioned elimination of pyruvate over time for selectively permeabilized cells of all strains used and with specific rates summarized in Table 4.13. Digitonin-permeabilized cells from the wild type cells showed the highest rate of pyruvate elimination with the cells corresponding to the *mpc1Δ* strain exhibiting the lowest rate of pyruvate elimination. Cells from the *mpc2Δ*

and the *mpc1Δmpc2Δ* strains exhibited a 31 % and 17 % decrease respectively of the specific pyruvate elimination rate when compared to wild type permeabilized cells. In all cases, the specific rates of pyruvate elimination were almost identical to the specific rates of $CO_2$ formed, exhibiting that these two amounts were metabolically directly linked.

Although the MPC transporter was incapable of transporting pyruvate to the mitochondrial matrix and to the pyruvate dehydrogenase complex in all mutant strains, strain *mpc1Δ* exhibited different kinetics of pyruvate elimination than strains *mpc2Δ* and *mpc1Δmpc2Δ*, although all strains were expected to yield similar values. Therefore except to pyruvate, the respiratory cosubstrate, malate, was also quantified chromatographically in order to shed more light in the metabolism of pyruvate.
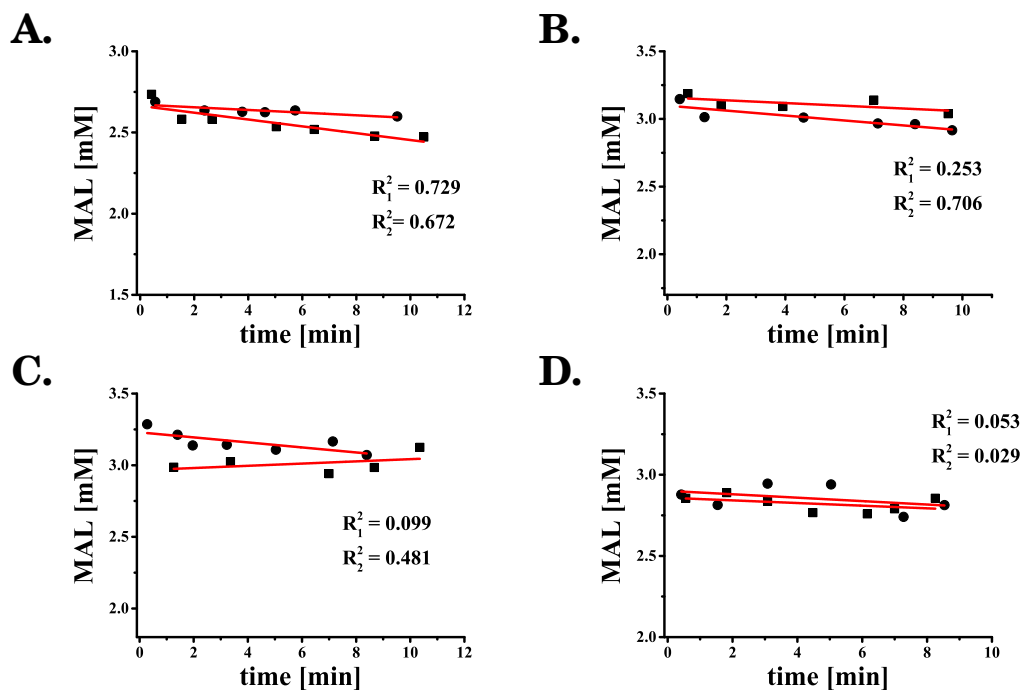


Figure 4.54: Metabolism of malate over time for experiments performed in the closed system at 30 °C . Figure [A] refers to the wild type digitonin-permeabilized cells, Figure [B] to cells from the *mpc1Δ* strain, Figure [C] to cells from the *mpc2Δ* strain and Figure [D] to cells from *mpc1Δmpc2Δ* strain. Conditions summarized in Figure 4.48. Red line indicates each curve of the regression analysis along with the $R^2$.

It is evident from all plots (Figures 4.54.A-D, that the total concentration of malate barely changed over time independent of the *S. pombe* strain used. This pointed towards the assumption that malate was part of a cycle where it was continuously consumed and replenished, therefore attaining a constant concentration over time. This could be possible by the combined activities of the cytosolic pyruvate carboxylase converting pyruvate to oxaloacetate, which was then converted to

malate by a cytosolic or a mitochondrial malate dehydrogenase and lastly malate could be converted to pyruvate by the malic enzyme, thus closing the cycle.

Combining these results with the $CO_2$ and acetaldehyde kinetics for the various strains, led to the interpretation that some kind of metabolic interplay took place in the selectively permeabilized cells under pyruvate oxidizing conditions based on the physical association of cytosolic enzymes to the outer mitochondrial membrane, as summarized with the reaction scheme of Figure 4.55. Oxaloacetate and malate are illustrated linked in the mitochondrial matrix via the known malate dehydrogenase activity. However the existence of a cytosolic malate dehydrogenase in *S. pombe* cells, has not been verified based on either sequence homology to known proteins (PomBase database) or by experimental results. The *S. pombe* Mdh1p is predicted to be mitochondrially localized and no other isoforms have been identified, whereas in *S. cerevisiae* there exist two isoforms of the malate dehydrogenase, a cytosolic (Mdh2p) and a mitochondrial one (Mdh1p). Therefore the existence of the *S. pombe* cytosolic malate dehydrogenase activity is marked with a questionmark in Figure 4.55.
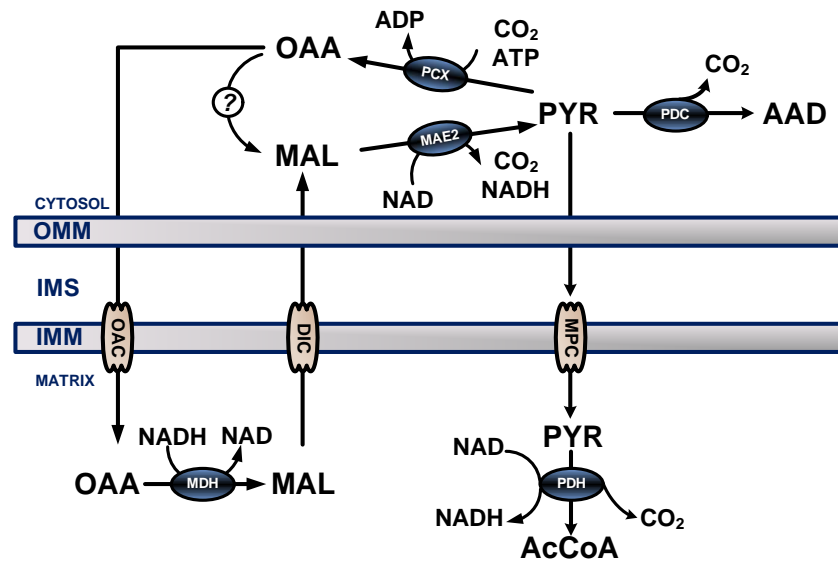


Figure 4.55: The hypothesized reaction network for pyruvate and malate metabolism with $CO_2$ formation in the *S. pombe* mitochondria-cytosol interface. Products that may occur from pyruvate (PYR) and malate (MAL) metabolism here are $CO_2$, acetaldehyde (AAD), oxaloacetate (OAA) and acetyl-CoA (AcCoA). Enzymes illustrated here are: PDC, pyruvate decarboxylase; PDH, pyruvate dehydrogenase complex; PCX, pyruvate carboxylase; MAE2, malic enzyme; MDH, malate dehydrogenase. The mitochondrial transporters docked on the inner mitochondrial membrane (IMM) for pyruvate is the MPC, the OAC for oxaloacetate and for malate the hypothesized DIC. OMM is the outer mitochondrial membrane. OMM and IMS represent the outer mitochondrial membrane and the mitochondrial intermembrane space.

#### 4.3.5.4 Spatial organization of the pyruvate metabolon

It has been shown in previous parts of this work, how mitochondrial membrane transporters like the non-specific OMM porin, interacted functionally with enzymes of the cytosol and of the mitochondrial intermembrane space allowing for an active metabolite channeling to increase the mitochondrial metabolism of cytosolic NADH. This spatial and regulatory organization into a metabolon allows for increased synergy and interaction in the cytosol of soluble enzymes in sequence or membrane-associated enzymes to membrane transporters (Moraes and Reithmeier, 2012). Also evidence continues to grow on enzymes being bound to the cytoskeleton which are not free to diffuse and escape the cytoplasm as it was revealed with experiments conducted with permeabilized CHO cells and fibroblasts (Menard et al., 2014). For example, after permeabilization of the cell membrane, enzymes of the glycolysis were retained inside the cells and continued to function, unless treated with inhibitors of actin polymerization that reversed the docking of these enzymes on the cytoskeleton and were subsequently released in the extracellular environment (Hudder et al., 2003).

There are various examples of such metabolons existing across different species. For example in plants like *A. thaliana*, where 5-10 % of glycolytic enzymes are associated with the outer mitochondrial membrane (Giegé et al., 2003; Graham et al., 2007), the microcompartmentation of enzymes and their organization into metabolons has been linked with regions of organelles where demand in ATP or pyruvate is higher. Also plant metabolons have been found to exist on the cytosolic side of the endoplasmatic reticulum membrane taking part in the plant's secondary metabolism (Jørgensen et al., 2005). In erythrocytes, the metabolism of $CO_2$ depends on a metabolon where a carbonic anhydrase is functionally bound on a plasma membrane chloride/bicarbonate exchanger (Sterling et al., 2001). In yeast it has been speculated that ADP uptake and metabolism into the mitochondria is organized into a metabolon with the porin, the adenine nucleotide translocator (ANT), the phosphate carrier and the ATP synthase being the major players (Clémençon, 2012). Such a metabolon has been proposed to exist in mammalian cells as well where the cytosolic hexokinase and glycerol kinase interact with the porin of the OMM to gain access to newly released mitochondrially synthesized ATP (reviewed by (Adams et al., 1991)).

Our experimental results could support the existence of a metabolon entailing the Mpc1p and the Mpc2p of the MPC machinery as well as enzymes of the cytosol that are metabolically linked to pyruvate as illustrated with Figure 4.56.
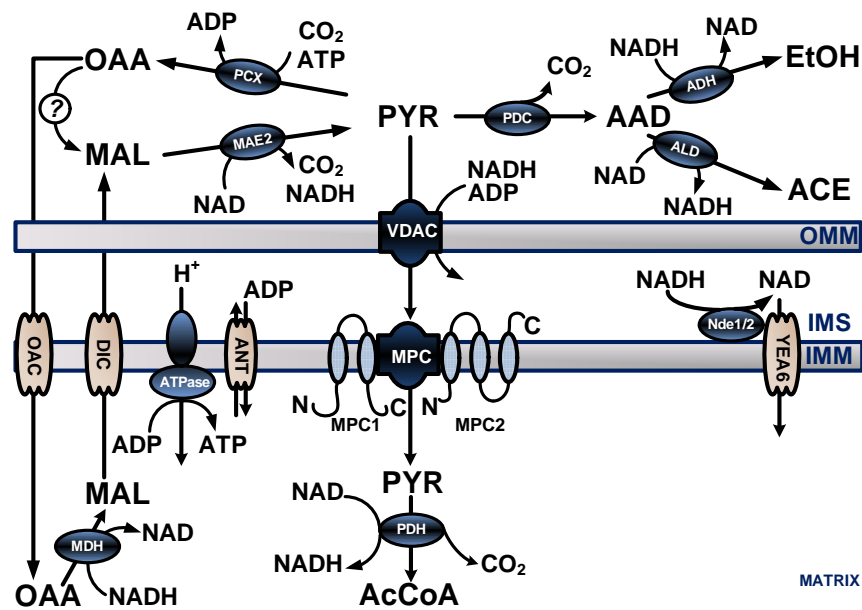
Figure 4.56: Proposed set of reactions for the metabolism of pyruvate at the cytosol-mitochondrium interface. Three compartments are illustrated (cytosol, mitochondrial intermembrane space (IMS), mitochondrial matrix) separated from each other by the outer (OMM) and inner mitochondrial membranes (IMM).Enzymes illustrated here are: PDC, pyruvate decarboxylase; MAE2, malic enzyme; PCX, pyruvate carboxylase; ADH, Alcohol dehydrogenase; MDH, malate dehydrogenase; ALD, aldehyde dehydrogenase; PDH, pyruvate dehydrogenase complex; NDE1/2, external mitochondrial NADH dehydrogenases; ATPase, mitochondrial matrix ATP synthase. The mitochondrial transporters docked on the OMM and IMM are: VDAC, voltage-dependent anion channel or porin; ANT, adenine nucleotide translocator; YEA6, NAD transporter; OAC, oxaloacetate carrier; DIC, hypothesized dicarboxylate carrier for malate; MPC, mitochondrial pyruvate carrier with its two subunits and their theoretical conformation in the IMM as adapted from *S. cerevisiae* (Bender et al., 2015).

Focusing on the outer mitochondrial membrane, the VDAC would be the functional link between the cytosolic pyruvate metabolism and the import of pyruvate to the IMS and then via the MPC machinery to the mitochondrial matrix. Therefore the players of the pyruvate metabolon in the cytosol could be the malic enzyme and the pyruvate carboxylase activities on one hand and the first step of the fermentative pathway on the other, i.e. the pyruvate decarboxylase activity. Interestingly, measurement of $^{14}CO_2$ production in *S. cerevisiae* isolated mitochondria in the presence of pyruvate revealed 20 % of this production being linked to the presence of the cytosolic pyruvate decarboxylase activity. This activity was then attributed to contamination of the mitochondrial fraction by the cytosolic pyruvate decarboxylase although the activity of another cytosolic enzyme (glucose 6-phosphate dehydrogenase) in this fraction was very low (< 5 % of total activity) (Urk et al., 1989).

After the channeling of pyruvate through the VDAC (we do not consider here passive diffusion of pyruvate through the OMM which can take place in cells) to the

IMS side of the MPC machinery, pyruvate can be directed to the pyruvate dehydrogenase complex residing in the mitochondrial matrix, which further links pyruvate metabolism to the respiratory chain and the TCA cycle. Another evidence to take into consideration would be the fact that both the Mpc1p and Mpc2p from *S. cerevisiae* were parts of a 150-kDa complex (Bricker et al., 2012) whereas Mpc1 along with Mpc3 formed a 300-kDa complex (Bender et al., 2015), leaving open the possibility that the yeast MPC machinery harbors additional components. A theoretical dimer comprising the mitochondrial pyruvate carrier complex would have a size of around 30-kDa in *S. cerevisiae* and in *S. pombe*.
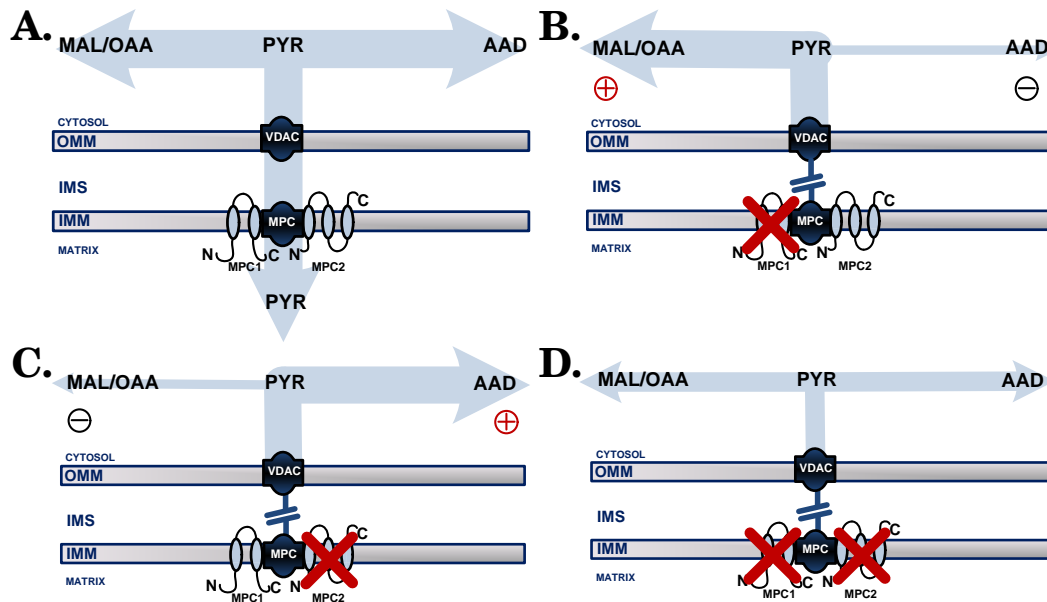


Figure 4.57: Proposed redistribution of the carbon fluxes of the cytosolic metabolism of pyruvate after the introduction of genetic perturbations in the MPC machinery for strain *mpc1∆* [B], strain *mpc2∆* [C] and strain *mpc1∆mpc2∆* [D] in comparison to the wild type strain [A].

More specifically, we have seen that the elimination of the Mpc1p subunit led to pyruvate metabolism being significantly reduced, while $CO_2$ and acetaldehyde did not accumulate to the same extent as in the wild type cells. Figure 4.57.B could pose as an explanation of what happens when the *mpc1* gene is not expressed any more. In this scenario the elimination of the pyruvate transporter activity would lead to accumulation of pyruvate in the cytosol. Pyruvate in the cytosol would be decarboxylated towards oxaloacetate while malic enzyme could replenish the cytosolic pyruvate pools. Recently it has been reported (Orlandi et al., 2014) that loss of the Mpc1p from *S. cerevisiae* cells, caused an increase in the activity of the malic enzyme encoded by *MAE1*. This supports the assumption that a redistribution of fluxes at the pyruvate node could be possibly caused by a perturbation in the activity of the MPC machinery.

The recycling of pyruvate in the cytosol through the anaplerosis would explain why its concentration did not change significantly compared to the wild type. The total malate/oxaloacetate pool could be replenished in a cyclic manner as malate and oxaloacetate are linked at least in the mitochondrial matrix through the malate dehydrogenase activity (Mdh1p) and these two acids can be transported throughout the inner mitochondrial membrane as it has been shown in previous parts. However it is unknown whether a cytosolic malate dehydrogenase exists in the cytosol of *S. pombe* cells.

The scenario of a high flux through the first step of the fermentative pathway seems unlikely. Such an alternative scenario where the PDC would be highly active but acetaldehyde be rapidly consumed by reactions downstream of it (fermentative pathway) was not supported by the experimental results. Firstly, this would be followed by a much more increased $CO_2$ formation even if the malic enzyme activity would be able to replenish the consumed cytosolic pyruvate pools, due to the combined activity of the pyruvate decarboxylase and malic enzyme. Furthermore, acetate was not detected in any samples yielded by selectively permeabilized cells nor was ethanol detected by the MIMS (change in the m/z = 45 or m/z = 46 intensities). Therefore, these findings point towards the fact that acetaldehyde was the end-product of pyruvate decarboxylation in the fermentative pathway and did not further react to form acetate or ethanol.

In the case of permeabilized cells where Mpc2p was eliminated from the MPC machinery, the *in situ* fluxes in the cytosol could have been redirected in the opposite direction compared to the Mpc1p-deficient strain. As illustrated in Figure 4.57.C, pyruvate, instead of accumulating as in the *mpc1*Δ strain, it could be more accessible to the pyruvate decarboxylase enzyme in the cytosol producing through this pathway acetaldehyde and $CO_2$ levels comparable to the wild type cells. Since in Mpc2p-deficient mitochondria, mitochondrial pyruvate uptake is expected to be blocked as in Mpc1p-deficient mitochondria (based on the physiological characterization of strains growing in batch cultures on glucose), the $CO_2$ produced had to originate from a different source since it could not be formed any more by the pyruvate dehydrogenase complex in the mitochondrial matrix. This could only be possible due to a higher $CO_2$ formation (and acetaldehyde formation) compensating for the non-functioning Pdhp because of a higher flux through the Pdcp (see Figure 4.56 for reaction scheme). Thus, the Mpc2p-deficient permeabilized cells, could exhibit $CO_2$ and acetaldehyde formation profiles that were similar (acetaldehyde) or slightly reduced ($CO_2$) compared to the wild type cells as described in previous parts.

The proposed redistribution of the pyruvate flux when the Mpc1p or the Mpc2p subunit was eliminated from *S. pombe* mitochondria, could point towards the mode

of regulation that each subunit exerts on the cytosolic side of the pyruvate metabolon. In principle, each subunit of the MPC machinery could be bound on the mitochondrial side of the VDAC which spans the OMM, in a manner similar as that speculated for the ANT and the VDAC (Brdiczka et al., 2006). Loss of one of the subunits could then lead to weaker binding of enzymes on the cytosolic face of the VDAC, that normally are part of the pyruvate metabolon. This translates to absence of both subunits of the MPC machinery in the double knockout would lead to loss of the MPC-bound regulation of the cytosolic enzymes that are connected to the cytosolic pyruvate node. The mitochondria of the $mpc1\Delta mpc2\Delta$ strain could therefore behave in a more distributed manner exhibiting activities of the fluxes towards pyruvate recycling in one direction and pyruvate decarboxylation towards the formation of acetaldehyde in the other direction, as illustrated in Figure 4.57.D. The combination of the *in situ* results of pyruvate, $CO_2$ and acetaldehyde formation, placed the double knockout strain between the single-knockout strains in terms of at least the activity of the flux towards the Pdcp. The assumption that the MPC machinery and its composition could exert control over the pyruvate utilization is not exotic altogether.

Only recently Bender et al., (Bender et al., 2015), formulated the hypothesis that the MPC machinery may regulate the activity of the cytosolic PDC by swapping its subunits based on the cultivation conditions. More specifically, *S. cerevisiae* cells growing in a glucose medium, possessed a MPC transporter with the Mpc1p and Mpc2p subunits (coined $MPC_{FERM}$) and a low mitochondrial pyruvate uptake capacity. On the other hand, cells growing on non-fermentative media, like glycerol, possessed a MPC machinery with Mpc1p and the Mpc3p (coined $MPC_{OX}$) as its functional subunits, allowing for higher mitochondrial pyruvate uptake and a lower flux through the Pdcp in the cytosol.

In *S. pombe* permeabilized cells, as analyzed in aforementioned parts, based on which subunit was deleted from the MPC machinery, the pyruvate metabolon was altered and the fluxes of pyruvate in the cytosol were redistributed each time. Pyruvate metabolism always varied when comparing selectively permeabilized cells missing either MPC subunit or both. This kind of regulation could signify a connection to the manner of regulation that the yeast MPC machinery possesses over the fermentative pathway and oxidation of pyruvate in the mitochondria as described previously. However the *S. pombe* MPC machinery tends to differ from its yeast counterpart. We have identified two genes (*mpc1*, *mpc2*) that express the functional subunits of the MPC machinery, whereas in *S. cerevisiae* three genes (*MPC1*, *MPC2*, *MPC3*) express functional parts of the transporter. In this regard the *S. pombe* MPC machinery is similar to the one of higher eukaryotes (human, *D. melanogaster*, *Trypanosoma brucei*) (Bricker et al., 2012; Štáfková et al., 2016) which also entails two

subunits, expressed by two genes (MPC1, MPC2). This attribute could however stem from the fact that the *S. pombe* genome is more conserved than that of *S. cerevisiae* since their divergence from their common ancestor (Hoffman et al., 2015), thus retaining mechanisms that are conserved in higher eukaryotes.

Interestingly, in cancer cells the most common deletion is that of the MPC1 locus with the MPC2 gene being more inconsistent (either overexpressed or deleted) (Schell et al., 2014a), adding along with other systematic changes to the poor oxidation of pyruvate in the mitochondria and its reduction towards lactate in the cytosol (Warburg effect). For example, the expression of the MPC1 gene in prostate cancer patients was found to be repressed leading towards a higher glycolytic activity in tumor cells, tumor growth and metastasis (Wang et al., 2016). Therefore the degree of regulation that the mitochondrial import of pyruvate exerts on neighbouring pathways can reveal the dynamic communication between the oxidative phosphorylation and cytosolic enzymatic activities and bring forth the evolutionary link that exists between the Warburg effect in mammalian cells and the Crabtree effect in yeast (Diaz-Ruiz et al., 2011; Vanderperre et al., 2015).

#### 4.3.5.5 Uptake of oxygen by wild type and pyruvate transporter-deficient mitochondria in the presence of pyruvate

The uptake of oxygen was monitored continuously in a sealed mini-reactor at 30 °C, in the presence of pyruvate, malate, NADH and ADP and compared between all strains. Based on the division of acetaldehyde formation in phase I and phase II (with phase I being indicative of an acetaldehyde lag phase with a duration of 2 minutes) the same time division was applied into oxygen kinetics.

As illustrated in Figure 4.58, the left column of the subfigures covers the first phase of oxygen uptake in the sealed reactor (phase I) and the right column the rest of each experiment's duration (phase II). With Figure 4.58.A & B for the selectively permeabilized wild type cells it is exhibited that oxygen uptake rates in the aforementioned phases differed from each other, just like acetaldehyde and $CO_2$ kinetics for the wild type. More specifically the initial rate of oxygen uptake in phase I (first 2 min) was reduced subsequently by 40 % in phase II (in mM/min). Therefore, oxygen uptake during the first two minutes coincided with the maximum oxygen uptake rate for the selectively permeabilized wild type cells incubated in the aforementioned substrates.

However this kind of transition from a higher to a lower respiration rate was not shared among the mitochondria of the MPC-deficient mutant strains. Instead all mutant strains possessed similar respiration rates to each other which were during phase I lower than that of the wild type permeabilized cells (see Table 4.14 for specific uptake rates). Additionally, the difference between the oxygen uptake

between phases I and II for all mutants was minimal. The presence of NADH in the reaction mix failed to rescue the respiration rate from being reduced due to the inability of the mitochondria to transport pyruvate. This finding points towards a more systematic effect of the MPC subunits on elements of the respiratory chain as well, influencing electron transport and subsequently oxygen uptake.

Apparently, the introduction of a non functioning MPC machinery in all mutants, caused a similar and reproducible drop in the respiration rate, regardless of which subunit(s) was absent from the MPC. Interestingly, the differences that the strains possessed with each other in terms of acetaldehyde and $CO_2$ formation did not seem to be reflected on their oxygen uptake profiles as well.

Our results are supported by similar findings concerning respiring *S. cerevisiae* whole cells. More specifically, loss of the Mpc1p protein in *S. cerevisiae* caused a decrease in respiration (Orlandi et al., 2014) during growth on a fermentable carbon source (glucose). The rate of oxygen consumption was also decreased in whole *S. cerevisiae* cells growing on a non-fermentable carbon source (glycerol) when either *MPC1*, *MPC3* or both of them were not expressed (Timón-Gómez et al., 2013), as predicted by the finding that subunits Mpc1p and Mpc3p form a functional pyruvate import machinery ($MPC_{OX}$) during growth on glycerol (Bender et al., 2015).
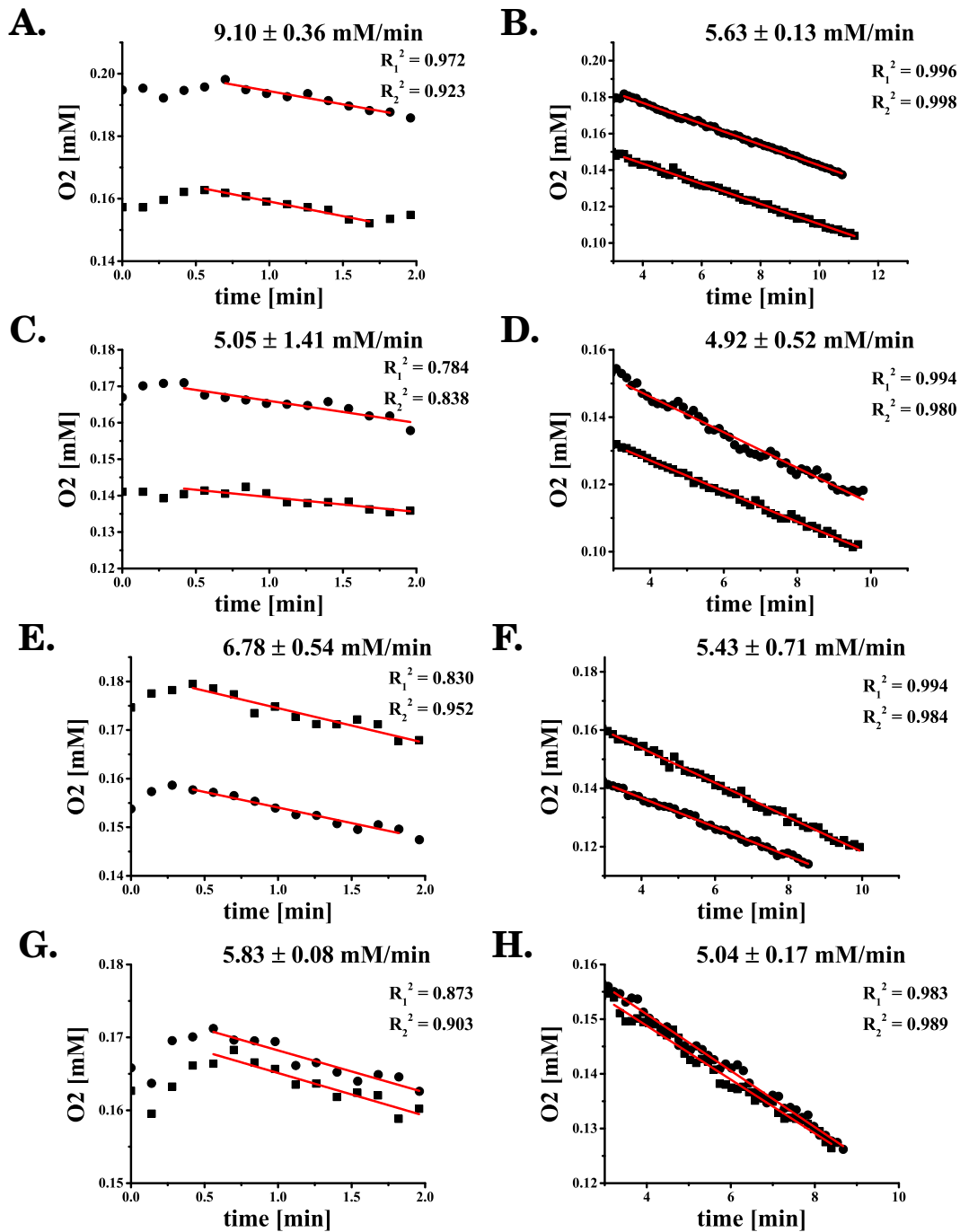
Figure 4.58: Uptake of oxygen over time for experiments performed in the closed system at 30 °C . Figures [A]-[B] representative of the wild type, Figures [C]-[D] of the *mpc1Δ* strain, Figures [E]-[F] of the *mpc2Δ* strain and Figures [G]-[H] of the *mpc1Δmpc2Δ* strain. Conditions summarized in Figure 4.48. Red line indicates each curve of the regression analysis along with the $R^2$.

Table 4.14: A comparison between the specific $O_2$ uptake rate ($q_{O_2}$) for all digitonin-permeabilized strains in the presence of pyruvate, malate, NADH and ADP in the sealed reactor. These are mean values along with their standard deviations from two experiments conducted with cells yielded from parallel cultivations.

| $q_{O_2}$ [nmol/(mg CDW×min)] | CBS 356 (WT) | *mpc1Δ* | *mpc2Δ* | *mpc1Δmpc2Δ* |
|---|---|---|---|---|
| Phase I | 5.7 ± 1.4 | 3.7 ± 1.2 | 3.5 ± 0.3 | 3.9 ± 0.0 |
| Phase II | 3.6 ± 0.5 | 3.6 ± 0.6 | 2.8 ± 0.4 | 3.4 ± 0.1 |

#### 4.3.5.6  Redox metabolomics in selectively permeabilized *S. pombe* mutant cells

The kinetics of NADH and NAD were compared between selectively permeabilized wild type cells and mutant cells (*mpc1Δ, mpc2Δ, mpc1Δmpc2Δ*). When digitonin-permeabilized cells are incubated in the presence of pyruvate, malate and ADP, NADH not only fuels the respiratory chain with electrons but along with NAD are involved in various other reactions as well. More specifically they are substrates for the malic enzyme and pyruvate carboxylase in the cytosol and the pyruvate dehydrogenase complex in the mitochondrial matrix (see Figure 4.56).

In wild type permeabilized cells both redox precursors were initially metabolized at a constant rate and eventually reached a phase, where NADH was completely eliminated from the reactor environment and NAD leveled off (Figures 4.59.A & B). Based on the linear relationship between time and the concentration of the precursors, where NADH was consumed and NAD accumulated, the specific elimination and formation rates respectively were calculated for the wild type and for the rest of the mutant strains (see Table 4.15). In wild type cells the fate of NADH was expected to be as follows. NADH could be oxidized by the NADH dehydrogenases that are docked on the IMM, as was described in aforementioned parts. However it is unknown whether both an IMM-facing and a mitochondrial matrix-facing dehydrogenase exist in *S. pombe* like in *S. cerevisiae*. What is certain however is that in such a case the external NADH dehydrogenase would be at all times activated in the presence of exogenous NADH. The mitochondrial NAD transporter (YEA6) could furthermore facilitate the transfer of NAD from the IMS to the mitochondrial matrix. Simultaneously, newly formed NAD could be reduced to NADH in the cytosol by the malic enzyme activity and in the mitochondrial matrix by the pyruvate dehydrogenase complex activity.
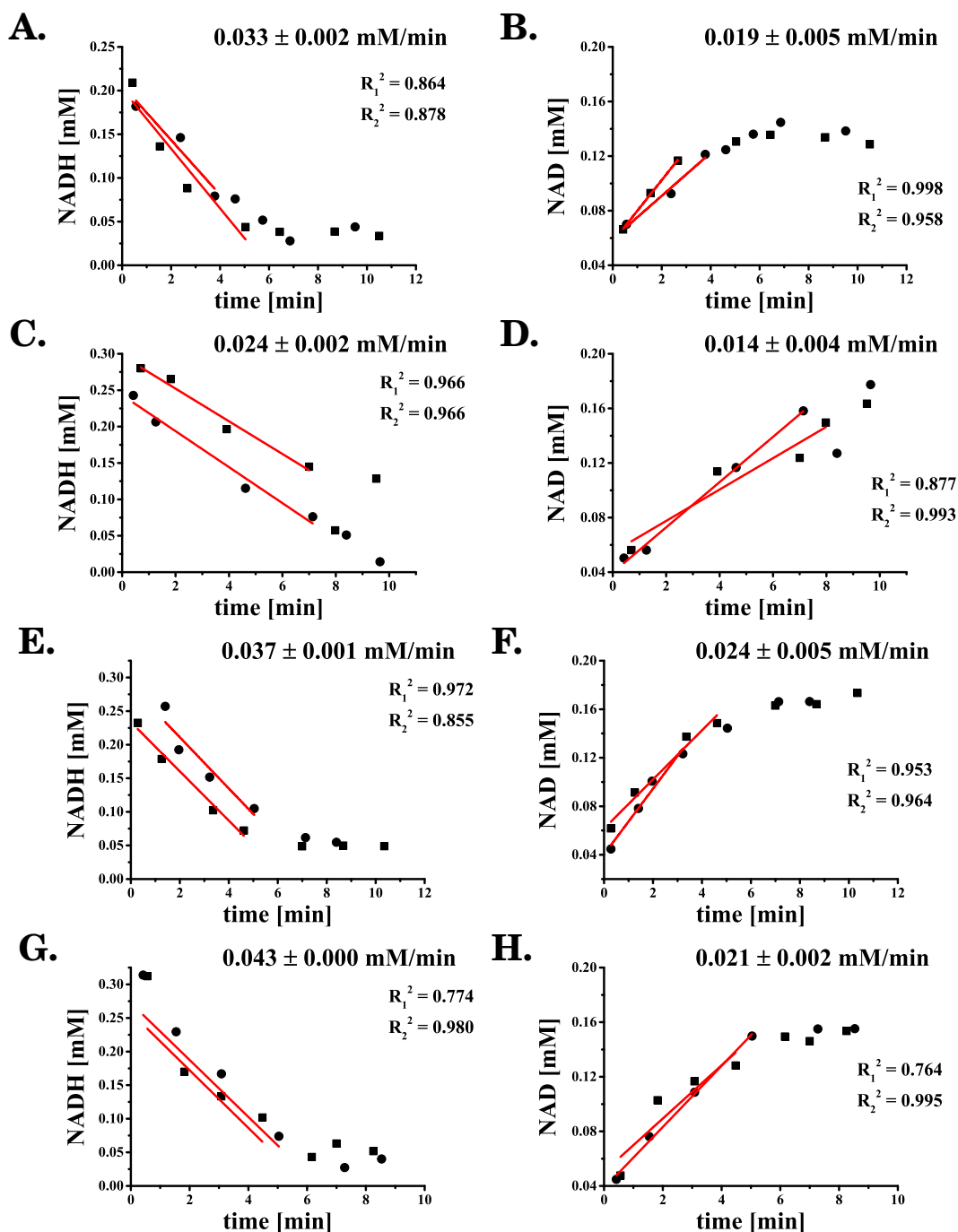
Figure 4.59: Elimination of NADH and formation of NAD over time for experiments performed in the closed system at 30 °C . Figures [A]-[B] refer to the wild type digitonin-permeabilized cells, Figures [C]-[D] to cells from the *mpc1Δ* strain, Figures [E]-[F] to cells from the *mpc2Δ* strain and Figures [E]-[F] to cells from *mpc1Δmpc2Δ* strain. Conditions summarized in Figure 4.48. Red line indicates each curve of the regression analysis along with the $R^2$.

**A.** 7.07 ± 2.54 mol/mol

$R_1^2 = 0.963$
$R_2^2 = 0.971$

**B.** 2.61 ± 0.75 mol/mol

$R_1^2 = 0.833$
$R_2^2 = 0.941$

**C.** 4.29 ± 0.37 mol/mol

$R_1^2 = 0.946$
$R_2^2 = 0.943$

**D.** 2.46 ± 0.33 mol/mol

$R_1^2 = 0.861$
$R_2^2 = 0.885$

**E.** 5.29 ± 0.30 mol/mol

$R_1^2 = 0.983$
$R_2^2 = 0.995$

**F.** 3.77 ± 1.03 mol/mol

$R_1^2 = 0.968$
$R_2^2 = 0.983$

**G.** 6.78 ± 1.63 mol/mol

$R_1^2 = 0.982$
$R_2^2 = 0.999$

**H.** 4.08 ± 0.07 mol/mol

$R_1^2 = 0.810$
$R_2^2 = 0.991$

Figure 4.60: Relationship between NADH and NAD relative to mitochondrial oxygen consumption. Figures [A]-[B] refer to the wild type digitonin-permeabilized cells, Figures [C]-[D] to cells from the *mpc1Δ* strain, Figures [E]-[F] to cells from the *mpc2Δ* strain and Figures [E]-[F] to cells from *mpc1Δmpc2Δ* strain. Conditions summarized in Figure 4.48. Red line indicates each curve of the regression analysis along with the $R^2$.

201

Table 4.15: A comparison between the specific elimination ($q_{NADH}$) and formation ($q_{NAD}$) rate for NADH and NAD respectively for all digitonin-permeabilized strains in the presence of pyruvate, malate, NADH and ADP in the sealed reactor. These are mean values along with their standard deviations from two experiments conducted with cells yielded from parallel cultivations.

| specific rate [nmol/(mg CDW×min)] | CBS 356 (WT) | *mpc1Δ* | *mpc2Δ* | *mpc1Δmpc2Δ* |
|---|---|---|---|---|
| $q_{NADH}$ | 21.0 ± 4.9 | 17.2 ± 2.0 | 19.2 ± 0.4 | 28.5 ± 0.4 |
| $q_{NAD}$ | 12.5 ± 5.2 | 10.3 ± 3.1 | 12.2 ± 2.4 | 14.0 ± 1.5 |

Table 4.16: A comparison between the molar yield for NADH ($Y_{NADH/O_2}$) and NAD ($Y_{NAD/O_2}$) respectively on oxygen for all digitonin-permeabilized strains in the presence of pyruvate, malate, NADH and ADP in the sealed reactor. These are mean values along with their standard deviations from two experiments conducted with cells yielded from parallel cultivations.

| molar yield [mol/mol] | CBS 356 (WT) | *mpc1Δ* | *mpc2Δ* | *mpc1Δmpc2Δ* |
|---|---|---|---|---|
| $Y_{NADH/O_2}$ | 6.30 ± 2.43 | 5.08 ± 0.44 | 5.29 ± 0.30 | 6.78 ± 1.63 |
| $Y_{NAD/O_2}$ | 2.61 ± 0.75 | 2.46 ± 0.33 | 3.77 ± 1.03 | 4.08 ± 0.07 |

The specific NAD formation rate ($q_{NAD}$) was almost identical for all strains examined, as well as the specific NADH elimination rate ($q_{NADH}$), which was slightly higher for the double knockout strain (see Table 4.15). However, the ratio of the two rates ($q_{NADH}/q_{NAD}$) was always higher than unity, indicating that the two redox precursors were not in balance under these conditions. These pointed towards a possible degradation of NADH during sampling for all cases, since it was eliminated with a faster rate than the rate with which NAD was formed.

As the 1:1 stoichiometry was reached between NADH and NAD when NADH was either exogenously supplied or generated *in situ* but not during the mitochondrial oxidation of pyruvate and malate, the activation of NAD(H) kinases (consumption of NAD(H) towards NADP formation) (Miyagi et al., 2009) that exist in the cytosol and in mitochondria was excluded. Also yeast cells in general do not possess NADH transhydrogenases (Rydström, 2006).

In Figure 4.60 the concentration of both redox precursors was plotted against the oxygen concentration measured in the mini-reactor and summarized for all strains under examination. What can be further noted from these results is that in all cases, NADH and oxygen were consumed simultaneously until the point where NADH and subsequently NAD entered a stationary phase uncoupled from oxygen consumption. This behavior was not shared by the *mpc1Δ* strain, where the more robust regeneration of NADH in the cytosol through the activities of pyruvate carboxylase and malic enzyme maintained a near linear relationship to oxygen consumption for the whole of the duration of an experiment. The yields for NADH and NAD on oxygen (see Table 4.16) did not reveal any major difference between the mutant strains and the wild type.

### 4.3.5.7   Adenosine nucleotides in selectively permeabilized *S. pombe* mutant cells

So far we have shown the systemic effects that have been caused by the deletion of either or both genes expressing functional subunits of the putative *S. pombe* mitochondrial pyruvate carrier. These effects could be summarized as a redistribution of fluxes at the pyruvate node in the cytosol and the reduction of the mitochondrial oxygen consumption even if an adequate concentration of NADH was readily present to be oxidized. The first part of the aforementioned effects could be explained by comparing pyruvate metabolism, $CO_2$ and acetaldehyde formation between the permeabilized cells of the wild type and the mutant strains.

In this part, the dynamic quantification of adenosine nucleotide attempts to shed more light on the oxidative phosphorylation efficiency, the transport of adenosine nucleotides throughout mitochondria and their metabolism in the cytosol when mitochondrial pyruvate import was expected to be inactive (MPC-deficient mutants).

Figure 4.61: AMP formation over time for experiments performed in the closed system at 30 °C . Subfigure [A] refers to the wild type digitonin-permeabilized cells, Subfigure [B] to cells from the *mpc1Δ* strain, Subfigure [C] to cells from the *mpc2Δ* strain and Subfigure [D] to cells from *mpc1Δmpc2Δ* strain. Conditions summarized in Figure 4.48. Red line indicates each curve of the regression analysis along with the $R^2$.
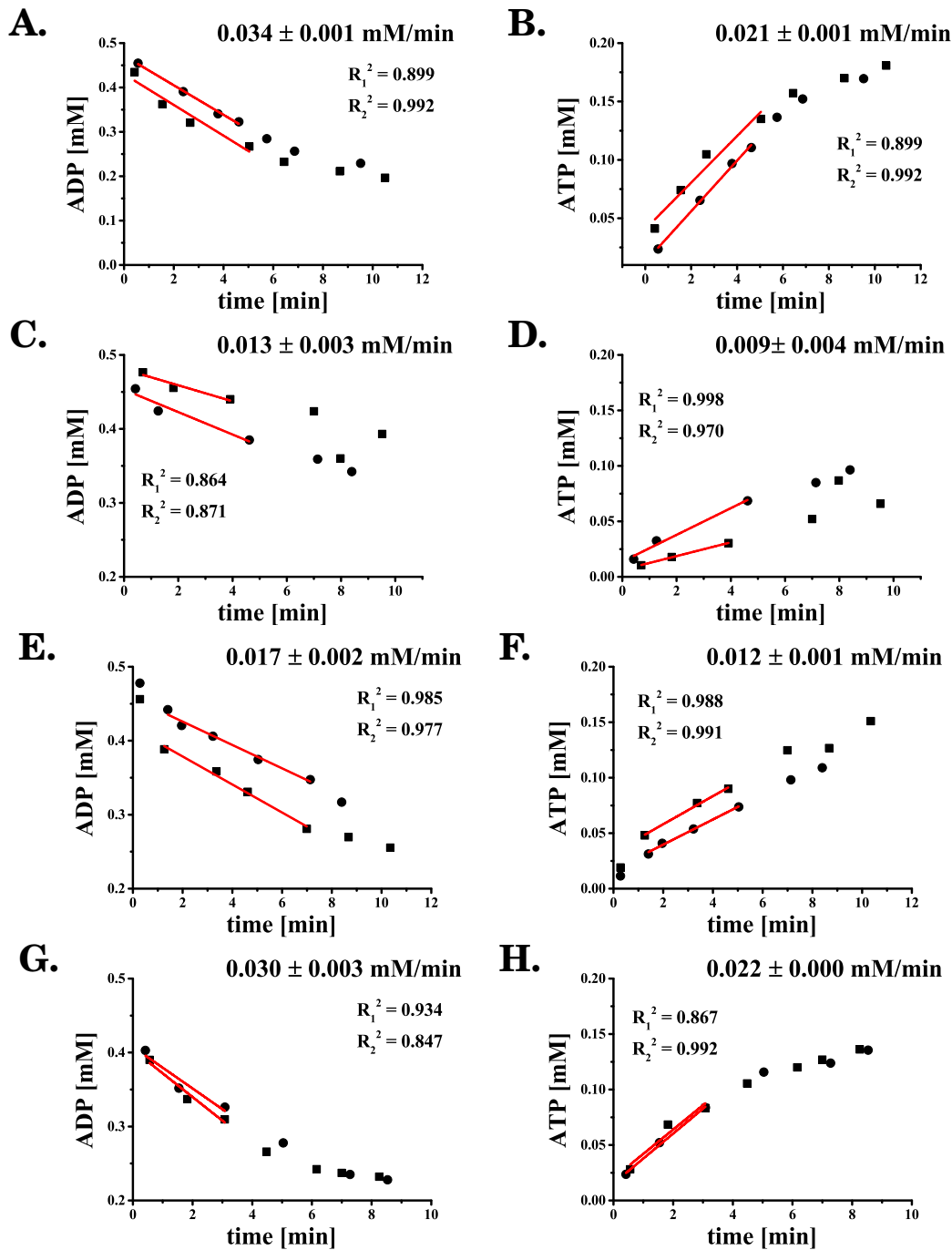
Figure 4.62: ADP elimination and ATP formation over time for experiments performed in the closed system at 30 °C . Subfigures [A]-[B] refer to the wild type digitonin-permeabilized cells, Subfigures [C]-[D] to cells from the *mpc1*Δ strain, Subfigures [E]-[F] to cells from the *mpc2*Δ strain and Subigures [E]-[F] to cells from *mpc1*Δ*mpc2*Δ strain. Conditions summarized in Figure 4.48. Red line indicates each curve of the regression analysis along with the $R^2$.
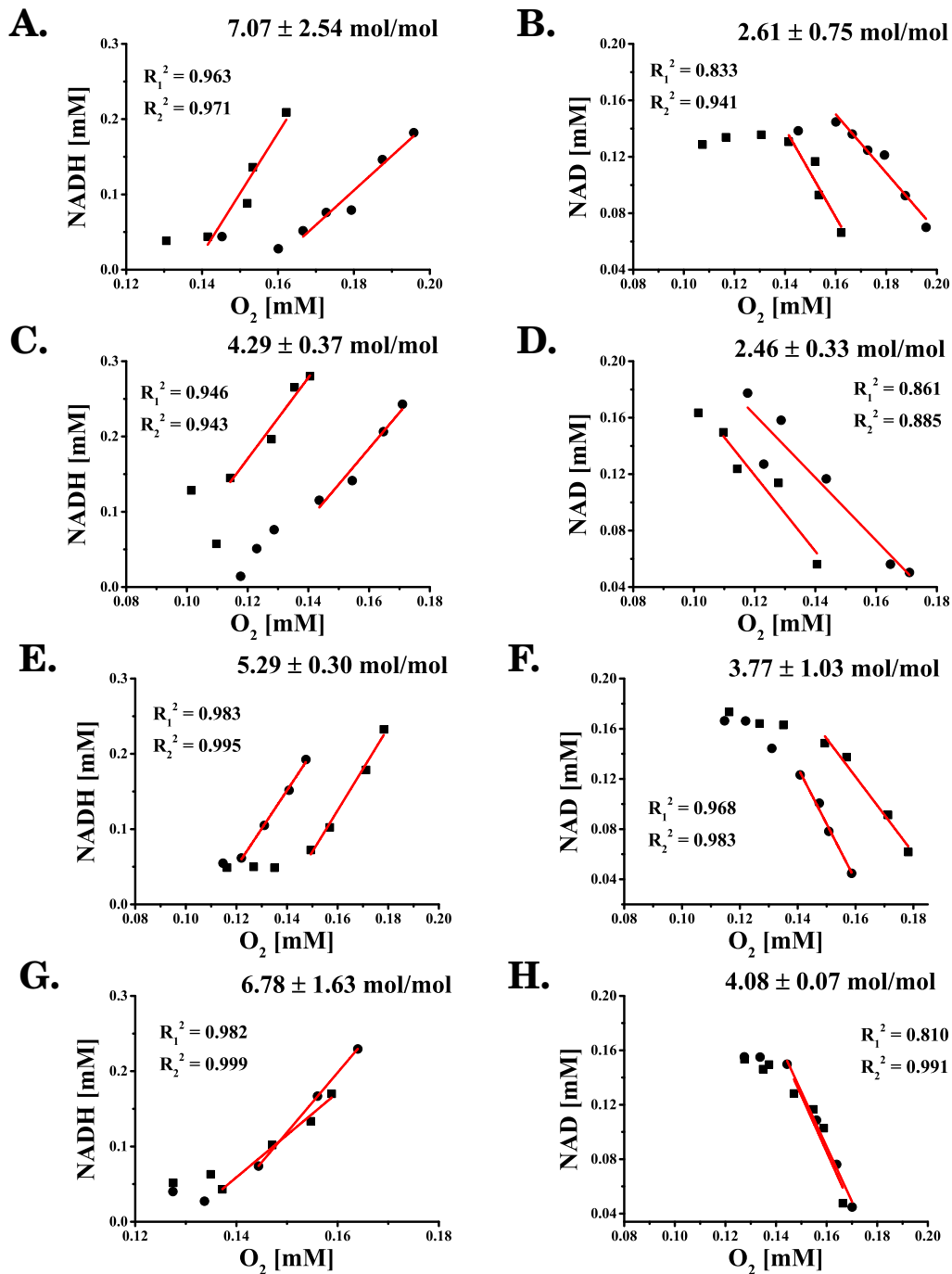
**A.** 1.06 ± 0.02 mol/mol — $R_1^2 = 0.99$, $R_2^2 = 0.99$

**B.** 0.94 ± 0.06 mol/mol — $R_1^2 = 0.97$, $R_2^2 = 0.99$

**C.** 0.93 ± 0.05 mol/mol — $R_1^2 = 0.93$, $R_2^2 = 0.97$

**D.** 0.98 ± 0.01 mol/mol — $R_1^2 = 0.97$, $R_2^2 = 0.91$

Figure 4.63: ATP formation over time for experiments performed in the closed system at 30 °C . Subfigure [A] refers to the wild type digitonin-permeabilized cells, Subfigure [B] to cells from the *mpc1Δ* strain, Subfigure [C] to cells from the *mpc2Δ* strain and Subigure [D] to cells from *mpc1Δmpc2Δ* strain. Conditions summarized in Figure 4.48. Red line indicates each curve of the regression analysis along with the $R^2$.

Table 4.17: A comparison between the specific elimination rate for ADP ($q_{ADP}$) and the specific formation rates for AMP ($q_{AMP}$) and ATP (($q_{ATP}$)) for all digitonin-permeabilized strains in the presence of pyruvate, malate, NADH and ADP in the sealed reactor. These are mean values along with their standard deviations from two experiments conducted with cells yielded from parallel cultivations.

| specific rate [nmol/(mg CDW×min)] | CBS 356 (WT) | *mpc1Δ* | *mpc2Δ* | *mpc1Δmpc2Δ* |
|---|---|---|---|---|
| $q_{ADP}$ | 21.7 ± 4.4 | 9.5 ± 2.7 | 8.9 ± 1.2 | 20.1 ± 1.7 |
| $q_{AMP}$ | 6.9 ± 0.3 | 2.3 ± 0.9 | 2.6 ± 0.3 | 8.1 ± 0.6 |
| $q_{ATP}$ | 13.2 ± 1.5 | 6.7 ± 3.3 | 6.2 ± 0.5 | 14.9 ± 0.3 |

Both adenosine nucleotides, ADP and ATP (Figures 4.62.A & B respectively), exhibited kinetic profiles similar to those when NADH (exogenous or formed *in situ*) and succinate were oxidized, as shown in previous parts. In selectively permeabilized wild type cells, the initial concentration of ADP (0.5 mM) was consumed lin-

early and then its elimination was significantly reduced (initial rate of elimination slowing down). The ADP elimination rate was calculated by the initial linear curve as illustrated Figure 4.62.A for wild type permeabilized cells. Initially the wild type permeabilized cells, continuously synthesized ATP while its formation rate levelled off during the end phase of a typical experiment (Figure 4.62.B). As postulated in 4.1.2, the reduction in the ATP formation rate could possibly be attributed to apyrases and ATPases hydrolysing ATP in the cytosol, similar for example to the *S. cerevisiae* E-type ATPases (Zhong and Guidotti, 1999) or others. A result of the activity of such ATPases is the formation of AMP as illustrated in Figure 4.61.

The formation of AMP was exclusively linked to the formation of ATP as was mentioned before and the adenylate kinase activity was inhibited with the addition of Ap5A. Furthermore when the concentration of newly synthesized ATP was plotted versus the sum of the concentration of ADP and newly formed AMP, the ratio of [ATP]/([ADP] + [AMP]) was close to unity, as calculated graphically for all strains (Figure 4.63.A-D).

In *mpc1Δ* permeabilized cells the ADP elimination rate was reduced by 57 % compared to the wild type with the specific ATP formation rate showing a similar decline by 49.2 % as well (see Table 4.17 for specific rates). Also the form of both curves changed and did not resemble anymore the hyperbolic curves typical for the wild type cells (Figures 4.62.C & D for ADP and ATP respectively). The specific rates of ADP elimination and ATP accumulation for strain *mpc2Δ* (Figures 4.62.E & F for ADP and ATP respectively) were reduced by 59 % and 53 % respectively compared to the wild type cells, approximating the degree of reduction found for strain *mpc1Δ* (see Table 4.17 for specific rates). Surprisingly the double knockout strain *mpc1Δmpc2Δ* (Figures 4.62.G & H for ADP and ATP respectively) did not exhibit a significant decrease of its specific ADP elimination and ATP accumulation rates compared to the wild type.

Based on these results, an apparent interpretation would be that permeabilized cells possessing single-gene deletions (*mpc1Δ* and *mpc2Δ*) had a reduced capacity to exchange cytosolic ADP for mitochondrial ATP on one hand and synthesize ATP in the mitochondrial matrix on the other, whereas the double knockout behaved similarly to the wild type mitochondria. However explaining the metabolism of ADP and ATP in this case could not be as straightforward due to the fact that ATP could be consumed in the cytosol by the activity of the pyruvate carboxylase and yield ADP (see Figure 4.56).
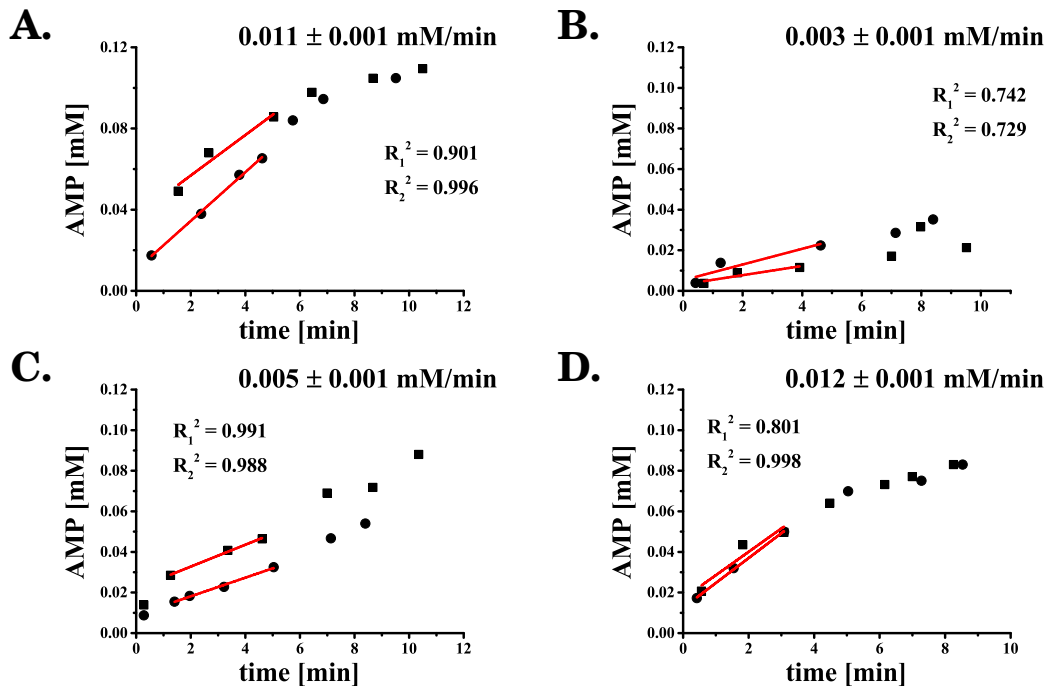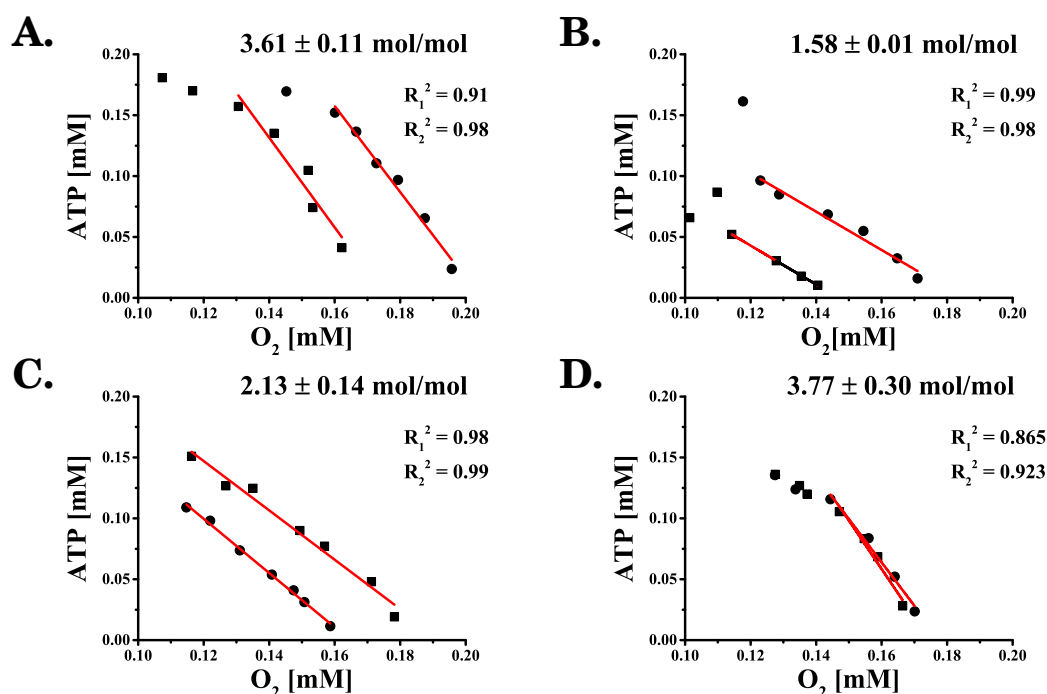
Figure 4.64: Yield of ATP on oxygen for experiments performed in the closed system at 30 °C . Subfigure [A] refers to the wild type digitonin-permeabilized cells, Subfigure [B] to cells from the *mpc1Δ* strain, Subfigure [C] to cells from the *mpc2Δ* strain and Subigure [D] to cells from *mpc1Δmpc2Δ* strain. Conditions summarized in Figure 4.48. Red line indicates each curve of the regression analysis along with the $R^2$.

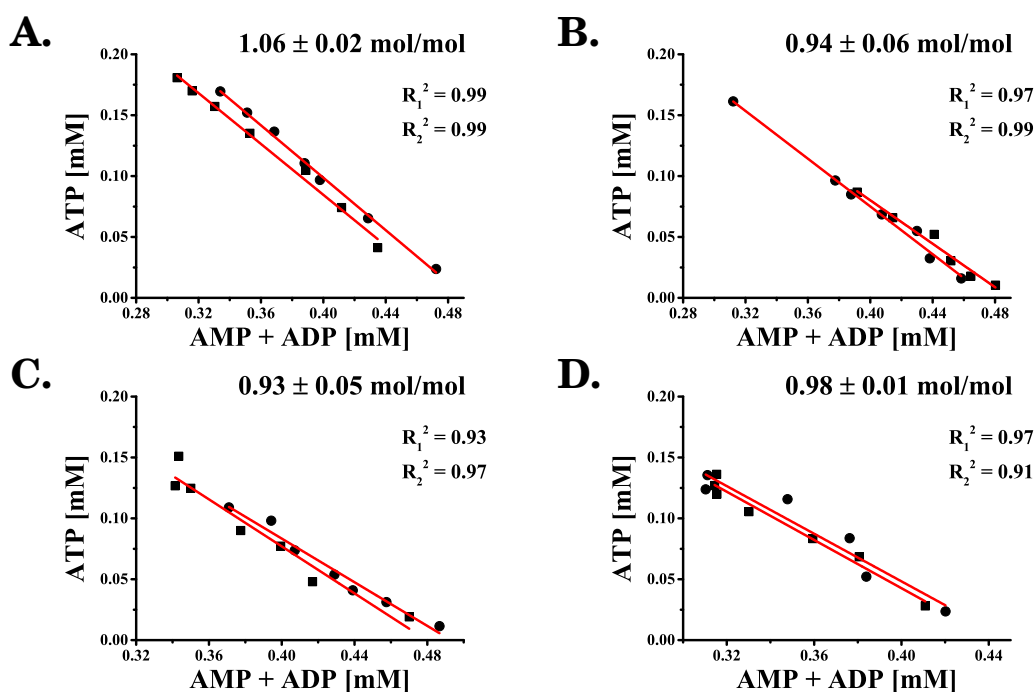Table 4.18: A comparison between the P/O ratio for all digitonin-permeabilized strains in the presence of pyruvate, malate, NADH and ADP in the sealed reactor. These are mean values along with their standard deviations from two experiments conducted with cells yielded from parallel cultivations.

|  | CBS 356 (WT) | *mpc1Δ* | *mpc2Δ* | *mpc1Δmpc2Δ* |
|---|---|---|---|---|
| P/O | 1.80 ± 0.05 | 0.79 ± 0.00 | 1.06 ± 0.07 | 1.89 ± 0.15 |

It has been postulated that carbon was recycled at some extent from cytosolic pyruvate towards the malate/oxaloacetate pool and back to pyruvate, throughout the various selectively permeabilized strains that were examined. Furthermore our findings suggest that the *mpc1Δ* possessed a higher flux through this cycle compared to the wild type and the other strains and this could partially explain the $P/O_{mpc1\Delta}$ ratio with a value of 0.79 ± 0.00 (see Table 4.18) being significantly lower (by 56 %) than the $P/O_{WT}$ ratio (P/O ratio calculated for each strain from ATP/$O_2$

ratio (in mol/mol) of Figure 4.64 and then divided by two: P/O = (ATP/O$_2$)/2). Therefore the decrease in mitochondrial respiration for strain *mpc1$\Delta$* was accompanied by a decrease in the activity of the mitochondrial ATP synthase and an increase of the flux through the ATP-consuming pyruvate carboxylase activity. This further decreased the ratio of ATP formed to O$_2$ consumed. It was also hypothesized that the substrate cycle from pyruvate to the malate/oxaloacetate pool and back in permeabilized cells of strain *mpc2$\Delta$* had an activity that was comparable to the wild type and the double knockout strain. The P/O$_{mpc2\Delta}$ ratio however was reduced by 41 % compared to the P/O$_{WT}$ ratio (Figures 4.64.A & C for the wild type and for strain *mpc2$\Delta$*, calculated P/O ratios in Table 4.18).

At the same time the permeabilized cells of the double knockout strain had an unchanged ratio of ATP formation to oxygen consumed compared to the wild type (Figures 4.64.A & D for the wild type and strain *mpc1$\Delta$mpc2$\Delta$* respectively) with both P/O ratios almost identical. We would have expected that the *mpc1$\Delta$mpc2$\Delta$* and *mpc2$\Delta$* would have similar P/O ratios due to the activity of the ATP-consuming pyruvate carboxylase in the cytosol, which would consume more ATP in the *mpc1$\Delta$* strain (justifying the low P/O ratio) than in the other two mutant strains. Therefore, the cytosolic pyruvate carboxylase could not be the sole contributor to the low P/O ratio observed.

An interpretation of this would be that additionally to the redistribution of pyruvate fluxes in the cytosol, the absence of only one of the mitochondrial pyruvate carrier subunits each time had an effect on the efficiency of the respiratory chain to transport electrons and led to a dysfunction in mitochondrial ATP formation (mitochondrial ATP synthase) as well.

The first part pointing towards an inefficient or dysfunctional electron transport chain could be substantiated by the decrease in oxygen uptake in all mitochondrial preparations of the mutant cells. The second part, that of a dysfunctional ATP synthase (evident by a low P/O regardless of inferred pyruvate carboxylase activity in the cytosol) but only in the case of single mutants could be explained in terms of the components of the MPC being part of a larger metabolon connected with the function of the ATP synthase. Such a hypothetical metabolon spanning the outer and inner mitochondrial membranes and connecting functionally the cytosol to the mitochondrial matrix and vice versa would have in its core the mitochondrial pyruvate carrier. Based on our results, we hypothesize that eliminating either one of the MPC subunits caused a change in the structure of the metabolon mainly affecting the functionality of the ATP synthase that is bound on the matrix side of the IMM. Once both subunits were not present in the metabolon, this kind of down-regulation due to conformational changes of the metabolon would be completely alleviated thus ensuring once more the proper functioning of the ATP synthase and

the generation of a P/O ratio identical to wild type mitochondria, even when the oxygen uptake was reduced.

These results further strengthen the proposed hypothesis that the MPC machinery is part of a larger transmembrane metabolon with the VDAC, the ANT and the ATP synthase being also functionally connected to each other. As such, the MPC could regulate the activity not only of cytosolic enzymes as it was shown in this work, but also of those residing in the mitochondrial matrix such as the ATP synthase. The MPC therefore could not only be a link of glycolysis to the TCA cycle but a component of a more extended metabolon functionally linking mitochondrial import to the oxidative phosphorylation mechanism. Combining this with the apparent influence that the MPC machinery exerts on the first step of the fermentative pathway, further places the MPC metabolon in a central position as a regulator of the Crabtree effect.

# Chapter 5

# Conclusions and Outlook

This work focused on establishing a novel method to analyse *in situ* functional mitochondria in *S. pombe* cells, by quantifying a plethora of parameters that are not assessed by traditional approaches. This method also aimed towards elucidating the role of mitochondrial transporters docked either on the outer or the inner mitochondrial membrane while taking into account the compartmentalized enzymatic make-up of the cell which would be activated in either side of these membranes in the presence of specific substrates. The strength of this approach lied on the fact that the internal cellular architecture was preserved intact and it could be established which systemic interactions took place at the cytosol-mitochondria interface.

The aforementioned parameters that were quantitatively assessed included $O_2$ generated at the mitochondrial respiratory chain, ATP which was formed by the ATP synthase and exchanged for cytosolic ADP by the adenine nucleotide translocator, redox precursors (NAD/NADH) fuelling dehydrogenases and finally carboxylic acids entering mitochondria (pyruvate, succinate) and their metabolic products (fumarate, malate, acetaldehyde, $CO_2$) either formed in the cytosol or in the mitochondrial matrix.

The foundation for setting up the aforementioned experimental methodology was based on achieving selective permeabilization of the plasma membrane of *S. pombe* cells with digitonin as the permeabilizing agent and maintaining functional and intact mitochondria in an appropriate synthetic, cytosol-mimicking buffer. The qualitative controls that were applied included the establishment of the respiratory control ratio (RCR) as an indicator of mitochondrial respiratory functionality during ADP-activated conditions and providing proof for the outer mitochondrial membrane integrity in the presence of externally supplied cytochrome *c*.

A proof of principle was implemented by externally supplying succinate to selectively permeabilized cells suspended either in a sealed, miniaturized reactor system or in a unsealed, unbaffled shake flask, with continuous quantification of $O_2$ in both systems. The successfully respiring mitochondria exhibited excellent coupling of

energy to respiration as pointed out by the high RCR values whereas it was established that both the ATP-forming ATP synthase and the mitochondrial antiporter for ATP and ADP (ANT) were simultaneously operating. It could be inferred for both the closed and the open system, that ATP-utilizing enzymatic activities outside of the mitochondria could be present in the cytosol of selectively permeabilized cells, such as ATPases and apyrases that would participate in a substrate cycle along with the ATP synthase.

The presence of such a cycle provided a solid explanation for the ADP and ATP pools levelling off after the initial continuous net elimination and formation phases respectively. The effect of competing enzymatic activities for ATP and ADP that were localized in the cytosol of selectively permeabilized cells, were reflected as a drop in the experimentally inferred P/O ratio for both the open and the closed system compared to the theoretical mechanistic ratio during succinate oxidation. As such, we could identify a possible caveat concerning the study of the mitochondrial activity of selectively permeabilizing cells when focusing on the P/O ratio accompanied by ADP not being completely exhausted and AMP being formed following the hydrolysis of ATP in the cytosol. The presence of AMP was made apparent in the open system and was marked as a difference compared to the closed system. Other differences between the closed and the open system related to the absolute rates of mitochondrial respiration and ADP and ATP net elimination and formation rates. The most probable cause that could generate such differences would be the continuous supply of exogenous $O_2$ in the open system compared to a limiting concentration of exogenous $O_2$ in the closed system. Therefore an interesting question arises concerning the effect of not only the concentration of oxygen on the mitochondrial respiratory chain but also whether a continuous supply of oxygen can maximize the efficiency of electron transport and of the ATP synthase.

Nevertheless, we were able to activate part of the TCA cycle during ADP-driven succinate oxidation with the subsequent synthesis of fumarate and exhibit that at least one mitochondrial carrier for succinate was active and potentially an additional one for fumarate and/or malate during this process. Even if the sequence analysis points out that *S. pombe* mitochondria lack a dicarboxylate carrier protein or a succinate-fumarate antiporter, we can confirm that a mechanism exists that actively transports succinate into the mitochondrial matrix and can be inhibited by phenylsuccinate. It is currently not possible to conclude whether such a transporter would be responsible for the transport of other dicarboxylates as well. Further studies remain to be performed in order to identify the gene expressing such a carrier in *S. pombe* and elucidate whether more transporters or antiporters are active during mitochondrial succinate uptake. In such a case it would also be of interest to discern the reason why *S. pombe* possesses a non-homologous mechanism to its

mammalian and yeast counterparts concerning transport-mediated succinate mitochondrial metabolism and whether this is connected to the evolutionary history of the fission yeast.

In the second part of this work, selectively permeabilized *S. pombe* cells were used to illustrate how the passage of exogenously supplied NADH is limited at the outer mitochondrial membrane and more specifically during its transport mediated by the voltage-dependant annion carrier (VDAC). *S. pombe* mutant cells containing a deletion for the gene sequence (*por1Δ*) inferred to be encoding for the VDAC were used to examine whether VDAC played any role in the mitochondrial oxidation of NADH when the latter was synthesized *in situ* by the cytosolic glyceraldehyde 3-phosphate dehydrogenase. Selectively permeabilized cells harboring the *por1* gene deletion exhibited a highly reduced mitochondrial respiration rate when compared to wild type mitochondria during ADP-driven respiration. Furthermore, the *por1Δ* mutant cells did not rapidly oxidize the newly synthesized NADH which accumulated in the cytosol instead of passing through the OMM to its site of oxidation in the mitochondrial intermembrane space (IMS) where the external mitochondrial NADH dehydrogenase resides.

These findings place the *S. pombe* Por1p at a central place in two functional areas. The first one has to do with the passage of large metabolites, such as the NADH, through the first barrier separating the cytosol from the mitochondrial matrix, namely the OMM. The second one implicates this protein to function in tandem with cytosolically-localized enzymes where metabolites central for the mitochondrial metabolism, such as NADH, are synthesized. This degree of cooperativity between elements of the mitochondrial membrane and the cytosol shows the high importance of metabolite channeling and its central position in energy homeostasis and the central metabolism. Interestingly, the use of selectively permeabilized cells is ideal to reveal such phenomena of metabolite channeling taking place, since the spatial subcellular organization is conserved, which would be impossible with the use of isolated mitochondria or with transporters reconstituted in liposomes.

In the final part of this work we focused on the mitochondrial pyrucate carrier machinery that has only been recently identified in *S. cerevisiae* (Bricker et al., 2012; Herzig et al., 2012). The quantification of the *in vivo* fluxes at the pyruvate node during steady state respirofermentative growth on $^{13}$C-labeled glucose revealed that carbon is mainly diverted towards ethanol biosynthesis indicative of the active Crabtree effect. Furthermore, it was revealed that the main carbon fluxes entering the mitochondria were directed towards mitochondrial acetyl-CoA from the cytosolic acetyl-CoA and pyruvate pools and towards mitochondrial oxaloacetate pools stemming from its cytosolic counterpart. However, the flux of pyruvate entering the mitochondria could not be resolved. Therefore, as a next step dele-

tion mutants were constructed for the gene sequences that were inferred based on homology to encode the two subunits of the MPC machinery in *S. pombe*, namely *mpc1* and *mpc2*. The three deletion mutants with the genotypes *mpc1Δ*, *mpc2Δ* and *mpc1Δmpc2Δ* were physiologically characterized during exponential growth on glucose and compared to wild type cells.

The first indicator that the MPC was successfully inactivated occurred when the deletion strains could only be cultivated with branched-chain amino acids (leucine, valine, isoleucine) being supplemented to the cultivation medium along with glucose. Normally, these amino acids are synthesized with pyruvate as the precursor in the mitochondria. However in *S. pombe* cells with no available pyruvate entering from the cytosol and without a mitochondrial pyruvate-forming malic enzyme (which is localized in the cytosol), no alternative precursor for BCAA biosynthesis exists. The specific growth rate of the deletion strains was significantly reduced as compared to wild type cells and they possessed a lower capacity to utilise glucose from the cultivation medium.

At the same time all deletion mutants had a largely increased accumulation of pyruvate in the extracellular space which was a direct effect of the introduction of a bottleneck at the pyruvate node. Due to this bottleneck, pyruvate was not able to be efficiently utilized through the remaining metabolic pathways (anaplerosis, ethanol and acetate biosynthesis) in the cytosol, leading to a higher secretion of pyruvate to the extracellular space in the mutant strains. A further finding supporting the existence of a bottleneck at the pyruvate node was the continuous accumulation of acetate during the exponential growth phase which was not the case for wild type cells, that normally begin to synthesize acetate only after glucose is depleted at the end of the exponential growth phase. Interestingly the introduction of a bottleneck at the pyruvate node did not affect the upper part of glycolysis as glycerol yields on glucose remained mostly unchanged for all strains under examination.

The comparison of ethanol yields on glucose did not signify large differences between the strains under examination. Interestingly, the deletion of single MPC subunits or both of them forced the cells to exhibit plasticity and robustness at the pyruvate node when coping with the increase of pyruvate availability in the cytosol. On one hand excess pyruvate formed was secreted to the extracellular space. On the other hand due to the blockage of mitochondrial pyruvate uptake (mitochondrial pyruvate serves as a source for acetyl-CoA), cells diverted the carbon flux towards cytosolic acetate formation. An alternative path to re-supply mitochondria with acetyl-CoA would be the utilization of the cytosolic acetyl-CoA synthetase with acetate as the substrate and the subsequent uptake of acetyl-CoA from the mitochondria by a hypothetical carnitine-acylcarnitine translocase. However neither a translocator for acetylcarnitine/carnitine is known to exist in *S. pombe*, nor mi-

tochondrial or cytosolic carnitine acetyltransferases (as in *S. cerevisiae*) which are needed for the mitochondrial uptake of cytosolic acetyl-CoA stemming from acetate.

Subsequently, a more targeted approach was applied in order to discern the effect of the different MPC deficiencies at the enzymatic activities of the cytosol-mitochondria interface *in situ* by utilizing in this case selectively permeabilized cells. Digitonin-permeabilized cells respired in the presence of pyruvate in a sealed mini-reactor coupled to the membrane inlet mass spectrometer.

The first product that was used to compare wild type permeabilized cells to knockout strains in the presence of pyruvate, malate, ADP and NADH was acetaldehyde generated by the pyruvate decarboxylase activity (first step of the ethanol biosynthetic pathway). Surprisingly, the knockout strains exhibited varying activities of the pyruvate decarboxylase. Acetaldehyde levels for the *mpc1Δ* strain were barely detectable whereas the *mpc2Δ* produced comparable levels to the wild type permeabilized cells. This was the first direct evidence that the MPC monomer make-up had a direct effect on the metabolic activity of an enzyme that was localized in the cytosol and not on the inner mitochondrial membrane where the mitochondrial transporter is docked. Further examination of $CO_2$ levels generated by multiple enzymatic activities (e.g mitochondrial pyruvate dehydrogenase complex, cytosolic pyruvate decarboxylase, cytosolic malic enzyme) for the wild type and the knockout strains correlated with our findings for acetaldehyde formation. More specifically $CO_2$ formation was largely reduced for the permeabilized *mpc1Δ* strain and only slightly for the *mpc2Δ* strain when compared to the wild type cells. At the same time the quantification of pyruvate being consumed correlated with the levels of acetaldehyde and $CO_2$ formation whereas malate levels for all strains remained constant.

On terms of mitochondrial functionality, the introduction of the MPC-deficiency, caused a similar and reproducible reduction of the respiration rate for all strains, regardless of which subunit was deleted from the MPC. Selectively permeabilized wild type cells exhibited the physiological transition from a high state 3 respiration (in the presence of ADP) to a lower state 4 respiration, with the respiration rate being decreased in the latter phase, whereas all deletion strains exhibited no distinct respiration states (even in the presence of ADP). All permeabilized preparations of MPC deletion strains exhibited similar capacity of their respiratory chain to utilize oxygen when compared to each other which approximated the uncoupled state 4 respiration of the permeabilized wild type cells. However when comparing the permeabilized preparations on the basis of experimentally inferred P/O ratios only the single-knockouts exhibited lower P/O values than the wild type whereas the double knockout *mpc1Δmpc2Δ* P/O ratio was not affected. This fact pointed towards an inefficient or dysfunctional electron transport chain and at the same time

a lower efficiency in producing ATP in the mitochondrial matrix and exchanging it for cytosolic ADP.
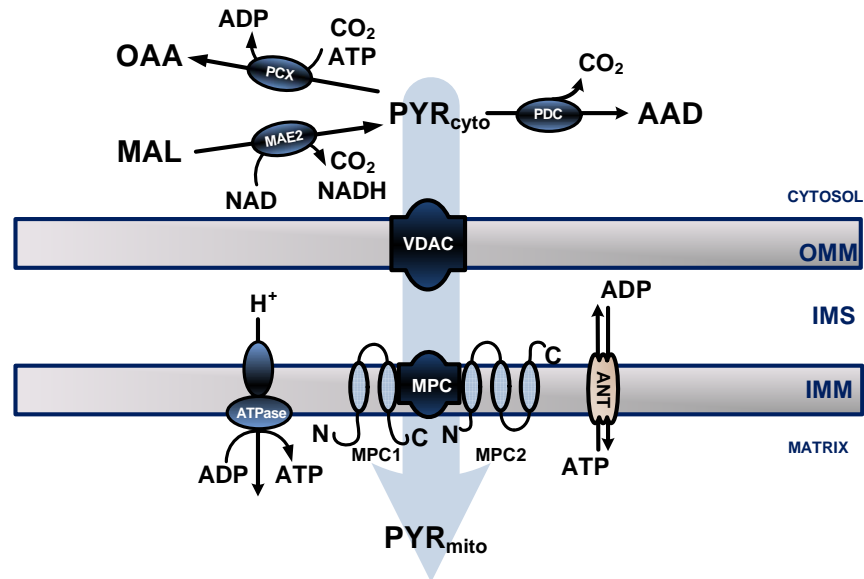


Figure 5.1: Hypothesized components of the pyruvate metabolon. Three compartments are illustrated (cytosol, mitochondrial intermembrane space (IMS), mitochondrial matrix) separated from each other by the outer (OMM) and inner mitochondrial membranes (IMM).Enzymes illustrated here are: PDC, pyruvate decarboxylase; MAE2, malic enzyme; PCX, pyruvate carboxylase; ATPase, mitochondrial matrix ATP synthase. The mitochondrial transporters docked on the OMM and IMM are: VDAC, voltage-dependent anion channel or porin; ANT, adenine nucleotide translocator; MPC, mitochondrial pyruvate carrier with its two subunits and their theoretical conformation in the IMM as adapted from *S. cerevisiae* (Bender et al., 2015).

These results can be interpreted by accepting that the monomers of the MPC are part of a larger metabolon interconnected spatially not only with the activities of cytosolic enzymes but also with the activities of the mitochondrial ATP synthase (see Figure 5.1). Such a metabolon would bridge functionally the cytosol (pyruvate decarboxylase, malic enzyme, pyruvate carboxylase) and the mitochondrial matrix (ATP synthase) via a mitochondrial transporter (MPC). More specifically, the Mpc1p monomer in our model is hypothesized to modulate the first step of the ethanol biosynthetic pathway (cytosolic pyruvate decarboxylase) and the Mpc2p monomer the cytosolic enzymatic activities linking pyruvate with the cytosolic oxaloacetate/malate pool (pyruvate carboxylase and malic enzyme respectively). Loss of the Mpc1p was hypothesized to divert the flux from cytosolic pyruvate away from the pyruvate decarboxylase activity, whereas loss of the Mpc2p subunit had no effect on this enzymatic activity.

The extended metabolon of pyruvate would be functionally interconnected with the VDAC docked on the outer mitochondrial membrane and the adenine nucleotide

translocator allowing for the continuous supply of the mitochondrial ATP synthase with ADP from the cytosol. Such a metabolon would therefore function based on metabolic compartmentalization manifested in the form of metabolite channeling and enzyme-transporter cooperativity. Therefore the MPC can be a major metabolic regulator for redistributing fluxes around the pyruvate node, thus influencing the Crabtree effect and safeguarding the optimal functionality of the oxidative phosphorylation.

Historically, although it was widely accepted that pyruvate entry into the mitochondrial matrix is transporter-mediated, the molecular identity of such a mechanism was only recently unearthed. However there are still many open questions concerning its metabolic role in higher organisms, the stoichiometry of the MPC components and the transcriptional regulation of the mechanism's components. Shedding more light on these questions along with the ongoing identification of inhibitors of the MPC from $\alpha$-cyano-4-hydroxycinnamate (CHC) and UK5099 (Halestrap and Denton, 1974; Halestrap, 1976; Hildyard et al., 2005) to thiazolidinediones (Divakaruni et al., 2013) may lead to discerning not only the metabolic significance of the MPC but also finding pharmacological agents for battling diseases where MPC may play a role. For example the MPC activity has been implicated in pathophysiologies such as diabetes, cancer and neurodegenerative diseases (Gray et al., 2013; Vigueira et al., 2014; Szlosarek et al., 2014; McCommis and Finck, 2015; Wang et al., 2016). Taking into account that the MPC is conserved from yeasts to plants and humans and that the MPC has been implicated into modulating the Warburg effect in cancer cells (Schell et al., 2014a,b) and the Crabtree effect in *S. cerevisiae* via subunit exchange under different growth conditions (Bender et al., 2015) further signifies the central importance of this mechanism. The identification of the MPC in *S. pombe* and our novel findings on the organization of the MPC into a larger metabolon expand the current state of knowledge and offer more insight on the spatial regulation of compartmentalized metabolic pathways.

It would be interesting to expand the analysis of the metabolism around the pyruvate node by applying metabolic flux analysis in *S. pombe* mutant cells lacking either or both of the MPC components. By supplying labeled substrates to growing *S. pombe* cells lacking a functional MPC mechanism different conditions can be explored (respiratory or respirofermentative growth) and at the same time how the *in vivo* carbon fluxes at the pyruvate node are distributed for each condition and genetic background. Applying $^{13}$C-MFA on MPC-knockdowns (reduced expression of *mpc* genes) in mammalian cells revealed increased fatty acid oxidation in order to replenish mitochondrial acetyl-CoA pools along with increased glutaminolysis and pyruvate secretion while maintaining growth (Vacanti et al., 2014).

In order to gain more insight into the role of the MPC mechanism on the Crab-

tree effect a suitable strategy would be to use members of the Crabtree-negative yeasts such as *Candida utilis* and delete the genes expressing the components of the MPC. Is the subunit composition of the MPC in Crabtree-negative yeasts different from that in Crabtree-positive yeasts? How would the fluxes at the pyruvate node be redistributed and how would mitochondria fuel the TCA cycle under such conditions? Would the loss of function of the MPC influence the sugar uptake of the cell and the activity of the pyruvate decarboxylase in the cytosol? The onset of the Crabtree effect (switching from glucose limitation to glucose excess) in Crabtree-positive yeasts correlates with an increased activity of the cytosolic pyruvate decarboxylase, whereas in Crabtree-negative yeasts the activity of this enzyme remains low and unchanged (Urk et al., 1990).

Therefore based on our findings where the MPC composition modulates the activity of the pyruvate decarboxylase in the Crabtree-positive *S. pombe* it would be of interest to examine how this relationship diversified in Crabtree-negative yeasts and possibly reveal a link between the pyruvate metabolon and the evolution and regulation of the Crabtree effect. Subsequently, modifying the activity of the MPC in Crabtree-positive yeasts could prove as a target for optimizing glucose utilization and reduce the waste of carbon through the formation of ethanol and increase biomass yields (Wardrop et al., 2004). Utilizing such a metabolic switch for supressing the Crabtree effect in Crabtree-positive yeasts could make them more promising hosts for the heterologous production of proteins in industrial growth media.

The renaissance of studying compartmentalized pyruvate metabolism between the cytosol and the mitochondria triggered by the molecular identification of the MPC along with the growing use of selectively permeabilized cells for *in situ* studies (Kuznetsov et al., 2008; Salabei et al., 2014) will increase our understanding of mitochondrial dysfunction in disease and reveal novel targets for optimizing yeast cells as hosts for the biotechnological production of high-value proteins.

# Chapter 6

# Bibliography

Acin-Perez, R. and Enriquez, J. A. (2014). The function of the respiratory supercomplexes: the plasticity model. *Biochimica et Biophysica Acta*, 1837(4):444–50.

Acín-Pérez, R., Fernández-Silva, P., Peleato, M. L., Pérez-Martos, A., and Enriquez, J. A. (2008). Respiratory Active Mitochondrial Supercomplexes. *Molecular Cell*, 32(4):529–539.

Adams, V., Griffin, L., Towbin, J., Gelb, B., Worley, K., and McCabe, E. R. B. (1991). Porin interaction with hexokinase and glycerol kinase: Metabolic microcompartmentation at the outer mitochondrial membrane. *Biochemical Medicine and Metabolic Biology*, 45(3):271–291.

Affourtit, C., Krab, K., Leach, G. R., Whitehouse, D. G., and Moore, a. L. (2001). New insights into the regulation of plant succinate dehydrogenase. On the role of the protonmotive force. *The Journal of Biological Chemistry*, 276(35):32567–74.

Agarwal, P. K., Uppada, V., and Noronha, S. B. (2013). Comparison of pyruvate decarboxylases from *Saccharomyces cerevisiae* and *Komagataella pastoris* (*Pichia pastoris*). *Applied Microbiology and Biotechnology*, 97(21): 9439–49

Agrimi, G., Brambilla, L., Frascotti, G., Pisano, I., Porro, D., Vai, M., and Palmieri, L. (2011). Deletion or overexpression of mitochondrial NAD+ carriers in *Saccharomyces cerevisiae* alters cellular NAD and ATP contents and affects mitochondrial metabolism and the rate of glycolysis. *Applied and Environmental Microbiology*, 77(7):2239–2246.

Aithal, H. N., Walsh-Reitz, M. M., and Toback, F. G. (1985). Regulation of glyceraldehyde-3-phosphate dehydrogenase by a cytosolic protein. *The American Journal of Physiology*, 249(1 Pt 1):C111–C116.

Aluvila, S., Kotaria, R., Sun, J., Mayor, J. A., Walters, D. E., Harrison, D. H., and Kaplan, R. S. (2010). The yeast mitochondrial citrate transport protein: molecular determinants of its substrate specificity. *Journal of Biological Chemistry*, 285(35):27314–27326.

Ansanay, V., Dequin, S., Camarasa, C., Schaeffer, V., Grivet, J. P., Blondin, B., Salmon, J. M., and Barre, P. (1996). Malolactic fermentation by engineered *Saccharomyces cerevisiae* as compared with engineered Schizosaccharomyces pombe. *Yeast*, 12(1 996):215–225.

Antoniewicz, M. R., Kelleher, J. K., and Stephanopoulos, G. (2007). Elementary Metabolite Units (EMU): a novel framework for modeling isotopic distributions. *Metabolic Engineering*, 9(1):68–86.

Aranda, A. and del Olmo, M. (2004). Exposure to acetaldehyde in yeast determines an induction of sulfur amino acid metabolism and polyamine transporter genes, which depends on Met4p and Haa1p transcription factors, respectively. *Applied and Environmental Microbiology*, 70(4):1913–1922.

Aravind, L., Watanabe, H., Lipman, D. J., and Koonin, E. V. (2000). Lineage-specific loss and divergence of functionally linked genes in eukaryotes. *Proceedings of the National Academy of Sciences of the United States of America*, 97(21):11319–11324.

Arco, A. D. and Satrustegui, J. (2005). New mitochondrial carriers: an overview. *Cellular and Molecular Life Sciences*, 62(19-20):2204–2227.

Avéret, N., Aguilaniu, H., Bunoust, O., Gustafsson, L., and Rigoulet, M. (2002). NADH is specifically channeled through the mitochondrial porin channel in *Saccharomyces cerevisiae*. *Journal of Bioenergetics and Biomembranes*, 34(6):499–506.

Avéret, N., Fitton, V., Bunoust, O., Rigoulet, M., and Guérin, B. (1998). Yeast mitochondrial metabolism: from *in vitro* to *in situ* quantitative study. *Molecular and Cellular Biochemistry*, 184(1-2):67–79.

Baburina, I., Dikdan, G., Guo, F., Tous, G. I., Root, B., and Jordan, F. (1998). Reactivity at the substrate activation site of yeast pyruvate decarboxylase: inhibition by distortion of domain interactions. *Biochemistry*, 37(5):1245–55.

Bähler, J., Wu, J.-Q., Longtine, M. S., Shah, N. G., McKenzie III, A., Steever, A. B., Wach, A., Philippsen, P., and Pringle, J. R. (1998). Heterologous Modules for Efficient and Versatile PCR-based Gene Targeting in *Scizosaccharomyces pombe*. *Yeast*, (14):943–951.

Bakker, B. M., Overkamp, K. M., van Maris AJ, Kötter, P., Luttik, M. a., van Dijken JP, and Pronk, J. T. (2001). Stoichiometry and compartmentation of NADH metabolism in *Saccharomyces cerevisiae*. *FEMS microbiology reviews*, 25(1):15–37.

Balasubramanian, M. K., Bi, E., and Glotzer, M. (2004). Comparative Analysis of Cytokinesis in Budding Yeast, Fission Yeast and Animal Cells. *Current Biology*, 14(18):R806–R818.

Becker, J., Klopprogge, C., and Wittmann, C. (2008). Metabolic responses to pyruvate kinase deletion in lysine producing *Corynebacterium glutamicum*. *Microbial Cell Factories*, 7:8.

Beckmann, K., Messinger, J., Badger, M. R., Wydrzynski, T., and Hillier, W. (2009). On-line mass spectrometry: Membrane inlet sampling. *Photosynthesis Research*, 102:511–522.

Beitz, E. (2000). TEXshade: shading and labeling of multiple sequence alignments using LATEX2 epsilon. *Bioinformatics (Oxford, England)*, 16(2):135–139.

Bender, T., Pena, G., and Martinou, J.-C. (2015). Regulation of mitochondrial pyruvate uptake by alternative pyruvate carrier complexes. *EMBO Journal*, 34(7):911–924.

Birnboim, H. C. and Doly, J. (1979). A rapid alkaline extraction procedure for screening recombinant plasmid DNA. *Nucleic Acids Research*, 7(6):1513–1524.

Blachly-Dyson, E., Song, J., Wolfgang, W. J., Colombini, M., and Forte, M. (1997). Multicopy suppressors of phenotypes resulting from the absence of yeast VDAC encode a VDAC-like protein. *Molecular and Cellular Biology*, 17(10):5727–5738.

Bolten, C. J. and Wittmann, C. (2008). Appropriate sampling for intracellular amino acid analysis in five phylogenetically different yeasts. *Biotechnology Letters*, 30:1993–2000.

Böttinger, L., Horvath, S. E., Kleinschroth, T., Hunte, C., Daum, G., Pfanner, N., and Becker, T. (2012). Phosphatidylethanolamine and cardiolipin differentially affect the stability of mitochondrial respiratory chain supercomplexes. *Journal of Molecular Biology*, 423(5):677–86.

Boubekeur, S., Bunoust, O., Camougrand, N., Castroviejo, M., Rigoulet, M., and Guérin, B. (1999). A mitochondrial pyruvate dehydrogenase bypass in the yeast *Saccharomyces cerevisiae*. *The Journal of Biological Chemistry*, 274(30):21044–8.

Boubekeur, S., Camougrand, N., Bunoust, O., Rigoulet, M., and Guérin, B. (2001). Participation of acetaldehyde dehydrogenases in ethanol and pyruvate metabolism of the yeast *Saccharomyces cerevisiae*. *European Journal of Biochemistry*, 268(19):5057–5065.

Boumans, H., Grivell, L. A., and Berden, J. A. (1998). The Respiratory Chain in Yeast Behaves as a Single Functional Unit. *Journal of Biological Chemistry*, 273(9):4872–4877.

Bradshaw, P. C. and Pfeiffer, D. R. (2006). Loss of NAD(H) from swollen yeast mitochondria. *BMC Biochemistry*, 7:3.

Bradshaw, P. C. and Pfeiffer, D. R. (2013). Characterization of the respiration-induced yeast mitochondrial permeability transition pore. *Yeast*, (30):471–483.

Brandina, I., Graham, J., Lemaitre-Guillier, C., Entelis, N., Krasheninnikov, I., Sweetlove, L., Tarassov, I., and Martin, R. P. (2006). Enolase takes part in a macromolecular complex associated to mitochondria in yeast. *Biochimica et Biophysica Acta - Bioenergetics*, 1757(9-10):1217–1228.

Braun, B. R., van het Hoog, M., D'Enfert, C., Martchenko, M., Dungan, J., Kuo, A., Inglis, D. O., Uhl, M. A., Hogues, H., Berriman, M., Lorenz, M., Levitin, A., Oberholzer, U., Bachewich, C., Harcus, D., Marcil, A., Dignard, D., Iouk, T., Zito, R., Frangeul, L., Tekaia, F., Rutherford, K., Wang, E., Munro, C. a., Bates, S., Gow, N. a., Hoyer, L. L., Köhler, G., Morschhäuser, J., Newport, G., Znaidi, S., Raymond, M., Turcotte, B., Sherlock, G., Costanzo, M., Ihmels, J., Berman, J., Sanglard, D., Agabian, N., Mitchell, A. P., Johnson, A. D., Whiteway, M., and Nantel, A. (2005). A human-curated annotation of the Candida albicans genome. *PLoS Genetics*, 1(1):0036–0057.

Brdiczka, D. G., Zorov, D. B., and Sheu, S. S. (2006). Mitochondrial contact sites: Their role in energy metabolism and apoptosis. *Biochimica et Biophysica Acta - Molecular Basis of Disease*, 1762(2):148–163.

Bricker, D. K., Taylor, E. B., Schell, J. C., Orsak, T., Boutron, A., Chen, Y.-C., Cox, J. E., Cardon, C. M., Van Vranken, J. G., Dephoure, N., Redin, C., Boudina, S., Gygi, S. P., Brivet, M., Thummel, C. S., and Rutter, J. (2012). A mitochondrial pyruvate carrier required for pyruvate uptake in yeast, Drosophila, and humans. *Science New York NY*, 337(6090):96–100.

Bryksin, A. V. and Matsumura, I. (2012). Overlap extension PCR cloning: a simple and reliable way to create recombinant plasmids. *Biotechniques*, 48(6):463–465.

Bryson, J. M., Coy, P. E., Gottlob, K., Hay, N., and Brooks Robey, R. (2002). Increased hexokinase activity, of either ectopic or endogenous origin, protects renal epithelial cells against acute oxidant-induced cell death. *Journal of Biological Chemistry*, 277(13):11392–11400.

Carlsen, H. N., Degn, H., and Lloyd, D. (1991). Effects of alcohols on the respiration and fermentation of aerated suspensions of baker's yeast. *Journal of General Microbiology*, 137(12):2879–2883.

Castegna, A., Scarcia, P., Agrimi, G., Palmieri, L., Rottensteiner, H., Spera, I., Germinario, L., and Palmieri, F. (2010a). Identification and functional characterization of a novel mitochondrial carrier for citrate and oxoglutarate in Saccharomyces cerevisiae. *Journal of Biological Chemistry*, 285(23):17359–17370.

Castegna, A., Scarcia, P., Agrimi, G., Palmieri, L., Rottensteiner, H., Spera, I., Germinario, L., and Palmieri, F. (2010b). Identification and functional characterization of a novel mitochondrial carrier for citrate and oxoglutarate in *Saccharomyces cerevisiae*. *Journal of Biological Chemistry*, 285(23):17359–70.

Catalina-Rodriguez, O., Kolukula, V. K., Tomita, Y., Preet, A., Palmieri, F., Wellstein, A., Byers, S., Giaccia, A. J., Albanese, C., and Avantaggiati, M. L. (2012). The mitochondrial citrate transporter , CIC , is essential for mitochondrial homeostasis. *Oncotarget*, 3(10):1220–1235.

Cavero, S., Vozza, a., Del Arco, a., Palmieri, L., Villa, a., Blanco, E., Runswick, M. J., Walker, J. E., Cerdán, S., Palmieri, F., and Satrústegui, J. (2003). Identification and metabolic role of the mitochondrial aspartate-glutamate transporter in *Saccharomyces cerevisiae*. *Molecular Microbiology*, 50(4):1257–1269.

Cederbaum, A. I., Lieber, C. S., and Rubin, E. (1974). The Effect of Acetaldehyde on Mitochondrial Function. *Archive of Biochemistry and Biophysics*, 161(1):26-39

Chappell, J. and Beevers, H. (1983). Transport of Dicarboxylic Acids in Castor Bean Mitochondria. *Plant Physiology*, 72(2):434–440.

Chardwiriyapreecha, S., Hondo, K., Inada, H., Chahomchuen, T., Sekito, T., Iwaki, T., and Kakinuma, Y. (2009). A simple and specific procedure to permeabilize the plasma membrane of *Schizosaccharomyces pombe*. *Bioscience, Biotechnology, and Biochemistry*, 73(9):2090–5.

Cherry, J. M., Hong, E. L., Amundsen, C., Balakrishnan, R., Binkley, G., Chan, E. T., Christie, K. R., Costanzo, M. C., Dwight, S. S., Engel, S. R., Fisk, D. G., Hirschman, J. E., Hitz, B. C., Karra, K., Krieger, C. J., Miyasato, S. R., Nash,

R. S., Park, J., Skrzypek, M. S., Simison, M., Weng, S., and Wong, E. D. (2012). *Saccharomyces* Genome Database: the genomics resource of budding yeast. *Nucleic Acids Research*, 40(D1):D700–D705.

Choudhary, C., Weinert, B. T., Nishida, Y., Verdin, E., and Mann, M. (2014). The growing landscape of lysine acetylation links metabolism and cell signalling. *Nature Reviews Molecular Cell Biology*, (15):536–550.

Christen, S. and Sauer, U. (2011). Intracellular characterization of aerobic glucose metabolism in seven yeast species by 13C flux analysis and metabolomics. *FEMS Yeast Research*, 11(3):263–72.

Christensen, B. and Nielsen, J. (1999). Isotopomer analysis using GC-MS. *Metabolic Engineering*, 1(4):282–290.

Claypool, S. M., Oktay, Y., Boontheung, P., Loo, J. A., and Koehler, C. M. (2008). Cardiolipin defines the interactome of the major ADP/ATP carrier protein of the mitochondrial inner membrane. *The Journal of Cell Biology*, 182(5):937–950.

Clémençon, B. (2012). Yeast mitochondrial interactosome model: Metabolon membrane proteins complex involved in the channeling of ADP/ATP. *International Journal of Molecular Sciences*, 13(2):1858–1885.

Clémençon, B., Rey, M., Trézéguet, V., Forest, E., and Pelosi, L. (2011). Yeast ADP/ATP carrier isoform 2: conformational dynamics and role of the RRRMMM signature sequence methionines. *Journal of Biological Chemistry*, 286(41):36119–31.

Colombini, M. (2004). VDAC: the channel at the interface between mitochondria and the cytosol. *Molecular and Cellular Biochemistry*, 256-257(1-2):107–115.

Compan, V., Pierredon, S., Krznar, P., Marchiq, I., Zamboni, N., Pouyssegur, J., and Martinou, J.-c. (2015). Monitoring Mitochondrial Pyruvate Carrier Activity in Real Time Using a BRET-Based Biosensor : Investigation of the Warburg Effect. *Molecular Cell*, (59):491–501.

Cordeiro, C. and Freire, A. P. (1995). Digitonin permeabilization of *Saccharomyces cerevisiae* cells for in situ enzyme assay. *Analytical Biochemistry*, 229(1):145–148.

Couzin, N., Trézéguet, V., Le Saux, a., and Lauquin, G. J. (1996). Cloning of the gene encoding the mitochondrial adenine nucleotide carrier of *Schizosaccharomyces pombe* by functional complementation in Saccharomyces cerevisiae. *Gene*, 171(1):113–7.

Crichton, P. G., Affourtit, C., and Moore, A. L. (2007). Identification of a mitochondrial alcohol dehydrogenase in *Schizosaccharomyces pombe*: new insights into energy metabolism. *The Biochemical Journal*, 401(2):459–64.

Dashko, S., Zhou, N., Compagno, C., and Piskur, J. (2014). Why, when, and how did yeast evolve alcoholic fermentation? *FEMS Yeast Research*, 14:826–832.

Dautant, A., Velours, J., and Giraud, M.-F. (2010). Crystal structure of the Mg.ADP-inhibited state of the yeast F1Fo-ATP synthase. *The Journal of Biological Chemistry*, 285(38):29502–10.

Davies, K. M., Anselmi, C., Wittig, I., Faraldo-Gomez, J. D., and Kuhlbrandt, W. (2012). Structure of the yeast F1Fo-ATP synthase dimer and its role in shaping the mitochondrial cristae. *Proceedings of the National Academy of Sciences*, 109(4):13602–13607.

Dawson, A. (1979). Oxidation of cytosolic NADH formed during aerobic metabolism in mammalian cells. *Trends in Biochemical Sciences*, 4(8):171–176.

de Jong-Gubbels, P., van Dijken, J. P., and Pronk, J. T. (1996). Metabolic fluxes in chemostat cultures of *Schizosaccharomyces pombe* grown on mixtures of glucose and ethanol. *Microbiology (Reading, England)*, 142(1996):1399–1407.

De Vries, S., Van Witzenburg, R., Grivell, L. a., and Marres, C. a. (1992). Primary structure and import pathway of the rotenone-insensitive NADH-ubiquinone oxidoreductase of mitochondria from *Saccharomyces cerevisiae*. *European Journal of Biochemistry / FEBS*, 203(3):587–592.

Decottignies, A., Sanchez-Perez, I., and Nurse, P. (2003). *Schizosaccharomyces pombe* Essential Genes: A Pilot Study. *Genome Research*, (13):399–406.

Deshpande, R., Yang, T. H., and Heinzle, E. (2009). Towards a metabolic and isotopic steady state in CHO batch cultures for reliable isotope-based metabolic profiling. *Biotechnology Journal*, 4(2):247–263.

Díaz-Ruiz, R., Avéret, N., Araiza, D., Pinson, B., Uribe-Carvajal, S., Devin, A., and Rigoulet, M. (2008). Mitochondrial oxidative phosphorylation is regulated by fructose 1,6-bisphosphate. A possible role in Crabtree effect induction? *The Journal of Biological Chemistry*, 283(40):26948–55.

Diaz-Ruiz, R., Rigoulet, M., and Devin, A. (2011). The Warburg and Crabtree effects: On the origin of cancer cell energy metabolism and of yeast glucose repression. *Biochimica et Biophysica Acta*, 1807(6):568–76.

225

Divakaruni, A. S., Wiley, S. E., Rogers, G. W., Andreyev, A. Y., Petrosyan, S., Loviscach, M., Wall, E. A., Yadava, N., Heuck, A. P., Ferrick, D. A., Henry, R. R., McDonald, W. G., Colca, J. R., Simon, M. I., Ciaraldi, T. P., and Murphy, A. N. (2013). Thiazolidinediones are acute, specific inhibitors of the mitochondrial pyruvate carrier. *Proceedings of the National Academy of Sciences of the United States of America*, 110(14):5422–5427.

Driouch, H., Melzer, G., and Wittmann, C. (2012). Integration of *in vivo* and *in silico* metabolic fluxes for improvement of recombinant protein production. *Metabolic Engineering*, 14(1):47–58.

Duarte, M., Peters, M., Schulte, U., and Videira, A. (2003). The internal alternative NADH dehydrogenase of *Neurospora crassa* mitochondria. *The Biochemical Journal*, 371(Pt 3):1005–1011.

Dudkina, N. V., Kouril, R., Peters, K., Braun, H.-P., and Boekema, E. J. (2010). Structure and function of mitochondrial supercomplexes. *Biochimica et Biophysica Acta (BBA) - Bioenergetics*, 1797(6-7):664–670.

Duvezin-Caubet, S., Caron, M., Giraud, M.-F., Velours, J., and di Rago, J.-P. (2003). The two rotor components of yeast mitochondrial ATP synthase are mechanically coupled by subunit $\delta$. *Proceedings of the National Academy of Sciences of the United States of America*, 100(23):13235–13240.

Feldhaus, P., Fröhlich, T., Goody, R. S., Isakov, M., and Schirmer, R. H. (1975). Synthetic inhibitors of adenylate kinases in the assays for ATPases and phosphokinases. *European Journal of Biochemistry*, 57:197–204.

Ferguson, S. J. (2010). ATP synthase: from sequence to ring size to the P/O ratio. *Proceedings of the National Academy of Sciences of the United States of America*, 107(39):16755–16756.

Fernfindez, M., Fernfindez, E., and Rodicio, R. (1994). ACR1 , a gene encoding a protein related to mitochondrial carriers , is essential for acetyl-CoA synthetase activity in Saccharomyces cerevisiae. *Molecular Genetics and Genomics*, (242):727–735.

Fernie, A. R., Carrari, F., and Sweetlove, L. J. (2004). Respiratory metabolism: glycolysis, the TCA cycle and mitochondrial electron transport. *Current Opinion in Plant Biology*, 7(3):254–61.

Fiechter, A. and Seghezzi, W. (1992). Regulation of glucose metabolism in growing yeast cells. *Journal of Biotechnology*, 27:27–45.

Forsburg, S. L. (2003). Overview of *Schizosaccharomyces pombe*. *Current Protocols in Molecular Biology*, (Supplement 64):13.14.1–13.14.3.

Forster, J., Famili, I., Palsson, B. O., and Nielsen, J. (2003). Genome-Scale Reconstruction of the *Saccharomyces cerevisiae* Metabolic Network. *Genome Research*, (13):244–253.

Fountoulakis, M. and Lahm, H.-W. (1998). Hydrolysis and amino acid composition analysis of proteins. *Journal of Chromatography A*, 826:109–134.

Freire, A. P., Margarida, A., and Cordeiro, C. (1998). An experiment illustrating metabolic regulation *in situ* using digitonin permeabilized yeast cells. *Biochemical Education*, 26:161–163.

Gall, J. M., Wong, V., Pimental, D., Havasi, A., Wang, Z., Pastorino, J. G., Bonegio, R., Schwartz, J. H., and Borkan, S. C. (2011). Hexokinase Regulates Susceptibility to Bax-Mediated Mitochondrial Membrane Injury after Ischemic Stress. *Kidney International*, 79(11):1207–1216.

Genova, M. L. and Lenaz, G. (2014). Functional role of mitochondrial respiratory supercomplexes. *Biochimica et Biophysica Acta*, 1837(4):427–43.

Giegé, P., Heazlewood, J. L., Roessner-Tunali, U., Millar, a. H., Fernie, A. R., Leaver, C. J., and Sweetlove, L. J. (2003). Enzymes of glycolysis are functionally associated with the mitochondrion in *Arabidopsis* cells. *The Plant Cell*, 15(9):2140–2151.

Giga-Hama, Y., Tohda, H., Takegawa, K., and Kumagai, H. (2007). *Schizosaccharomyces pombe* minimum genome factory. *Biotechnology and Applied Biochemistry*, 46:147–155.

Goldstein, A. L. and McCusker, J. H. (1999). Three new dominant drug resistance cassettes for gene disruption in *Saccharomyces cerevisiae*. *Yeast*, 15(14):1541–1553.

Gombert, A. K., Moreira dos Santos, M., Christensen, B., and Nielsen, J. (2001). Network identification and flux quantification in the central metabolism of *Saccharomyces cerevisiae* under different conditions of glucose repression. *Journal of Bacteriology*, 183(4):1441–1451.

Gonzalvez, F., Pariselli, F., Dupaigne, P., Budihardjo, I., Lutter, M., Antonsson, B., Diolez, P., Manon, S., Martinou, J.-C., Goubern, M., Wang, X., Bernard, S., and Petit, P. X. (2005). tBid interaction with cardiolipin primarily orchestrates

mitochondrial dysfunctions and subsequently activates Bax and Bak. *Cell death and Differentiation*, 12(6):614–26.

Graham, J. W. A., Williams, T. C. R., Morgan, M., Fernie, A. R., Ratcliffe, R. G., and Sweetlove, L. J. (2007). Glycolytic enzymes associate dynamically with mitochondria in response to respiratory demand and support substrate channeling. *The Plant Cell*, 19(11):3723–3738.

Gray, L. R., Tompkins, S. C., and Taylor, E. B. (2013). Regulation of pyruvate metabolism and human disease. *Cellular and Molecular Life Sciences*, 71(14):2577-604

Gross, a., Pilcher, K., Blachly-Dyson, E., Basso, E., Jockel, J., Bassik, M. C., Korsmeyer, S. J., and Forte, M. (2000). Biochemical and genetic analysis of the mitochondrial response of yeast to BAX and BCL-X(L). *Molecular and Cellular Biology*, 20(9):3125–3136.

Güldener, U., Heck, S., Fiedler, T., Beinhauer, J., and Hegemann, J. H. (1996). A new efficient gene disruption cassette for repeated use in budding yeast. *Nucleic Acids Research*, 24(13):2519–2524.

Gutiérrez-Aguilar, M. and Baines, C. P. (2013). Physiological and pathological roles of mitochondrial SLC25 carriers. *Biochemical Journal*, 454(3):371–386.

Gutiérrez-Aguilar, M., Pérez-Vázquez, V., Bunoust, O., Manon, S., Rigoulet, M., and Uribe, S. (2007). In yeast, Ca2+ and octylguanidine interact with porin (VDAC) preventing the mitochondrial permeability transition. *Biochimica et Biophysica Acta - Bioenergetics*, 1767(10):1245–1251.

Hackenbrock, C., Chazotte, B., and Gupte, S. S. (1986). The Random Collision Model and a Critical Assessment of diffusion and collision in Mitochondrial Electron Transport. *Journal of Bioenergetics and Biomembranes*, 18(5):331–368.

Haferkamp, I. and Schmitz-Esser, S. (2012). The plant mitochondrial carrier family: functional and evolutionary aspects. *Frontiers in Plant Science*, 3(January):1–19.

Hagman, A. and Piškur, J. (2015). A Study on the Fundamental Mechanism and the Evolutionary Driving Forces behind Aerobic Fermentation in Yeast. *Plos One*, 10(1):e0116942.

Hagman, A., Säll, T., Compagno, C., and Piskur, J. (2013). Yeast "make-accumulate-consume" life strategy evolved as a multi-step process that predates the whole genome duplication. *PloS one*, 8(7):e68734.

Hagman, A., Säll, T., and Piskur, J. (2014). Analysis of the yeast short-term Crabtree effect and its origin. *FEBS Journal*, 281:4805–4814.

Halachmi, D., Ghislain, M., and Eilam, Y. (1992). An intracellular ATP-dependent calcium pump within the yeast *Scizosaccharomyces pombe*, encoded by the gene cta3. *European Journal of Biochemistry*, 1008(207):1003–1008.

Halestrap, A. P. (1976). The Mechanism of the Inhibition of the Mitochondrial Pyruvate Transporter by a-Cyanocinnamate Derivatives. *Biochemical Journal*, (156):181–183.

Halestrap, A. P. and Denton, R. M. (1974). Specific inhibition of pyruvate transport in rat liver mitochondria and human erythrocytes by alpha-cyano-4-hydroxycinnamate. *Biochemical Journal*, 138(2):313–316.

Hanahan, D. and Harbor, C. S. (1983). Studies on transformation of Escherichia coli with plasmids. *Journal of Molecular Biology*, (166):557–580.

Heiland, S., Radovanovic, N., Höfer, M., Winderickx, J., and Lichtenberg, H. (2000). Multiple hexose transporters of *Schizosaccharomyces pombe*. *Journal of Bacteriology*, 182(8):2153–62.

Heinemeyer, J., Braun, H. P., Boekema, E. J., and KouÅŹil, R. (2007). A structural model of the cytochrome c reductase/oxidase supercomplex from yeast mitochondria. *Journal of Biological Chemistry*, 282(16):12240–12248.

Hentges, P., Van Driessche, B., Tafforeau, L., Vandenhaute, J., and Carr, A. M. (2005). Three novel antibiotic marker cassettes for gene disruption and marker switching in *Schizosaccharomyces pombe*. *Yeast*, 22(13):1013–1019.

Herzig, S., Raemy, E., Montessuit, S., Veuthey, J.-L., Zamboni, N., Westermann, B., Kunji, E. R. S., and Martinou, J.-C. (2012). Identification and functional expression of the mitochondrial pyruvate carrier. *Science New York*, 337(6090):93–6.

Heslot, H., Goffeau, a., and Louis, C. (1970). Respiratory metabolism of a "petite negative" yeast *Schizosaccharomyces pombe* 972h-. *Journal of Bacteriology*, 104(1):473–81.

Hildyard, J. C., Ammala, C., Dukes, I. D., Thomson, S. A., and Halestrap, A. P. (2005). Identification and characterisation of a new class of highly specific and potent inhibitors of the mitochondrial pyruvate carrier. *Biochimica et Biophysica Acta*, 1707(2-3):221–230.

Hildyard, J. C. and Halestrap, A. P. (2003a). Identification of the mitochondrial pyruvate carrier in *Saccharomyces cerevisiae*. *The Biochemical Journal*, 374(Pt 3):607–611.

Hildyard, J. C. W. and Halestrap, A. P. (2003b). Identification of the mitochondrial pyruvate carrier in *Saccharomyces cerevisiae*. *The Biochemical Journal*, 374(Pt 3):607–611.

Hinkle, P. C. (2005). P/O ratios of mitochondrial oxidative phosphorylation. *Biochimica et Biophysica Acta*, 1706(1-2):1–11.

Hoefer, M. and Nassar, F. (1987). Aerobic and Anaerobic Uptake of Sugars in *Schizosaccharomyces pombe*. *Journal of General Microbiology*, 133(1987):2163–2172.

Hoffman, C. S. and Winston, F. (1987). A ten-minute DNA preparation from yeast efficiently releases autonomous plasmids for transformation of *Escherichia coli*. *Gene*, 57:267–272.

Hoffman, C. S. and Winston, F. (1991). Glucose repression of transcription of the *Schizosaccharomyces pombe* fbp1 gene occurs by a cAMP signaling pathway. *Genes and Development*, 5(4):561–571.

Hoffman, C. S., Wood, V., and Fantes, P. A. (2015). An Ancient Yeast for Young Geneticists: A Primer on the *Schizosaccharomyces pombe* Model System. *Genetics*, 201(2):403–423.

Hollien, J., Lin, J. H., Li, H., Stevens, N., Walter, P., and Weissman, J. S. (2009). Regulated Ire1-dependent decay of messenger RNAs in mammalian cells. *Journal of Cell Biology*, 186(3):323–331.

Hollien, J. and Weissman, J. S. (2006). Decay of Endoplasmic Reticulum-Localized mRNAs During the Unfolded Protein Response. *Science*, 313(July):104–107.

Huang, L. S., Shen, J. T., Wang, A. C., and Berry, E. a. (2006). Crystallographic studies of the binding of ligands to the dicarboxylate site of Complex II, and the identity of the ligand in the "oxaloacetate-inhibited" state. *Biochimica et Biophysica Acta - Bioenergetics*, 1757(9-10):1073–1083.

Hübner, G., Weidhase, R., and Schellenberger, a. (1978). The mechanism of substrate activation of pyruvate decarboxylase: a first approach. *European Journal of Biochemistry / FEBS*, 92(1):175–181.

Hudder, A., Nathanson, L., and Deutscher, M. P. (2003). Organization of mammalian cytoplasm. *Molecular and Cellular Biology*, 23(24):9318–26.

Idiris, A., Bi, K., Tohda, H., Kumagai, H., and Giga-Hama, Y. (2006). Construction of a protease-deficient strain set for the fission yeast *Schizosaccharomyces pombe*, useful for effective production of protease-sensitive heterologous proteins. *Yeast*, 23(2):83–99.

Idiris, A., Tohda, H., Sasaki, M., Okada, K., Kumagai, H., Giga-Hama, Y., and Takegawa, K. (2010). Enhanced protein secretion from multiprotease-deficient fission yeast by modification of its vacuolar protein sorting pathway. *Applied Microbiology and Biotechnology*, 85(3):667–677.

Ikeda, S., Nikaido, K., Araki, K., Yoshitake, A., Kumagai, H., and Isoai, A. (2004). Production of recombinant human lysosomal acid lipase in *Schizosaccharomyces pombe*: development of a fed-batch fermentation and purification process. *Journal of Bioscience and Bioengineering*, 98(5):366–373.

Imai, Y. and Yamamoto, M. (1994). The fission yeast mating pheromone P-factor: its molecular structure, gene structure, and ability to induce gene expression and G1 arrest in the mating partner. *Genes & Development*, 8(3):328–338.

Jansen, M. L., Krook, D. J., De Graaf, K., van Dijken, J. P., Pronk, J. T., and de Winde, J. H. (2006). Physiological characterization and fed-batch production of an extracellular maltase of *Schizosaccharomyces pombe* CBS 356. *FEMS Yeast Research*, 6(6):888–901.

Jault, J. M., Comte, J., Gautheron, D. C., and Di Pietro, a. (1994). Preparation of highly phosphorylating mitochondria from the yeast *Schizosaccharomyces pombe*. *Journal of Bioenergetics and Biomembranes*, 26(4):447–56.

Jørgensen, K., Rasmussen, A. V., Morant, M., Nielsen, A. H., Bjarnholt, N., Zagrobelny, M., Bak, S., and Møller, B. L. (2005). Metabolon formation and metabolic channeling in the biosynthesis of plant natural products. *Current Opinion in Plant Biology*, 8(3):280–291.

Joseph-Horne, T., Hollomon, D. W., and Wood, P. M. (2001). Fungal respiration: a fusion of standard and alternative components. *Biochimica et Biophysica Acta*, 1504(2-3):179–95.

Joyalt, J. L. and Aprilles, J. R. (1992). The ATP-Mg/Pi Carrier of Rat Liver Mitochondria Catalyzes a Divalent Electroneutral Exchange. *The Journal of Biological Chemistry*, 261(21):19198–19203.

Kaplan, R. S., Mayor, J. A., A, G. D., and O., W. D. (1995). High level expression and characterization of the mitochondrial citrate transport protein from Saccharomyces cerevisiae. *The Journal of Biological Chemistry*, 270(8):4108–4114.

Kaur, R., Ingavale, S. S., and Bachhawat, A. K. (1997). PCR-mediated direct gene disruption in *Schizosaccharomyces pombe*. *Nucleic Acids Research*, 25(5):1080–1081.

Kawamata, H., Starkov, A. a., Manfredi, G., and Chinopoulos, C. (2010). A kinetic assay of mitochondrial ADP-ATP exchange rate in permeabilized cells. *Analytical Biochemistry*, 407(1):52–7.

Kerscher, S., Droese, S., Zwicker, K., Zickermann, V., and Brandt, U. (2002). *Yarrowia lipolytica*, a yeast genetic system to study mitochondrial complex I. *Biochimica et Biophysica Acta - Bioenergetics*, 1555(1-3):83–91.

Kesten, D., Kummer, U., Sahle, S., and Hübner, K. (2015). A new model for the aerobic metabolism of yeast allows the detailed analysis of the metabolic regulation during glucose pulse. *Biophysical Chemistry*, 206:40–57.

Kim, D.-U., Hayles, J., Kim, D., Wood, V., Park, H.-O., Won, M., Yoo, H.-S., Duhig, T., Nam, M., Palmer, G., Han, S., Jeffery, L., Baek, S.-T., Lee, H., Shim, Y. S., Lee, M., Kim, L., Heo, K.-S., Noh, E. J., Lee, A.-R., Jang, Y.-J., Chung, K.-S., Choi, S.-J., Park, J.-Y., Park, Y., Kim, H. M., Park, S.-K., Park, H.-J., Kang, E.-J., Kim, H. B., Kang, H.-S., Park, H.-M., Kim, K., Song, K., Song, K. B., Nurse, P., and Hoe, K.-L. (2010). Analysis of a genome-wide set of gene deletions in the fission yeast *Schizosaccharomyces pombe*. *Nature Biotechnology*, 28(6):617–23.

Kimmig, P., Diaz, M., Zheng, J., Williams, C. C., Lang, A., Aragón, T., Li, H., and Walter, P. (2012). The unfolded protein response in fission yeast modulates stability of select mRNAs to maintain protein homeostasis. *eLife*, 2012(1):1–20.

Klein, T., Lange, S., Wilhelm, N., Bureik, M., Yang, T.-H., Heinzle, E., and Schneider, K. (2014). Overcoming the metabolic burden of protein secretion in *Schizosaccharomyces pombe*. A quantitative approach using 13C based metabolic flux analysis. *Metabolic Engineering*, 21:34–45.

Klement, T., Dankmeyer, L., Hommes, R., van Solingen, P., and Büchs, J. (2011). Acetate-glycerol cometabolism: Cultivating *Schizosaccharomyces pombe* on a non-fermentable carbon source in a defined minimal medium. *Journal of Bioscience and Bioengineering*, 112(1):20–25.

Klingenberg, M. (1989). Molecular Aspects of the Adenine Nucleotide Carrier from Mitochondria. *Archive of Biochemistry and Biophysics*, 270(1):1–14.

Klingenberg, M. (2008). The ADP and ATP transport in mitochondria and its carrier. *Biochimica et Biophysica Acta*, 1778(10):1978–2021.

Kmita, H. and Budzinska, M. (2000). Involvement of the TOM complex in external NADH transport into yeast mitochondria depleted of mitochondrial porin1. *Biochimica et Biophysica Acta - Biomembranes*, 1509(1-2):86–94.

Komoszynski, M. and Wojtczak, A. (1996). Apyrases (ATP diphosphohydrolases, EC 3.6.1.5): function and relationship to ATPases. *Biochimica et Biophysica Acta*, 1310:233–241.

Krawchuk, M. D. and Wahls, W. P. (1999). High-efficiency Gene Targeting in *Schizosaccharomyces pombe*: Using a Modular, PCR-based Approach with Long Tracts of Flanking Homology. *Yeast*, 15(13):1419–1427.

Kukuruzinska, M. A., Bergh, M. L., and Jackson, B. J. (1987). Protein Glycosylation in Yeast. *Annual Review of Biochemistry*, 56:915–944.

Kunji, E. R. S. and Crichton, P. G. (2010). Mitochondrial carriers function as monomers. *Biochimica et Biophysica Acta - Bioenergetics*, 1797(6-7):817–831.

Kurtzman, C. P. and Robnett, C. J. (2003). Phylogenetic relationships among yeasts of the 'Saccharomyces complex' determined from multigene sequence analyses. *FEMS Yeast Research*, 3(4):417–432.

Kuznetsov, A. V., Veksler, V., Gellerich, F. N., Saks, V., Margreiter, R., and Kunz, W. S. (2008). Analysis of mitochondrial function in situ in permeabilized muscle fibers, tissues and cells. *Nature Protocols*, 3(6):965–76.

Labaille, F., Colson, a. M., Petit, L., and Goffeau, a. (1977). Properties of a mitochondrial suppressor mutation restoring oxidative phosphorylation in a nuclear mutant of the yeast *Schizosaccharomyces pombe*. *Journal of Biological Chemistry*, 252(16):5716–5723.

Lançar-Benba, J., Foucher, B., and Saint-Macary, M. (1996). Characterization, purification and properties of the yeast mitochondrial dicarboxylate carrier (*Saccharomyces cerevisiae*). *Biochimie*, 78:195–200.

LaNoue, K. F. and Schoolwerth, a. C. (1979). Metabolite transport in mitochondria. *Annual Review of Biochemistry*, 48:871–922.

Lee, a. C., Xu, X., Blachly-Dyson, E., Forte, M., and Colombini, M. (1998). The role of yeast VDAC genes on the permeability of the mitochondrial outer membrane. *The Journal of Membrane Biology*, 161(2):173–81.

Lemasters, J. J., Hill, C., and Carolina, N. (1984). The ATP-to-Oxygen Stoichiometries of Oxidative Phosphorylation by Rat Liver Mitochondria. *The Journal of Biological Chemistry*, 259(21):13123–13130.

Lemasters, J. J. and Holmuhamedov, E. (2006). Voltage-dependent anion channel (VDAC) as mitochondrial governator - Thinking outside the box. *Biochimica et Biophysica Acta - Molecular Basis of Disease*, 1762(2):181–190.

Li, C.-L., Wang, M., Ma, X.-Y., and Zhang, W. (2014). NRGA1, a Putative Mitochondrial Pyruvate Carrier, Mediates ABA Regulation of Guard Cell Ion Channels and Drought Stress Responses in *Arabidopsis*. *Molecular Plant*, (7):1508–1521.

Luttik, M. a. H., Overkamp, K. M., Kötter, P., De Vries, S., Van Dijken, J. P., and Pronk, J. T. (1998). The *Saccharomyces cerevisiae* NDE1 and NDE2 genes encode separate mitochondrial NADH dehydrogenases catalyzing the oxidation of cytosolic NADH. *Journal of Biological Chemistry*, 273(38):24529–24534.

Mannella, C. a. (1998). Conformational changes in the mitochondrial channel protein, VDAC, and their functional implications. *Journal of Structural Biology*, 121(2):207–18.

Manon, S. and Guérin, M. (1998). Investigation of the yeast mitochondrial unselective channel in intact and permeabilized spheroplasts. *Biochemistry and Molecular Biology international*, 44(3):565–575.

Matsuyama, A., Arai, R., Yashiroda, Y., Shirai, A., Kamata, A., Sekido, S., Kobayashi, Y., Hashimoto, A., Hamamoto, M., Hiraoka, Y., Horinouchi, S., and Yoshida, M. (2006). ORFeome cloning and global analysis of protein localization in the fission yeast *Schizosaccharomyces pombe*. *Nature Biotechnology*, 24(7):841–847.

Matsuzawa, T., Ohashi, T., Hosomi, A., Tanaka, N., Tohda, H., and Takegawa, K. (2010). The gld1+ gene encoding glycerol dehydrogenase is required for glycerol metabolism in *Schizosaccharomyces pombe*. *Applied Microbiology and Biotechnology*, 87(2):715–727.

McCommis, K. S. and Finck, B. N. (2015). Mitochondrial pyruvate transport: a historical perspective and future research directions. *Biochemical Journal*, 3(466):443–454.

McDonald, A. and Vanlerberghe, G. (2004). Branched mitochondrial electron transport in the Animalia: presence of alternative oxidase in several animal phyla. *IUBMB Life*, 56(June):333–341.

McDowall, M. D., Harris, M. A., Lock, A., Rutherford, K., Staines, D. M., Bähler, J., Kersey, P. J., Oliver, S. G., and Wood, V. (2015). PomBase 2015: updates to the fission yeast database. *Nucleic Acids Research*, 43(Database issue):D656–D661.

Menard, L., Maughan, D., and Vigoreaux, J. (2014). The Structural and Functional Coordination of Glycolytic Enzymes in Muscle: Evidence of a Metabolon? *Biology*, 3(3):623–644.

Metelkin, E., Demin, O., Kovács, Z., and Chinopoulos, C. (2009). Modeling of ATP-ADP steady-state exchange rate mediated by the adenine nucleotide translocase in isolated mitochondria. *The FEBS Journal*, 276(23):6942–55.

Milakovic, T. and Johnson, G. V. W. (2005). Mitochondrial respiration and ATP production are significantly impaired in striatal cells expressing mutant huntingtin. *The Journal of Biological Chemistry*, 280(35):30773–82.

Miyagi, H., Kawai, S., and Murata, K. (2009). Two Sources of Mitochondrial NADPH in the Yeast *Saccharomyces cerevisiae*. *Journal of Biological Chemistry*, 284(12):7553–7560.

Moore, A. L., Walters, A. J., Thorpet, J., Fricaud, A.-C., and Watts, F. Z. (1992). *Schizosaccharomyces pombe* Mitochondria : Morphological , Respiratory and Protein Import Characteris tics. *Yeast*, 8(1 992):923–933.

Moraes, T. F. and Reithmeier, R. A. F. (2012). Membrane transport metabolons. *Biochimica et Biophysica Acta - Biomembranes*, 1818(11):2687–2706.

Moreadith, R. W. and Fiskum, G. (1984). Isolation of mitochondria from ascite tumor cells permeabilized with digitonin. *Analytical Biochemistry*, 137:360–367.

Mourier, A., Devin, A., and Rigoulet, M. (2009). Active proton leak in mitochondria: A new way to regulate substrate oxidation. *Biochimica et Biophysica Acta - Bioenergetics*, 1797(2):255–261.

Mourier, A. and Larsson, N.-G. (2011). Tracing the trail of protons through complex I of the mitochondrial respiratory chain. *PLoS Biology*, 9(8):e1001129.

Mourier, A., Vallortigara, J., Yoboue, E. D., Rigoulet, M., and Devin, A. (2008). Kinetic activation of yeast mitochondrial d-lactate dehydrogenase by carboxylic acids. *Biochimica et Biophysica Acta - Bioenergetics*, 1777(10):1283–1288.

Neiman, a. M., Stevenson, B. J., Xu, H. P., Sprague, G. F., Herskowitz, I., Wigler, M., and Marcus, S. (1993). Functional homology of protein kinases required for sexual differentiation in *Schizosaccharomyces pombe* and *Saccharomyces cerevisiae* suggests a conserved signal transduction module in eukaryotic organisms. *Molecular Biology of the Cell*, 4(1):107–120.

Nicholls, D. G. and Ferguson, S. J. (2002). *Bioenergetics*. Academic Press, third edition.

Nohl, H. and Schönheit, K. (1996). The effect of the exogenous NADH dehydrogenase of heart mitochondria on the transmembranous proton movement. *Archives of Biochemistry and Biophysics*, 331(2):259–264.

Noji, H., Yasuda, R., Yoshida, M., and Kinosita, K. J. (1997). Direct observation of the rotation of F1 ATP-ase. *Nature*, 386:299–302.

Ohnishi, T., Kawaguchi, K., and Hagihara, B. (1966). Preparation and Some Properties of Yeast Mitochondria. *Journal of Biological Chemistry*, 241(8):1797–1806.

Oliveira, P. J., Santos, D. J., and Moreno, a. J. (2000). Carvedilol inhibits the exogenous NADH dehydrogenase in rat heart mitochondria. *Archives of Biochemistry and Biophysics*, 374(2):279–285.

Orlandi, I., Coppola, D. P., and Vai, M. (2014). Rewiring yeast acetate metabolism through MPC1 loss of function leads to mitochondrial damage and decreases chronological lifespan. *Microbial Cell* 1(12):393–405.

Osothsilp, C. and Subden, R. E. (1986). Malate transport in *Schizosaccharomyces pombe*. *Journal of Bacteriology*, 168(3):1439–1443.

Osumi, M. (2012). Visualization of yeast cells by electron microscopy. *Journal of Electron Microscopy*, 61(6):343–365.

Oyedotun, K. S., Sit, C. S., and Lemire, B. D. (2007). The *Saccharomyces cerevisiae* succinate dehydrogenase does not require heme for ubiquinone reduction. *Biochimica et Biophysica Acta - Bioenergetics*, 1767(12):1436–1445.

Påhlman, I. L., Larsson, C., Averet, N., Buiioust, O., Boubekeur, S., Gustafsson, L., and Rigoulet, M. (2002). Kinetic regulation of the mitochondrial glycerol-3-phosphate dehydrogenase by the external NADH dehydrogenase in *Saccharomyces cerevisiae*. *The Journal of Biological Chemistry*, 277(31):27991–27995.

Pallotta, M. L. (2012). Mitochondrial involvement to methylglyoxal detoxification: D-Lactate/Malate antiporter in *Saccharomyces cerevisiae*. *Antonie van Leeuwenhoek*, 102(1):163–75.

Palmieri, F. (2004). The mitochondrial transporter family (SLC25): physiological and pathological implications. *Pflugers Archiv: European Journal of Physiology*, 447(5):689–709.

Palmieri, F. (2013). Molecular Aspects of Medicine The mitochondrial transporter family SLC25 : Identification , properties and physiopathology. *Molecular Aspects of Medicine*, 34:465–484.

Palmieri, F., Agrimi, G., Blanco, E., Castegna, A., Di Noia, M. A., Iacobazzi, V., Lasorsa, F. M., Marobbio, C. M., Palmieri, L., Scarcia, P., Todisco, S., Vozza, A., and Walker, J. (2006). Identification of mitochondrial carriers in *Saccharomyces cerevisiae* by transport assay of reconstituted recombinant proteins. *Biochimica et Biophysica Acta*, 1757:1249–1262.

Palmieri, F. and Pierri, C. L. (2010). Structure and function of mitochondrial carriers - Role of the transmembrane helix P and G residues in the gating and transport mechanism. *FEBS Letters*, 584(9):1931–1939.

Palmieri, F., Pierri, C. L., De Grassi, A., Nunes-Nesi, A., and Fernie, A. R. (2011). Evolution, structure and function of mitochondrial carriers: a review with new insights. *The Plant Journal : For Cell and Molecular Biology*, 66(1):161–81.

Palmieri, F., Prezioso, G., Quagliariello, E., and Klingenberg, M. (1971). Kinetic Study of the Dicarboxylate Carrier in Rat Liver Mitochondria. *European Journal of Biochemistry*, 22:66–74.

Palmieri, L., Agrimi, G., Runswick, M. J., Fearnley, I. M., Palmieri, F., and Walker, J. E. (2001). Identification in *Saccharomyces cerevisiae* of two isoforms of a novel mitochondrial transporter for 2-oxoadipate and 2-oxoglutarate. *The Journal of Biological Chemistry*, 276(3):1916–22.

Palmieri, L., Lasorsa, F. M., De Palma, A., Palmieri, F., Runswick, M. J., and Walker, J. E. (1997). Identification of the yeast ACR1 gene product as a succinate-fumarate transporter essential for growth on ethanol or acetate. *FEBS Letters*, 417(1):114–118.

Palmieri, L., Lasorsa, F. M., Iacobazzi, V., Runswick, M. J., Palmieri, F., and Walker, J. E. (1999a). Identification of the mitochondrial carnitine carrier in *Saccharomyces cerevisiae*. *FEBS Letters*, 462:472–476.

Palmieri, L., Lasorsa, F. M., Vozza, A., Agrimi, G., Fiermonte, G., Runswick, M. J., Walker, J. E., and Palmieri, F. (2000). Identification and functions of new transporters in yeast mitochondria. *Biochimica et Biophysica Acta*, 1459:363–369.

Palmieri, L., Palmieri, F., Runswick, M. J., and Walker, J. E. (1996). Identification by bacterial expression and functional reconstitution of the yeast genomic sequence encoding the mitochondrial dicarboxylate carrier protein. *FEBS Letters*, 399(3):299–302.

Palmieri, L., Vozza, A., Agrimi, G., De Marco, V., Runswick, M. J., Palmieri, F., and Walker, J. E. (1999b). Identification of the yeast mitochondrial transporter for

oxaloacetate and sulfate. *The Journal of Biological Chemistry*, 274(32):22184–22190.

Palmieri, L., Vozza, a., Hönlinger, a., Dietmeier, K., Palmisano, a., Zara, V., and Palmieri, F. (1999c). The mitochondrial dicarboxylate carrier is essential for the growth of *Saccharomyces cerevisiae* on ethanol or acetate as the sole carbon source. *Molecular Microbiology*, 31(2):569–77.

Pär, H. J., Nordström, K. J., Schiöth, H. B., and Fredriksson, R. (2011). The Solute Carrier Families Have a Remarkably Long Evolutionary History with the Majority of the Human Families Present before Divergence of Bilaterian Species. *Molecular Biology and Evolution*, 28(4):1531–1541.

Perry, C. G. R., Kane, D. a., Lanza, I. R., and Neufer, P. D. (2013). Methods for assessing mitochondrial function in diabetes. *Diabetes*, 62(April):1041–1053.

Phillips, M. L. and Williams, G. R. (1973). Effects of 2-Butylmalonate, 2-Phenylsuccinate, Benzylmalonate and p-Iodobenzylmalonate on the oxidation of Substrates by Mung Bean Mitochondria. *Plant Physiology*, 51:225–228.

Picard, M., Taivassalo, T., Ritchie, D., Wright, K. J., Thomas, M. M., Romestaing, C., and Hepple, R. T. (2011). Mitochondrial structure and function are disrupted by standard isolation methods. *PloS One*, 6(3):e18317.

Picault, N., Hodges, M., Palmieri, L., and Palmieri, F. (2004). The growing family of mitochondrial carriers in *Arabidopsis. Trends in Plant Science*, 9(3):138–46.

Postma, E., Verduyn, C., Scheffers, W. a., and Van Dijken, J. P. (1989). Enzymic analysis of the crabtree effect in glucose-limited chemostat cultures of *Saccharomyces cerevisiae*. *Applied and Environmental Microbiology*, 55(2):468–77.

Postmus, J., Tuzun, I., Bekker, M., Müller, W. H., de Mattos, M. J. T., Brul, S., and Smits, G. J. (2011). Dynamic regulation of mitochondrial respiratory chain efficiency in *Saccharomyces cerevisiae*. *Microbiology (Reading, England)*, 157(Pt 12):3500–11.

Prentice, H. L. (1991). High efficiency transformation of *Schizosaccharomyces pombe* by electroporation. *Nucleic Acids Research*, 20(3):621.

Pronk, J. T., Steensmays, H. Y., and Van Dijken, J. P. (1996). Pyruvate Metabolism in *Saccharomyces cerevisiae*. *Yeast*, 12:1607–1633.

Queiroz, J. H. D., Uribelarrea, J.-l., and Pareilleux, A. (1993). Estimation of the energetic biomass yield and efficiency of oxidative phosphorylation in cell-recycle

cultures of *Schizosaccharomyces pombe*. *Applied Microbiology and Biotechnology*, (39):609–614.

Rampelt, H. and Laan, M. V. D. (2015). Metabolic remodeling : a pyruvate transport affair. *EMBO Journal*, 34(7):835–837.

Rasmussen, U. F. and Rasmussen, H. N. (1985). The NADH oxidase system (external) of muscle mitochondria and its role in the oxidation of cytoplasmic NADH. *The Biochemical Journal*, 229(3):631–641.

Reeves, R. E. and Sols, A. (1973). Regulation of *Escherichia coli* phosphofruktokinase *in situ*. *Biochemical and Biophysical Research Communications*, 50(2):459–466.

Reinders, A. and Ward, J. M. (2001). Functional characterization of the alpha-glucoside transporter Sut1p from *Schizosaccharomyces pombe*, the first fungal homologue of plant sucrose transporters. *Molecular Microbiology*, 39(2):445–454.

Remize, F., Andrieu, E., and Dequin, S. (2000). Engineering of the pyruvate dehydrogenase bypass in *Saccharomyces cerevisiae*: role of the cytosolic Mg2+ and mitochondrial K+ acetaldehyde dehydrogenases Ald6p and Ald4p in acetate formation during alcoholic fermentation. *Applied and Environmental Microbiology*, 66(8):3151–9.

Rhind, N., Furnari, B., and Russell, P. (1997). Cdc2 tyrosine phosphorylation is required for the DNA damage checkpoint in fission yeast. *Genes and Development*, 11(4):504–511.

Rigoulet, M., Aguilaniu, H., Avéret, N., Bunoust, O., Camougrand, N., Grandier-Vazeille, X., Larsson, C., Pahlman, I.-L., Manon, S., and Gustafsson, L. (2004). Organization and regulation of the cytosolic NADH metabolism in the yeast *Saccharomyces cerevisiae*. *Molecular and Cellular Biochemistry*, 256-257(1-2):73–81.

Robey, R. B. and Hay, N. (2006). Mitochondrial hexokinases, novel mediators of the antiapoptotic effects of growth factors and Akt. *Oncogene*, 25(34):4683–4696.

Ruprecht, J. J., Hellawell, A. M., Harding, M., Crichton, P. G., Mccoy, A. J., and Kunji, E. R. S. (2014). Structures of yeast mitochondrial ADP / ATP carriers support a domain-based alternating-access transport mechanism. *Proceedings of the National Academy of Sciences*, 111(4):426–434.

Russell, P. and Nurse, P. (1986). *Schizosaccharomyces pombe* and *Saccharomyces cerevisiae*: a look at yeasts divided. *Cell*, 45(6):781–782.

Russell, P. R. and Hall, B. D. (1983). The primary structure of the alcohol dehydrogenase gene from the fission yeast *Schizosaccharomyces pombe*. *The Journal of Biological Chemistry*, 258(1):143–149.

Rydström, J. (2006). Mitochondrial NADPH, transhydrogenase and disease. *Biochimica et Biophysica Acta - Bioenergetics*, 1757(5-6):721–726.

Saks, V. A., Veksler, V. I., Kuznetsov, A. V., Kay, L., Sikk, P., Tiivel, T., Tranqui, L., Olivares, J., Winkler, K., Wiedemann, F., and Kunz, W. S. (1998). Permeabilized cell and skinned fiber techniques in studies of mitochondrial function *in vivo*. *Molecular and Cellular Biochemistry*, 184(1-2):81–100.

Salabei, J. K., Gibb, A. a., and Hill, B. G. (2014). Comprehensive measurement of respiratory activity in permeabilized cells using extracellular flux analysis. *Nature Protocols*, 9(2):421–38.

Sambrook, J., Fritsch, E. F., and Maniatis, T. (1989). *Cold Spring Harbor Laboratory Molecular Cloning : A Laboratory Manual*. Cold Spring Harbor Lab Press, Publications Dept, New York, 2nd edition.

Satrustegui, J., Pardo, B., and Del Arco, A. (2007). Mitochondrial transporters as novel targets for intracellular calcium signaling. *Physiological Reviews*, 87(1):29–67.

Schägger, H. and Pfeiffer, K. (2000). Supercomplexes in the respiratory chains of yeast and mammalian mitochondria. *The EMBO Journal*, 19(8):1777–83.

Scheffler, I. E. (1999). Mitochondrial Electron Transport Chain and Oxidative Phosphorylation. In *Mitochondria*, chapter 5, pages 141–246. Wiley-Liss, first edition.

Schell, J., Olson, K., Jiang, L., Hawkins, A., Van Vranken, J., Xie, J., Egnatchik, R., Earl, E., DeBerardinis, R., and Rutter, J. (2014a). A Role for the Mitochondrial Pyruvate Carrier as a Repressor of the Warburg Effect and Colon Cancer Cell Growth. *Molecular Cell*, 56(3):400–413.

Schell, J., Olson, K., and Rutter, J. (2014b). The mitochondrial pyruvate carrier as a mediator of the Warburg Effect and its impact on cancer growth and metabolism. *Cancer & Metabolism*, 2(Suppl 1):O14.

Schneider, K. (2011). *Auswirkungen der MAE1-Gendeletion auf den Zentralstoffwechsel von Saccharomyces cerevisiae unter verschiedenen Physiologien*. Saarbrücken.

Schneiter, R. and Daum, G. (2006). Extraction of Yeast Lipids. In Xiao, W., editor, *Yeast Protocol*, pages 41–45. Humana Press.

Schonauer, M. S., Kastaniotis, A. J., Kursu, V. a. S., Hiltunen, J. K., and Dieckmann, C. L. (2009). Lipoic acid synthesis and attachment in yeast mitochondria. *The Journal of Biological Chemistry*, 284(35):23234–42.

Seixas da-Silva, W., Gomez-Puyou, A., Gomez-Puyou, M. T. D., Moreno-Sanchez, R., Felice, F. G. D., Meis, L. D., Oliveira, M. F., and Galina, A. (2004). Mitochondrial Bound Hexokinase Activity as a Preventive Antioxidant Defense. *The Journal of Biological Chemistry*, 279(38):39846–39855.

Serrano, R., Gancedo, J. M., and Gancedo, C. (1973). Assay of yeast enzymes *in situ*: A potential tool in regulation studies. *European Journal of Biochemistry*, 34:479–482.

Shoshan-Barmatz, V., Israelson, a., Brdiczka, D., and Sheu, S. (2006). The Voltage-Dependent Anion Channel (VDAC): Function in Intracellular Signalling, Cell Life and Cell Death. *Current Pharmaceutical Design*, 12(18):2249–2270.

Sohn, S. B., Kim, T. Y., Lee, J. H., and Lee, S. Y. (2012). Genome-scale metabolic model of the fission yeast *Schizosaccharomyces pombe* and the reconciliation of *in silico/in vivo* mutant growth. *BMC Systems Biology*, 6(1):49.

Štáfková, J., Mach, J., Biran, M., Verner, Z., Bringaud, F., and Tachezy, J. (2016). Mitochondrial pyruvate carrier in *Trypanosoma brucei*. *Molecular Microbiology*, 00:n/a–n/a.

Stanley, G. a., Douglas, N. G., Every, E. J., Tzanatos, T., and Pamment, N. B. (1993). Inhibition and stimulation of yeast growth by acetaldehyde. *Biotechnology Letters*, 15(12):1199–1204.

Stanley, G. a. and Pamment, N. B. (1993). Transport and Intracellular Accumulation of Acetaldehyde in *Saccharomyces cerevisiae*. *Biotechnology and Bioengineering*, 42:24–29.

Stein, L. R. and Imai, S. I. (2012). The dynamic regulation of NAD metabolism in mitochondria. *Trends in Endocrinology and Metabolism*, 23(9):420–428.

Stephanopoulos, G., Aristidou, A. A., and Nielsen, J. (1998). *Metabolic Engineering: Principles and Methodologies*. Academic Press.

Sterling, D., Reithmeier, R. a. F., and Casey, J. R. (2001). A transport metabolon: Functional interaction of carbonic anhydrase II and chloride/bicarbonate exchangers. *Journal of Biological Chemistry*, 276(780):47886–47894.

Stevenson, B. J., Liu, J.-W., and Ollis, D. L. (2008). Directed evolution of yeast pyruvate decarboxylase 1 for attenuated regulation and increased stability. *Biochemistry*, 47(9):3013–3025.

Suga, M. and Hatakeyama, T. (2001). High efficiency transformation of *Schizosaccharomyces pombe* pretreated with thiol compounds by electroporation. *Yeast*, 18:1015–1021.

Szlosarek, P., Lee, S., and Pollard, P. (2014). Rewiring Mitochondrial Pyruvate Metabolism: Switching Off the Light in Cancer Cells? *Molecular Cell*, 56(3):343–344.

Timón-Gómez, A., Proft, M., and Pascual-Ahuir, A. (2013). Differential regulation of mitochondrial pyruvate carrier genes modulates respiratory capacity and stress tolerance in yeast. *PloS One*, 8(11):e79405.

Todisco, S., Agrimi, G., Castegna, A., and Palmieri, F. (2006). Identification of the mitochondrial NAD+ transporter in *Saccharomyces cerevisiae*. *The Journal of Biological Chemistry*, 281(3):1524–1531.

Tohda, H., Okada, H., Giga-hama, Y., Okayamab, H., and Kumagai, H. (1994). A Copy-Number-Controlled Expression Vector for the Fission Yeast *Schizosaccharomyces pombe*. *Gene*, 150:275–280.

Toth, P. P., Sumerix, K. J., Ferguson-Miller, S., and Suelter, C. H. (1990). Respiratory control and ADP:O coupling ratios of isolated chick heart mitochondria. *Archives of Biochemistry and Biophysics*, 276(1):199–211.

Traba, J., Froschauer, E. M., Wiesenberger, G., Satrústegui, J., and Del Arco, A. (2008). Yeast mitochondria import ATP through the calcium-dependent ATP-Mg/Pi carrier Sal1p, and are ATP consumers during aerobic growth in glucose. *Molecular Microbiology*, 69(3):570–85.

Trézéguet, V., Zeman, I., David, C., Lauquin, G. J., and Kolarov, J. (1999). Expression of the ADP/ATP carrier encoding genes in aerobic yeasts; phenotype of an ADP/ATP carrier deletion mutant of *Schizosaccharomyces pombe*. *Biochimica et Biophysica Acta*, 1410(3):229–36.

Tsai, C. S., Aveledo, A. J., McDonald, I. J., and Johnson, B. F. (1987). Diauxic growth of the fission yeast *Schizosaccharomyces pombe* in mixtures of D-glucose and ethanol or acetate. *Canadian Journal of Microbiology*, 33(7):593–597.

Urk, H. V., Schipper, D., Breedveld, G. J., Mak, P. R., Scheffers, W. A., and Van Dijken, J. P. (1989). Localization and kinetics of pyruvate-metabolizing enzymes in

relation to aerobic alcoholic fermentation in *Saccharomyces cerevisiae* CBS 8066 and *Candida utilis* CBS 621. *Biochimica et Biophysica Acta*, 992:78–86.

Urk, H. V., Voll, W. S. L., Scheffers, W. A., and Dijken, J. P. V. (1990). Transient-State Analysis of Metabolic Fluxes in Transient-State Analysis of Metabolic Fluxes in Crabtree-Positive and Crabtree-Negative Yeasts. *Applied and Environmental Microbiology*, 56(1):281–287.

Vacanti, N. M., Divakaruni, A. S., Green, C. R., Parker, S. J., Henry, R. R., Ciaraldi, T. P., Murphy, A. N., and Metallo, C. M. (2014). Regulation of Substrate Utilization by the Mitochondrial Pyruvate Carrier. *Molecular Cell*, (56):1–11.

Van Hoek, P., Flikweert, M. T., Van Der Aart, Q. J. M., Steensma, H. Y., Van Dijken, J. P., and Pronk, J. T. (1998). Effects of pyruvate decarboxylase overproduction on flux distribution at the pyruvate branch point in *Saccharomyces cerevisiae*. *Applied and Environmental Microbiology*, 64(6):2133–2140.

Van Urk, H., Bruinenberg, P. M., Veenhuis, M., Scheffers, W. a., and Van Dijken, J. P. (1989). Respiratory capacities of mitochondria of *Saccharomyces cerevisiae* CBS 8066 and *Candida utilis* CBS 621 grown under glucose limitation. *Antonie van Leeuwenhoek*, 56(3):211–20.

Van Winden, W. a., Wittmann, C., Heinzle, E., and Heijnen, J. J. (2002). Correcting mass isotopomer distributions for naturally occurring isotopes. *Biotechnology and Bioengineering*, 80(4):477–479.

Vanderperre, B., Bender, T., Kunji, E. R., and Martinou, J.-C. (2015). Mitochondrial pyruvate import and its effects on homeostasis. *Current Opinion in Cell Biology*, 33:35–41.

Vélot, C., Mixon, M. B., Teige, M., and Srere, P. A. (1997). Model of a quinary structure between Krebs TCA cycle enzymes: A model for the metabolon. *Biochemistry*, 36(47):14271–14276.

Vemuri, G. N., Eiteman, M. a., McEwen, J. E., Olsson, L., and Nielsen, J. (2007). Increasing NADH oxidation reduces overflow metabolism in *Saccharomyces cerevisiae*. *Proceedings of the National Academy of Sciences of the United States of America*, 104(7):2402–7.

Verduyn, C., Stouthamer, a. H., Scheffers, W. a., and van Dijken, J. P. (1991). A theoretical evaluation of growth yields of yeasts. *Antonie van Leeuwenhoek*, 59(1):49–63.

Videira, A. (1998). Complex I from the fungus *Neurospora crassa*. *Biochimica et Biophysica Acta - Bioenergetics*, 1364(2):89–100.

Vignais, P. V. (1976). The mitochondrial adenine nucleotide translocator. *Journal of Bioenergetics*, 8:9–17.

Vigueira, P. a., McCommis, K. S., Schweitzer, G. G., Remedi, M. S., Chambers, K. T., Fu, X., McDonald, W. G., Cole, S. L., Colca, J. R., Kletzien, R. F., Burgess, S. C., and Finck, B. N. (2014). Mitochondrial pyruvate carrier 2 hypomorphism in mice leads to defects in glucose-stimulated insulin secretion. *Cell Reports*, 7(6):2042–53.

Viljoen, M., Subden, R. E., Krizus, A., and Van Vuuren, H. J. (1994). Molecular analysis of the malic enzyme gene (mae2) of *Schizosaccharomyces pombe*. *Yeast*, 10(5):613–624.

Viljoen, M., Volschenk, H., Young, R. A., and van Vuuren, H. J. (1999). Transcriptional regulation of the *Schizosaccharomyces pombe* malic enzyme gene, mae2. *The Journal of Biological Chemistry*, 274(15):9969–9975.

Vogelstein, B. and Gillespie, D. (1979). Preparative and analytical purification of DNA from agarose. *Proceedings of the National Academy of Sciences of the United States of America*, 76(2):615–619.

von Jagow, G. and Klingenberg, M. (1970). Pathways of Hydrogen in Mitochondria of *Saccharomyces carlsbergensis*. *European Journal of Biochemistry*, 12:583–592.

von Meyenburg, H. K. (1969). Energetics of the Budding Cycle of *Saccharomyces cerevisiae* during Ghicose Limited Aerobic Growth. *Archives of Microbiology*, 66:289–303.

Wahrheit, J., Nonnenmacher, Y., Sperber, S., and Heinzle, E. (2015). High-throughput respiration screening of single mitochondrial substrates using permeabilized CHO cells highlights control of mitochondria metabolism. *Engineering in Life Sciences*, 15(2):184–194.

Wang, L., Xu, M., Qin, J., Lin, S.-c., Lee, H.-j., Tsai, S. Y., and Tsai, M.-j. (2016). MPC1 , a key gene in cancer metabolism , is regulated by COUPTFII in human prostate cancer. *Oncotarget*, 7(12):14673–14683.

Wardrop, F. R., Liti, G., Cardinali, G., and Walker, G. M. (2004). Physiological responses of Crabtree positive and Crabtree negative yeasts to glucose upshifts in a chemostat. *Annals of Microbiology*, 54(1):103–114.

Watt, I. N., Montgomery, M. G., Runswick, M. J., Leslie, A. G. W., and Walker, J. E. (2010). Bioenergetic cost of making an adenosine triphosphate molecule in animal mitochondria. *Proceedings of the National Academy of Sciences of the United States of America*, 107(39):16823–16827.

Wenz, T., Hielscher, R., Hellwig, P., Schägger, H., Richers, S., and Hunte, C. (2009). Role of phospholipids in respiratory cytochrome bc1 complex catalysis and supercomplex formation. *Biochimica et Biophysica Acta (BBA) - Bioenergetics*, 1787(6):609–616.

Weyler, C., Bureik, M., and Heinzle, E. (2015). Selective oxidation of UDP-glucose to UDP-glucuronic acid using permeabilized *Schizosaccharomyces pombe* expressing human UDP-glucose 6-dehydrogenase. *Biotechnology Letters*, 38(3):1–5.

Wiechert, W. (2001). 13C metabolic flux analysis. *Metabolic Engineering*, (3):195–206.

Wiechert, W., Möllney, M., Isermann, N., Wurzel, M., and De Graaf, A. a. (1999). Bidirectional reaction steps in metabolic networks: III. Explicit solution and analysis of isotopomer labeling systems. *Biotechnology and Bioengineering*, 66:69–85.

Wikstrom, M. and Hummer, G. (2012). Stoichiometry of proton translocation by respiratory complex I and its mechanistic implications. *Proceedings of the National Academy of Sciences*, 109(12):4431–4436.

Wilson, J. E. (1997). Homologous and Heterologous Interactions between Hexokinase and Mitochondrial Porin: Evolutionary Implications. *Journal of Bioenergetics and Biomembranes*, 29(1):97–102.

Wittmann, C. and De Graaf, A. (2005). Metabolic Flux Analysis in *Corynebacterium glutamicum*. In Eggeling, L. and Bott, M., editors, *Handbook of Corynebacterium glutamicum*, pages 277–304. CRC Press.

Wittmann, C., Hans, M., and Heinzle, E. (2002). *In vivo* analysis of intracellular amino acid labelings by GC / MS. *Analytical Biochemistry*, 307:379–382.

Wittmann, C. and Heinzle, E. (1999). Mass spectrometry for metabolic flux analysis. *Biotechnology and Bioengineering*, 62(6):739–750.

Wittmann, C. and Heinzle, E. (2001). Modeling and experimental design for metabolic flux analysis of lysine-producing *Corynebacteria* by mass spectrometry. *Metabolic Engineering*, 3(2):173–191.

Wittmann, C. and Heinzle, E. (2005). Metabolic Activity Profiling by 13C Tracer Experiments and Mass Spectrometry in *Corynebacterium glutamicum*. In Barredo, J., editor, *Microbial Processes and Products*, chapter 10, pages 191–204. Humana Press.

Wittmann, C. and Heinzle, E. (2008). Metabolic Network Analysis and Design in *Corynebacterium glutamicum*. In Burkovski, A., editor, *Corynebacteria: Genomics and Molecular Biology*, pages 79–112. Caister Academic Press.

Wood, V., Gwilliam, R., Rajandream, M. A., Lyne, M., Lyne, R., Stewart, A., Sgouros, J., Peat, N., Hayles, J., Baker, S., Basham, D., Bowman, S., Brooks, K., Brown, D., Brown, S., Chillingworth, T., Churcher, C., Collins, M., Connor, R., Cronin, A., Davis, P., Feltwell, T., Fraser, A., Gentles, S., Goble, A., Hamlin, N., Harris, D., Hidalgo, J., Hodgson, G., Holroyd, S., Hornsby, T., Howarth, S., Huckle, E. J., Hunt, S., Jagels, K., James, K., Jones, L., Jones, M., Leather, S., McDonald, S., McLean, J., Mooney, P., Moule, S., Mungall, K., Murphy, L., Niblett, D., Odell, C., Oliver, K., O'Neil, S., Pearson, D., Quail, M. A., Rabbinowitsch, E., Rutherford, K., Rutter, S., Saunders, D., Seeger, K., Sharp, S., Skelton, J., Simmonds, M., Squares, R., Squares, S., Stevens, K., Taylor, K., Taylor, R. G., Tivey, A., Walsh, S., Warren, T., Whitehead, S., Woodward, J., Volckaert, G., Aert, R., Robben, J., Grymonprez, B., Weltjens, I., Vanstreels, E., Rieger, M., Schafer, M., Muller-Auer, S., Gabel, C., Fuchs, M., Dusterhoft, A., Fritzc, C., Holzer, E., Moestl, D., Hilbert, H., Borzym, K., Langer, I., Beck, A., Lehrach, H., Reinhardt, R., Pohl, T. M., Eger, P., Zimmermann, W., Wedler, H., Wambutt, R., Purnelle, B., Goffeau, A., Cadieu, E., Dreano, S., Gloux, S., Lelaure, V., Mottier, S., Galibert, F., Aves, S. J., Xiang, Z., Hunt, C., Moore, K., Hurst, S. M., Lucas, M., Rochet, M., Gaillardin, C., Tallada, V. A., Garzon, A., Thode, G., Daga, R. R., Cruzado, L., Jimenez, J., Sanchez, M., del Rey, F., Benito, J., Dominguez, A., Revuelta, J. L., Moreno, S., Armstrong, J., Forsburg, S. L., Cerutti, L., Lowe, T., McCombie, W. R., Paulsen, I., Potashkin, J., Shpakovski, G. V., Ussery, D., Barrell, B. G., and Nurse, P. (2002). The genome sequence of *Schizosaccharomyces pombe*. *Nature*, 415(6874):871–880.

Wood, V., Harris, M. a., McDowall, M. D., Rutherford, K., Vaughan, B. W., Staines, D. M., Aslett, M., Lock, A., Bähler, J., Kersey, P. J., and Oliver, S. G. (2012). PomBase: A comprehensive online resource for fission yeast. *Nucleic Acids Research*, 40(October 2011):695–699.

Xu, Y. (2000). The Yeast Mitochondrial Citrate Transport Protein. Probing the roles of cysteines, Arg181 and Arg189 in transporter function. *The Journal of Biological Chemistry*, 275(10):7117–7124.

Yanagida, M. (2002). The model unicellular eukaryote, *Schizosaccharomyces pombe*. *Genome biology*, 3(3):2003.1–2003.4.

Yang, T. H., Bolten, C. J., Coppi, M. V., Sun, J., and Heinzle, E. (2009). Numerical bias estimation for mass spectrometric mass isotopomer analysis. *Analytical Biochemistry*, 388(2):192–203.

Yang, T. H., Frick, O., and Heinzle, E. (2008). Hybrid optimization for 13C metabolic flux analysis using systems parametrized by compactification. *BMC Systems Biology*, 2:29.

Yang, T. H., Wittmann, C., and Heinzle, E. (2006). Respirometric 13C flux analysis, Part I: Design, construction and validation of a novel multiple reactor system using on-line membrane inlet mass spectrometry. *Metabolic Engineering*, 8(5):417–431.

Zhang, J. W. and Lazarow, P. B. (1995). PEB1 (PAS7) in *Saccharomyces cerevisiae* encodes a hydrophilic, intra-peroxisomal protein that is a member of the WD repeat family and is essential for the import of thiolase into peroxisomes. *The Journal of Cell Biology*, 129(1):65–80.

Zhang, M., Mileykovskaya, E., and Dowhan, W. (2002). Gluing the Respiratory Chain Together. Cardiolipin is required for supercomplex formation in the inner mitochondrial membrane. *The Journal of Biological Chemistry*, 277(46):43553–43556.

Zhong, X. and Guidotti, G. (1999). A yeast Golgi E-type ATPase with an unusual membrane topology. *The Journal of Biological Chemistry*, 274(46):32704–32711.

Zizi, M., Forte, M., Blachly-Dyson, E., and Colombini, M. (1994). NADH regulates the gating of VDAC, the mitochondrial outer membrane channel. *The Journal of Biological Chemistry*, 269(3):1614–1616.

# Appendix

## Plasmid Maps
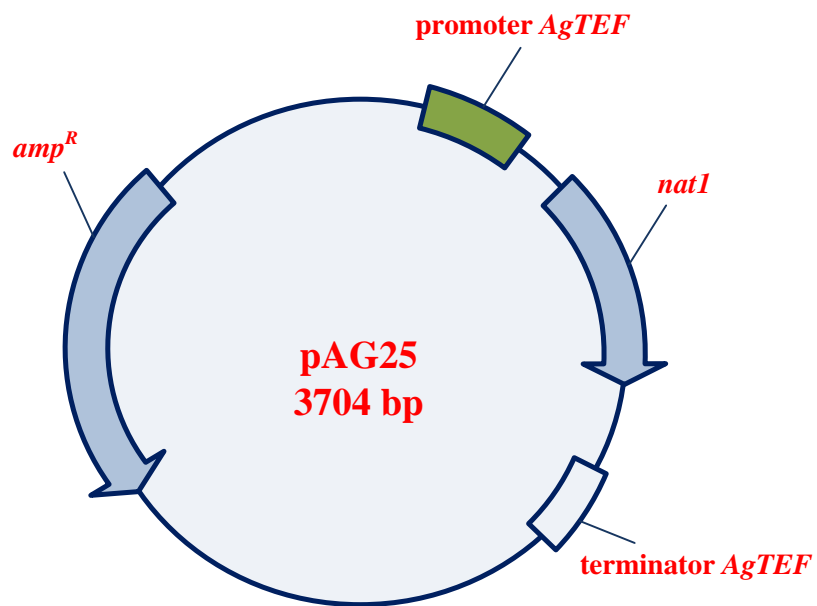


Figure 1: Plasmid map for vector pAG25
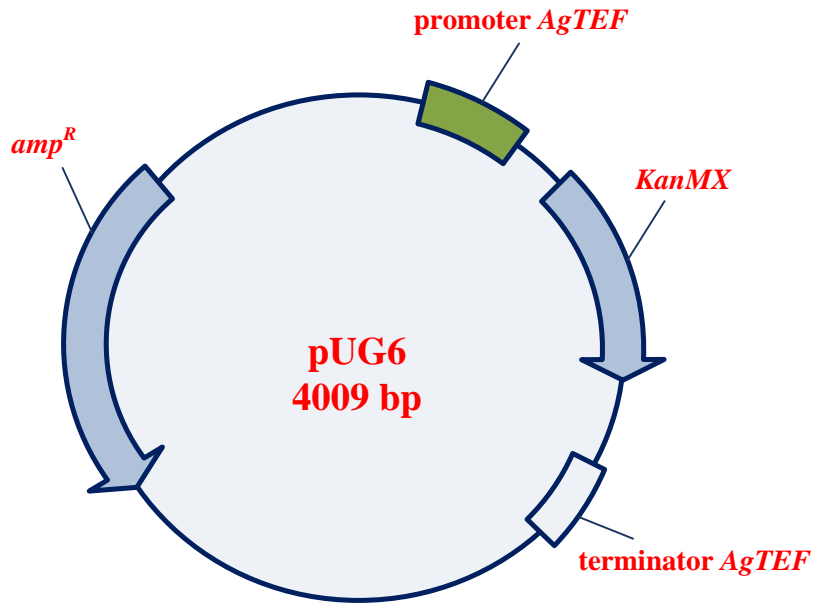
Figure 2: Plasmid map for vector pUG6

# *In vivo* fluxes

## Central metabolism model for $^{13}$C-based flux analysis

Table 1: Model of the *S. pombe* CBS 356 central metabolism used for the MFA during 99 % [1-$^{13}$C]-glucose uptake at a steady-state. where relative carbon fluxes are illustrated based on a 100 % glucose uptake rate (glucose$_{ex}$), standardized for an experimentally measured q$_{glucose}$ = 10.51 ± 1.49 [mmol/(g CDW · h)].

| Reaction | Reactant | Product |
| --- | --- | --- |
| **1** | Glucose 6-P $\leftrightarrow$ | Fructose-6P |
| **2** | Fructose 6-P $\rightarrow$ | glyceraldehyde 3-P + dihydroxyacetone-P |
| **3** | glyceraldehyde 3-P $\leftrightarrow$ | dihydroxyacetone-P |
| **4** | glyceraldehyde 3-P $\rightarrow$ | 3-phosphoglycerate + NADH |
| **5** | 3-phosphoglycerate $\rightarrow$ | phosphoenolpyruvate |
| **6** | phosphoenolpyruvate $\rightarrow$ | pyruvate[cyt] |
| **7** | pyruvate[cyt] $\rightarrow$ | pyruvate[mit] |

| 8  | oxaloacetate[cyt] $\leftrightarrow$ | oxaloacetate[mit] |
| 9  | acetyl-CoA[cyt] $\rightarrow$ | acetyl-CoA[mit] |
| 10 | pyruvate[mit] $\rightarrow$ | $CO_2$ + acetyl-CoA[mit] + NADH |
| 11 | malate[mit] $\rightarrow$ | malate[cyt] |
| 12 | malate[cyt] $\rightarrow$ | $CO_2$ + pyruvate[cyt] + NADH |
| 13 | pyruvate[cyt] + $CO_2$ $\rightarrow$ | oxaloacetate[cyt] |
| 14 | glucose-6P $\rightarrow$ | pentose 5-P + $CO_2$ + 2NADPH |
| 15 | pentose 5-P $\leftrightarrow$ | glyceraldehyde 3-P + sedoheptulose 7-P |
| 16 | glyceraldehyde 3-P + sedoheptulose 7-P $\leftrightarrow$ | fructose 6-P + erythrose 4-P |
| 17 | pentose 5-P + erythrose 4-P $\leftrightarrow$ | fructose 6-P + glyceraldehyde 3-P |
| 18 | oxaloacetate[mit] + acetyl-CoA[mit] $\rightarrow$ | isocitrate |
| 19 | isocitrate $\rightarrow$ | $\alpha$-ketoglutarate + $CO_2$ + NADPH |
| 20 | $\alpha$-ketoglutarate $\rightarrow$ | succinate + $CO_2$ + NADH |
| 21 | succinate $\rightarrow$ | fumarate + FADH |
| 22 | fumarate $\leftrightarrow$ | malate[mit] |
| 23 | malate[mit] $\rightarrow$ | oxaloacetate[mit] + NADH |
| 24 | pyruvate[cyt] $\rightarrow$ | acetaldehyde+$CO_2$ |
| 25 | acetaldehyde $\rightarrow$ | acetate+NADH |
| 26 | acetate $\rightarrow$ | acetyl-CoA[cyt] |
| 27 | 3-phosphoglycerate $\rightarrow$ | serine + NADH |
| 28 | serine $\leftrightarrow$ | glycine + MTF |
| 29 | oxaloacetate[cyt] $\rightarrow$ | aspartate[cyt] |
| 30 | oxaloacetate[mit] $\rightarrow$ | aspartate[mit] |
| 31 | aspartate[cyt] + 2NADPH $\rightarrow$ | threonine |

| 32 | threonine $\leftrightarrow$ | glycine + acetaldehyde + NADH |
|----|------------------------------|-------------------------------|
| 33 | pyruvate[mit] + NADPH $\rightarrow$ | oxoisovalerate + $CO_2$ |
| 34 | phosphoenolpyruvate + erythrose 4-P + NADPH $\rightarrow$ | shikimate 3-P |
| 35 | pyruvate[cyt] $\rightarrow$ | alanine |
| 36 | pyruvate[mit] $\rightarrow$ | alanine |
| 37 | oxoisovalerate $\rightarrow$ | valine |
| 38 | phosphoenolpyruvate + shikimate 3-P $\rightarrow$ | phenylalanine + $CO_2$ |
| 39 | threonine + pyruvate[mit] + NADPH $\rightarrow$ | isoleucine + $CO_2$ |
| 40 | aspartate[cyt] + MTF + 2NADPH $\rightarrow$ | methionine |
| 41 | acetaldehyde + NADH $\rightarrow$ | ethanol$_{ex}$ |
| 42 | dihydroxyacetone-P + NADH $\rightarrow$ | glycerine$_{ex}$ |
| 43 | pyruvate[cyt] $\rightarrow$ | pyruvate$_{ex}$ |

Table 2: Experimental values of proteinogenic amino acids mass isotopomers measured via GC/MS and their relevant experimental error from samples taken from parallel cultivations for *S. pombe* CBS 356 during respirofermentative growth on 99 % 1-[$^{13}$C]-glucose

| Amino acid fragment | Mass isotopomer | Sample 1 | Sample 2 | error propagation [%] |
|---|---|---|---|---|
| ala (m/z 260) | $m_0$ | 0.536 | 0.538 | 0.7 |
| | $m_1$ | 0.452 | 0.451 | 0.6 |
| | $m_2$ | 0.011 | 0.011 | 0.0 |
| | $m_3$ | 0.000 | 0.001 | 0.0 |
| ala (m/z 232) | $m_0$ | 0.543 | 0.545 | 0.6 |
| | $m_1$ | 0.451 | 0.449 | 0.6 |
| | $m_2$ | 0.006 | 0.006 | 0.0 |
| gly (m/z 246) | $m_0$ | 0.967 | 0.966 | 0.2 |
| | $m_1$ | 0.031 | 0.032 | 0.1 |
| | $m_2$ | 0.003 | 0.003 | 0.1 |
| val (m/z 288) | $m_0$ | 0.297 | 0.299 | 0.8 |
| | $m_1$ | 0.481 | 0.481 | 0.3 |
| | $m_2$ | 0.213 | 0.212 | 0.4 |
| | $m_3$ | 0.007 | 0.007 | 0.0 |
| | $m_4$ | 0.000 | 0.000 | 0.0 |
| | $m_5$ | 0.000 | 0.000 | 0.0 |
| val (m/z 260) | $m_0$ | 0.300 | 0.301 | 0.8 |
| | $m_1$ | 0.480 | 0.480 | 0.3 |
| | $m_2$ | 0.211 | 0.211 | 0.5 |
| | $m_3$ | 0.007 | 0.007 | 0.0 |
| | $m_4$ | 0.001 | 0.000 | 0.0 |
| ile (m/z 200) | $m_0$ | 0.279 | 0.281 | 0.8 |
| | $m_1$ | 0.468 | 0.467 | 0.4 |
| | $m_2$ | 0.231 | 0.230 | 0.4 |
| | $m_3$ | 0.021 | 0.021 | 0.0 |
| | $m_4$ | 0.001 | 0.001 | 0.0 |
| | $m_5$ | 0.000 | 0.000 | 0.0 |
| ser (m/z 390) | $m_0$ | 0.552 | 0.554 | 0.6 |

|  |  |  |  |  |
|---|---|---|---|---|
|  | $m_1$ | 0.437 | 0.436 | 0.6 |
|  | $m_2$ | 0.010 | 0.010 | 0.0 |
|  | $m_3$ | 0.000 | 0.000 | 0.0 |
| ser (m/z 362) | $m_0$ | 0.563 | 0.565 | 0.6 |
|  | $m_1$ | 0.432 | 0.430 | 0.6 |
|  | $m_2$ | 0.005 | 0.005 | 0.0 |
| phe (m/z 336) | $m_0$ | 0.218 | 0.220 | 0.9 |
|  | $m_1$ | 0.421 | 0.421 | 0.2 |
|  | $m_2$ | 0.284 | 0.282 | 0.5 |
|  | $m_3$ | 0.067 | 0.066 | 0.2 |
|  | $m_4$ | 0.004 | 0.004 | 0.0 |
|  | $m_5$ | 0.002 | 0.002 | 0.1 |
|  | $m_6$ | 0.001 | 0.001 | 0.0 |
|  | $m_7$ | 0.002 | 0.002 | 0.1 |
|  | $m_8$ | 0.001 | 0.001 | 0.0 |
|  | $m_9$ | 0.001 | 0.001 | 0.0 |
| phe (m/z 302) | $m_0$ | 0.977 | 0.977 | 0.1 |
|  | $m_1$ | 0.022 | 0.023 | 0.1 |
|  | $m_2$ | 0.000 | 0.001 | 0.0 |
| phe (m/z 234) | $m_0$ | 0.222 | 0.225 | 0.9 |
|  | $m_1$ | 0.422 | 0.422 | 0.1 |
|  | $m_2$ | 0.280 | 0.278 | 0.6 |
|  | $m_3$ | 0.066 | 0.065 | 0.2 |
|  | $m_4$ | 0.005 | 0.005 | 0.0 |
|  | $m_5$ | 0.002 | 0.002 | 0.1 |
|  | $m_6$ | 0.001 | 0.001 | 0.0 |
|  | $m_7$ | 0.001 | 0.001 | 0.0 |
|  | $m_8$ | 0.001 | 0.001 | 0.0 |
| asp (m/z 418) | $m_0$ | 0.490 | 0.492 | 0.6 |
|  | $m_1$ | 0.462 | 0.460 | 0.6 |
|  | $m_2$ | 0.046 | 0.047 | 0.1 |
|  | $m_3$ | 0.001 | 0.002 | 0.0 |

|  |  |  |  |  |
|---|---|---|---|---|
|  | $m_4$ | 0.000 | 0.000 | 0.0 |
| glu (m/z 432) | $m_0$ | 0.269 | 0.271 | 0.8 |
|  | $m_1$ | 0.456 | 0.455 | 0.4 |
|  | $m_2$ | 0.241 | 0.240 | 0.4 |
|  | $m_3$ | 0.031 | 0.032 | 0.1 |
|  | $m_4$ | 0.002 | 0.002 | 0.0 |
|  | $m_5$ | 0.000 | 0.000 | 0.0 |
| thr (m/z 404) | $m_0$ | 0.493 | 0.493 | 0.6 |
|  | $m_1$ | 0.460 | 0.459 | 0.6 |
|  | $m_2$ | 0.045 | 0.046 | 0.0 |
|  | $m_3$ | 0.001 | 0.001 | 0.0 |
|  | $m_4$ | 0.000 | 0.000 | 0.0 |
| thr (m/z 376) | $m_0$ | 0.506 | 0.507 | 0.5 |
|  | $m_1$ | 0.457 | 0.455 | 0.5 |
|  | $m_2$ | 0.037 | 0.037 | 0.0 |
|  | $m_3$ | 0.001 | 0.001 | 0.0 |
| average experimental error of the mass isotopomer fractions [%] |  |  |  | **0.26** |

Table 3: Calculated and simulated mass isotopomers for all proteinogenic amino acids for *S. pombe* CBS 356 during respirofermentative growth on 99 % 1-[$^{13}$C]-glucose.

| | $m_0$ | $m_1$ | $m_2$ | $m_3$ | $m_4$ | $m_5$ | $m_6$ | $m_7$ | $m_8$ | $m_9$ |
|---|---|---|---|---|---|---|---|---|---|---|
| **ala (m/z 260)** | | | | | | | | | | |
| measured | 0.537 | 0.452 | 0.011 | 0.0005 | | | | | | |
| simulated | 0.535 | 0.450 | 0.015 | 0.0001 | | | | | | |
| **ala (m/z 232)** | | | | | | | | | | |
| measured | 0.544 | 0.450 | 0.006 | | | | | | | |
| simulated | 0.544 | 0.450 | 0.006 | | | | | | | |
| **gly (m/z 246)** | | | | | | | | | | |
| measured | 0.966 | 0.031 | 0.0025 | | | | | | | |
| simulated | 0.961 | 0.038 | 0.0004 | | | | | | | |
| **val (m/z 288)** | | | | | | | | | | |
| measured | 0.298 | 0.481 | 0.213 | 0.007 | 0.0004 | 0.0002 | | | | |
| simulated | 0.291 | 0.486 | 0.214 | 0.009 | 0.0001 | 0.000 | | | | |
| **val (m/z 260)** | | | | | | | | | | |
| measured | 0.301 | 0.480 | 0.211 | 0.007 | 0.0005 | | | | | |
| simulated | 0.296 | 0.490 | 0.209 | 0.005 | 0.0000 | | | | | |
| **ile (m/z 200)** | | | | | | | | | | |
| measured | 0.280 | 0.467 | 0.230 | 0.021 | 0.0014 | 0.0004 | | | | |
| simulated | 0.278 | 0.478 | 0.226 | 0.017 | 0.0003 | 0.000 | | | | |
| **ser (m/z 390)** | | | | | | | | | | |
| measured | 0.553 | 0.437 | 0.010 | 0.0002 | | | | | | |
| simulated | 0.550 | 0.434 | 0.016 | 0.0001 | | | | | | |
| **ser (m/z 362)** | | | | | | | | | | |
| measured | 0.564 | 0.431 | 0.005 | | | | | | | |
| simulated | 0.560 | 0.432 | 0.008 | | | | | | | |
| **phe (m/z 336)** | | | | | | | | | | |
| measured | 0.219 | 0.421 | 0.283 | 0.066 | 0.004 | 0.002 | 0.001 | 0.002 | 0.001 | 0.001 |
| simulated | 0.214 | 0.429 | 0.283 | 0.068 | 0.006 | 0.0003 | 0.000 | 0.000 | 0.000 | 0.000 |

phe (m/z 302)

| | | | |
|---|---|---|---|
| measured | 0.977 | 0.023 | 0.0004 |
| simulated | 0.970 | 0.029 | 0.0002 |

phe (m/z 234)

| | | | | | | | | | |
|---|---|---|---|---|---|---|---|---|---|
| measured | 0.224 | 0.422 | 0.279 | 0.066 | 0.005 | 0.002 | 0.001 | 0.001 | 0.001 |
| simulated | 0.217 | 0.434 | 0.281 | 0.063 | 0.005 | 0.0002 | 0.000 | 0.000 | 0.000 |

asp (m/z 418)

| | | | | | |
|---|---|---|---|---|---|
| measured | 0.491 | 0.461 | 0.047 | 0.001 | 0.0002 |
| simulated | 0.488 | 0.457 | 0.053 | 0.001 | 0.000 |

glu (m/z 432)

| | | | | | | |
|---|---|---|---|---|---|---|
| measured | 0.270 | 0.455 | 0.241 | 0.032 | 0.002 | 0.000 |
| simulated | 0.263 | 0.469 | 0.240 | 0.028 | 0.001 | 0.000 |

thr (m/z 404)

| | | | | | |
|---|---|---|---|---|---|
| measured | 0.493 | 0.460 | 0.045 | 0.001 | 0.000 |
| simulated | 0.502 | 0.456 | 0.041 | 0.001 | 0.000 |

thr (m/z 376)

| | | | | |
|---|---|---|---|---|
| measured | 0.506 | 0.456 | 0.037 | 0.001 |
| simulated | 0.511 | 0.456 | 0.033 | 0.0004 |

Table 4: Relative intracellular and extracellular *in vivo* fluxes relative to the glucose uptake rate ($q_{glucose}$ = 10.51 ± 1.49 [mmol/(g CDW · h)]) during aerobic-fermentative growth of *S. pombe* CBS 356 on glucose. The confidence interval for 95 % is based on 100 monte carlo simulations. Reaction numbers are the same as in Table 1.

| Reaction | Flux [%] | Confidence interval [%] |
| --- | --- | --- |
| 1 | 89.1 | 0.00 |
| 2 | 93.9 | 0.17 |
| 3 | 80.3 | 0.06 |
| 4 | 176.1 | 0.22 |
| 5 | 174.5 | 0.23 |
| 6 | 172.9 | 0.25 |
| 7 | 6.7 | 0.62 |
| 8 | 7.4 | 0.02 |
| 9 | 4.0 | 0.47 |
| 10 | 4.3 | 0.64 |
| 11 | 5.1 | 0.45 |
| 12 | 5.1 | 0.45 |
| 13 | 9.0 | 0.38 |
| 14 | 8.2 | 0.45 |
| 15 | 2.8 | 0.05 |
| 16 | 2.8 | 0.07 |
| 17 | 2.0 | 0.08 |
| 18 | 8.4 | 0.45 |
| 19 | 8.4 | 0.45 |
| 20 | 6.1 | 0.49 |
| 21 | 6.1 | 0.49 |
| 22 | 6.1 | 0.12 |
| 23 | 1.0 | 0.09 |
| 24 | 161.4 | 0.48 |
| 25 | 9.6 | 0.46 |
| 26 | 9.6 | 0.46 |
| 27 | 0.6 | 0.03 |

| | | |
|---|---|---|
| **28** | 0.6 | 0.00 |
| **29** | 1.6 | 0.04 |
| **30** | 0.04 | 0.02 |
| **31** | 0.7 | 0.04 |
| **32** | 0.6 | 0.00 |
| **33** | 0.4 | 0.01 |
| **34** | 0.3 | 0.0 |
| **35** | 0.4 | 0.03 |
| **36** | 0.3 | 0.03 |
| **37** | 0.4 | 0.01 |
| **38** | 0.3 | 0.00 |
| **39** | 0.3 | 0.00 |
| **40** | 0.1 | 0.00 |
| **41** | 151.9 | 0.21 |
| **42** | 13.6 | 0.39 |
| **43** | 0.5 | 0.10 |

# Curriculum Vitae

## Personal information

Date of Birth    05.12.1983

Nationality    Greek

## Education

| | |
|---|---|
| 09/2009–06/2016 | PhD candidate, Biochemical Engineering group, University of Saarland, Germany |
| 10/2006–04/2009 | Master of Science (Biotech.), Faculty of Natural Science and Technology III, University of Saarland, Germany |
| 9/2001–7/2006 | Diploma in Biology, Department of Biological Applications and Technologies, University of Ioannina, Greece |

## Training

| | |
|---|---|
| 2012 | UniGR Meeting on Systems Biology, Lultzhausen, Luxemburg |
| 2011 | Omix workshop, Jülich |
| 2010 | Biosystems Engineering, Bioreactors and Cell Factories workshop, Braunwald, Switzerland |

## List of publications under preparation

**Delis V.**, Schneider K., Heinzle E. Identification of the *Schizosaccharomyces pombe* voltage-dependent anion-selective channel and role in metabolite channeling into the mitochondrium.

**Delis V.**, Schneider K., Heinzle E. The mitochondrial pyruvate carrier of *Schizosaccharomyces pombe*. *In situ* characterization of the mitochondrial pyruvate metabolism in a mini-reactor system.

# Declaration of original authorship

I hereby declare that this dissertation is my own original work except where otherwise indicated. All data or concepts drawn directly or indirectly from other sources have been correctly acknowledged. This dissertation has not been submitted in its present or similar form to any other academic institution either in Germany or abroad for the award of any other degree.

Saarbrücken, June 2016

Vasileios Delis